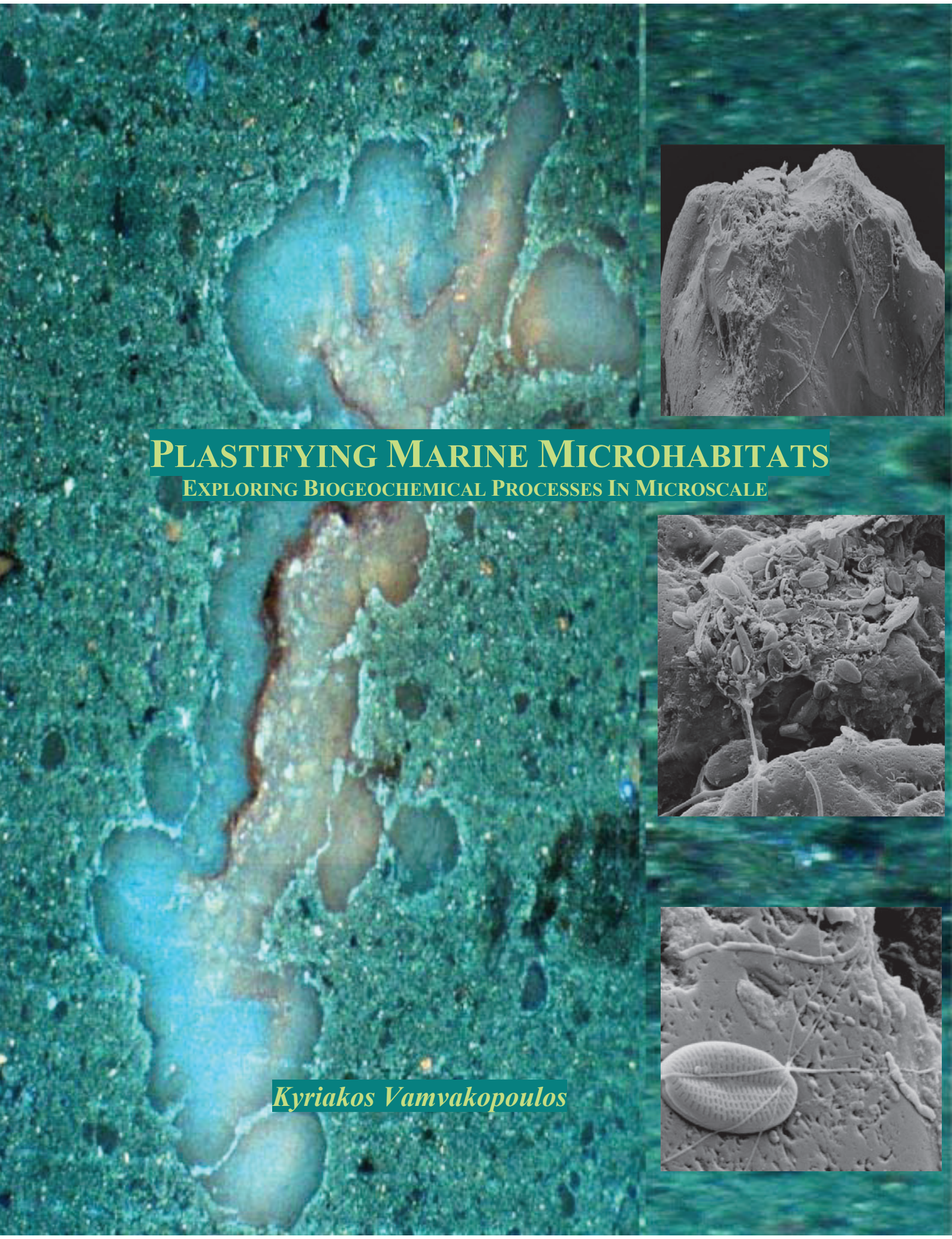

PLASTIFYING MARINE MICROHABITATS

EXPLORING BIOGEOCHEMICAL PROCESSES IN MICROSCALE

Kyriakos Vamvakopoulos

Plastifying Marine Microhabitats
Exploring biogeochemical processes in microscale

Dissertation
Zur Erlangung des Doktorgrades der
Naturwissenschaften

-Dr. rer. Nat.-

Department of Biology
University of Bremen
Germany

Kyriakos Vamvakopoulos
Bremen 2011

1. Gutachter	Prof. Dr. Bo Barker Jørgensen Max Planck Institute for Marine Microbiology & University of Bremen Bremen, Germany
2. Gutachter	PD Dr. Sabine Kasten Alfred Wegener Institute for Polar and Marine Research Bremerhaven, Germany
Prüfer	Prof. Dr. Christian Wild Leibniz Center for Tropical Ecology & University of Bremen Bremen, Germany
Prüfer	Dr. Gunter Wegener Max Planck Institute for Marine Microbiology Bremen, Germany

Weitere Mitglieder des Prüfungsausschusses

Dipl. Biologin Judith Klatt
Joseph Marshal

Datum des Promotionskolloquiums

14. Dezember 2011

To my Family

Table of contents

Acknowledgements

I am most grateful to my advisor Ole Larsen for that he gave me the possibility to be a part of his team, for mentoring, commenting and his genius ideas.

I am also grateful to Bo Barker Jørgensen for giving me the opportunity to work at the Max Planck Institute for Marine Microbiology in Bremen, for the inspiring discussions and for reviewing the thesis.

I would also very much like to thank Sabine Kasten for reviewing the thesis.

Christian Wild and Gunter Wegener are thanked for being part of the thesis committee.

Thanks to Tim Ferdelman for providing me with support and feedback throughout my PhD.

William Bill Davison and Niko Finke are thanked for reviewing and commenting on some parts of the thesis.

Katharina Kohls is thanked a lot for keeping me in good mood and shape with the in-office badminton brakes, the endless hours of laughing (mobbing included), the vital discussions on common scientific issues and the practical help and advice with parts of the thesis. Special thanks to Lars Holmqvist, a great scientist, colleague and friend. Many thanks also to Ami Bachar for the fruitful discussions on hypersaline mats.

All TREAD participants are thanked. Ronnie Glud, Annie Glud and Henrik Stahl for their hospitality at the Marine Biological Laboratory of Helsingør and their support on method optimization. Jacqueline Schmidt is thanked for her patient with the flumes, the excellent maintenance of the set up and the high quality of the project background data. Ann-Charlotte M. Toes from the TU Delft is acknowledged for providing the *shewanella* strains and her help with molecular work and discussion. Hao Zhang and Sophie-Tankere Muller are thanked for sharing their experience on heavy metals. Anders Tengberg is thanked for the nice atmosphere and the Russian lessons during the exhausting sampling campaigns.

To Ursula Werner, Lev Neretin, Jochen Nüster, Gaute Lavik, Hans Røy, Lubos Polerecky, Elsabe Julies, Olivera Kuijpers, Simone Böer, Markus Billerbeck, Friederike Hoffmann, Felix Janssen, Enoma Omoregie and Sergio Contreras my heartfelt thanks.

Gabriele Schüßler, Gabriele Klockgether, Kirsten Imhoff, Imke Busse, Tomas Wilkop and Martina Alisch are thanked very much for practical lab help and the pleasant time.

Many thanks for their technical assistance and advice on construction and testing of numerous set ups to the following technicians: Alfred Kutsche, Georg Herz, Harald Osmers, Paul Färber, Volker Meyer and Bernd Stickfort.

The Max Planck Institute for Iron Research and Monika Nellessen are thanked for giving me the opportunity to use their labs.

Rolf Tippkötter and Thilo Eickhorst are thanked for practical help on embedding, sectioning, polishing and electron microscopy. Katrin Praest (fa. Struers) is thanked for providing help with polishing media and protocols.

I gratefully acknowledge the support from the European Union (contract EVK3-CT-2002-00081) and the Max-Planck-Society.

Thesis abstract

Microorganisms are omnipresent in the environment and sediments have proven to be the largest repository for bacteria growing deep into the geosphere. Only fairly recently it was understood that sediment bacteria play a crucial role in the global carbon cycling and thereby exert control on global climate and cycling of nutrients and other elements. Research has only just begun to reveal the detailed processes in the intimate relationship between microorganisms and minerals in natural sediments, aided by development of new analytical methods and techniques.

To retain the physical structure of the investigated materials (sediments and microbial mats) samples were impregnated with a polyester. Special efforts were paid to minimize changes in biological, chemical and physical disturbance during the preparation. The work comprised development or adaption of techniques and materials for sampling, water replacement, impregnation and section preparation for obtaining undisturbed sections. Crucial for the preservation and identification of bacteria after the plastification procedure were two points: low curing temperatures and post-embedding water permeability of the specimen. From the plethora of embedding materials the most suitable according to the previous requirements found to be the Glycolmethacrylate (GMA).

The developed method was applied in detailed studies of biogeochemistry and environmental microbiology. Impregnating sediments and microbial mats with GMA enabled characterization of the sediment structure (2D arrangement of particles), and analysis of elemental composition of matrix background and individual particles. Once the impregnated blocks were hard they were cut and polished flat to yield petrographic quality specimens. Due to the high water permeability it was proven possible to investigate bacteria with some selected molecular techniques without disturbing or deplastifying the sample.

Estuarine environments are among the most intensely exploited zones and the sediments become the ultimate receptacle of many anthropogenic contaminants including heavy and trace metals. To understand the fate and behavior of heavy metals in micrometer scale along minerals in a North Sea metal polluted silty environment we applied scanning

electron microscopy (SEM) and energy dispersive X-ray analysis (EDS) on solidified sediment sections. Results from high resolution in situ measurements and other methods were combined to provide a better description of the sediment biogeochemical processes. The combination of techniques allowed us to describe processes at a spatial resolution close to that of individual bacteria or microniches. The results showed that pyrite (FeS_2) was the most dominant iron sulfide in the sediments and that the composition was highly variable from pure pyrites to pyrites almost dominated by impurities. The sediments were found to be very heterogeneous as the processes were investigated with a combination of diffusive gradients in thin films gel (DGT) and planar optodes (PO) prior to sediment embedding. A crucial role in the oxidation process played fauna activity and burrow construction as indicated by the presence of oxidized aggregates found mixed into reduced sediment matrix. Elemental mapping was used to search copper bearing minerals that proved to be heterogeneously distributed within the sediments. Analyzing the Cu-hotspots revealed that copper is predominantly associated with Fe-oxides and sulfides. The Fe-sulfides contained traces of all contaminants and the copper concentrations ranged from 0.2 to 3% Cu (on an atomic basis). The Cu containing sulfides cover a range from a few percentage of Cu substitution in pyrite over chalcopyrite ($CuFeS_2$) to almost pure chalcocite (Cu_2S).

The different high resolution data collected in the EU project TREAD were used to verify model developments on two different scales. The data described major sediment processes with a focus on turn-over and fluxes of heavy metals over the sediment water interface. The data were in the first instance used to develop a detailed sediment process model called 3DTREAD. Several tests were made confirming that the model produced similar temporal and spatial distribution of solute concentrations as measured with high resolution gels (DET/DGT) and optodes. The model describes also solid and solute interaction and was used to calculate the concentration patterns around oxidizing pyrite grains. The detailed process model formed the basis for a simplified process model that was developed as an EcoLAB template to be used with shallow water equation models. The EcoLAB simulations of heavy metals in sediments and the overlaying water are solved together with hydrodynamic and sediment transport models. This model has been used on several commercial sediment management projects by DHI.

The developed method for sediment preparation was also applied to sub-samples taken from long sediment cores from the Arkona Basin in the southwestern Baltic Sea. This investigation aimed at studying the geochemical alteration of sulfur and iron species across different sedimentary units. The study showed that elemental sulfur precipitates within iron minerals. In accordance to this observation, analysis of sulfur species in the pore water confirmed the presence of various forms of elemental sulfur (S_8), colloidal sulfur (S^0), polysulfides (S_n^{2-}) and polythionates ($S_nO_6^{2-}$).

Additionally, the work includes investigation of nodules found in sediments from the Black Sea. Semi-quantitative analysis using electron microprobe of embedded magnetic nodules from sediment samples (388 cm depth), showed that greigite and greigitized pyrite (pyrite core surrounded by greigite) were the dominant magnetic minerals. In the case of greigitized pyrite the association of these two phases follows a well defined pattern with pyrite becoming completely overgrown by greigite. Magnetic susceptibility analysis and x-ray diffraction (XRD) confirmed the presence of these phases in this sediment horizon.

Insights in spatial distribution of microorganisms were derived by identifying microorganisms in embedded undisturbed sediment samples adopting staining and fluorescence in situ hybridization (FISH) protocols. Hereby the structure of bacteria in sediments and microbial mats could be studied at a high level of detail. The spatial distribution of two specific groups within the Chloroflexaceae family was studied in a hypersaline mat following the plastification procedure and subsequent fluorescence in situ hybridization. The presence of Chloroflexaceae was further confirmed by 16S rRNA gene clone library analysis and by hyperspectral imaging of pigments.

Assuming low degree of disturbance caused by the sediment treatment, the mineral-bacteria interaction could be studied. The analysis showed that the microbial community is associated with mineral surfaces while other constituents are appearing to form microniches in the sediment matrix – presumably associated with substrate availability. Applying successively SEM and epifluorescence microscopy over the same plastified sediment sections in vertical profiles of 6x1 cm and overlapping results has showed that in the flumes microbial attachment on minerals surface was very scarce with less than

one association per square centimeter. Thus, direct bacteria-mineral associations could only have minor influence the Fe cycle in this miniaturized and semi-closed environment.

Capturing bacteria in a biota-friendly matrix and revealing their direct relation to substrate at a high spatial resolution allow us to conclude that this methodological approach could be a strong tool to explore in situ intact bacteria microniches from many sedimentary environments.

Zusammenfassung

Mikroorganismen sind in unserer Umwelt ubiquitär, und Sedimente machen das größte Gebiet ihr Vorkommen aus. Es ist nicht lange her, als es klar wurde, dass gerade Bakterien die im Sediment leben, eine entscheidende Rolle im globalen Kohlenstoffkreislauf spielen, und dadurch das globale Klima und die Kreisläufe von Nährstoffen und anderen wichtigen Elementen beeinflussen können. Die Forschung hat gerade durch die Entwicklung neuer analytischer Methoden und Techniken begonnen, die Prozesse der intimen Beziehung zwischen Mikroorganismen und Mineralien in natürlichen Sedimenten detailliert aufzudecken. In dieser Hinsicht war das Ziel der vorliegenden Doktorarbeit die Entwicklung einer Methode, welche die Untersuchung der Interaktion von Bakterien und Sedimentpartikeln ermöglichen soll. Darüber hinaus wurde diese Methode in Untersuchungen angewendet, die sich mit der Verteilung von Mineralien, der Elementen Zusammensetzung wichtiger Substrate (Eisenoxide & -sulfide), dem Aufspüren der räumlichen Beziehungen zwischen Substraten und Organismen und der in situ Identifizierung und Charakterisierung von Mikroben in komplexen natürlichen Proben befassen.

Die Arbeit ist in zwei Abschnitten unterteilt. Der erste Abschnitt der Arbeit beinhaltet die technische Entwicklung um die Erhaltung der physikalischen Struktur der untersuchten Umweltproben zu ermöglichen (Sedimente, Böden, Hart- und Weichgewebe). Um das Probenmaterial zu verfestigen, wurde ein Polyester verwendet. Im Anschluss wurden Dünnschliffe oder polierte Blöcke für Untersuchungszwecke präpariert. Viel Wert wurde dabei auf die Verminderung jeglicher Störungen auf das biologische, chemische und physikalische System gelegt. Die Möglichkeiten für die Probenahme, Entwässerung, Imprägnierung und Probenvorbereitung für hauptsächlich mikroskopische Zwecke werden erläutert. Entscheidend für den Erhalt und die Identifizierung von Bakterien nach der Einbettung waren zwei Punkte: niedrige Aushärtungstemperaturen und Wasser Permeabilität der ausgehärteten Polyestermatrix. Aus der Vielzahl von Einbettungsmedien hat sich Glycolmethacrylate (GMA) am besten bewährt.

In dem zweiten Abschnitt soll die Methode in ausführlichen Studien der Biogeochemie und Mikrobiologie angewendet werden. So sollen in imprägnierten Blocke Details der

Sediment Matrix analysiert. Die Tatsache der hohen Wasserpermeabilität der imprägnierten Schnitte soll uns ermöglichen, molekulare Techniken einzusetzen, um die eingebetteten Bakterien identifizieren und untersuchen zu können.

Ästuare gehören zu den am intensivsten genutzten Gebieten und die Sedimente zum ultimativen Empfänger vieler anthropogener Schadstoffe, darunter Schwer- und Spurenmetalle. Um das Verhalten von Metallen in Mikrometer-Skala in der Festphase in Metall-belasteten Nordsee-Sedimenten studieren zu können, haben wir Rasterelektronenmikroskopie (REM) und energiedispersive Röntgenanalyse (EDS) an eingebetteten Sedimenten angewendet. In situ Messungen mit hoher Auflösung wurden mit anderen Methoden kombiniert, um eine bessere Beschreibung der biogeochemischen Prozesse liefern zu können. Dies erlaubte uns, Prozesse in der Skala eines Bakteriums oder einer Mikronische zu beschreiben. Die Ergebnisse zeigten, dass Pyrit (FeS_2) mit einer sehr variablen Zusammensetzung aus reinem und verunreinigtem Pyrit, das häufigste Eisensulfid in unseren Sedimenten war. Die Sedimente haben sich als sehr heterogen erwiesen, wie Untersuchungen mit kombinierten Messungen von Diffusionsgradienten in dünnen Gel-Filmen (DGT) und Planar Optode (PO) vor den Einbettungen zeigten. Eine entscheidende Rolle bei dem Oxidationsprozess spielten Bioirrigation, Fauna Aktivität und Röhrenbau. Bioturbation verursacht eine Vermischung der Sedimentpartikel, was durch die Präsenz von oxidierten Aggregaten in reduzierten Sedimentschichten angezeigt wird.

Element Mapping wurde verwendet, um kupferhaltige Mineralien aufzusuchen, die nachweislich heterogen innerhalb der Sedimente verteilt waren. Die Analyse des Cu-Hotspots hat gezeigt, dass Kupfer überwiegend mit Eisenoxiden und -sulfiden assoziiert ist. Die Eisensulfide enthielten Spuren von vielen verschiedenen Verunreinigungen und auch Kupfer in einem Bereich zwischen 0,2 bis 3% Cu (auf atomarer Basis). Die kupferhaltigen Sulfide decken einen Bereich von wenigen Prozenten Cu-Substitutionen in Pyrit über Chalkopyrit ($CuFeS_2$) bis fast reines Chalkosin (Cu_2S).

Eine Reihe von verschiedenen hochauflösenden Daten vom EU-Projekt TREAD wurden gesammelt und verwendet, um Modell-Entwicklungen auf zwei unterschiedlichen Skalen zu überprüfen. Die Daten beschreiben wichtige Prozesse in Sedimenten mit dem

Schwerpunkt auf Umsatz und Flux von Schwermetallen über die Sediment-Wasser Grenzfläche. Diese Daten wurden zunächst verwendet, um ein detailliertes Sediment-Prozess-Modell genannt 3DTREAD zu entwickeln. Mehrere Tests haben bestätigt, dass die durch das Modell produzierte zeitliche und räumliche Verteilung der Konzentrationen gelöster Stoffen ähnlich ist, wie solche aus Messungen durch hoch auflösende Gele (DET / DGT) und Optoden. Das Modell beschreibt auch feste und gelöste Interaktionen und wurde benutzt, um Konzentrationsmuster ringsum oxidierender Pyrit-Körner zu berechnen. Das detaillierte Prozessmodell bildete die Grundlage für ein vereinfachtes Prozessmodell, welches als EcoLAB Vorlage entwickelt wurde, um eine Verwendung mit Gleichungsmodellen in seichten Gewässern zu ermöglichen. Die EcoLAB Simulationen von Schwermetallen sowohl in Sedimenten als auch im Wasser wurden mit Modellen der Hydrodynamik und des Sedimenttransportes ergänzt. Dieses Modell wurde in mehreren kommerziell verwendeten Sedimenten-Management Projekten von DHI verwendet.

Die Methode wurde auch in Proben von langen Sedimentkernen aus dem Arkona Becken der südwestlichen Ostsee angewendet. Dadurch wurde die Untersuchung der geochemischen Veränderungen von Schwefel und Eisen in verschiedenen Sediment Abschnitten angestrebt. Die Studie zeigte, dass elementarer Schwefel in Eisen-Mineralien ausfällt. Diese Beobachtung wurde durch Porenwasser-Messungen bestätigt. Dadurch wurden verschiedene Formen von elementarem Schwefel (S_8), kolloidalem Schwefel (S^0), Polysulfide (S_n^{2-}) und Polythionate ($S_nO_6^{2-}$) gemessen.

Darüber hinaus beinhaltet diese Arbeit Untersuchungen an Mineralien in Sedimenten aus dem Schwarzen Meer. Semi-quantitative Analyse mittels Elektronenmikroskopie von eingebetteten magnetischen Partikeln aus Sedimentproben aus 388 cm Tiefe haben gezeigt, dass Greigit und greigitiziertes Pyrit (Pyrit-Kern umgeben von Greigit) die dominierenden magnetischen Mineralien Fraktionen ausmachen. Im Falle von greigitiziertem Pyrit folgt das Verhältnis der beiden Phasen immer einem genau definierten Muster, wobei Pyrit vollständig von Greigit umgehüllt wird. Magnetische Suszeptibilität und Röntgen-Diffraktometrie (XRD) haben das Vorhandensein dieser Phasen in diesem Sedimenthorizont bestätigt.

Einsichten in die räumliche Verteilung von Mikroorganismen in eingebetteten und ungestörten Sedimentproben wurden durch Färbungsreaktionen und Fluoreszenz-in-situ-Hybridisierung ermöglicht. Auf diese Weise konnte die Struktur der Bakteriengemeinschaften in Sedimenten und mikrobiellen Matten detailliert untersucht werden. In einer hypersaline Matte war es uns möglich durch Einbettung und Fluoreszenz-in-situ-Hybridisierung, die räumliche Verteilung von Chloroflexaceae Stämmen zu untersuchen. Die Anwesenheit von Chloroflexaceae wurde durch 16S rRNA-Genbanken und hyperspektrale Abbildung von Pigmenten bestätigt.

Auch Mineral-Bakterien Assoziationen konnten beobachtet werden. Unsere Analyse hat gezeigt, dass ein geringer Teil der mikrobiellen Gemeinschaften auf Oberflächen von Mineralien ansässig sind. Viel mehr formen die Bakterien Mikronischen, die wahrscheinlich Substrat abhängig sind. Sukzessive Anwendung von SEM und Epifluoreszenzmikroskopie auf die gleichen Sediment Schnitte in vertikalen Profilen von 6 x 1 cm und nachfolgender Überlappung der Bilder hat gezeigt, dass in unseren Aquarien die mikrobielle Besiedlung an Oberflächen von Fe-Mineralien mit weniger als ein Bakterien-Mineralien-Assoziation pro Quadratzentimeter Sediment sehr knapp war. Deshalb konnten direkte Bakterien-Mineralien-Assoziationen den Fe-Zyklus in diesem kleinen und halb geschlossenen Durchflusskanal nur gering beeinflussen.

Das Plastifizieren von Bakterien innerhalb ihrer Umweltproben und die hoch auflösende Visualisierung ihrer räumlichen Struktur im Bezug auf ihre Substrate zeigte, dass dieser methodischer Ansatz hilfreich sein konnte, um in situ intakte bakterielle Mikronischen aus vielen sedimentären Habitaten zu erforschen.

Introduction

Sediment processes resulting from biological, chemical and physical processes, have been intensely studied in the past century. The spatial resolution of is limited by the adopted technologies and rationale behind the studies. As an example, contaminated sediments are usually investigated at vertical resolutions in the order of meters corresponding to accuracy of dredging activities. This is in strong contrast to the actual processes occurring at a micrometer scale. It is therefore essential for our understanding of processes to investigate these at highest possible resolution. Most of the research to date has employed wet chemical techniques to obtain porewater gradients typically at centimetre resolution. Major breakthroughs have been provided through the advances using radiotracers (Jørgensen 1978) and various kinds of microsensors (Revsbech & Jørgensen 1986; Revsbech 1989; de Beer & Sweerts 1989; de Beer et al. 1997; Kühl et al. 1998) and gel technologies (Davison et al. 1994) enabling high spatial and temporal resolution of process studies. With advances in molecular ecology it has become possible to identify microorganisms based on their functional genes allowing quantification of organism groups in sub-millilitre sediment samples (Muyzer & Ramsing 1995; Lloyd et al. 2010).

Only in the most recent past has it been possible to align microbiological and biogeochemical investigations to achieve results at comparable spatial resolution significantly advancing our understanding of sediment processes (Jørgensen 2006). However, many techniques focus on mixed sediment samples with volumes in the order of millilitres. In many marine sediments such volumes may cover microenvironments with grossly different redox environment housing billions of genetically diverse microorganisms (Torsvik et al. 1996; Nealson 1997; Llobet-Brossa et al. 1998). Therefore, it is easier to quantify an overall process, than it is to justify the presence and function in situ of an individual microbial species and characterize its niche (Tate 1986).

With concentration-depth profiles of solid-phase components and pore waters, typically measured at centimetre resolution significant heterogeneity at sub-centimetre scale where steep chemical gradients place anaerobes, microaerophiles and aerobes in close proximity are lost (Happer et al. 1999; Bernhard et al. 2003). It remains therefore analytical challenging to identify and study individual organisms in an ecological context in

environmental samples. Molecular tools, imaging mass spectrometry (Kuypers and Jørgensen 2007) and culturing experiments have paid large contributions to identify and characterize isolated microbes to understand their in situ role and function. However, to investigate the structural heterogeneity and to understand the role of localized concentration gradients it is necessary to study this system at the same scale as the processes take place.

Methods to embed undisturbed soil samples in resin followed by examination with microscopy have been used to characterize the structure, fabric and mineral transformations giving rise to the discipline of soil micromorphology. During the development of these methods soil scientists had a strong focus on the abiotic transformations. Postma and Altemüller (1990) made the first investigations using various staining techniques to examine in situ the distribution of microorganisms and their relation to minerals and organic matter in soil thin sections and polished blocks. Postma and Altemüllers work was based on the classical soil thin section approach introduced by Kubiena in 1936. The established methods cannot be readily applied to study marine sediments due to the salt content and low permeability in fine-grained marine sediments. Therefore the development of a biota friendly, non-destructive embedding method for highly hydrated samples such as sediments and microbial mats is the primary focus of the current thesis. Furthermore, we should apply the method and combine results with high-resolution techniques to investigate biogeochemical processes at sub-millimetre scale with regard to the iron-sulfur cycle in natural and contaminated marine sediments.

Established high resolution methods

High resolution spatial investigations include microsensor profiling, small-volume sediment and pore water sampling (Revsbech & Jørgensen 1986; Aller and Aller 1986) often correlated with organism abundances. Microelectrode profiles suggest vertically distinct oxygenated and anoxic-sulfidic layers yielding a mosaic of chemically heterogeneous microhabitats both in vertical and horizontal dimensions (Lovley & Phillips 1986; Davison et al. 1991). Recent advances in instrumentation have helped detect and characterize submillimetre-scale microhabitats. Rather than the one-dimensional microelectrode approach; planar optodes (PO), gel measurements by diffusive equilibrium (DET), diffusive gradient (DGT) thin films and hyperspectral

imaging are able to resolve the solute structure in 2D with focus on chemical species like oxygen, sulfide and metals with a spatial resolution of some tens of microns (Zhang & Davison 1995; Glud et al. 1996; Fones et al. 1998; Stahl et al. 2006, Kühl & Polerecky 2008). To date most of the information on microbial ecology is obtained from sediments with disrupted spatial arrangement (Deflaun 1983; Gelder 1983; Mayer 1986). The application of imaging mass spectrometry of single cells in combination with biogeochemical and molecular ecological techniques has provided very promising results (Halm et al. 2009). One of the main problems is to preserve the 3 dimensional configuration of the microenvironment and to avoid major disturbances of the microorganisms upon and during collection and processing of sediment (Curry 2002).

Plastifying marine sediments

Synthetic resins used for biogeochemical purposes should possess as much as possible from the properties listed below:

Low viscosity	Allows fast and thorough penetration into the finest pores.
Low curing temperature	Minimizes the likelihood of sample disturbance as a result of elevated temperature, especially critical for heat-sensitive materials/cells.
Slow polymerization rate	Permits maintenance of high fluidity for a long duration and in conjunction with low viscosity affects thorough sample impregnation. Also minimizes cracking and birefringence due to strain as a result of rapid polymerization.
Long pot life	Permits storage of a reasonable quantity of resin for a reasonable duration without deterioration in quality.
Low shrinkage coefficient	Minimizes sample disturbance due to sympathetic movement of units with the shrinking impregnant.
Medium hardness	Permits cutting, grinding and polishing of sections without undue difficulty. Too soft results in the displacement and dislodgement of fabric units as well as the embedding of grinding grains in the impregnant; too hard is difficult to work with.
High strength	Able to withstand routine sectioning treatments without showing plastic deformations or brittle failure.
High melting point	Frictional heat emanated during and grinding may not be absorbed sufficiently quickly by the lubricant-cum coolant.
Minimum reaction with organic liquids	Common organic solvent such as acetone, ethanol used as diluents, degreasants or in the substitution of pore fluid should not react deleteriously with the impregnant. Also paraffin oil used a coolant-cum-lubricant should be inert to the impregnant.
Desirable optical properties	Ideally the impregnant should be optically isotropic free from birefringent strain colorless with a refractive index to permit the application of optical techniques.

Table 1. Attributes of an ideal impregnant for microstructural studies (Jim 1985).

Resin type	Resin	Viscosity (mPas)	Shrinkage . %	Density (g/cm^3)	H_2O solubility
Polyester	Crystic 17449	380	7.5	1.11	-
	Palatal P50-01	280	7	1.12	-
	Synolite 544	280	7	1.12	-
	Vestopal 160	800	7.5	1.1	-
Acrylic	LR White	-	2	1.07	-
	RWL Medium	-	3	-	-
Epoxy	Araldite BY158+HY1012 Scotchcast	200	6.4	1.06	-
Melamine	Nanoplast	-	-	1.21	+
Methacrylate	Hydroxypropyl Methacrylate Butyl methacrylate	-	-	1.08	++
	Hydroxyethyl methacrylate (Glycolmethacrylate)	70	6	1.06	++

Table 2. List of the properties of some of the most common referred resins. Polyester, acrylic and epoxy data from Tippkötter & Ritz (1996). Melamine from Bachhuber & Frösch (1983). Methacrylate from Rosenberg et al. (1960); Leduc & Holt (1965).

Many different resins are used for sediment preparation with the most common groups listed at Tab. 2. Most of these resins are not advantageous for marine sediments (in particular clays) because of the relatively high viscosities preventing thorough penetration into the sediments. The viscosity of the resin is therefore essential for the quality of the impregnation (Tippkötter & Ritz 1996). This kind of difficulty may be circumvented by using methacrylates meeting the desirable attributes of low viscosity, density and hydrophilicity. In the group of the water-miscible methacrylates hydroxyethyl methacrylate (GMA) can penetrate tissues easier than hydroxypropyl-methacrylate (HPMA) and should be preferred (Leduc & Bernhard 1967).

A variety of methods for plastification of samples have been described historically (Alexander & Jackson 1954; Bowles 1968; Frankel 1970; Jim 1985; Tippkötter et al. 1986; Kuehl et al. 1988; Watling 1988; Postma & Altemüller 1990; Baerwald et al. 1991; Lamoureux 1994; Tippkötter & Ritz 1996; Fisk et al. 1999; Nunan et al. 2001; Curry et al. 2002). As referred in these works the common steps for resin impregnation are: i) **dehydration** ii) **infiltration with impregnant** iii) **resin polymerization**.

For example, dehydration may take place either via evacuation or replacement of pore fluid (s. Tab. 3). In general, air-drying may cause significant shrinkage of samples and freeze-drying may create fissures. The main impact of solvent substitution on the

sediment matrix and structure is the potential dissolution and removal of organic matter fractions. Hence, solvent substitution remains the preferred method for dehydration of sediment samples leaving the matrix intact and producing minimal shrinkage (Murphy 1986). Samples with high content of smectite and vermiculite should be prone to shrinkage and rearrangement of particles in the sediment matrix. Further details on imfiltration and polymerization are listed in the method chapter.

Techniques	Variants	Comments
Evacuation of pore fluid	Direct evaporation a) air drying b) oven-drying	Generally unsuitable for fine-textured samples with high natural moisture content because of the possibility of change in arrangement and orientation of sediment constituents) Shrinkage Tremendous stresses of surface tension
	Removal of liquid-air interface a) freeze-drying b) critical point drying	Reduce shrinkage of samples to a minimum (<0.5%) Formation of ice-crystals Need complex procedures and special equipment Can only deal with small-sized samples
Replacement of Pore fluid	One-step replacement by water-miscible impregnant	Osmotic shock should be avoided by using a series of water-impregnant mixtures at increasing impregnant concentration, with initial moisture content of the mixture matched with that of the samples Considerable shrinkage still occurs Undesirable optical properties, mainly birefringence and unsuitable refractive index Possible formation of clay-impregnant complex with aberrant optical properties
	Two-step replacement by water-miscible solvent followed by solvent-miscible impregnant	A concentration series of water-solvent mixtures should preferably be used to replace interstitial moisture gradually and avoid osmotic shock and slaking of samples Vapor exchange, which allows slow substitution of water by a volatile solvent and hence minimizes sample disturbance The solvent may form complexes with clay minerals resulting in excessive expansion of basal spacing

Table 3: Details and comments on various methods for pore fluid evacuation/replacement prior resin embedding (adopted from Jim 1985).

Apart from resins, paraffin and agar (agar is a polysaccharide agarose in which the hydrogen bonds of the hydroxyl groups cross link as the solution cools to room temperature) are two media widely used in biology to stabilize tissue structure. The main

advantage of agar- and paraffin-embedding is that they do not require chemical pre-treatment of the sample. They provide the physical stabilization necessary to maintain bacteria attached in surfaces, e.g. roots and sponges, and enable in situ hybridization (Macnaughton 1996; Hoffmann et al. 2003). Unfortunately, they have several disadvantages over resin media. Cast of sediment blocks in agar and paraffin may be easy but cutting, staining, washing, and blocking on slides should be extremely careful to prevent lost of sediment material, in addition samples cannot used for conventional SEM examination due to the high vapour pressure of water.

Exploring plastified microniches, tools & possibilities

There are a couple of microscopical methods applied in plastified sections such as polarized light microscopy (PM), epifluorescence microscopy (EM), confocal laser scanning microscopy (CLSM) and scanning electron microscopy (SEM).

The use of polarized light in microscopy allows mineral identification. If the thickness (length of light pass) of a mineral grain is known, then the refractive index and other optical properties can be used to accurately determine the mineralogy. PM may also be used for the examination of intergrain matrices, organic matter and the weathering states of grains (Fisk et al. 1999).

In contrast, EM is particularly important for the identification and characterization of microorganisms but is not wholly satisfactory for the examination of structure and composition. For example in Figures 2 & 3 fluorescent microscopy shows some aspects of bacteria distribution but image information is not sufficient for precise study of micromorphology.

To enhance the focal depth resolution in optical microscopy pointed laser light is used in CLSM that enables virtual sectioning of samples and thus make possible a 3D description of the investigated specimen / area (MacNaughton et al. 1994). Using CLSM thickness of the specimen is not a limiting factor since light from out-of-focus planes is physically excluded by the detector pinhole. In addition, the series of 2D digital images obtained by CLSM may allow 3D rendering and reconstructions (Fig. 4). However, characterizing sediments by digital imaging would require massive amounts of data storage, specialized algorithms or automated scanning and enormous computing power for reconstruction into 3D images. Confocal microscopy has been widely used in environmental microbiology (Lawrence et al. 1991; Ghiorse et al. 1996; DeLeo et al. 1997), but its use to examine bacteria in sediments has so far been limited.

High resolution images over a wide range of magnifications and with a good focus depth may also be provided with the SEM. SEM is powerful in revailing details of complex geometries and fine details of individual cells. A limitation of SEM is illustrated in figure 5(1c). The figure exhibits what appears to be a bacterial aggregate, however, it is unclear

whether the structure is composed of bacteria or single minerals growing over a protruding structure of the substrate. Since SEM only images the surface of a sample volumetric reconstruction of serial images from multiple layers is not possible.

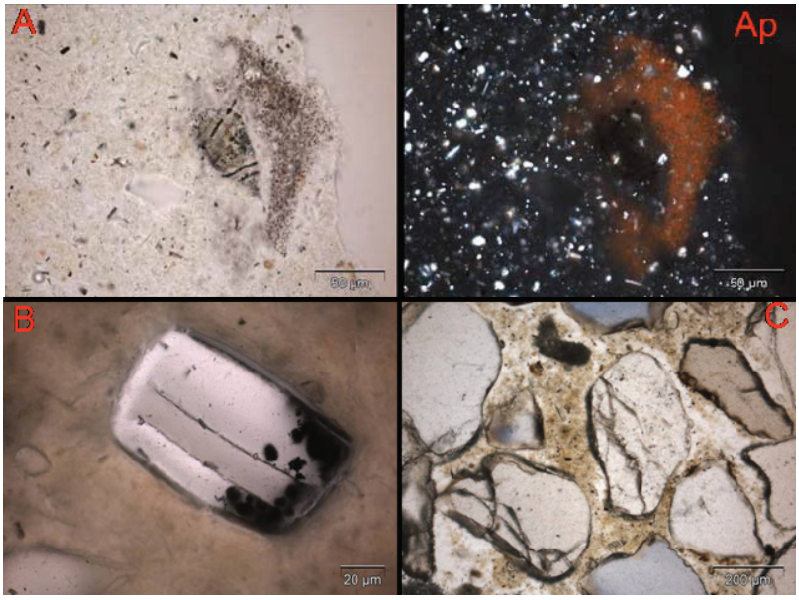

Figure 1: Impregnated sediment thin sections. Transmitted light image provides information on pore spaces and spatial arrangement of grains (A). The same microscopic field under polarized light; yellow reddish structures are iron oxides (Ap). Shell-like structure with iron sulfide precipitates enclosed (B). Sand particles embedded in an organic matrix (C).

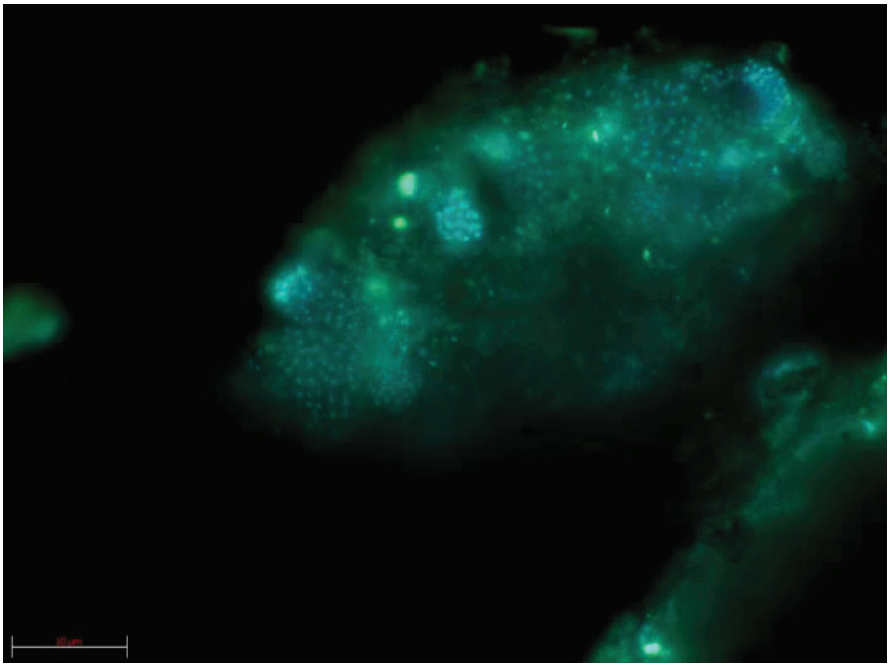

Figure 2. EM on a sandy sediment section embedded in GMA and stained with DAPI. Bright dots are bacteria cells. Quartz grains are black colored. Scale bar 10 µm.

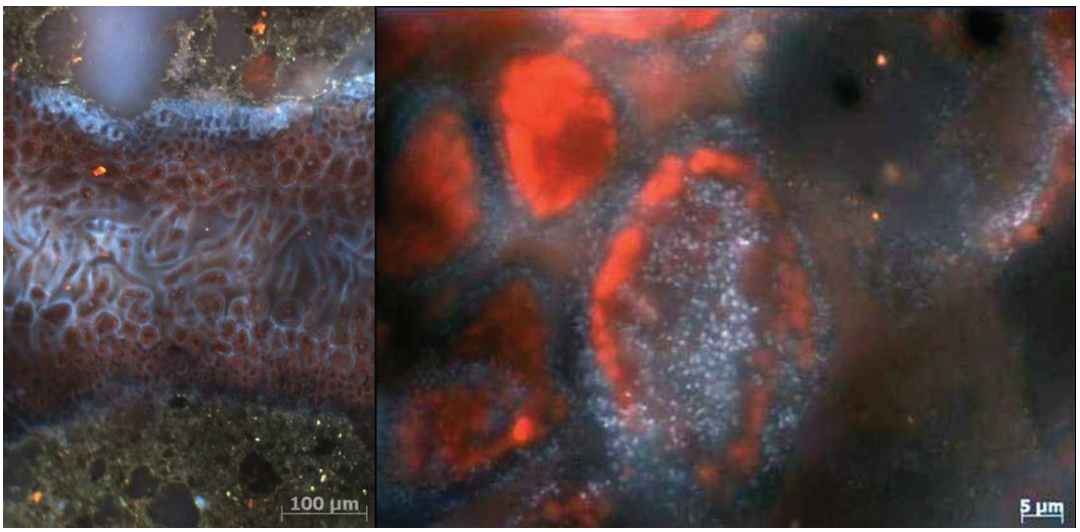

Figure 3: EM on a silty sediment section embedded in GMA and stained with DAPI. **Left**: The grey-blue signals are areas with a high bacteria density.

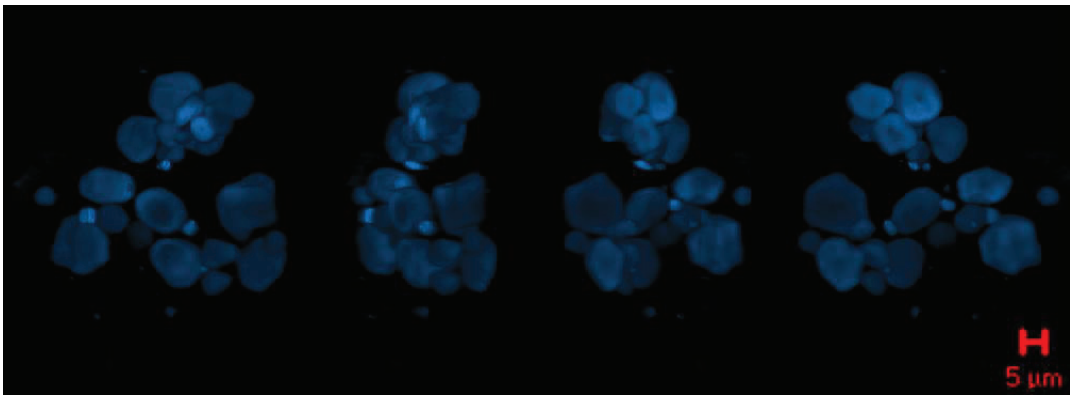

Figure 4. Sediment particles embedded in GMA and stained with DAPI. CLSM serial images digitally processed and reconstructed (y axis).

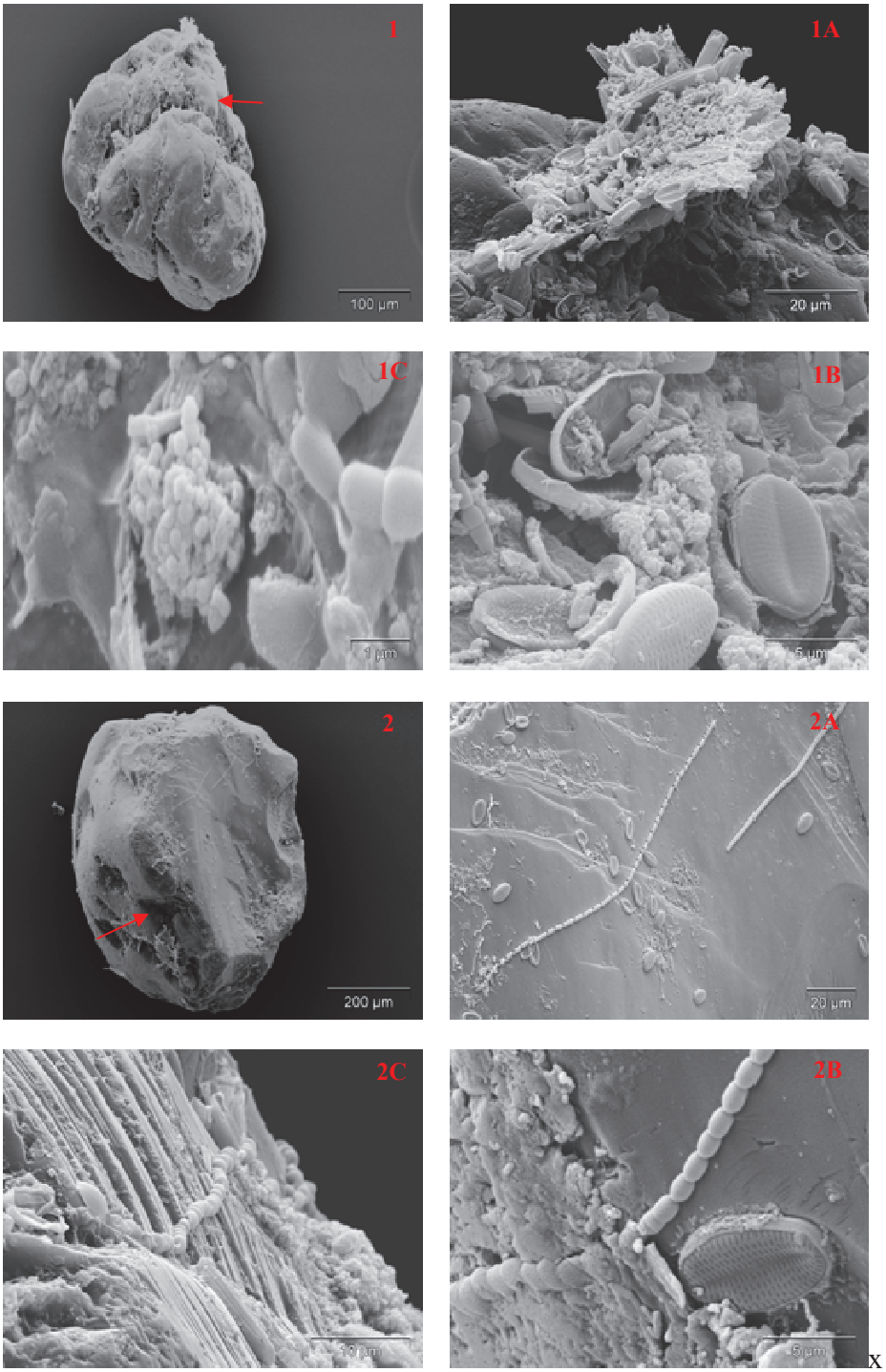

Figure 5: SEM micrographs from single sand grains (1, 2). Close-ups on a detritus assemblage (1A, 1B) and a bacterial-like looking aggregate (1C). Cyanobacteria filaments attached on grain surface (2A, 2C), partially embedded in exopolymers (2C). With SEM filamentous bacteria may well be identified when exposed on the surface. Usually identification is difficult and uncertain when microorganisms are embedded in an assemblage of fragments of filaments, algae, minerals and detritus.

Biogeochemistry of microhabitats

The above pictures demonstrate that organic matter is not homogenously distributed in sediments. Particulate organic matter deposited in sediments gives rise to the bloom of bacteria decomposing the organic matter. The structure of the sediments has direct influence on the rate of organic matter mineralization and therefore on the global biogeochemical cycles. The sediment structures are important for transport processes within the sediments and influence the rate of organic matter decomposition (Ranson et al. 1997). Organic carbon captured in the sediment matrix may get oxidized completely to CO_2 using O_2 as electron acceptor. After depletion of O_2, microbes may utilize other electron acceptors like nitrate, manganese and iron (oxyhydr)oxides, and sulfate. In the absence of these electron acceptors organic matter itself may act as electron acceptor and methane is formed (Fig. 6).

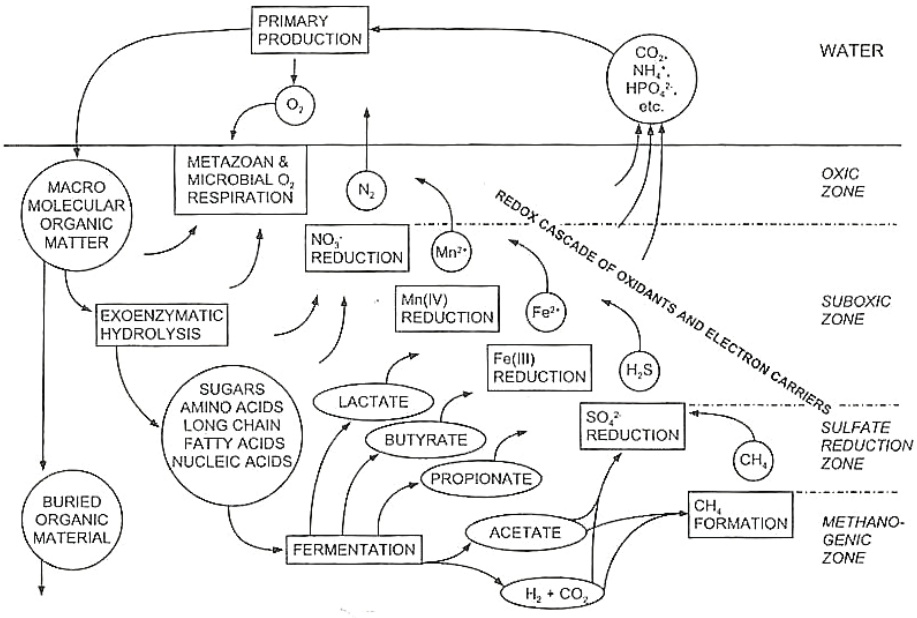

Figure 6. Pathways of organic carbon degradation in marine sediments and their relation to the geochemical zonations and consumption of oxidants. Figure reproduced from Jørgensen 2006 (after Fenchel & Jørgensen 1977).

The quantitatively most important metal in sediments is iron usually entering the sediments as Fe(III) being reduced to Fe(II) and ultimately buried as pyrite. Heavy metals are strongly influenced by the sediment biogeochemistry as they can be adsorbed to Fe(III)-oxides and hydroxides and included into Fe-sulphides. Many examples are

available describing the sediment processes affecting the heavy metal cycling (Brown et al. 1999; Zoumis et al. 2001; Eggleton et Thomas 2004; Banfield et al. 2005), dissimilatory and assimilatory reactions (Lovley 1991; Nealson & Saffarini 1994; Straub et al. 1996; Kostka et al. 1999), and chemical transformations (Haese 2006). Numerous works describe the bulk processes involved but limited information is available about the detailed reactions at molecular scale. It is of course extremely difficult and complicated to work in those scales, e.g. the double layer of metal oxide-aqueous solution interfaces is of the order of 4 Å with the overlying solvent region of interest being between 20-30 Å. Considering now that a single microbial cell layer is approximately 5000 Å and a biofilm or an aggregate contains some 100s of bacteria then we have almost an infinite distance with an inherent complexity in terms of interfacial chemistry (Brown et al. 1999). In the last years major biogeochemical processes like sulfate and iron reduction/oxidation have been studied in great detail (Jørgensen 1982; Lovley & Phillips 1986; Canfield et al. 1993). Utilizing radiolabelled tracers the reduction of pore water sulfate to sulfide via dissimilatory sulfate reduction has been accurately quantified and shown to be the dominant pathway of anaerobic organic carbon oxidation in ocean margin sediments (Jørgensen 1982). In freshwater environments iron(III)oxides are the most important electron acceptors, whereas their quantitative importance as terminal electron acceptor in marine systems is much lower (Canfield et al 1993; Roden & Wetzel 1996; Thamdrup 2000). Jakobsen and Postma (1996) explained this difference by the energy yielded under partial equilibrium conditions. In most marine sediments, iron oxides are reduced by sulfide and form a range of iron(II) mono- and bi-sulphides. Iron oxides play a key role in the formation of pyrite (Aller & Rude 1988; Berner 1984; Wilkin & Barnes 1997). Manganese oxides are, due to their higher oxidation potential, able to oxidize Fe(II), and sulfide to sulphate, or to pyrite. In addition to precipitation and dissolution of iron minerals complexation, sorption and desorption of trace metals control trace metal availability in the sediment systems (Jenne 1968; Manceau et al. 2002). However, llittle is known about trace metal associations with oxides and sulfides in sediment systems (i.e. coprecipitated or adsorbed on the minerals, or precipitated as discrete metal sulfides) (Huerta-Diaz et al. 1996). The complexity of biogeochemical processes affecting copper availability is well illustrated regarding copper. When copper enters into the sediment

system, it is usually bound in organic matter. During early diagenesis, the organic matter is oxidized and the copper is released. Copper can then adsorb to transition metal oxides and hydroxides or be incorporated into sulphides. However, sulphides are usually reoxidized releasing copper several times before ultimately buried in the sedimentary record (Schmidt & Forster 1977; Sawlan & Murray 1983).

Additional factors influencing the biogeochemical cycling in the sediments include bioturbation caused by sediment in-fauna, in particular burrowing macro fauna. Through reworking the substrate, enlarging the interface sediment-water, and enhancing irrigation bioturbating fauna is modifying geochemical gradients affecting redox conditions and associated processes (Meysman et al. 2006). Although the effects of bioturbation are clear, the actual mechanisms behind them are less established (Murray et al. 2002).

In general, sediment redox chemistry is largely controlled by microbial activity. Dissimilatory iron and manganese oxide reducers have been studied in detail with the aim of investigating the need for physical contact to transfer electrons from the microorganisms to the electron acceptors (Lovley 1991; Nealson & Saffarini 1994). Results from experiments with pure cultures have revealed a range of mechanisms for electron transfer including the use of electron carriers (Neilands 1995; Lovley & Chapelle 1995; Lovley et al. 1996; Caccavo & Das 2002) and production of protons locally altering pH to ease dissolution of oxides prior to reduction (Ehrlich 1996; Lower et al. 2001; Frankel & Bazylinski 2003). In few investigations it has been possible to document the need for physical contact between the microorganisms and electron acceptor (Nevin & Lovley 2002; Reguera et al. 2005). Given the particle size and the size of microorganisms it has due to lack of analytical methods yet not been possible to elucidate the pathways in natural sediments. Current methods meet their limits in the attempt to quantify metabolic products of individual organisms due to the low amounts used per organism. Recent advances have enabled high resolution studies of DNA, biomarkers and photo pigments from biomats sectioned in 0.25–0.5 mm. This high resolution is however, still coarse when considering the size of individual cells being less than 0.5 μm^3 (Nunan et al. 2001).

References

Aller JY and Aller RC (1986) Evidence for localized enhancement of biological activity associated with tube and burrow structures in deep-sea sediments at the HEBBLE site, western North Atlantic. *Deep-Sea Research* **33**: 755-790.

Aller RC and Rude PD (1988) Complete oxidation of solid phase sulfides by manganese and bacteria in anoxic marine sediments. *Geochimica et Cosmohimica Acta* **52**: 751-765.

Banfield JF, Tyson GW, Allen EE and Whitaker RJ (2005) The search for a molecular-level understanding of the processes that underpin the earth's biogeochemical cycles. *Reviews in Mineralogy & Geochemistry* **59**: 1-7.

Berner RA (1984) Sedimentary pyrite formation: An update. *Geochimica et Cosmohimica Acta* **48**: 605-615.

Bernhard JM, Visscher PT and Bowser SS (2003) Submillimeter life positions of bacteria, protists, and metazoans in laminated sediments of the Santa Barbara Basin. *Limnol Oceanogr* **48**: 813-828.

Brown JEJr, Henrich VE, Casey VE, Clark DL, Eggleston C, Felmy A, Goodman DW, Grätzel M, Maciel G, McCarthy MI, Sverjensky DA, Toney MF and Zachara JM (1999) Metal oxide surfaces and their interactions with aqueous solutions and microbial organisms. *Chem Rev* **99**: 77-174.

Canfield DE, Thamdrup B and Hansen JW (1993) The anaerobic degradation of organic matter in Danish coastal sediments: Iron reduction, manganese reduction, and sulfate reduction. *Geochimica et Cosmohimica Acta* **57**: 3867-3883.

Curry KJ, Abril M, Avant JB, Curry C, Bennett RH and Hulbert MH (2002) A technique for processing undisturbed marine sand sediments and reconstructing fabric and porometry. *Journal of Sedimentary Research* **72**: 933-937.

Davison W, Grime GW, Morgan JAW and Clarke K (1991) Distribution of dissolved iron in sediment pore waters at submillimetre resolution. *Nature* **352**: 323-324.

deBeer D & Sweerts J-PRA (1989) Measurement of a nitrate gradients with an iron selective microelectrode. *Anal.Chim.Acta* **219**: 351-356.

deBeer D, Schramm A, Santegoeds CM & Kühl M (1997) A nitrite microsensor for profiling environmental biofilms. *Applied and Environmental Microbiology* **63** (3): 973-977.

Deflaun MF and Meyer LM (1983) Relationships between bacteria and grain surfaces in intertidal sediments. *Limnol Oceanogr* **28**: 873-881.

DeLeo PC, Baveye P and Ghiorse WC (1997) Use of confocal laser scanning microscopy on soil thin-sections for improved characterization of microbial growth in unconsolidated soils and aquifer materials. *Journal of Microbiological Methods* **30**: 193-203.

Eggleton J and Thomas KV (2004) A review of factors affecting the release and bioavailability of contaminants during sediment disturbance events. *Environmental International* **30**: 973-980.

Ehrlich HL (1996) How microbes influence mineral growth and dissolution. *Chemical Geology* **132**: 5-9.

Fisk AC, Murphy SL and Tate III RL (1999) Microscopic observations of bacterial sorption in soil cores. Biol Fertil Soils 28: 111-116.

Fletcher M and Marshall KC (1982) Are Solid Surfaces of Ecological Significance to Aquatic Bacteria. Plenum Press, New York, 236 pp.

Fones GR, Davison W and Grime GW (1998) Development of constrained DET for measurements of dissolved iron in surface sediments at sub-mm resolution. *The Science of the Total Environment* **221**: 127-137.

Frankel RB and Bazylinski DA (2003) Biologically induced mineralization by bacteria. *Reviews in Mineralogy & Geochemistry* **54** (1): 95-114.

Gelder SR (1983) Enhancement of histochemically demonstrated organic matenals on sand-silt grains using polarized light. *Tech Inf Bull* **1**: 11-12.

Glud RN, Ramsing NB, Gundersen JK and Klimant I (1996) Planar optrodes: a new tool for fine scale measurements of two-dimensional O_2 distribution in benthic communities. *Marine Ecology Progress Series* **140**: 217-226.

Halm H, Musat N, Lam P, Langlois R, Musat F, Peduzzi S, Lavik G, Schubert CJ, Singha B, LaRoche J and Kuypers MMM (2009) Co-occurrence of denitrification and nitrogen fixationvin a meromictic lake, Lake Cadagno (Switzerland). *Environmental Microbiology* **11**: 1945-1958.

Harper MP, Davison W and Tych W (1999) One-dimensional views of three-dimensional sediments. *Environ Sci Technol* **33**: 2611-2616.

Hoffmann F, Janussen D, Dröse W, Arp G and Reitner J (2003) Histological investigation of organisms with hard skeletons: a case study of siliceous sponges. *Biotechnic & Histochemistry* **78**: 191-199.

Hudson-Edwards KA (2003) Sources, mineralogy, chemistry and fate of heavy metal-bearing particles in minng-affected river systems. *Mineralogical Magazine* **67**: 205-217.

Huerta-Diaz MA, Tessier A and Carignan R (1996) Geochemistry of trace metals associated with reduced sulfur in freshwater sediments. *Applied Geochemistry* **13**: 213-233.

Jenne EA (1968) Controls on Mn, Fe, Co, Ni, Cu, and Zn concentrations in soils and water: The significant role of hydrous Mn and Fe oxides. in: Trace inorganics in water. American Chemical Society. *Advances in chemistry* (**21**): 337-387.

J¢rgensen BB (1978) A comparison of methods for the quantification of bacterial sulfate reduction in coastal marine sediments 1. Measurement with radiotracer techniques. *Geomicrobiology Journal* **1** (1):11-27.

J¢rgensen BB (1982) Mineralization of organic matter in the seabed - the role of sulphate reduction. *Nature* **296**: 643-645.

J¢rgensen BB and Nelson DC (2004) Sulfide oxidation in marine sediments: Geochemistry meets microbiology. In: Amend JP, Edwards KJ and Lyons TW (eds) Sulfur Biogeochemistry, pp 63-81. The geological society of America.

Jȼrgensen BB (2006) Bacteria and marine biogeochemistry. In: Schulz HD and Zabel M (eds) Marine Geochemistry, pp 169-206.

Kostka JE, Haefele E, Viehweger R and Stucki JW (1999) Respiration and dissolution of iron(III)-containing clay minerals by bacteria. *Environ Sci Technol* **33**: 3127-3133.

Kühl M and Polerecky L (2008) Functional and structural imaging of phototrophic microbial communitites and symbioses. *Aquatic Microbial Ecology* **53**: 99-118.

Kuypers MMM and Jȼrgensen BB (2007) The future of single-cell environmental microbiology. *Environmental Microbiology* **9**, 6-7.

Llobet-Brossa E, Rosselló-Mora R and Amann RI (1998) Microbial community composition of Wadden Sea sediments as revealed by fluorescence in situ hybridization. *Appl Environ Microbiol* **64**: 2691-2696.

Lloyd KG, MacGregor BJ and Teske A (2010) Quantitative PCR methods for RNA and DNA in marine sediments: maximizing yield while overcoming inhibition. *FEMS Microbiology Ecology* **72** (1): 143-151.

Lovley DR and Phillips EJP (1986) Organic matter mineralization with reduction of ferric iron in anaerobic sediments. *Applied and Environmental Microbiology* **51**: 683-689.

Lovley DR (1991) Dissimilatory Fe(III) and Mn(IV) reduction. *Microb.Rev.* **55** (2): 259-287.

Lower SK, Hochella MF Jr and Beveridge TJ (2001) Bacterial recognition of mineral surfaces: Nanoscale interactions between Shewanella and a-FeOOH. *Science* **292** (5520): 1360-1363.

Macnaughton SJ, Booth T, Embley TM and O´Donnell AG (1996) Physical stabilization and confocal microscopy of bacteria on roots using 16S rRNA targeted, fluorescent-labeled oligonucleotide probes. *Journal of Microbiological Methods* **26**: 279-285.

Manceau A, Marcus MA and Tamura N (2002) Quantitative speciation of heavy metals in soils and sediments by synchrotron X-ray techniques. *Reviews in Mineralogy & Geochemistry* **49** (1): 341-428.

Mayer LM (1985) Geochemistry of humic substances in estuarine environments. In: Aiken GR, McKnight DM, Wershaw DL and MacCarthy P (eds) Hurnic substances in soil, sediment, and water. Geochernistry, isolation, and characterization, pp 211-232. John Wiley & Sons, New York.

Meysman FJR, Middelburg JJ and Heip CHR (2006) Bioturbation: a fresh look at Darwin's last idea. *Trends in Ecology and Evolution* **21**: 688-695.

Murphy CP (1986) Thin section preparation of soils and sediments. A B Academic Publishers, UK.

Murray JMH, Meadows A and Meadows PS (2002) Biogeomorphological implications of microscale interactions between sediment geotechnics and marine benthos: a review. *Geomorphology* **47**: 15-30.

Muyzer G and Ramsing NB (1995) Molecular methods to study the organization of microbial communities. *Wat- Sci.Tech.* **32**: 1-9.

Nealson KH (1997) Sediment bacteria: Who´s there, what are they doing, and what´s new? *Annu.Rev.Earth Planet.Sci.* **25**: 403-434.

Nealson KH and Saffarini D (1994) Iron and manganese in anaerobic respiration: environmental significance, physiology, and regulation. *Ann.Rev.Microbiol.* **48**: 311-343.

Nevin KP and Lovley DR (2002) Mechanisms for Fe(III) oxide reduction in sedimentary environments. *Geomicrobiology Journal* **19**: 141-159.

Postma D and Jakobsen R (1996) Redox zonation: Equilibrium constraints on the Fe(III)/SO_4^- reduction interface. *Geochimica et Cosmohimica Acta* **60** (17): 3169-3175.

Postma J and Altemüller H-J (1989) Bacteria in thin soil sections stained with the fluorescent brightener calcofluor white M2R. *Soil Biology & Biochemistr*y **22**: 89-96.

Ransom B, Bennett RH, Baerwald R and Shea K (1997) TEM study of in situ organic matter on continental margins: occurrence and the "monolayer" hypothesis. *Marine Geology* **138**: 1-9.

Reguera G, McCarthy KD, Mehta T, Nicoll JS, Tuominen MT and Lovley DR (2005) Extracellular electron transfer via microbial nanowires. *Nature* **23**: 1098-1101.

Revsbech NP (1989) An oxygen microsensor with a guard cathode. *Limnol.Oceanogr.* **34** (2): 474-478.

Revsbech NP and Jørgensen BB (1986) Microelectrodes: their use in microbial ecology. *Advances in Microbial Ecology* **9**: 293-352.

Roden EE and Wetzel RG (1996) Organic carbon oxidation and suppression of methane production by microbial Fe(III) oxide reduction in vegetated and unvegetated freshwater wetland sediments. *Limnol.Oceanogr.* **41** (8): 1733-1748.

Sawlan JJ and Murray JW (1983) Trace metal remobilization in the interstitial waters of red clay and hemipelagic marine sediments. *Earth and Planetary Science Letters* **64** (2): 213-230.

Stahl H, Glud A, Schröder CR, Klimant I, Tengberg A and Glud RN (2006) Time-resolved pH imaging in marine sediments with a luminescent planar optode. *Limnol Oceanogr*: Methods **4**: 336-345.

Schmidt RL and Forster WO (1977) Copper in the marine environment - Part II. *C R C Critical Reviews in Environmental Control* **8** (1-4): 247-291.

Straub KL, Benz M, Schink B and Widdel F (1996) Anaerobic, nitrate-dependent microbial oxidation of ferrous iron. *Appl Environ Microbiol* **62**: 1458-1460.

Tate RL (1986) Importance of autecology in microbial ecology. In: Tate RL (ed) Microbial Ecology, pp 1-26. Wiley-Interscience, USA.

Thamdrup B (2000) Bacterial manganese and iron reduction in aquatic sediments. In: Advances in microbial ecology, edited by B. Schrink, New York: Kluiver Academic/Plenum p. 41-84.

Torsvik V, Sørheim R and Goksøyr J (1996) Total bacterial diversity in soil and sediment communities - a review. *Journal of Industrial Microbiology* **17**: 170-178.

Watling L (1988) Small-scale features of marine sediments and their importance to the study of deposit-feeding. *Marine Ecology Progress Series* **47**: 135-144.

Weise W and Rheinheimer G (1978) Scanning Electron Microscopy and Epifluorescence Investigation of Bacterial Colonization of Marine Sand Sediments. *Microbial Ecology* **4**: 175-188.

Wilkin RT and Barnes HL (1997) Formation processes of framboidal pyrite. *Geochimica et Cosmohimica Acta* **61** (2): 323-339.

Zhang H and Davison W (1995) Performance characteristics of diffussion gradients in thin films for the in situ measurment of trace metals in aqueous solution. *Anal Chem* **67**: 3391-3400.

Zoumis T, Schmidt A, Grigorova L and Calmano W (2001) Contaminants in sediments: remobilisation and demobilisation. *The Science of the Total Environment* **266**: 195-202, 2001.

Thesis outline

The primary aim of the thesis is to develop a method for study in situ the distribution and interaction of bacteria and particulates in different marine sedimentary environments and microbial mats. Mineral distribution and elemental composition of important substrates like iron oxides and sulfides should be investigated. Spatial relationships among substrates and organisms should be detected. Microbes in complex natural samples should be identified and characterized.

It is fundamental for understanding the processes involved in sediments to reveal in situ details in scales as small as possible, ideally to those scales where the processes take place. Plastification of sediments should make possible the preservation of the entire structure and its biotic and abiotic constituents. It is difficult to conceive of detailed studies of sediment or mats of the morphologically almost unified bacteria by means of optical microscopy without staining or hybridizing the cells. This calls for an embedding media which should be water permeable in solid state.

Therefore, we should try to examine in detail existing protocols and impregnation media with a view to adopting, revising and improving one or other of them trying to reduce physical and chemical stress. Once the protocol will be successful developed, applied and verified in different marine habitats it will be necessary to stress out the possibilities of handling and treating of the solidified blocks.

Particular emphasis should be placed on the in situ identification possibilities of microbial communities in natural samples. Existing bacteria staining and FISH protocols should be adapted and applied on plastified sections.

Recording in detail the characteristics of sediments at a micrometer / sub-micrometer level requires sophisticated and microscopic techniques at the limit of visible light resolution. Observation and magnification of samples at those scales should be widely tested with optical and electron microscopes. To act as a support for other analyses and to form a basis for the choice of further selective mineralogical, chemical and physical analyses images derived from the impregnated blocks should be linked to other high

resolution techniques. These efforts and progresses should be represented in the following chapters.

Part 1, Method

A protocol for plastifying marine sediments and postembedding staining of microbes enclosed in the resin-matrix

Kyriakos Vamvakopoulos[1] & Ole Larsen[2]

[1#]Max-Planck-Institute for Marine Microbiology, Celsiusstr. 1, D-28359 Bremen, Germany

[2]DHI-NTU Water & Environment Research Centre and Education Hub, 200 Pandan Loop #08-03, Singapore

Abstract

It is essential for understanding biogeochemical processes in sediments to work with virtually undisturbed samples in scales as small as possible, ideally to those scales where the processes take place. To maintain spatial structure and study microorganisms and mineral constituents in high resolution sediment samples were plastified with Glycolmethacrylate (GMA), a water permeable polyester. Postembedding staining of sediment sections with the DNA-specific fluorescent dye 4´-6-diamidino-2-phelylindole (DAPI) enabled us to identify bacteria enclosed in the matrix. We report the experimental approaches in order to minimize the mechanical, thermal and chemical disturbance and optimize the results during sampling, fixation, embedding, sectioning and staining. As a result of these modifications a simple protocol for sediment plastification was developed.

Introduction

Many recent ecological studies on the marine microbenthos retrieved from highly heterogenic sediments were aiming on observation and characterization of bacteria mainly in a cm^3 scale. Comparing bacterial cell volume of ca. 0.1-0.2 μm^3 (Kuwae & Hosokawa 1999) to the cm^3 volume previously mentioned we easily realize the scale problem of these approaches. In such a million of μm^3 volume of chemically heterogeneous microhabitats (Davison et al. 1991; Harper et al. 1999; Bernhard et al. 2005) parameters like colonization strategies of the attached bacteria, structure of microcolonies, 3D distribution of a single specie, chemical, physical and biological properties either are not included in the ecological study or they are too general and thus inadequate to understand and describe ecological niches.

High quality in situ description of microhabitats taking into consideration sedimentological, microstructural, geochemical and biological properties, requires a non destructive approach which can ensure sample integrity during lab analysis and preferably application of different methods on a well defined area without altering sample properties (Baerwald et al. 1999). This can be achieved through impregnation of sediments. Thereby the pores of the unconsolidated material are permeated by a low-viscosity liquid which hardens into a solid upon thermal curing or cooling (Jim 1985). This results in preservation of structures and matrices within a framework of a medium which permits the preparation of sections and applications of established microscopic techniques. Kubiena (1938) published first a protocol on sediment impregnation revealing geological aspects of soil microenvironments in plastified sections. This technique enabled microbiological observations (Alexander & Jackson 1954; Tippkötter et al. 1986; Postma & Altemüller 1990; Tippkötter & Ritz 1996; Fisk et al. 1999; Nunan et al. 2001) and was also applied in moist or marine sedimentary environments (Bowles 1968; Frankel 1970; Jim 1985; Kuehl et al. 1988; Watling 1988; Baerwald et al. 1991; Lamoureux 1994; Curry et al. 2002). In most of these works polyester, epoxy or acrylic resins were preferred due to material properties required for high quality sections. These plastics are hydrophobic and require dehydration with alcohol or other organic solvents. Additionally, the polymers obtained are not water permeable, a property which is

imperative for postembedding chemical treatment. Glycolmethacrylate (GMA) was introduced as a low viscosity water-miscible polyester which is water-permeable when solidifies (Rosenberg et al. 1960). This property may enable staining reactions of biological or non biological structures enclosed in the plastic. Progress in in-situ-nucleic-acid-hybridization enabled identification of cells in their environment (Gall & Pardue 1969; Amann et al. 1995). GMA impregnation combined with in-situ-hybridization of cells enclosed in the polyester matrix was successfully performed in treponemes (Moter et al. 1998), plants (Takechi et al. 1999), wheat embryos (Mochida & Tsujimoto 2001), corals (Hoffmann et al. 2003) and a hypersaline mat (Bachar et al. 2008). Accordingly, GMA seems to be the ideal medium for plastifying highly hydrated marine sediments allowing chemical treatment after hardening for microscale investigations and bacteria identification.

In this paper we present a plastification protocol for fine and coarse sediments with focus on results optimization during sampling, fixation, embedding, sectioning and staining of microorganisms minimizing mechanical, thermal and chemical disturbance.

Method

The method we developed was tested on two contrasting types of marine sediments: a) sandy sediment with well sorted grain size distribution dominated by of particles between 200-600 μm, and b) a silty mud only containing particles smaller than 20 μm. The two types of sediment differed not only in particle size distribution but also with respect to their porosity (sand=0.37; silty mud=0.82) and permeability. The permeability is particularly important for the method since the resin must be transported into the sediment during impregnation.

Our method of preparation involves several individual steps: **a**) sampling undisturbed sediment **b**) fixation of biota in the samples **c**) fluid replacement (muddy sediments) **d**) polyester embedding **e**) sectioning **f**) DNA staining.

Sampling of undisturbed sediment

All samples were taken using rectangular metal frames (steel VA 1.4571) of 60 x 37 x 18 mm with material strength 0.5 mm. Metal frames used for fine sediment embeddings were additionally laterally perforated with 2 rows of 1 mm Ø of diameter. The investigated samples were obtained from mesocosms used for the EU Project TREAD EVK3-CT-2002-00081.

Sampling was carried out according to Fig. 1. We deployed a flat plastic sheet of 200 x 200 mm, material strength 1 mm vertically in the sediment. The metal frame for the embedding was placed on the top of the sediment and manually pushed onto the plastic sheet in an angle of 90°. The back of the metal frame was closed by vertical insertion of a thin stainless steel mesh (thickness of 1 mm) and was sandwiched between the two sheets. The sample was lifted up by pressing both sheets and placed horizontally on a table with the mesh facing upward. The mesh was removed carefully, and the excess sediment was cut away with a knife. A thin plastic mesh Ø 0.5 mm was glued with Loctite fast glue on the edges of the metal frame. The frame was then rotated 180° so the plastic sheet was facing upwards and the mesh downwards. Thereafter the sediment was transferred into a container (plastic box 12x12x5 cm) with glass beads (Ø 3 mm) covering the bottom. Next, sterile filtered seawater was added to make the plastic sheet float and detach from the sediment leaving a smooth and undisturbed sediment surface.

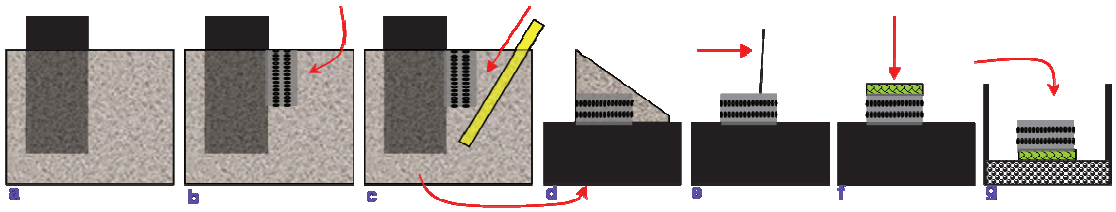

Figure 1. Sequence for sampling: **a**) plane surface is inserted into the sediment **b**) metal frame is pushed into the sediment and against the plane surface **c**) a plastic jig is pushed into the sediment at an angle until it is completely under the frame **d**) jig, metal frame and plane are moved out of the sediment and turned 90° left **e**) excess sediment is removed with a blade from the top of the metal frame **f**) a net is glued over the edges **g**) sample is turned 180° and placed in a container with glass beads on the bottom.

Fixation and fluid replacement

Immediately after sampling the sediments were fixed in 4.5 % formaldehyde in sea water for 12 h. The fixative was rinsed out with phosphate buffer saline (PBS) 1,37 M NaCl, 85 mM Na_2HPO_4 x 2 H_2O, 27 mM KCl, 15 mM KH_2PO_4. It is assumed that the fixation is less effective for impermeable sediments where the transport into the sediment matrix is determined by diffusion than in the sands. Experiments were conducted to test the effect of longer fixation time. After fixation and rinsing, the fine sediment samples were dehydrated by successive 12 h immersions in aqueous ethanol (20, 40, 60, 80, 90, 96 $^{v}/_{v}$).

Embedding

Plastification was carried out through polymerization of a solution based on GMA:

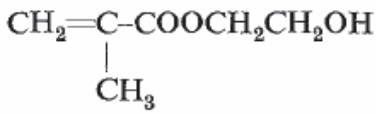

The GMA solution together with accelerator and hardener are included in a Kit with the commercial name Technovit 7100 sold by Heraeus Kulzer. The monomer is a transparent, hygroscopic, colorless liquid with density 1.065 (at 20 °C) and viscosity 0.701 poise (at 20 °C) that is completely miscible with ethanol (Roseberg et al. 1960). We used only anhydrous monomer (up to 3 % aqueous solutions possible). The polymerisation of the GMA monomer mixture was initiated by adding 0.6 g of benzoic peroxide to 100 ml of GMA (SolA). Caution, benzoic peroxide should only be added if using anhydrous GMA due to the risk of explosion. After mixing of SolA with benzoic peroxide the solution is stable at frozen storage (-22 °C) for several weeks. To ensure a complete penetration of GMA into the sediment matrix and its micropores the fine grained sediment samples were first soaked in ethanol / SolA 1:1 and in pure SolA for 12 h each at -22 °C. Endpolymerization was accelerated by mixing for 30´´ 120 ml SolA in 8 ml of a barbituric acid derivative with chloride ions (SolP). In room temperature the well mixed final embedding solution (SolA/SolP 15:1) should be applied within 5 minutes while after the solution viscosity and density are rapidly increasing.

Samples were saturated with the embedding mixture SolP and were fully cured after 4 days at -22 °C, 1 day at +4 °C and 1 day at +40 °C. Plastifying coarse sediments is much easily and quick and requires only immersion of the samples in the embedding mixture

SolP for 1 day at +4 °C. The reaction is completed after 8 h at +45 °C. This mixture works fine for standard DNA staining reactions.

GMA as a water-miscible solution should be handled with care while repeated exposure of the skin to the liquid monomer can produce allergic reactions. The polymerized GMA can be handled without difficulty (Leduc & Bernhard 1967).

All times given above were adjusted according to the degree of permeability of the sediment block. The steps until post-curing were performed under 4 °C. Solution exchange was done from down to up. The sediment block remained immobile and stable in the embedding devices till complete resin-impregnation in order to avoid perturbation and loss of material. No pressure / vacuum were applied trying to avoid any damage of the sediment fine texture (Watling 1988; Baerwald et al. 1991; Boës & Fagel 2005). Samples kept wet in any stage of embedding.

Sectioning

After hardening, the impregnated sample was removed from its metal form, trimmed and sectioned with 2 kinds of manual cut off machines: 1) a micro band saw (MBS 240/E, Proxxon) with a diamond blade 0.3 mm thick and 3 mm broad. 2) a rotary microtome (HM 505 E, Microm) with a stainless steel knife. Samples were carefully cut without using cooling water since the cured GMA is water permeable. Sectioning of coarse sediments was only possible with diamond blades, while fine sediments were cut with both the microtome and the band saw. Samples were sawed to suitable size to fit the object slides (10x10 mm) and to the microtome.

Staining and imaging

Microtome sections were immediately used for staining reactions while the sawed sections needed additionally treatment. The blocks of sandy sediments were flattened by rubbing on a glass surface coated with 1 µm aluminium oxide powder (Struers) suspended in liquid paraffin**.** Sections were ready for staining after rinsing with ethanol and drying for 10 minutes at 40 °C.

Bacterial cells in the sections were stained with the DNA-specific fluorescent dye 4´-6-diamidino-2-phelylindole (DAPI) (Porter & Feig, 1980). They were covered with DAPI-

solution 2.5 µg ml^{-1} distilled water for 10 minutes in the dark, rinsed 2-3 times with distilled water and dried for 15´ minutes at 45 °C. Prior to optical examination stained sections were bonded on cleaned polished glass slides with epoxy glue, or carbon adhesive tabs 12 mm in diameter (Pelco), or double-stick tape. Epifluorescence microscopy was performed with an Axio Imager M1 microscope (Zeiss) equipped with a Plan Apochromat objective (Zeiss). For image acquisition and processing two setups were used, an AxioCam MPc (Zeiss) camera with the software package AxioVision 4.3, and a CoolSnap HQ (Photometrics) camera with the software package Metamorph Imaging 6.2.

Results

The low viscosity of the GMA and the partial water solubility resulted to an optimal impregnation by capillary action even in impermeable muddy sediments. No remarkable volume contraction of the polymerized block could be observed. The low curing temperature and the non aggressive components prevented probably the loss of biological information.

Best results were obtained by plastifying sediments in rectangular (perforated) steel frames. This helps in orienting samples and marking with appropriate reference numbers. The glass beads on the bottom of the box elevated the sediment slightly above the base of the container and promoted circulation of fluids under the sediment. The combination of metal / silicon / glass provided stability; neutral chemical behavior and flexibility during the removal of the hardened sediment blocks form the moulds. Between frames and boxes there was enough space for the exchange of solutions avoiding flushing away of the sediment surface.

For the high permeable coarse sediments the chemical impact was minimized by avoiding ethanol dehydration. In the muddy sediments ethanol resulted most probably to some solubilisation of the organic matrix causing a slight yellow-brown coloration in the dehydration solution. The quantities normally dissolved are minute (Tippkötter & Ritz 1996). Perhaps in organic-rich sediments may modify the volume of the sample by extraction of the soluble organics. Osmotic shock could be avoided by using a series of water-impregnant mixtures at increasing impregnant concentration, with initial moisture

content of the mixture matched with that of the samples (Jim 1985). We tried dehydration in 10 % steps without observing any differences after microscopical examination to those samples dehydrated as proposed in the methodology part. Longer dehydration is disadvantageous meaning added mechanical and chemical pressure through more solutions exchange and the increase of ethanol residence within the sediment.

Impregnation was always satisfactory without using pressure or vacuum. The low viscosity of the GMA enabled sediment saturation by capillarity (Lamoureux 1994). Increasing the ambient temperature from -22 °C to 4 °C and to 40 °C is necessary in order to increase the polymerization rate. During the polymerization the temperature increases and the polymerization rate decreases. Increasing temperature can compensate the energy lost and accelerate the polymerization rate (Boës & Fagel 2005).

Hardness decreased with increased water content. Inadequate dehydrated samples resulted to incomplete polymerization with a white milky and soft mass as end-product. The hardened GMA was colorlessness with a low refractive index and without any autofluorescence under UV. GMA transparency was lost when water content exceeded 40 %. Postembedding staining with DAPI worked fine for bacteria visualization (Fig. 3).

It was not possible to dissolve the GMA polymer by immersing sections in organic solvents like acetone, ether, toluene, xylene, butyl acetate, 2-methoxyethylacetate and dichloromethane. The polymers obtained swell in ethanol, acetone and particularly water. Swelling was minimized by using barium chloride (0.5 M). Swelling is not permanently and samples return to their original form and consistency after drying. The drying period depends on sample volume, surrounding temperature and solution applied, e.g. sections of 100-200 µm after immersion in DAPI solution were incubated for 30´ at 40 °C to obtain their original form and consistency. Incubating coarse sediment sections in water for 30 min at room temperature has softened the polymer and enabled us to unhinge readily single grains out of the matrix.

The temperature development and the duration of the polymerization depend on the ambient temperature (Fig 2). The peaks indicate the hardening of the GMA. At room temperature GMA hardens after ca. 1 hour with a peak at 68 °C. At 4 °C hardening is

completed after ca. 12.5 h with a maximum T° of 13.5 °C. At -22.5 °C the slowly reaction was completed after ca. 150 h with a max T °C at -21 °C.

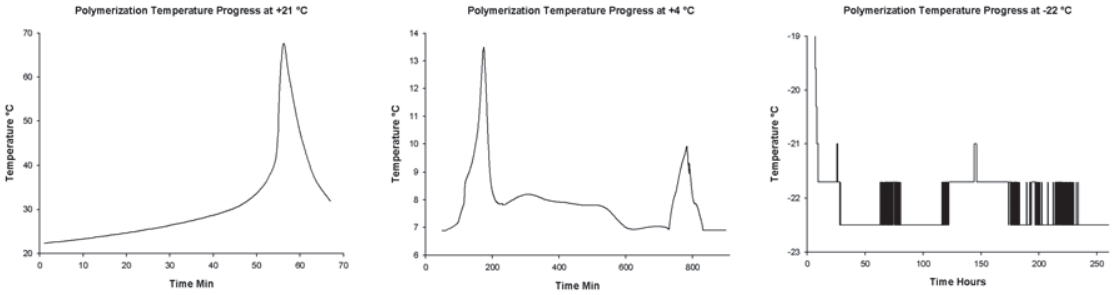

Figure 2. T° progress during polymerization of 2 ml GMA.

Plastifications of coarse sediments were optimal at +4 °C and of fine sediments at -22.5 °C. For the fine sediments slowly polymerization reaction is imperative. In case that a polymerization should take place at room temperature we advise the use of a metal underground or water bath for transferring heat out of the sample.

The diamond grains on the band saw cut evenly and uniformly through both hard and soft phases of the specimen. There was no evidence of material burns, smearing and chipping during trimming of impregnated sediment blocks with the diamond band saw. We think that trimming with the lowest band speed at 180 m / min helped to avoid an increase of the frictional heat. Polymerized material was not brittle and therefore serial thin sections of fine sediment could be sliced with the microtome (fine sediment). Microtomy did not work at all with quartz grains. The thickness of the sections is not so important since epifluorescence microscopy is based on incident illumination. GMA sections were stable under the electron beam (Larsen et al. 2007).

Stain reactions in GMA sections should happen before mounting on glass slides. We experienced sections detachment from glass slides when immersed in water based solutions. Bacteria cannot penetrate the GMA polymer matrix and thus post embedding treatment cannot contaminate the material enclosed. Optimal DAPI concentration & infiltration time for staining purposes is reported in the methodology part. EM optical examination showed that bacterial cells were gut preserved in the matrix. Furthermore, it was possible to determine the degree and type of aggregation (Fig. 3). Bacteria aggregates in coarse sediment sections were relatively small with a max diameter of ca. 10 μm close to each other (Fig. 3, C & D). Bacteria aggregates in fine sediment sections were more voluminous, densely packed, contained high number of bacteria and were patchy distributed (Fig. 3 F, G).

Embeddings in polycarbonate (PC) frames or cores caused fractures on the PC during polymerization at 4 °C. This could be explained through the temperature differences between outer and inner part of the PC during the exothermal polymerization.

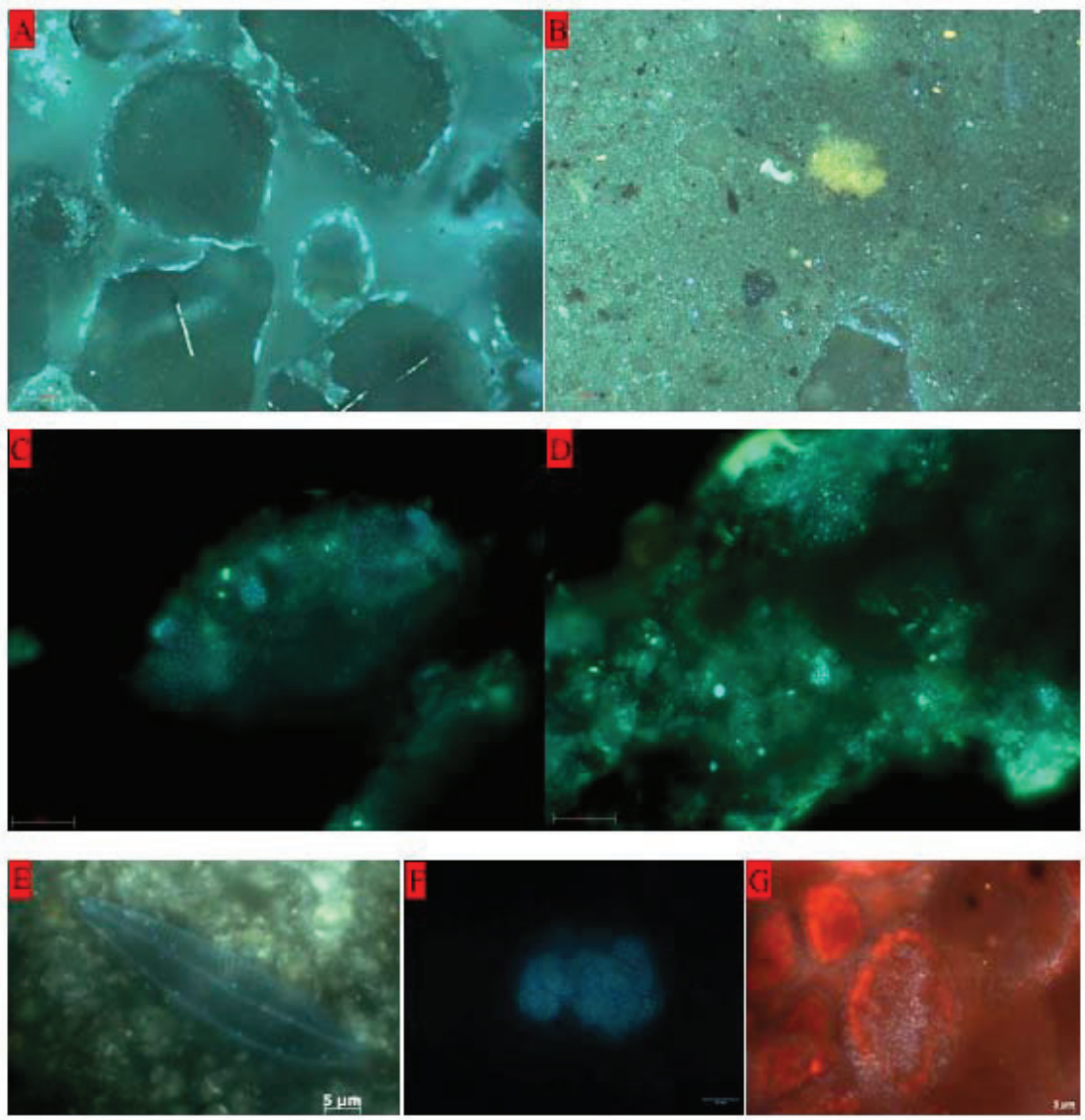

Figure 3. GMA embedded sections stained with DAPI, epifluorescence microscopy. Coarse (**A**, **C**, **D**) and fine sediments (**B**, **E**, **F**, **G**). Sand grains (black) surrounded by microbial life (bright blue) (**A**). The interspace between the grains was partially colonized from roughly round (Ø < 10 µm) bacterial aggregates (**C**, **D**). In fine sediments bacteria aggregates may exceed by far the 10 µm diameter range (**F** & **G**). Diatoms may serve as a substrate for bacterial growth (**E**).

Discussion

The whole sediment bulk with its cracks, cavities and pores was successfully fixed and embedded. No special skills were required for the production of reproducible sections. No deformations and shrinkage were observed. Polymerization proceeded at a uniform rate at the temperatures tested. Curing of the GMA never exceeded the 40 °C limit.

Higher temperatures may lead to fast polymerization and cracks (Ashley 1973). This is an advantage in comparison with other polyester / epoxy / acrylic resins which require ambient temperatures between 50-60 °C (Tippkötter & Ritz 1996). Also, GMA in contrast to some epoxy resins does not contain styrene which is a cancer risk for the operator. (Tippkötter & Ritz 1996; Boës & Fagel 2005). Dehydration is based on ethanol instead of acetone which is a less aggressive organic solvent. For highly permeable sediments the dehydration steps could be skipped.

The total time required for a complete plastification procedure was less compared to similar works in soils (Nunan et al. 2001) and sediments (Bernhard et al. 2003). Depending on material permeability, sample volume and reaction conditions polymerization may last from a few hours (Cook & Roy 2006) to few days (Bachar et al. 2008). Microbial population assessments without sonicating sediment samples could be performed under the EM or CLSM within any sections or blocks adequate plastified and with a flattened surface. Microscopic observation could be difficult if the surface is uneven. For better results glass slides should also be flattened because they are not of uniform thickness (Tippkötter & Ritz 1996).

Preembedding staining cannot guarantee identification of all microorganisms. Stains applied after fixation but before plastification might loose brightness during the embedding process (Postma & Altemüller 1990). Additionally, optimal preembedding stain concentration in samples of few cubic centimeters is difficult to be standardized due to stain interactions / absorbance related to the natural heterogeneity in available surfaces, chemical constituents (e.g. organics, reactive components etc), makro- and meiofauna content, porosity. Also, if stains should be applied before dehydration then ethanol cannot be used since it is detrimental to the staining effect (Anderson and Slinger 1975).

Our focus was to develop a reliable bacteria staining technique for resin-embedded samples avoiding deplastification prior microscopical analysis. Postembedding DAPI staining of GMA sections gave excellent reproducible results. DAPI stained adequately bacteria in a non-specific fashion and did not interact with the GMA (Fig. 3); in contrast to e.g. acridine orange which stains non specific soils and sediment constituents providing high background fluorescence overlaying single cells signals. Acridine orange

can additionally be adsorbed from resins (Postma & Altemüller 1990). DAPI stains in general DNA thus it is impossible to discriminate between the majorities of bacterial cells. To distinguish between bacterial groups sections should be hybridized (Manz et al. 2000, Bachar et al. 2008). During staining of GMA sections the structures are sterically fixed in the impregnant and thus the possibility of formation of artefacts is reduced.

If we assume that particulates can be transported down-core by fluid percolation during the plastification process then size sorting with bacteria deeper in the sediment column should be expected and elongated specimens (e.g. filaments) should exhibit a particular orientation in response to fluid motion. In hundreds of sections examined bacteria / filaments / elongated structures imaged throughout our samples were not apparently orientated. In agreement with the reports of Bernhard et al. (2003) and Bachar et al. (2008) processing during plastification does not appear to displace organisms.

In Figure 3 we see some examples on the form of bacterial distribution and aggregation in two types of sediments. The possibility is given to estimate lengths and widths of the aggregates both horizontally and vertically. Difficulties arise in dense colonies were signals will overlap. A further limitation in cells enumeration in dense microbial aggregates may arise from the limited depth of microscope focus and the overshadowing effect of the background signal of cells lying in out-of-focus planes. 3D maps of the aggregates with the use of a confocal laser scanning microscope (CLSM) could be a good alternative enabling additionally volume estimation (DeLeo et al. 1997). Automatic cell counting and measuring with a CLSM could be a further option according to a method described by Bloem et al. (1995) on soil smears. Non-specific background staining and debris autofluorescence could be removed through automated image processing procedures (Nunan et al. 2001). Biological structures encapsulated in the GMA matrix could be further studied by using enzymes (Rosenberg et al. 1960).

The fact that our method does not obliterate life positions of benthic organisms and their associated substrate could be helpful in studies focused on sediment structure, shape, chemical nature of grains and microbial distribution lighting up heterogeneity and microniches diversity. Interactions of microbes and minerals could be revealed by combining scanning electron microscopy (SEM) and x-ray elemental analysis (EDS) for

substrate analysis with EM on DAPI-stained sections showing position, form and number of microbes attached to a characterized surface. An additional option in analysis of sediment embedded in GMA is the use of a beta imager (Cook and Roy 2006). In general, while information is kept and stabilized in the matrix a number of methods could be successively applied in a well defined area revealing details of microniches.

Conclusions

We could successfully improve and adapt current protocols for impregnating marine / wet sediments and identify bacteria enclosed in the resin matrix. Our experiments showed that highly permeable sediments can be fixed and plastified within a day circumventing dehydration. Impermeable clays could sufficiently consolidate within few days. We could reveal the spatial distribution of DAPI-stained microbes indicating the high degree of preservation of biological material. Once the sediment plastified it can be kept undisturbed in the impregnant matrix for a very long period of time, perhaps several years maintaining biogeochemical information from a given sampling point for a long period. The fact that information is kept in the matrix and the possibility of combining methods on the microscale bears the potential to make the method a strong tool in microbial ecology studies.

Acknowledgements

The authors gratefully acknowledge the support from the European Union (contract EVK3-CT-2002-00081) and all participants of the TREAD project. We are most grateful to: Bo Barker Jørgensen, Tim Ferdelman and the Max-Planck-Society for support, Ronnie Glud and Henrik Stahl for their genius ideas optimizing sampling, Rolf Tippkötter and Thilo Eickhorst for practical help on embedding and sectioning, and Katrin Praest (fa. Struers) for her help with polishing media and protocols.

References

Amann RI, Ludwig W and Schleifer K-H (1995) Phylogenetic identification and in situ detection of individual microbial cells without cultivation. *Microb. Rev.* **59**:143-169.

Anderson FES and Jackson RM (1954) Examination of soil micro-organisms in their natural environment. *Nature* **174**: 750-751.

Bachar A, Polerecky L, Fisher J, Vamvakopoulos K, deBeer D, Jonkers M (2008) Two-dimensional mapping of photopigments distribution and activity of *Cloroflexus*-like bacteria in a hypersaline microbial mat. *FEMS Microbiology Ecology* **65**: 424-448.

Baerwald R, Burkett PJ, Bennett RH (1991) Techniques for the preparation of submarine sediments for electron microscopy. *Microstructure of finegrained sediments* (Bennett RH, Bryant WR, Hulbert MH, eds), pp. 309-331. Springer-Verlag, New York.

Bernhard JM, Visscher PT, and Bowser SS (2005) Submillimeter life positions of bacteria, protists, and metazoans in laminated sediments of the Santa Barbara Basin. *Limnol.Oceanogr.* **48** (2): 813-828.

Bloem J, Veninga M, and Shepherd J (1995) Fully automatic determination of soil bacterium numbers, cell volumes and frequencies of dividing cells by confocal laser scanning microscopy and image analysis. *Applied and Environmental Microbiology* **61** (3): 926-936.

Boës X and Fagel N (2005) Impregnation method for detecting annual laminations in sediment cores: An overview. *Sedimentary Geology* **179**: 185-194.

Bowles FA (1968) Microstructure of sediments: investigation with ultrathin sections. *Science* **159** (3820): 1236-1237.

Cook PLM and Roy H (2006) Advective relief of CO2 limitation in microphytobenthos in highly productive sandy sediments. *Limnol.Oceanogr.* **51** (**4**): 1594-1601.

Curry KJ et al. (2002) A technique for processing undisturbed marine sand sediments and reconstructing fabric and porometry. *Journal of Sedimentary Research* **72** (6): 933-937.

Davison W et al. (1991) Distribution of dissolved iron in sediment pore waters at submillimetre resolution. *Nature* **352** (6333): 323-324.

DeLeo PC, Baveye P, and Ghiorse WC (1997) Use of confocal laser scanning microscopy on soil thin-sections for improved characterization of microbial growth in unconsolidated soils and aquifer materials. *Journal of Microbiological Methods* **30**: 193-203.

Fisk AC, Murphy SL, and Tate III RL (1999) Microscopic observations of bacterial sorption in soil cores. *Biol Fertil Soils* **28**: 111-116.

Frankel L (1970) A technique for investigating microorganism associations. *Journal of Paleontology* **44** (3): 575-577.

Gall JG, Pardue ML (1969) Formation and detection of RNA-DNA hybrid molecules in cytological preparation. *Proc Natl Acad Sci* 63: 378-383.

Harper MP, Davison W, and Tych W (1999) One-dimensional views of three-dimensional sediments. *Environ.Sci.Technol.* **33**: 2611-2616.

Hoffmann F et al. (2003) Histological investigation of organisms with hard skeletons: a case study of siliceous sponges. *Biotechnic & Histochemistry* **78** (3-4): 191-199.

Jim CY (1985) Impregnation of moist and dry unconsolidated clay samples using spurr resin for microstuctural studies. *Journal of Sedimentary Petrology* **55**: 597-599.

Kubiena WL. 1938. *Micropedology.*Collegiate Press, Ames, Iowa.

Kuehl SA, Nittrouer CA, and DeMaster DJ (1998) Microfabric study of fine-grained sediments: observations from the Amazon subaqueous delta. *J.Sedim.Petrol.* **58**:12-23.

Kuwae T and Hosokawa Y (1999) Determination of abundance and biovolume of bacteria in sediments by dual staining with 4',6-diamidino-2-phenylindole and acridine orange: relationship to dispersion treatment and sediment characteristics. *Applied and Environmental Microbiology* **65** (8): 3407-3412.

Lamoureux SF (1994) Embedding unfrozen lake sediments for thin section preparation. *J.Paleolimnol.* **10**:141-146.

Larsen O et al. (2007) Transport and reactions of contaminants in sediments. *Sediment dynamics and pollutant mobility in rivers* (Westrich B, Förstner U, eds). Springer-Verlag, Berlin.

Leduc EH and Bernhard W (1967) Recent modifications of the glycol methacrylate embedding procedure. *J. Ultrastructure Research*. **19**: 196-199.

Macnaughton SJ et al. (1996) Physical stabilization and confocal microscopy of bacteria on roots using 16S rRNA targeted, fluorescent-labeled oligonucleotide probes. *Journal of Microbiological Methods* **26**: 279-285.

Manz W et al. (2000) Widefield deconvolution epifluorescence microscopy combined with fluorescence in situ hybridization reveals the spatial arrangement of bacteria in sponge tissue. *Journal of Microbiological Methods* **40**: 125-134.

Mochida K and Tsujimoto H (2001) Development of a genomic *in situ* hybridization method using Technovit 7100 sections of early wheat embryo. *Biotechnic & Histochemistry* **76** (5 & 6): 257-260.

Moter A et al. (1998) Fluorescence in situ hybridization shows spatial distribution of as yet uncultured treponemes in biopsies from digital dermatitis lesions. *Microbiology* **144**: 2459-2467.

Numan N et al. (2001) Quantification of the in situ distribution of soil bacteria by large-scale imaging of thin sections of undisturbed soil. *FEMS Microbiology Ecology* **36**: 67-77.

Porter KG and Feig YS (1980) The use of DAPI for identifying and counting aquatic microflora. *Limnol.Oceanogr.* **25** (5): 943-948.

Postma J and Altemüller H-J (1989) Bacteria in thin soil sections stained with the fluorescent brightener calcofluor whte M2R. *Soil Biology & Biochemistry* **22** (1): 89-96.

Ransom B et al. (1997) TEM study of in situ organic matter on continental margins: occurrence and the "monolayer" hypothesis. *Marine Geology* **138**: 1-9.

Rosenberg M, Bartl P, and Lesko J (1960) Water-soluble methacrylate as an embedding medium for the preparation of ultrathin sections. *J.Ultrastructure Research* **4**: 298-303.

Takechi K et al. (1999) *In situ* RNA hybridization using Technovit resin in *Arabidopsis thaliana*. *Plant Molecular Biology Reporter* **17**: 43-51.

Tippkötter R, Ritz K, and Darbyshire JF (1986) The preparation of soil thin sections for biological studies. *J.Soil Sci.* **37**: 681-690.

Tippkötter R and Ritz K (1996) Evaluation of polyester, epoxy and acrylic resins for suitability in preparation of soil thin sections for in situ biological studies. *Geoderma* **69**: 1996-31.

Watling L (1988) Small-scale features of marine sediments and their importance to the study of deposit-feeding. *Marine Ecology Progress Series* **47**: 135-144.

White D, FitzPatrick EA, and Killham K (1994) Use of stained bacterial inocula to assess spatial distribution after introduction into soil. *Geoderma* **63**: 245-254.

Part 2, Applications

Transition metal oxides and sulfides in marine sediments and their associated heavy metals

Kyriakos Vamvakopoulos[1], Niko Finke[2], Ole Larsen[3]

[1#]Max-Planck-Institute for Marine Microbiology, Celsiusstr. 1, D-28359 Bremen, Germany

[2]NordCEE - Nordic Center for Earth Evolution, Campusvej 55, 5230 Odense M, Danmark

[3]DHI-NTU Water & Environment Research Centre and Education Hub, 200 Pandan Loop #08-03, Singapore

Key words: iron oxides and sulfides, heavy metals, sediments, flume

#Corresponding author: Kyriakos Vamvakopoulos, Max-Planck-Institute for Marine Microbiology, Celsiusstr. 1, D-28359 Bremen, Germany, T: +49(0)421 2028 608, F: +49(0)421 2028 690, E-mail: kvamvako@mpi-bremen.de

Abstract

In a linear flume marine mesocosm experiment over a period of almost three years we tried to identify accumulation sites of heavy metals on transition metal oxides and sulfides in sediments and to evaluate the control exerted by the governing biogeochemical process at high spatial resolution. On Glycolmethacrylate (GMA) embedded sediments we applied scanning electron microscopy (SEM) and energy dispersive spectroscopy (EDS). Non-stoichiometric and stoichiometric pyrite (FeS_2) phases were the dominant fractions within the iron sulfide group (fraction >2µm). The Fe-sulfides contained traces of all contaminants and the copper concentrations ranged from 0.2 to 3% Cu (on an atomic basis). The copper sulfides cover a range from a few percentage of Cu substitution in pyrite over chalcopyrite ($CuFeS_2$) to almost pure chalcocite (Cu_2S). Bioturbation mix the sediment particles as indicated by the presence of oxidized aggregates found mixed into reduced sediment matrix. Combining EDS elemental mapping of substrate and bacteria staining with the DNA specific fluorescent dye 4´-6-diamidino-2-phelylindole (DAPI) the mineral-bacteria interaction in solidified sediment sections could be studied at a high level of detail. In the flume microbial attachment on minerals was very scarce, thus direct bacteria-mineral associations could only have minor influence the Fe cycle.

Introduction

Our present understanding of carbon and electron acceptor cycling in sediments is largely based on the measurement of porewater and sediment properties in large sampling volumes. Standard methods of porewater sampling and analysis require water volumes typically exceeding 10 mL (Lewis 2007). Normal fine-grained marine sediments contain in the corresponding volume of sediments in the order of 10^{10}-10^{11} microorganisms and almost the same number of particles exerting control on all biogeochemical processes (Llobet-Brossa et al. 1998). When on top of this, the difference in particle reactivity and processes are regarded it is only to expect that the sediments are more heterogeneous than recognizable with standard analytical methods.

The high heterogeneity of sediment systems is in fact well recognized and has been investigated using various high resolution technologies like microsensors (Revsbech & Jørgensen 1986), planar optodes (Glud et al. 1992; Stahl et al. 2006) and gel technologies (Davison et al. 1994). The results achieved using these high resolution methods have significantly improved our understanding of the temporal and spatial dynamics of solute structure and process rates in sediments. Microsensors have been used to study the spatial and temporary dynamics of oxygen and other solutes in the upper layers of sediments and biofilms (Kühl et Revsbech 2001) and using planary sensing systems (Glud et al. 2005) could quantify the effects of macrozoobenthos on the overall oxygen budget.

The importance of organic matter reactivity for early diagenesis has been shown by quantifying the oxygen consumption rate at highly reactive packages of organic matter incorporated sediments (Glud et al. 2005). High spatial variability of dissolved transition and heavy metals as well as sulfides has been demonstrated using diffusive gradients in thin-films (DGT) that reveal the ability of sediments to resupply the solutes (Naylor et al. 2004). These and other observations demonstrate the existence of small niches of very high reactivity that contribute to the bulk of total sediment reactions. Examples of the sediment heterogeneity that give rise to solute structures involve packages of reactive organic matter that through its decomposition gives rise to a bloom of different microorganisms around it leading to formation of microniches (Jørgensen 1977a; Fones et al. 1998). Another example could be the oxidation of a iron sulfide aggregate in the

uppermost sediment volume, brought up through bioturbation, releasing Fe^{2+} and trace elements during its oxidation.

Since the discovery of polarization of light in 1808 by the mathematician Etienne Louis Malus polarization microscopy has been the core technology to characterize crystalline materials. In fact, exploitation of most natural resources depends on our ability to investigate and interpret the structure of igneous and sedimentary rocks. Soil science significantly advanced after Kubiena's developments within soil micromorphology summarized in his classical work from 1938 (Kubiena 1938). This was based on inventions enabling the preparation of undisturbed soil samples that were resin embedded and formed into solid blocks maintaining the original orientation and structure of the soil systems. With the recent advances in analytical capability including among other electron microscopy and electron microprobing, mineral and water interactions have been studied in detail on embedded samples (Bisdom et Ducloux 1983; Hudson-Edwards et al. 2003). Embedding soils and sediments with synthetic resins however, requires the removal of water and hence dead and living organic tissues might be decomposed or loose their spatial arrangement. Recent advances in embedding technology have made it possible to embed undisturbed marine sediments preserving the structure and biological tissue allowing characterization of the spatial arrangement of natural microbial assemblages (Vamvakopoulos et Larsen in prep.).

Bacteria and mineral interactions have been intensively studied under controlled laboratory conditions in the recent past. Particularly these methods have been applied within medicine in studies of enamel corrosion (Zhang et al. 2010) and in environmental systems in studies for instance of electron transfer between microorganisms and ferric oxides (Granthama et Dove 1996). The active use of minerals as electron acceptor by bacteria has been demonstrated and diverse mechanisms including the production of (extra-) cellular enzymes and chelates acting as electron shuttles has been intensively studied (Neilands 1995; Lovley et Chapelle 1995; Lovley et al. 1996; Caccavo et Das 2002). Many factors are expected to influence the interaction between microbes and mineral substrate under natural conditions including the solid phase reactivity, surface chemistry and solution composition.

Marine sediments are the ultimate repository of contaminants and in ports, contamination with heavy metals, in particular copper, are of serious environmental concern (Larsen et al. 2007). Understanding the biogeochemical processes governing these sediments is crucial for efficient sediment management and pollution control. Transition metals play an important role as sinks for metal contaminants in marine sediments; they adsorb contaminants on their oxides and incorporate them into their sulfides (Khalid et al. 1978; Large et al. 2001; Vaughan et al. 2002 Hudson-Edwards 2003, Vaughan 2006; Lesven et al. 2010). These processes are likely also to occur in sediment microniches (and hence they are not comprehensively investigated using standard investigation techniques) (Huerta-Diaz et al. 1996). Despite the high environmental importance, fundamental questions still remain concerning the direct pathways of heavy metal interaction with transition metals. For example, the association of heavy metals with sulfides is only partially understood. It still remains an open question if the heavy metals are co-precipitated or adsorbed on Fe-sulfides, or precipitated as discrete metal sulfides (Huerta-Diaz et al. 1996). Most of the research to date has employed wet chemical extraction techniques and thermodynamic arguments, rather than direct in situ investigations to infer the speciation and distribution of heavy metals in sediments. In many cases, the precise effects of these processes on the heavy metal bearing particles are poorly understood (Hudson-Edwards 2003). As an example of the advantages of in-situ investigations, Hochella et al. (2005) showed that the major sink for Al in acid mine drainage sites was an amorphous (Si, Al) oxyhydroxide, and not the $Al(OH)_3$ predicted based on the thermodynamics.

To assess and understand the fate of heavy metals in marine sediments we constructed a €flume with contaminated sediments simulating field conditions. The flume was maintained over a period of almost three years to control flow and level of water, particulate movement and mixing, nutrients levels and macrofauna abundance. During the course of the experiment, we integrated methods to study the solute and solid structure and composition at high spatial resolution. Hereby, the aim was to identify accumulation sites of heavy metals on transition metal oxides and sulfides, to reveal mineral-bacteria interactions by mapping simultaneously substrate elements and bacteria

attached and to evaluate the control exerted by the governing biogeochemical process framework on heavy metal mobility in marine sediments.

Materials

Sediment flume

A sediment originating from a North Sea harbor basin at 11 m depth was transferred to the laboratory in undisturbed blocks. It was installed in a linear flume of 30x120 cm with unidirectional water movement of 4 cm/s. Illumination followed a 12 h day/night cycle and had a light intensity at the sediment surface of 40-50 μE m^{-2} while the room temperature was kept constant at 15 °C throughout the experiment (30 months). During the experiment water was added to maintain a salinity of $30^0/_{00}$. After an initial "baseline" period, the flume was given 3 treatments: 1) Addition of bioturbating fauna - the polychaete *Hediste diversicolor* (100 individuals) was added after 5 months; 2) 4 months after fauna addition an algal bloom was mimicked by adding a mixture of 80% Spirulina (Aldrige) and 20% macroalgae collected from a local beach corresponding to 30 g C/m^2; 3) Additional fauna (*H. diversicolor* (100) and *Arenicola marina* (50)) was added 8 months after adding organic matter. The survival rate for *H. diversicolor* was max 5 months and for *A. marina* up to 2 months.

Sediment properties

The sediment, typical for many estuarine systems, was fine-grained and contained predominantly clays and silts (77.4%). Fine and medium sands (9.1% and 13,5% respectively) made up the reminder. The total organic carbon content was 2.5-3% of dry weight depending on the sediment depth. The bulk concentrations (mg/kg dry weight) of selected heavy metals averaged over 5 y of monitoring were high: Zn 742 ± 114, Cu 558 ± 115, Pb 128 ± 10 and Cd 0.9 ± 0.49 (data were kindly provided by the local port authority).

Methods

Porewater and sediment were investigated using conventional techniques in addition to the high resolution investigations of solids using scanning electron microscopy. Three

sediment cores were taken a few cm apart in the center of the flumes, while two cores were taken at the opposite ends of the flume.

Porewater analysis

The sediment was carefully pressed out of the core liner in 1 cm slices and transferred into the porewater squeezer. The squeezer works by pressing the sediment onto a Watston GF/F filter by applying N_2 gas over a Latex Dental dam. The squeezed porewater was trapped in acid (1 M HCl) and the metals were analyzed on an ICP-MS.

HCl extractable Fe, Mn and Cu in sediment cores

The sediment was carefully pressed out of the core liner in 1 cm slices (except the upper one which was only 0.5 cm thick) and transferred to a acid washed centrifuge tube containing 20 ml anoxic 0.5 M HCl. The samples were shaken for 1 hour at room temperature and darkness before spinning down. The clear supernatant was analyzed with ICP-MS and results presented per volume of sediment.

Sulfate reduction rates

Parallel cores were incubated for sulfate reduction rate measurements. 50 kBq ^{35}S-sulfate were incubated in every depth horizon. After 6 h the incubations were stopped transferring the sediment to a 20% Zn-Acetate solution and frozen. The ^{35}S-labeled reduced sulfur fraction was extracted by the cold chromium distillation method (Kallmeyer et al. 2004) in single samples for most time points. Sulfate reduction rates were calculated as described by Jørgensen (1978).

DIC

Samples for DIC measurements were transferred into 1.5 ml glass vials and closed without headspace. The samples were stored cold and measured within 48 hours. (DIC) was measured via flow injection analysis with a conductivity detector (Hall and Aller 1992). 50 µl of sample were injected into a stream of 10 mM HCl. The CO_2 diffuses across a Teflon membrane into a stream of 10 mM NaOH. The conductivity change of the NaOH solution was measured on a VWR Scientific EC meter, Model 1054.

Ammonia

The water samples for ammonia were filtered through 0.2 µm PTFE filter (Sartorius) and frozen. Ammonia concentrations were obtained with a nutrient analyzer (Skalar SAN system).

Microscopy

Sampling & Plastifying

Sediment sampling and preparation from Flume C was performed by using metal frames of 60 x 37 x 8 mm. Samples were immediately transferred and fixed in filter-sterilized 4.5 % formaldehyde in seawater for 12 h at 4 °C. Prior to embedding with the 2-hydroxy-ethyl-methacrylate (GMA) resin the samples were dehydrated by successive 12 h immersions in aqueous ethanol (50, 70, 80, 90, 96 $^{v}/_{v}$). After dehydration the blocks were pre-embedded with 50% ethanol and 50% 2-hydroxy-ethyl-methacrylate before finally immersed in 100% 2-hydroxy-ethyl-methacrylate resin. Consolidated sediment blocks were trimmed in pieces with a surface of 1 cm^2. The surface of the pieces was polished with 1 µm sized Al_2O_3. Thin sections were prepared for epifluorescence microscopy either using a rotary HM 505E cryomicrotome (Microm) for standard specimens, or by making standard petrographic thin-section gluing the blocks to the glass slides, cutting off the blocks and polishing by hand as described in Murphy (1986).

Microscopy

Bacterial cells in the sections were stained with the DNA-specific fluorescent dye 4´-6-diamidino-2-phelylindole (DAPI) (Porter et Feig 1980) and evaluated using an Epifluorescence microscope (Zeiss Axio M1 equipped with Plan Apochromat). For image acquisition and processing two setups were used, an AxioCam MPc (Zeiss) camera with the software package AxioVision 4.3, and a CoolSnap HQ (Photometrics) camera with the software package Metamorph Imaging 6.2. The square centimetre sized impregnated sediment blocks were carbon coated prior to investigation in a Cambridge 2500 scanning electron microscope (SEM). The system was coupled to an EDAX energy dispersive spectrometer for standard free semi-quantitative chemical analysis. Only semi-

quantitative spot analyses are reported here based on analysis for 200 s at an acceleration voltage of 15 kV. Oxygen and carbon were excluded from the EDAX-spot measurements.

Results

Organic matter mineralization

The selected sediment contains fresh organic material from primary production in the estuary. The sediment becomes anoxic almost directly below the sediment-water interface due to the degradation of organic matter consuming dissolved oxygen. Due to the low permeability of the sediment, the solute exchange over the sediment – water interface is dominated by diffusion and turbating processes. The redox processes related to organic matter degradation were studied in the TREAD EU FP5 project and have been described in some detail by Tankere-Muller et al. (2007). The main terminal electron accepting processes for organic matter degradation in the sediment are iron oxide reduction and sulfate reduction. The relative importance of each process varies over short distances and also over time. The solute concentrations presented in Figure 1 are the average of 5 parallel cores. For all analysis, concentrations in the upper layers showed less variation than deeper in the sediment (data not shown). The higher homogeneity in the top layer is likely due to mixing by macrofauna especially active in the surface layers. Figure presents the water chemistry in the flume at one sampling time. The increases in Mn^{2+} and Fe^{2+} over depth are associated with an increase in TIC. This suggests ongoing reduction of iron oxides according to the reaction:

$$CH_2O + 4FeOOH + 7H_2CO_3 \rightarrow 4Fe^{2+} + 8HCO_3^- + 6H_2O \qquad \text{(Eq. 1)}$$

Organic matter is also degraded by sulfate reduction as evident from the measured sulfate reduction rates:

$$CH_2O + SO_4^{2-} \rightarrow 2HCO_3^- + H_2S \qquad \text{(Eq. 2)}$$

During the experiment, the organic matter was added to the flumes resulting in increase in sulfate reduction rates of about one order of magnitude. In the upper sediment layers where sulfate reduction may occur in vicinity of iron(III)-(hydr)oxides reoxidation of sulfide and production of Fe^{2+} is likely to occur:

$$H_2S + 2FeOOH + 4H_2CO_3 \rightarrow S^0 + 2Fe^{2+} + 4HCO_3^- \qquad \text{(Eq. 3)}$$

The degradation of organic matter is also indicated by the increase of NH_4 over depth reflecting the release of N-components from sedimentary organic matter. There is a concomitant increase in DIC and ammonia indicating that precipitation of carbonates is limited in the sediments.

Dissolved and extractable Fe, Mn and Cu

Concentrations of dissolved and extracted Fe, Mn and Cu are illustrated in Figure . Both Fe and Mn increase with depth from about 7 and 10 μM in the upper sediment to ~400 and 50 μM respectively. The dissolved ions are likely to be dominated by the species of Fe^{2+}, Mn^{2+} and Cu^{2+}. The increase in concentration of Fe and Mn is linked to reductive dissolution of the Fe(III)- and Mn(IV)-(oxy)hydrooxides. The high iron concentrations in the deeper parts of the flume act as sink for sulfide and may be responsible for the very low concentrations of free sulfide (data not shown) indicating that sulfide minerals are precipitating or reoxidized according to Eq. 4.

$$HS^- + Fe^{2+} + HCO_3^- \rightarrow FeS + H_2CO_3 \qquad \text{(Eq. 4)}$$

As illustrated in Figure 1 more Fe can be extracted at increasing depth by 0.5M HCl. This can be explained if the upper sediment layers contain iron(III) oxides that with depth are transformed into FeS and $FeCO_3$ that are more easily extractable with HCl (Heron et al. 1994). The solid phases of manganese extractable with 0.5M HCl show only minor variations over depth indicating only minor changes in Mn-mineralogy.

The dissolved Cu concentration decreases from 661 nM in the uppermost sediment to 159 nM at 6 cm depth. The Cu concentration in porewater is largely controlled by organic ligands, oxy-hydroxides that adsorb Cu and precipitation with e.g. sulfides. Usually, Cu enters into the sediment cycle bound to organic matter and is ultimately buried in Cu-sulfides. Cu is more readily extractable from the surface layers than the deeper layers of the investigated sediments. The total Cu is the same in all depths (data not shown) and the difference in Cu availability measured with HCl is due to the difference in speciation and mineralogy over depth. Likely sources for the high amounts of extractable and dissolved Cu in the surface layer include Cu associated with organic matter and Cu adsorbed to and bound in reactive iron(III)-(hydr)oxides. At increasing depth less Cu can be extracted indicating the formation of stable Cu(II) sulfides.

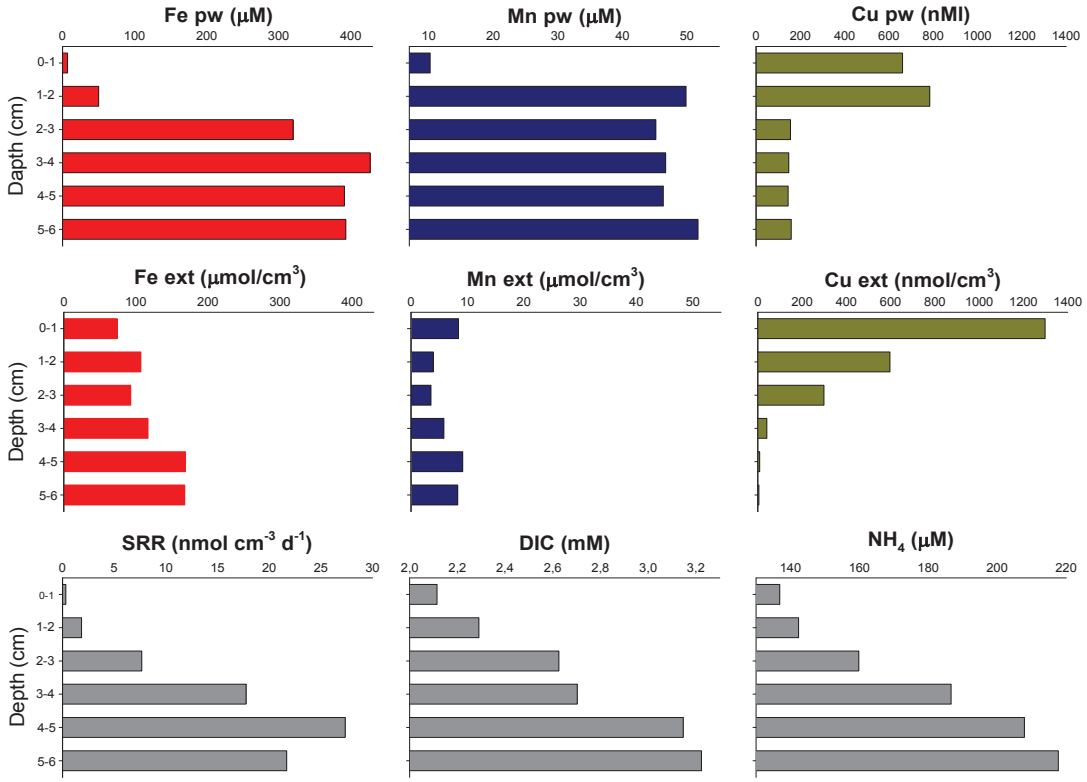

Figure 1. Porewater and extracted concentrations of Fe, Mn and Cu. Sulfate reduction rates (SRR), concentrations of dissolved inorganic carbon (DIC) and ammonia (NH_4).

To improve the understanding of Fe, Mn and Cu distribution in the sediments the Fe, Mn and Cu containing particles were sought characterized in microscope.

Microscopy

Spot analyses of Cu and Fe bearing minerals

Undisturbed sediment samples were prepared at the sampling campaigns during the flume experiment. The sediment blocks were investigated with SEM using both secondary and backscatter electron images. In the impregnated samples, the backscatter electron intensity depends largely on the atomic mass of the elements. Oxides and sulfides of iron and copper under study in this work appeared bright and clear in the microscope. After three of the sampling campaigns the specimens were observed in a 5 mm broad band throughout the max depth of 6 cm (from sediment surface and downward) quantifying the

minerals in different categories. Sediments from all campaigns were investigated to detect and analyze heavy metal particles and aggregates larger than the SEM electron beam resolution of ca.1-2 µm. The chemical composition of the aggregates and individual particles were characterized using semi-quantitative EDS total more than 700 spot analyses in the course of the experiment. Based on the elemental ratio after EDS-spot analysis, examined minerals were grouped into Fe-sulfides, Cu-sulfides, and Fe-aggregates. In total 204 spot analyses of sulfide minerals were conducted of which, based on atomic weight ratios, 153 were iron sulfides (pyrite and greigite) with impurities of heavy metals (less than 8% on atomic basis). The remaining 51 sulfide aggregates and particles were copper sulfides including pure chalcopyrite ($CuFeS_2$), chalcocite (Cu_2S) and covellite (CuS) as well as intermediate phases. Additionally, 63 large aggregates of iron(III)-(hydr)oxides ($FeO(OH)\ nH_2O$) were found and investigated.

Iron sulfides

Typical SEM micrographs of Fe-sulfides found in the sediments are displayed in Figure 2. In the investigated sediments Fe-sulfides exhibit morphologies varying from microcrystalline aggregates FeS (Figure 5), to framboidal aggregates of greigite Fe_3S_4 (Figure 2) and to larger individual crystals of pyrite FeS_2 (Figure 2). Despite our extensive investigation distinct grains of FeS exceeding the 1 µm resolution limit could not be observed. The Fe:S continuum from ca. 0.8 to ca. 0.35 (Figure 7) shows that ideal mineral formulas are rather rare, while the compositional range between greigite and pyrite is in good agreement with published observations (Wilkin & Barnes 1997).

An interesting aspect of greigite formation is the patchy occurrence of a few framboids in mutual contact. The elemental composition of these clusters point clearly towards greigite (Figure 2). The individual grains in those clusters are characterized by the same Fe:S ratio. Magnetic attraction as a property of aggregation of greigite spheres has already been reported (Wilkin & Barnes 1997; Large et al. 2001) and perhaps this process is responsible for the spatial distribution of greigite observed. Different metal ions are seen to substitute for Fe and are incorporated in the sulfides as revealed by the elemental map (Figure 2 A2).

According to the Fe:S ratios, pyrite was present in every sample studied. It was found in all depths in the sediment (Figure 8) and exhibited a wide range of morphologies. Changing the composition from greigite to pyrite leads to a loss of structural cations (Rimstidt & Vaughan 2003). Even subtle differences in stoichiometry influence electrical properties and may in turn significantly affect reactivity (Rimstidt & Vaughan 2003). Equally, this recrystallization leads to a loss of included ions and loss of mineral reactivity (Jean & Bancroft 1986).

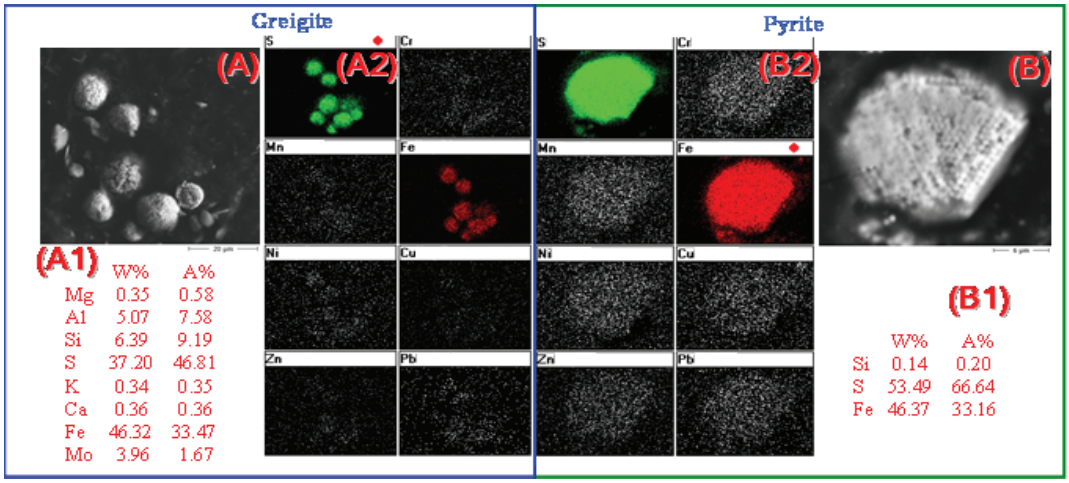

Figure 2. Typical SEM micrographs of Fe-sulfides (A & B). EDS spot reveals that the cluster of many individual framboids tightly packed next to each other is greigite (A1, Fe/S=0.72) in contrast to the individual crystal of pyrite (B1, Fe/S=0.5). EDS maps over the exposed mineral surface shows traces (<1%) of Cr, Mn, Ni, Cu, Zn and Pb in both minerals (A2 & B2).

Cu Sulfides

According to elemental analysis following EDS spot measurements about one quarter of all investigated sulfide particles contained more than 5% of copper. Based on elemental ratio the identified copper sulfides included pure chalcopyrite ($CuFeS_2$), chalcocite (Cu_2S) and covellite (CuS) as well as intermediate phases. Traces of other heavy metals were present as see from the compositional maps of every copper sulfide under study.

The minerals presented in Figure 3 (A2 & B2) contained trace amounts of Cr, Mn and Zn that were evenly distributed across the mineral. The results of spot analyses (Figure 3 A1 & B1) did not confirm the presence of Cr, Mn and Zn since each of these elements made up less than 1 % of the total atomic weight and was not included in the calculations.

Most of the copper containing sulfides grains were in a range of a few micrometers up to few tens of micrometers in diameter as the minerals presented in Figure 3 (A & B). Due to the small particle size, the backscatter electrons did not provide sufficient resolution to describe individual crystals. At the scale of resolution some copper sulfides appeared amorphous while other resembled aggregates or flocs (Figure 3 A1) and yet other displayed a framboidal structure (Figure 3 B1).

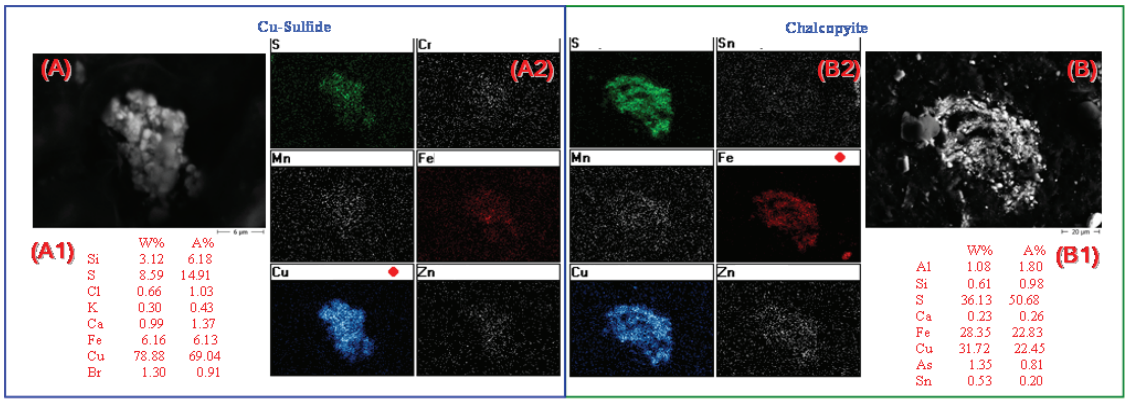

Figure 3. SEM micrographs of Cu containing phases (A & B). EDS spot reveals a floccular copper dominated mineral (A1, Cu/S=4.6) and a chalcopyrite (B1). EDS maps over the exposed mineral surface shows traces (<1%) of Cr, Mn and Zn in the copper sulfide (A2) and of Mn and Zn in the chalcopyrite (B2).

Siderite

The bright particles/aggregates observed at low resolution turned out to mainly contain iron and light elements (O, C), that cannot be quantified, in addition to traces of heavy metals. An example of one of these particles is presented in Figure 4. The aggregates consisted of small crystals about 1 µm across. Iron is omnipresent in the sediments entering the sedimentary cycle predominantly as iron(III)-(hydr)oxides that may be reduced to form secondary Fe(II) minerals in the sediments. Sedimentary iron(III)-(hydr)oxides are usually found dispersed in the sediments as small crystals (10-500 nm) often attached to surfaces of other mineral grains or associated with organic matter (Cornell & Schwertmann 1996). The morphology of images presented by Pye (1984) supported by the compositional analysis suggests that the particles in our study are siderite rather than oxides.

Some of the siderites display a rip like structure with rips organized parallel to each other. The rips are approximately 50-70 µm wide and 1 mm long (Figure 6). The semi-quantitative EDS-spot measurement revealed an iron content of 98.6 % with traces of Mn, Si and Ca. EDS-elemental mapping showed a homogeneous distribution of incorporated trace metals. Around the rim of some investigated siderites, dense bacterial colonies were found. The colony presented in Figure 6 was ~50 µm in length and 30 µm in width. The colonization of siderite was quantified to extend about 2.5 % of the total circumference. No change in aggregate composition could be measured with EDS. Apart from the biofilm growing at the sediment-water interface colonies associated with siderite appeared to represent a major pool of sediment bacteria beneath the 3 mm top of sediments zone. The siderite aggregates had all sharp edges that appear unaltered by microbial growth.

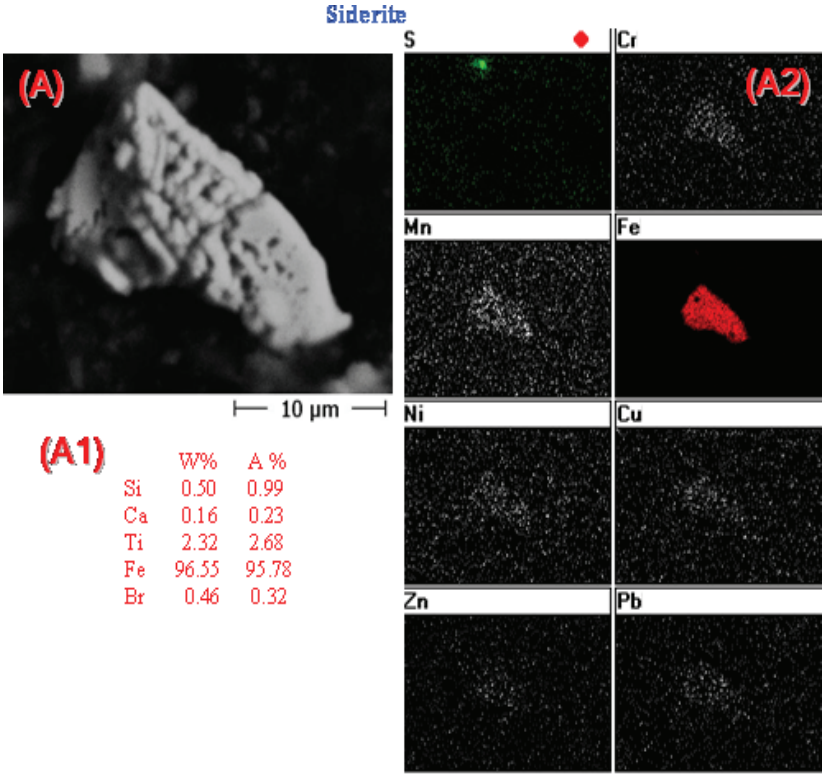

Figure 4. SEM micrographs of a siderite (A). EDS spot reveals a iron dominated mineral (A1). EDS maps over the exposed mineral surface shows traces (<1%) of Cr, Mn, Ni, Cu and Pb (A2).

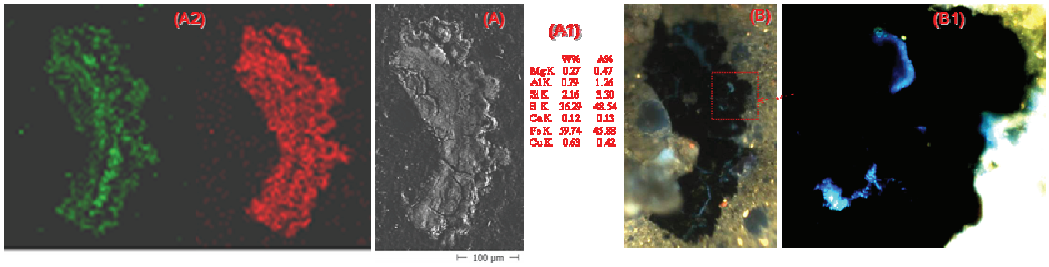

Figure 5. Secondary electron micrograph of an iron sulfide mineral (A). EDS spot measurement reveals an iron mono sulfide (A1, Fe/S ≈1). EDS maps over the exposed mineral surface shows heterogeneous distribution of iron (red) and sulfur (green) (A2). The bright blue spots in B & B1 images are signals of bacteria stained with DAPI under UV light.

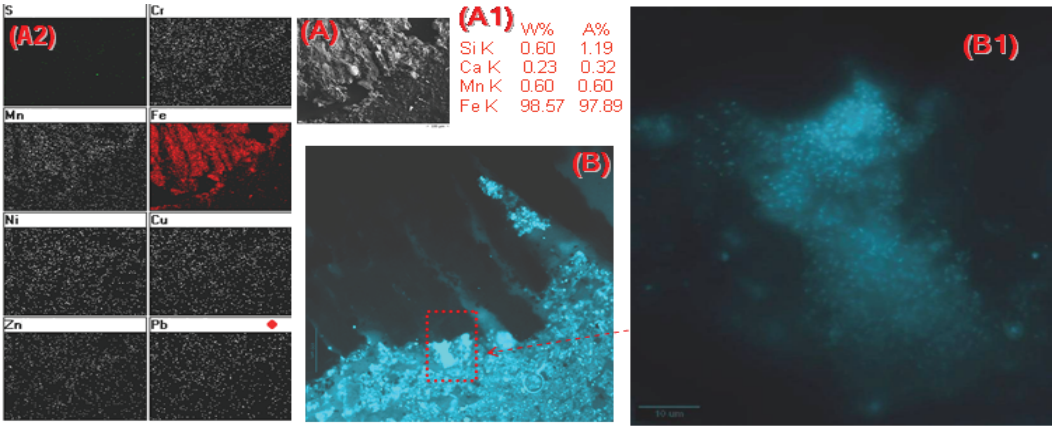

Figure 6. Secondary electron micrograph of an iron mineral (A). EDS spot measurement reveals that 98.6% of total weight is iron (A1). EDS maps over the exposed mineral surface shows only traces of Mn and Zn (A2). The bright blue spots in B & B1 images are signals of bacteria stained with DAPI under UV light.

Iron monosulfides

At all campaigns large iron sulfide aggregates were found. An example of such an iron-sulfide aggregate is displayed in the composite Figure 5. EDS spot measurements showed them to be dominated by Fe-mono-Sulfides (Figure 5 A1; Fe:S≈1). Only copper in less than 1% of total weight was found to be substituted into the minerals. Similar associations between Cu and iron sulfides have already been reported (Davison et al. 1992).

In the presented aggregate two discrete fronts could be revealed (Figure 5 A). The right hand side of the aggregate is more irregular than the left hand side showing a sharp peripheral line with semicircles rimed by cells. At high resolutions, the circular structures display a fan-like morphology. EDS-mapping over the fan-like structures showed that these areas contained less sulfur compared to the more bulky part of the aggregate (Figure 5 A2). We interpret this as Fe-mono-sulfides under transformation to pyrite. The highest S concentrations are found along the porous structures that was shown to be associated with microorganisms that appeared directly attached to the FeS mineral surface (Figure 5 B & B1).

Discussion

Compositional changes over time

To understand the dynamics of the Fe-S system we used quantitative EDS to analyze single iron sulfide minerals ranging up to 20 μm across, up to a max sediment depth of 6 cm within a 2 years period. Only grains exceeding the resolution of the electron beam being of 1-2 microns were considered. The Fe:S atomic ratio was used to categorize the examined specimens. Of the examined iron sulfides 13% have a Fe:S ratio between 0.8-0.6 and 76% between 0.6-0.4, these ratios are characteristic for greigite (Fe_3S_4, Fe:S=0.75) and pyrite (FeS_2, Fe:S=0.5). It is not clear to what extend the high Fe:S ratios could be attributable to pyrrhotite/troilite types of minerals, but based on the particle size and morphology greigite is assumed to prevail among the particles with high Fe:S ratios. Particles was found with Fe:S ratios indicating continuous transition from greigite to pyrite though the end-phases pyrite and greigite were most frequently found. It is unclear if this continuous variation represents a “solid solution series” or a continuous mixing of end-phase minerals.

Over the two years the flumes were maintained, only fauna addition appeared to increase the Fe:S ratio of the sedimentary sulfides (Figure 7). Burrowing macrofauna mix reduced microniches into the oxidized zone or vice versa and pump respiratory water down into the sediment affecting considerably the redox conditions (Jørgensen 1977b; Davis 1993). Emery and Rittendberg (1952) explained the occurrence of pyrite in oxidizing sediments off Southern California by the occurrence of reduced microniches existing in oxidized

upper sediment layers. The investigated sediment was highly heterogeneous as evident from solute structure reported in Tankere-Müller et al (2007). The solid sulphides were clearly affected by addition of fauna that increased the Fe:S ratio which suggests oxidation of pyrite and formation of fresh FeS concomittantly. Changes in the Fe:S ratio over depth indicate the greigite formation zone exists between the first and the third cm (Figure 8). However, it is important to remember that the variation of environmental conditions mimicked in the flume was smaller than similar sediment would experience when natural conditions influence the dynamics of the sediment.

Trace elements

It is commonly found that oxides and sulfides act as scavengers for trace metals (Khalid et al. 1978; Ferris et al. 1987; Kornicker & Morse 1991; Morse & Arakaki 1993; Morse 1993; Hochella Jr et al. 2005). Applying EDS-elemental mapping we were able to quantify traces of different heavy metals and observed them to be homogeneously distributed over the mineral bulk. The investigated pyrites contained different trace metals as frequently found (Abraitis et al. 2004, Huerta-Diaz et al. 1992). The trace metal concentrations in the investigated sulfides changed during the experiment. As an example, it was found that initially 6.8% of all investigated sulfide minerals contained Cu and this number increased to 58.1% after 1.5 years (Figure 9). Changes in concentration of sediment sulfide could not be detected during the course of the experiment during which no Cu was added. This indicates that around 50% of the sediment sulfides were turned over during 1.5 year. Other heavy metals (Zn and Pb) were also found to accrete in the sulphides while the concentration of elements as Mn, Cr and Ni in the solid sulphides increased initially then decreased during the experiment. Tankere-Muller et al. (2007) report the solute composition and confirmed the presence of the transition metals Cr and Ni that only are included as traces in the sulphides. These results clearly support the idea that particularly Cu is ultimately buried as a sulfide in marine sediments. In practical terms, this indicates that reoxidation of contaminated sediments must be controlled and such process must be considered in sediment management.

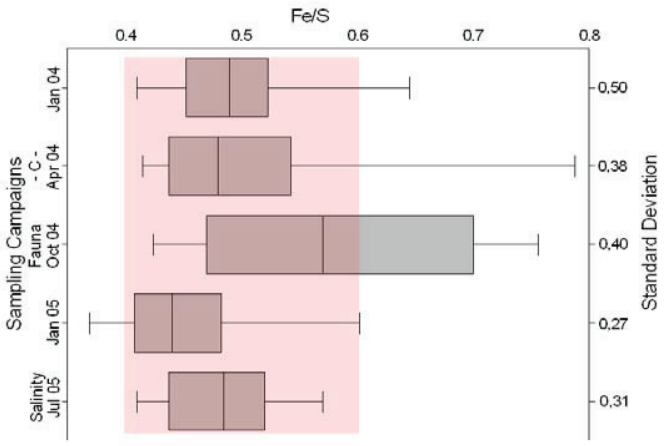

Figure 7. Fe/S ratio over time. Mesocosm was objected to three main treatments: April 04 addition of organic matter at 30 g C/m^2, October 04 addition of the polychaetes *H. diversicolor* and *Arenicola marina* (50-80 individuals), and July 05 exchange of seawater with brackish water. The boundary of the box closest to zero indicates the 25th percentile, the line within the box marks the median, and the boundary of the box farthest from zero indicates the 75th percentile. Whiskers (error bars) above and below the box indicate the 90th and 10th percentiles. With pink is the ratio highlighted indicating pyrite.

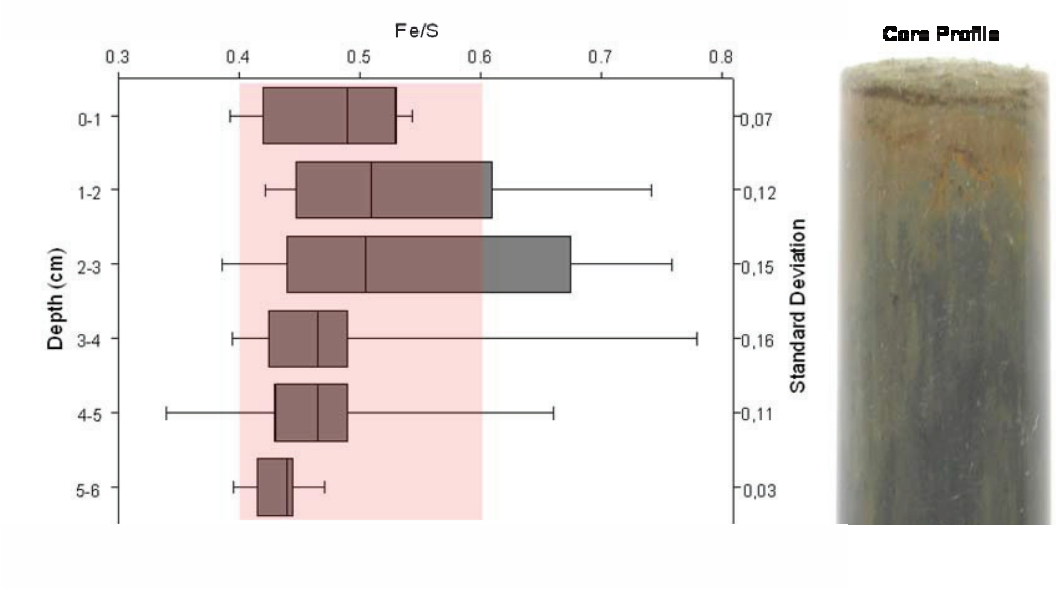

Figure 8. Fe/S over depth. The Fe/S ratio shows that most of the Fe-S minerals lie in the compositional range between greigite and pyrite. The boundary of the box closest to zero indicates the 25th percentile, the line within the box marks the median, and the boundary of the box farthest from zero indicates the 75th percentile. Whiskers (error bars) above and below the box indicate the 90th and 10th percentiles. With pink is the ratio highlighted indicating pyrite.

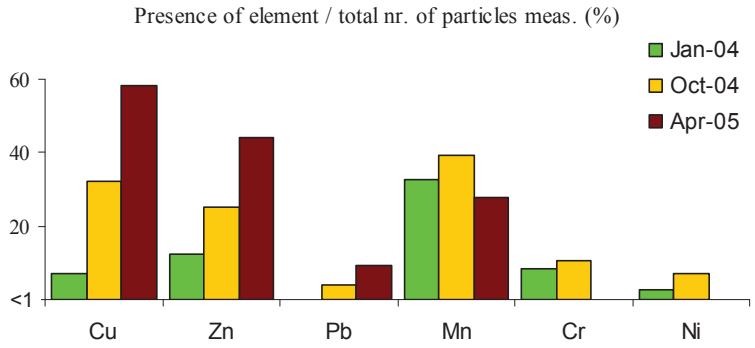

Figure 9. Frequency of Cu, Zn, Pb, Mn, Cr and Ni presence in EDS spot measurements of sulfides (total number).

Bacterial distribution

Novel methodology (Vamvakopoulos et Larsen in prep.) based on DAPI staining showed that bacteria were not homogenously distributed in the sediments. The bacteria were found in microniches except in a few millimeters at the top of the sediment where they were more homogenous. The abundances in the upper mm are very high and bacteria are ubiquitous (Figure 10 left). Nearly all observed bacterial colonies occur in dense almost spherical colonies without any minerals in their vicinity (Figure 10 right).

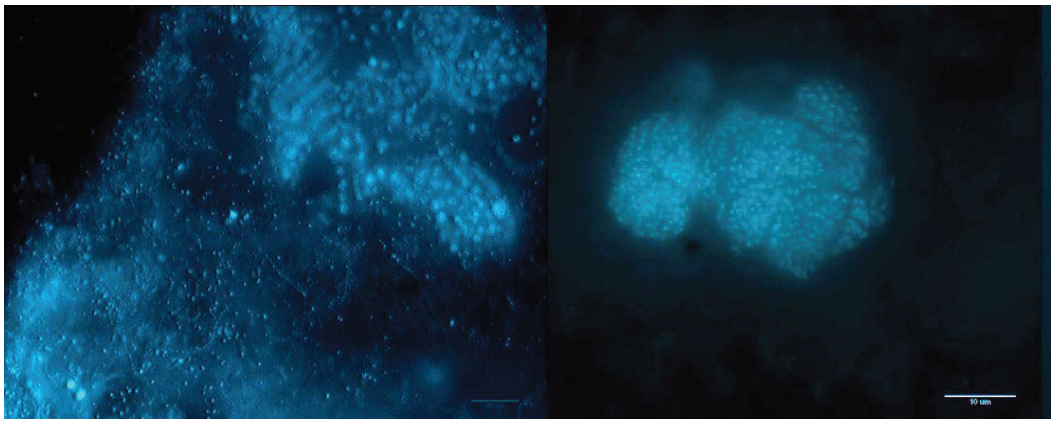

Figure 10. Bacterial distribution, DAPI staining / epifluorescence microscopy. At the water-sediment interface (left) the bacteria are present in extreme high numbers (scale bar 20 µm). Further deeper (right) they mainly occur in discrete colonies (scale bar 10 µm).

Examination of microorganism density using DAPI counting and Figure 5 illustrated that Fe-bearing minerals interpreted as siderite were associated with dense bacterial colonies. Similar high cell counts were not found in the vicinity of sulfides. The high densities

around siderite suggest that siderite is formed at locations where organic matter mineralization rates are high and Fe^{2+} is available in high concentrations, as exemplified in Eq. 1. We assume that the siderite formation is controlled by local high concentrations of CO_3^{2-} originating from the mineralization of organic matter rather than Fe^{2+} that is found across the entire sediment. The small crystallites in the siderite particles come in contrast with the size of the overall mineral grains often exceeding 1 mm in size (Figure 6 A). This suggest that CO_3^{2-} and Fe^{2+} diffusing towards the mineral extend over a significant time to support mineral growth.

Microbes attached on iron sulfide seem to be distributed in low abundance throughout the mineral matrix. In connection with the previous described oxide this would also mean that microbial Fe(III) reduction dominates over the microbial catalyzed redox processes. Space limitation and perhaps lack of organic supply are possible demonstrated at the low cell numbers. To sustain the channels the growth rate of the mineral should be the same or slower than the dissolution rate via bacterial activity.

The fact that niches in bacterial population could be identified in the sediment suggests that at least some of the microniches frequently observed with other methodologies (2D optrodes, DET/DGT) translates directly into microbial activity and is not only related to chemical processes. Growth of large siderite grains suggests that fresh organic matter is rapidly oxidized to supersaturate the interstitial waters with siderite. In our experiment changes in organic matter availability that affected the overall turnover rates by about one order of magnitude did not change the mineralogy or presence of microorganisms in any conclusive way. Since the overall fluxes in sediment increased as a result of organic matter addition, this indicates that microniches could have increased their turn-over rate substantially or more likely that the organic matter was predominantly oxidized in the upper sediment layers. Wave action and other physical forces would in natural sediments have affected the mixing and act to increase the heterogeneity of the sediment system. Thus, it is possible that mixing during a bloom event as mimicked by addition of organic matter only affect the sulfide mineral formation if external physical forces act to mix the sediment more rigorously than macrofauna is able to.

Acknowledgements

The following are acknowledged for their advice and help: William Davison, Monika Nellessen, Jacqueline Schmidt, Annie Glud and Ronnie Glud. This work was funded by the project TREAD contract EVK3-CT-2002-00081.

References

Abraitis P. K., Pattrick R. A. D., and Vaughan D. J. (2004) Variations in the compositional, textural and electrical properties of natural pyrite: a review. *Int. J. Miner. Process.* **74**, 41-59.

Bisdom E. B. A. and Ducloux J. (1983) *Submicroscopic studies of soils*. Elsevier.

BLMP (2002) Meeresumwelt 1997-1998. *Bundesamt für Seeschifffahrt und Hydrographie (BSH), Hamburg und Rostock* .

Brady K. S. et al. (1986) Influence of sulfate on Fe-oxide formation: comparisons with a stream receiving acid mine dranage. *Clays and Clay Minerals* **34**, 266-274.

Brown J. E. Jr. et al. (1999) Metal oxide surfaces and their interactions with aqueous solutions and microbial organisms. *Chem. Rev.* **99**, 77-174.

Butler I. B. and Rickard D. (2000) Framboidal pyrite formation via the oxidation or iron (II) monosulfide by hydrogen sulphide. *Geochimica et Cosmohimica Acta* **64**, 2665-2672.

Caccavo F. Jr. and Das A. (2002) Adhesion of dissimilatory Fe(III)-reducing bacteria to Fe(III) minerals. *Geomicrobiology Journal* **19**, 161-177.

Canfield D. S. (1989) Reactive iron in marine sediments. *Geochimica et Cosmohimica Acta* **53**, 619-632.

Canfield D. S., Raiswell R., and Bottrell S. (1992) The reactivity of sedimentary iron minerals toward sulfide. *American Journal of Science* **292**, 659-683.

Cappellen v. P. and Wang Y. (1996) Cycling of iron and manganese in surface sediments: a general theory for the coupled transport and reaction of carbon, oxygen,

nitrogen, sulfur, iron, and manganese. *American Journal of Science* **296**, 197-243.

Cornwell J. C. and Morse J. W. (1987) The characterization of iron sulfide minerals in anoxic marine sediments. *Marine Chemistry* **22**, 193-206.

Craig J. R., Vokes F. M., and Solberg T. N. (1998) Pyrite: physical and chemical textures. *Mineralium Deposita* **34**, 82-101.

Davis W. R. (1993) The role of bioturbation in sediment resuspension and its interaction with physical shearing. *J. Exp. Mar. Biol. Ecol.* **171**, 187-200.

Davison W., Fones G. R., and Grime G. W. (1997) Dissolved metals in surface sediment and a microbial mat at 100-μm resolution. *Nature* **387**, 885-888.

Davison W., Grime G. W., and Woof C. (1992) Characterization of lacustrine iron sulfide particles with proton-induced X-ray emission. Limnol.Oceanogr. **37** (8):1770-1777.

Davison W., Zhang H., and Grime G. W. (1994) Performance characteristics of gel probes used for measuring the chemistry of pore waters. *Environ. Sci. Technol.* **28**, 1623-1632.

DeVries C. R. and Wang F. (2003) In situ two-dimensional highresolution profiling of sulfide in sediment interstitial waters. *Environ. Sci. Technol.* **37**, 792-797.

Emerson D. and Ghiorse W. C. (1992) Isolation, cultural maintenance, and taxonomy of a sheath forming strain of *Lephothrix discophora* and characterization of manganese-oxidizing activity associated with the sheath. *Applied and Environmental Microbiology* **58**, 4001-4010.

Emery K. O. and Rittenberg S. C. (1952) Early diagenesis of California Basin sediments in relation to origin of oil. *AAPG Bulletin* **36**, 735-806.

Ferdelman T. G. et al. (1997) Sulfate reduction and methanogenesis in a Thioploca-dominated sediment off the coast of Chile. *Cosmochim. Acta* **61**, 3065-3079.

Ferris F. G., Fyfe W. S., and Beveridge T. J. (1987) Bacteria as nucleation sites for authigenic minerals in a metal-contaminated lake sediment. *Chemical Geology* **63** , 225-232.

Fones G. R., Davison W., and Grime G. W. (1998) Development of constrained DET for measurements of dissolved iron in surface sediments at sub-mm resolution. *The Science of the Total Environment* **221**, 127-137.

Fones G. R. et al. (2001) High-resolution metal gradients measured by in situ DGT/DET deployment in Black Sea sediments using an autonomous benthic lander. *Limnol. Oceanogr.* **46**, 982-988.

Giblin A. E., Luther G. W., and Valiela I. (1986) Trace metal solubility in salt marsh sediments contaminated with sewage sludge. *Estuarine, Coastal and Shelf Science* **23**, 477-498.

Glud R. N., Ramsing N. B., and Revsbech N. P. (1992) Photosynthesis and photosynthesis-coupled respiration in natural biofilms quantified with oxygen microsensors. *J. Phycol.* **28**, 51-60.

Glud R. N. et al. (1996) Planar optrodes: a new tool for fine scale measurements of two-dimensional O_2 distribution in benthic communities. *Marine Ecology Progress Series* **140**, 217-226.

Glud R. N. et al. (2001) An in situ instrument for planar O_2 optode measurements at benthic interfaces. *Limnol. Oceanogr.* **46**, 2073-2080.

Glud R. N. et al. (2005) Distribution of oxygen in surface sediments from central Sagami Bay, Japan: In situ measurements by microelectrodes and planar optodes. *Deep-Sea Research* **Part I 52**, 1974-1987.

Glud R. N. et al. (2009) In situ microscale variation in distribution and consumption of O2: A case study from a deep ocean margin sediment (Sagami Bay, Japan). *Limnol. Oceanogr.* **54**, 1-12.

Granthama M. C. and Dove P. M. (1996) Investigation of bacterial-mineral interactions using Fluid Tapping Mod Atomic Force Microscopy. *Geochimica et Cosmohimica Acta* **60**, 2473-2480.

Hall P. O. J. and Aller R. C. (1992) Rapid, small-volume, flow injection analysis for ΣCO_2, and $NH4^+$ in marine and freshwaters. *Limnol. Oceanogr.* **37**, 1113-1119.

Heron G. et al. (1994) Speciation of Fe(II) and Fe(III) in contaminated aquifer sediments using chemical extraction techniques. *Environ. Sci. Technol.* **28**, 1698-1705.

Hochella M. F. Jr. et al. (2005) Direct observation of heavy metal-mineral asociation from the Clark Fork River Superfund Complex: Implications for metal transport and bioavailability. *Geochimica et Cosmohimica Acta* **69**, 1651-1663.

Hudson-Edwards K. A. (2003) Sources, mineralogy, chemistry and fate of heavy metal-bearing particles in minng-affected river systems. *Mineralogical Magazine* **67**, 205-217.

Hudson-Edwards K. A. and Edwards S. J. (2005) Mineralogical controls on storage of As, Cu, Pb and Zn at the abandoned Mathiatis massive sulphide mine, Cyprus. *Mineralogical Magazine* **69**, 695-706.

Huerta-Diaz M. A. and Morse J. W. (1992) Pyritization of trace metals in anoxic marine sediments. *Geochimica et Cosmohimica Acta* **56**, 2681-2702.

Huerta-Diaz M. A., Tessier A., and Carignan R. (1996) Geochemistry of trace metals associated with reduced sulfur in freshwater sediments. *Applied Geochemistry* **13**, 213-233.

J¢rgensen B. B. (1977a) Bacterial Sulfate Reduction within Reduced Microniches of Oxidized Marine Sediments. *Marine Biol.* **41**, 7-17.

J¢rgensen B. B. (1977b) The sulfur cycle of a coastal marine sediment (Limfjorden, Denmark). *Limnol. Oceanogr.* **22**, 814-832.

J¢rgensen B. B. (1978) A comparison of methods for the quantification of bacterial sulfate reduction in coastal marine sediments 1. Measurement with radiotracer techniques. *Geomicrobiology Journal* **1**, 11-27.

J¢rgensen B. B. (1982) Mineralization of organic matter in the seabed - the role of sulphate reduction. *Nature* **296**, 643-645.

Jean G. E. and Bancroft G. M. (1986) Heavy metal adsorption of aqueous heavy metals on inorganic minerals. *Geochimica et Cosmohimica Acta* **50**, 1433-1444.

Jeroschewski P., Steukart C., and Kuhl M. (1996) An amperometric microsensor for the determination of H_2S in aquatic environments. *Anal. Chem.* **68**, 4351-4357.

Kallmeyer J. et al. (2004) A cold chromium distillation procedure for radiolabeled sulfide applied to sulfate reduction measurements. *Limnol. Oceanogr.* **Methods 2**, 171-180.

Khalid R. A., Patrick W. H. Jr., and Gambrels R. P. (1978) Effect of dissolved oxygen on chemical transformations of heavy metals, phosphorus, and nitrogen in an estuarine sediment. *Estuarine and CoastaL Marine Science* **6**, 21-35.

Kornicker W. A. and Morse J. W. (1991) Interactions of divalent cations with the surface of pyrite. *Geochimica et Cosmohimica Acta* **55**, 2159-2171.

Kraemer S. M., Butler A., and Borer P. (2005) Siderophores and the dissolution of iron-bearing minerals in marine systems. *Reviews in Mineralogy & Geochemistry* **59**, 53-84.

Kristensen E. and Kostka J. E. (2005) In *Interactions between Macro- and Microorganisms in Marine Sediments* (ed. E. Kristensen, J. E. Kostka, and R. Haese). Chap. 7, American Geophysical Union.

Kubiena W. L. (1938) *Micropedology*. Collegiate Press, Ames, Iowa.

Kuhl M. et al. (1998) H_2S microsensor for profiling biofilms and sediments: application in an acidic lake sediment. *Aquatic Microbial Ecology* **15**, 201-209.

Kuhl M. and Revsbech N. P. (2011) In *The benthic boundary layer* (ed. B. P. Boudreau and B. B. J¢rgensen). pp. 180-210. T. Oxford Univ. Press.

Large D. J. et al. (2001) Petrographic observations of iron, copper, and zinc sulfides in freshwater canal sediment. *Journal of Sedimentary Research* **71**, 61-69.

Larsen O., Postma D., and Jakobsen R. (2006) The reactivity of iron oxides towards reductive dissolution with ascorbic acid in a shallow sandy aquifer (Rømø, Denmark). *Geochimica et Cosmohimica Acta* **70**, 4827-4835.

Larsen O. et al. (2007) In *Sediment dynamics and pollutant mobility in rivers* (ed. B. Westrich and U. Förstner). Chap. 8, pp. 306-316. Springer.

Lesven L. et al. (2010) On metal diagenesis in contaminated sediments of the Deule river (northern France). *Applied Geochemistry* **25**, 1361-1373.

Lewis B. (2007) Operating procedure: Porewater sampling. *U. S. Environmental Protection Agency* 1-16.

Liger E., Charlet L., and Cappellen v. P. (1999) Surface catalysis of uranium(VI) reduction by iron(II). *Geochimica et Cosmohimica Acta* **63**, 2939-2955.

Llobet-Brossa E., Rosselló-Mora R., and Amann R. I. (1998) Microbial community composition of Wadden Sea sediments as revealed by fluorescence in situ hybridization. *Appl. Environ. Microbiol.* **64**, 2691-2696.

Lovley D. R. and Chapelle F. H. (1995) Deep subsurface microbial processes. *Reviews of Geophysics* **33**, 365-381.

Lovley D. R. et al. (1996) Humic substances as electron acceptors for microbial respiration. *Nature* **382**, 445-448.

Morse J. W. and Cornwell J. C. (1987) Analysis and distribution of iron sulfide minerals in recent anoxic marine sediments. *Marine Chemistry* **22**, 55-69.

Morse J. W. and Arakaki T. (1993) Adsorption and coprecipitation of divalent metals with mackinawite (FeS). *Geochimica et Cosmohimica Acta* **57**, 3635-3640.

Morse J. W. (1993) Interactions of trace metals with authigenic sulfide minerals: implications for their bioavailability. *Marine Chemistry* **46**, 1-6.

Murphy C. P. (1986) *Thin section preparation of soils and sediments*. A B Academic Publishers.

Naylor C. et al. (2004) Simultaneous release of sulphide with Fe,Mn, Ni and Zn in marine harbour sediment measured using a combined metal/sulphide DGT probe. *Sci. Total Environ.* **328**, 275-286.

Nealson K. H. and Saffarini D. (1994) Iron and manganese in anaerobic respiration: environmental significance, physiology, and regulation. *Ann. Rev. Microbiol.* **48**, 311-343.

Neilands J. B. (1995) Siderophores: structure and function of microbial iron transport compounds. *The journal of biological chemistry* **270**, 26723-26726.

Nowell A. R. M. and Jumars P. A. (1987) Flumes: theoretical and experimental considerations for simulation of benthic environments. *Oceanogr. Mar. Biol. Ann. Rev.* **25**, 91-112.

Oxford Instruments NanoAnalysis (2006) An introduction to energy-dispersive and wavelength-dispersive x-ray microanalysis. *Microscopy and Analysis X-Ray Supplement (Euro)* **102**, S5-S8.

Parkman R. H. et al. (1999) Reactions of copper and cadmium ions in aqueous solution with goethite, lepidocrocite, mackinawite, and pyrite. *American Mineralogist* **84** , 407-419.

Porter K. G. and Feig Y. S. (1980) The use of DAPI for identifying and counting aquatic microflora. *Limnol. Oceanogr.* **25**, 943-948.

Pye K. (1984) SEM analysis of siderite cements of intertidal marsh sediments, Norfolk, England. *Marine Geology* **56**, 1-12.

Revsbech N. P. and Jørgensen B. B. (1986) Microelectrodes: their use in microbial ecology. *Advances in Microbial Ecology* **9**, 293-352.

Rimstidt J. D. and Vaughan D. J. (2003) Pyrite oxidation: A state-of-the-art assessment of the reaction mechanism. *Geochimica et Cosmohimica Acta* **67**, 873-880.

Shaw T., Gieskes J., and Jahnke R. (1990) Early diagenesis in different depositional environments: The response of transition metals in pore water. *Geochimica et Cosmohimica Acta* **54**, 1233-1246.

Stahl H. et al. (2006) Time-resolved pH imaging in marine sediments with a luminescent planar optode. *Limnol. Oceanogr. : Methods* **4**, 336-345.

Stockdale A., Davison W., and Zhang H. (2009) Micro-scale biogeochemical heterogeneity in sediments: A review of available technology and observed evidence. *Earth-Science Reviews* **92**, 81-97.

Tankere-Muller S. et al. (2007) Fine scale remobilisation of Fe, Mn, Co, Ni, Cu and Cd in contaminated marine sediment. *Marine Chemistry* **106**, 192-207.

Vaughan D. J., Pattrick R. A. D., and Wogelius R. A. (2002) Minerals, metals and molecules: ore and envrironmental mineralogy in the new millennium. *Mineralogical Magazine* **66**, 653-676.

Vaughan D. J. (2006) Sulfide mineralogy and geochemistry: introduction and overview. *Reviews in Mineralogy & Geochemistry* **61**, 1-5.

Warnken K. W., Zhang H., and Davison W. (2014) Performance characteristics of suspended particulate reagent-iminodiacetate as a binding agent for diffusive gradients in thin films. *Anal. Chim. Acta* **508**, 41-51.

Webster J. G., Swedlund P. J., and Webster K. S. (1998) Trace metal adsorption onto an acid mine drainage iron(III) oxy hydroxy sulfate. *Environmental Science & Technology* **32**, 1361-1368.

Wilkin R. T. and Barnes H. L. (1997) Formation processes of framboidal pyrite. *Geochimica et Cosmohimica Acta* **61**, 323-339.

Zhang H. and Davison W. (1995) Performance characteristics of diffussion gradients in thin films for the in situ measurment of trace metals in aqueous solution. *Anal. Chem.* **67**, 3391-3400.

Zhang X. et al. (2010) Monitoring bacterial-demineralization of human dentine by electrochemical impedance spectroscopy. *Journal of Dentistry* **38**, 138-148.

Transport and reactions of contaminants in sediments

[1]Ole Larsen, [2]Bill Davison, [3]Kyriakos Vamvakopoulos, [4]Flemming Møhlenberg

[13]DHI-NTU Water & Environment Research Centre and Education Hub, 200 Pandan Loop #08-03, Singapore

[2]Lancaster University, Environmental Sciences Bailrigg, LA1 4YQ Lancaster, UK

[3]Department of Biogeochemistry, Max Planck Institute for Marine Microbiology, Celsiusstrasse 1, DE-28359 Bremen, Germany

[4]DHI Water and Environment, DK-2730 Hørsholm, Denmark

Book chapter at "Sediment Dynamics and Pollutant Mobility in Rivers" Bernhard Westrich and Ulrich Förstner (eds.), (2007) Springer

Introduction

Many of the sediments in our coastal environments are contaminated with various metals. The highest concentrations of contaminants are found in harbours, where antifouling paints and industrial activities are the main sources. In the past years there has been a strong focus on TBT that is known to be highly toxic and to affect the hormonal balance of many animals. Almost all substitutes for TBT are based on Cu-complexes. Copper is known to form strong complexes with natural organic matter and the total Cu-concentration in sediments is found to correlate with the concentration of organic matter (see Fig. 1).

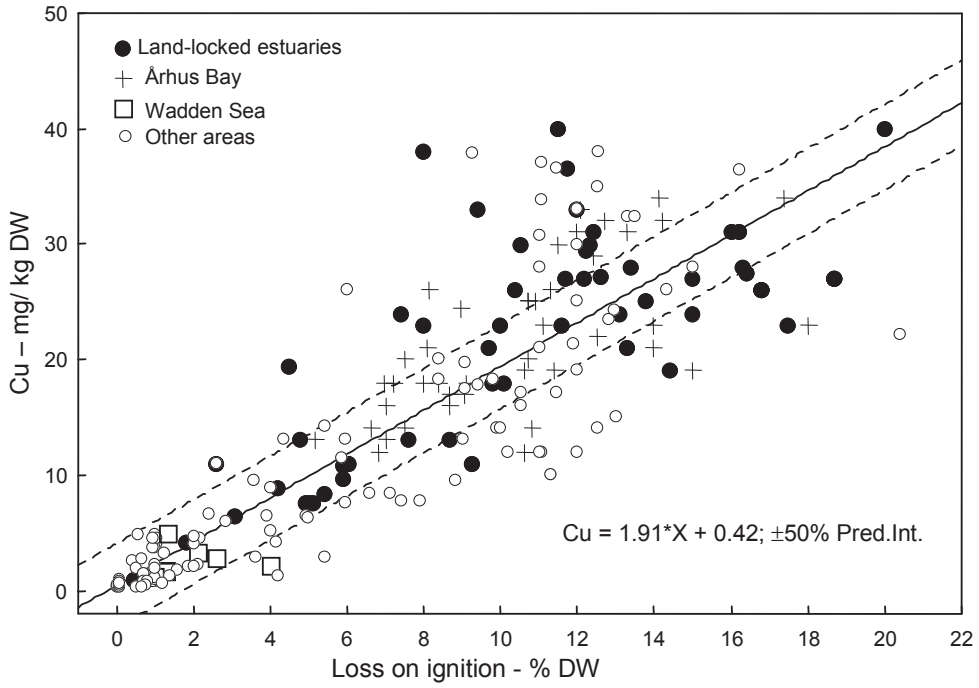

Figure 1. The bulk copper concentration displayed against the loss on ignition in a variety of estuarine sediments. Loss on ignition corresponds mainly to loss from organic matter although it also includes weight loss from carbonates and hydrated minerals (the data originates from Møhlenberg et al. 2007).

Recent investigations have shown that Cu concentrations in the marine environment can be very high in estuaries with heavy boat traffic (Comber et al. 2002) and in many areas exceed the sediment quality guideline values (e.g., CCME 1999; Long et al. 1998), and few studies have demonstrated that Cu may be one of the most important constraints on

benthic fauna. Chapman (1990) suggested an integrated approach (Sediment Quality Triad) to evaluate effects of contaminated sediments consisting of three complementary components including chemical analysis of contaminants, sediment toxicity, and assessment of resident biota such as changes in benthic community structure. An example of the third SQT component is shown in Fig. 2.

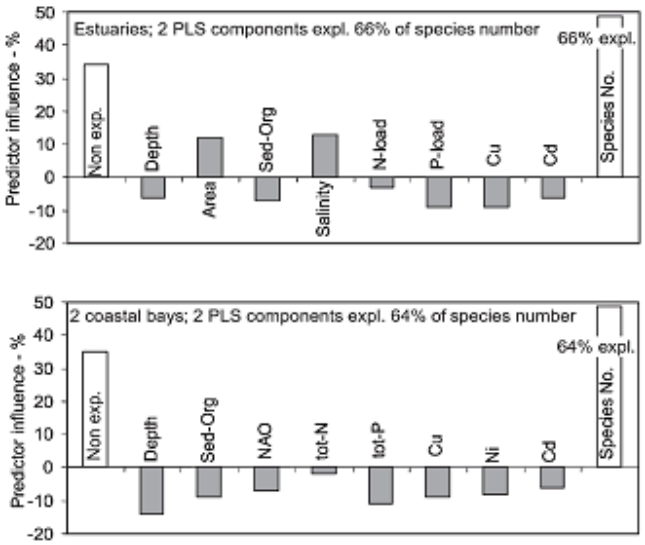

Figure 2. PLS analysis of 60 data sets from various European estuaries and 38 data sets from 2 coastal bays. Sixty-four and 66% of the variation of total species number could be explained using 2 PLS components. The heavy metals Cu and Cd (estuaries) and Cu, Ni and Cd accounted for 18 and 23% of the variation in species richness. In these coastal waters heavy metals are as important as nutrients for the faunal biodiversity (the data originates from Møhlenberg et al. 2007).

Using ca. 80 synoptic samples, linkages between forcing factors (sediment contaminants and water quality) and effects (benthic invertebrate species abundance) were analyzed using Partial Least Squares regressions (Møhlenberg et al. 2007). Initially, more than 60 potential predictors were included in PLS regressions, and significant predictors were identified by cross-validation or boot-strapping. Overall, the "natural" conditions such as salinity, station depth and sediment organic carbon were the most influential predictors of species richness and diversity. Depending on the location considered or the grouping of data, either nutrient concentrations or sediment contaminants, especially copper and cadmium, were the second most important factor affecting benthic communities, accounting for up to 25% of the variation in species richness (Fig. 2). Using field

experiments Lenihan et al. (2003) demonstrated that copper mainly caused reductions among crustaceans and echinoderms, while organic enrichment of sediments promoted annelids, but had variable effects on crustaceans and echinoderms. Hence, the effects of copper enrichments in sediment seem to be manifested through elimination of "sensitive" species leading to reductions in species richness, as shown in Fig. 2.

Predictive geochemical models, both numerical and conceptual, of elemental transformations and particularly remobilization underpin the assessment of risk posed by heavy metals in many environmental situations. The increased use of metals (e.g. copper) may critically affect the risk to intensively utilized coastal and estuarine environments. This environmental problem raises a question at a more fundamental level: what are the controls on heavy metals in marine sediments? The environmental chemistry of heavy metals has been studied during the past decades, with considerable research interest concentrated on Cd, Pb, and Cu (e.g., Serbst et al. 2003; Burnton et al. 2005; Chapman et al. 1998). For routine monitoring most sediment samples are collected directly from dredgers and analyzed as mixed bulk samples. Typically, bulk parameters like content of Corg and total concentrations of heavy metals are measured and the results are taken as representative for a large sediment volume. However, recent studies (Glud et al. 1996; Shuttleworth et al. 1999; Fenchel and Glud 1998) are showing that the geochemical structure of sediments is much more complicated than previously thought. Existing models are based on a 1-dimensional view of sediments with zones of microbial/chemical activity systematically layered. Biological activity is largely seen as a physical process that pertubates this state. This picture has largely developed from measurements based on horizontally slicing sediments and performing measurements on porewaters and the solid phase of the resulting volumetrically averaged sample. Measurements at one thousandth of this volumetric scale (DGT/DET/optodes/electrodes) have revealed a detailed solute structure, which suggests that sediment processes occur in microniches (Fones et al. 1998). This new perception of sediments suggests that sediments cannot be regarded as horizontally uniform, and consequently the use of one-dimensional models is called into question. Moreover, as microniches are likely to be short lived (days/weeks), the dynamic nature of the geochemical processes must be considered. At present, the transport, reactions and dynamics of copper and other heavy metals in marine sediments are known

at scales much larger than the scale of the bacteria and associated microniches (1–50 μm) involved in these processes. This poses a new question: how does analytical scale affect the interpretation of sediment geochemistry in terms of processes and reactions?

The dredged sediment in Europe amounts to more than 200 000 000 m^3 yr^{-1}. Although most of the sediment is not contaminated, large amounts contain high concentrations of heavy metals. The most contaminated sediments are treated as chemical waste and the costs for disposal exceed 100 Euro m^{-3}. Due to the high costs of sediment treatment and strong competition between harbours a unified European legislation concerning contaminated sediments is desirable. Such legislation should be based on the ecotoxicity and sediment processes rather than politically defined maximum concentrations in sediments. In response to the lack of understanding of fundamental processes a project under the FP5 of the European Union was initiated to investigate the importance of the individual processes and their spatial distribution within sediments. The project partners were: TU-Delft, Lancaster University, University of Copenhagen and the Max Planck Institute for marine microbiology. In this section we report selected results from the EU project TREAD (EVK3-CT-2002-00081), with the focus on copper.

The investigation includes the study of heavily contaminated harbor sediment whose locality may not be published.

Experimental Approach

Based on the conceptual model of processes in sediments occurring at microniches an analytical program was launched to enable the assessment of local fluxes and concentrations in sediments at high temporal and spatial resolution. Using high resolution techniques we attempted to investigate the fluxes of solutes (within sediments and through the sediment-water interface) in contaminated marine sediments upon disposal in the environment. Two sediments were selected: a fine-grained (silt) harbor sediment with low benthic activity and a permeable sand with high benthic activity. The harbor sediment was heavily contaminated with heavy metals while the sand from Sylt (Germany) represents pristine marine sand. The investigation included, besides a careful field site description, the sampling of several large undisturbed sediment blocks (0.18 m^2, 10 cm depth) that were brought to the laboratory facility in Bremen. The sediments were

installed in four mesocosms to mimic disposal of dredged material in the environment: (1) dumping at a site with high current velocities (silt was added to the sandy sediment, mimicking resuspension during a dredging event or disposal in a high current environment – mesocosm A), (2) dumping the sediment after reworking the sediment at a low energy environment (the silt was homogenized and slightly oxidized before settling in mesocosm D) and their respective control systems (undisturbed sand – mesocosm B and undisturbed harbor sediments – mesocosm C). The environmental controls of the 4 mesocosms were varied simultaneously throughout the two years the experiment lasted. Light, temperature and water flow were kept constant while, at different times, fresh supplies of benthic fauna and organic material were added and the salinity adjusted.

Novel techniques were used to detect and quantify key processes at the scale of their occurrence in sediments, including different forms of microsensors (electrodes and optodes), gel-sampling techniques and microscopy. More traditional measuring approaches (bulk flux measurements and extracted pore water profiles), integrating the activity of larger sediment volumes, provided comparisons with the high-resolution measurements.

Heavy Metals at the Field Site

Heavy metal content is routinely measured in harbor sediments by the authorities and is discussed here with kind permission. Literature data on the heavy metal concentration in North Sea sediments and data from the contaminated site are available for the fine fraction (<20 μm) of the sediment. Measurements of Hg, Cd, Pb, Cu and Zn, as well as organic tin from North Sea and Weser and Elbe sediments (BLMP 2002) and the contaminated and investigated site are shown in Table 1.

	Average	Average maximum	Maximum	Harbor site
Hg	0.38	0.52	1.5	0.9 ± 0.49
Cd	0.66	1.4	4.4	1.4 ± 0.29
Pb	77	111	234	128 ± 10
Cu	25	40	81	558 ± 115
Zn	227	375	903	742 ± 114
Monobutyltin	0.39	–	3.5	0.76 ± 0.28
Dibutyltin	0.45	–	5.5	4 ± 1.5
Tributyltin	0.34	–	1.4	78.8 ± 44.5
Tetrabutyltin	1.24	–	39.4 (6.0)	0.7 ± 0.094

Table 1. Sediment data of 10 different stations throughout the North Sea, Weser and Elbe (BLMP 2002) and the sampling location measured by the harbor authorities. Data for the inorganic metal concentrations were provided as minimum, average and maximum data for the 10 locations and are averaged accordingly. The value in brackets indicates the next smaller value. For the arbor site, data from 4 different sites around the sampling locatin were provided, the measurment from the closest site are presentes here averaged over 5 years of monitoring. Concentrations of the inorganic elements are given in mg kg-1 dry weight; the concentration of the butyl-tin species are given in µg kg-1 dry weight. The measurments were made on the fine fraction of the sediment <20 µm.

The heavy metal concentrations in the harbor sediments are similar to the maximum concentrations reported in the literature while the concentrations of copper are elevated 10–20 fold compared to the North Sea and river sediments. The highest literature value was found in a harbor area in northern Bremen, but the concentrations here were still more than five times lower than the lowest measurements from our study sediments. The butyl-tin concentrations measured in the Elbe between 1991 and 1997 also show distinct differences to those at our field site. While the concentrations of the different compounds are very similar in the Elbe, the harbor site shows large differences in the concentrations of the different compounds. The concentrations of butyl-tin vary at the different stations within the same harbor basin and the same year by a factor of up to 40. However, for all measurements the concentration of tributyl-tin was always highest, followed by di-, mono- and finally tetrabutyl-tin. As copper and tin are used in anti fouling paints for ships, it is not surprising to find high concentrations in the harbor basins, especially those close to a shipyard like our site. Similarly the site close to Bremen Harbor and one Elbe site, possibly close to Hamburg Harbor, showed the highest concentrations for Cu. These concentrations are still lower than at our site, but the samples originate from outside the harbor.

A comparison of the metal concentrations measured over a period of more than 20 years (6 years for the butyl-Sn) show that the concentrations decrease (BLMP 2002). This trend is less pronounced for Cd and Pb. Such a trend could not be seen in the measurements from the harbor basin, but the available data only cover 5 years. Any trend would be disguised in the high scatter of the small data set.

Heavy metal data are not available in the literature for the Sylt location or similar sites. This site is, however, very likely typical of the low end of the concentration spectrum.

Comparison of the data obtained within our project with literature data is a little difficult, as the literature data were measured in the fine fraction of the sediment. Our measurements (Fig. 2) were carried out in the total sediment, comprising mainly fine sand for the Sylt site, and ~70% fine material for the contaminated site.

Results

Bulk Concentrations of Copper in Sediments

The copper concentrations in all sediments were measured, after extraction with 6M HCl and many fold dilution, by ICP-MS. The concentrations were measured in five different sediment cores from the two control mesocosms (undisturbed sand from Sylt (B) and harbor sediment (C)). The average concentration (line) and the results from each individual sample are displayed in Fig. 3.

In both sediments the concentrations are significantly higher in the uppermost sediment layers despite bioturbation mixing the sediments. A further pronounced feature is that the horizontal variability is as large as the vertical variability in both sediments. The total copper concentration in the harbor sediment is about 80 times higher than the concentrations found in the sand.

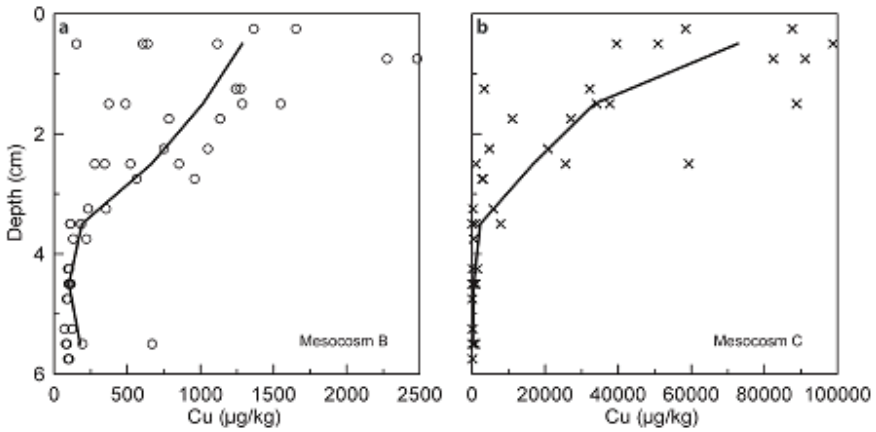

Figure 3. Copper concentration measured in sediments from mesocosm B and C. Each core was sliced in 1 cm slices. The concentration of copper was measured in two samples from each depth and the mean is represented by the symbols in the plot. Five cores was analysed and the mean of all five cores is shown as a line. Mesocosm B (circles) is the undisturbed sand from Sylt; C (crosses) is the undisturbed harbor sediment. The cores were sampled a few cm apart.

Bulk Concentrations of Copper in Porewater

The concentrations of dissolved heavy metals in the porewaters of all mesocosms were also measured. The results after about one year of the experiment are showed in Fig. 4 (corresponding to the same time as the sediment profiles presented in Fig. 3). The pore water from the harbor sediments (C and D) have higher concentrations of dissolved Cu than the pore waters from the sand (A and B) (3 to 9 times, depending on the sampling depth). In all sediments the Cu concentration in the porewater decreases with depth. The variations between the sampled cores are in the same range for the two ecosystems, indicating that the concentrations do not to any large extend depend on the transport path (advective vs. diffusive). The variation between 5 different cores sampled from mesocosms B and C is shown in Fig. 4b.

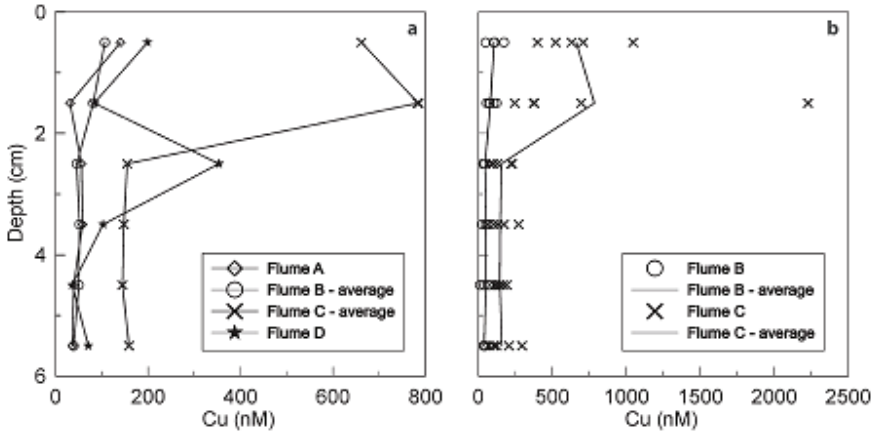

Figure 4. a Copper concentration measured in porewater extracted by centrifugation of the sediment under anoxic conditions through a 0.2-µm filter. Each result is the average of duplicate determinations. Additionally, the results from mesocosm B and C are averaged values of results from 5 different cores. A represents the results from sand with a surface layer of harbor sludge; B is the undisturbed sand from Sylt; C is the undisturbed harbor sediment; D is the homogenized harbor sediment. **b** Results from 5 individual cores of mesocosm B (circles) and C (crosses) and their average values. The cores were sampled a few cm apart.

The lack of systematic variation between the individual measurements suggests that any structure in the solute composition is not resolved at a cm scale.

The solute composition was investigated at high resolution using DET (diffusive equilibria in thin-films). Two cm wide strips of gel (0.8–1.2 mm thick), either continuous or segmented and mounted in a plastic support, were inserted into the sediment. Solutes in the porewater of the sediment equilibrate with the water within the gel within the typically 56 hours deployment time. The solute sampled in this way corresponds to a volume of only about 20 µl. Results from DET deployments in the harbor sediments are presented in Fig. 8.5. The location of the sediment water-interface is represented by zero.

The two high resolution porewater profiles are much smoother than the profiles displayed in Fig. 4. The high resolution measurements show that the Cu concentration peaks exactly at the sediment water-interface within the 2 mm resolution of the measurement. The high concentrations at the sediment water interface suggest that there is a local source at the surface, which is probably release from the reactive organic material that is rapidly oxidized and from associated oxidants, such as manganese oxides. With this rapid remobilization, Cu diffuses upwards and downwards from the sediment surface layer.

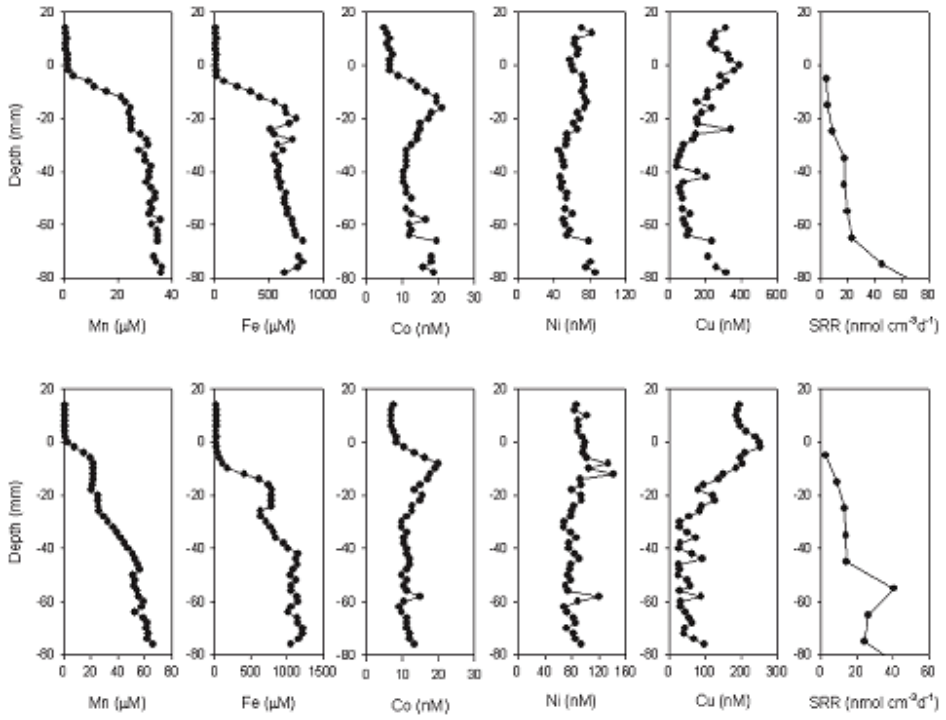

Figure 5. Concentration of metals measured with DET from the harbor sediments. The results presented in the upper panel originates were from mesocosm C (control) while the lower panel are results from the homogenized harbor sludge (the results were published in Tankere-Muller et al. 2006).

Fluxes of Copper in the Sediment

With DGT (Diffusive Gradients in Thin-film) a method is available to quantify the remobilization in sediments. The essential part of DGT probes is a cation exchanger protected behind a thin gel layer. When the probe contacts the sediment, solutes diffuse into the diffusive gel and the cations are trapped in the ion exchanger. After approximately 24 h deployment the probes were retrieved and cut into 3 mm squares that were treated with acid. Cations were measured in the eluate. The measured accumulation of Cu on the resin allows calculation of the average flux from the sediment to the resin over the deployment period. DGT measurements (Fig. 6) can be interpreted as an average concentration at the surface of the device during the deployment time. This is usually lower than the bulk concentration because (a) supply from solid phase to solution is kinetically limited and (b) only part of the Cu organically complexed is measured by

DGT when the diffusion coefficient for the free metal ion is used in the calculation. In this work the ratio of the DGT-derived concentration of Cu to the concentration in porewater measured by DGT was between 0.3 and 1.2, indicating that Cu was not dominated by large organic complexes and that there was an appreciable supply from solid phase to solution. It is therefore a good approximation to attribute the DGT-measured flux to the resupply flux of Cu to the porewaters. If anything this is likely to underestimate the magnitude of the highly localized flux, as the DGT maxima were defined by single data points. Measurement at higher vertical resolution than the 3 mm used for DGT would probably reveal higher maxima.

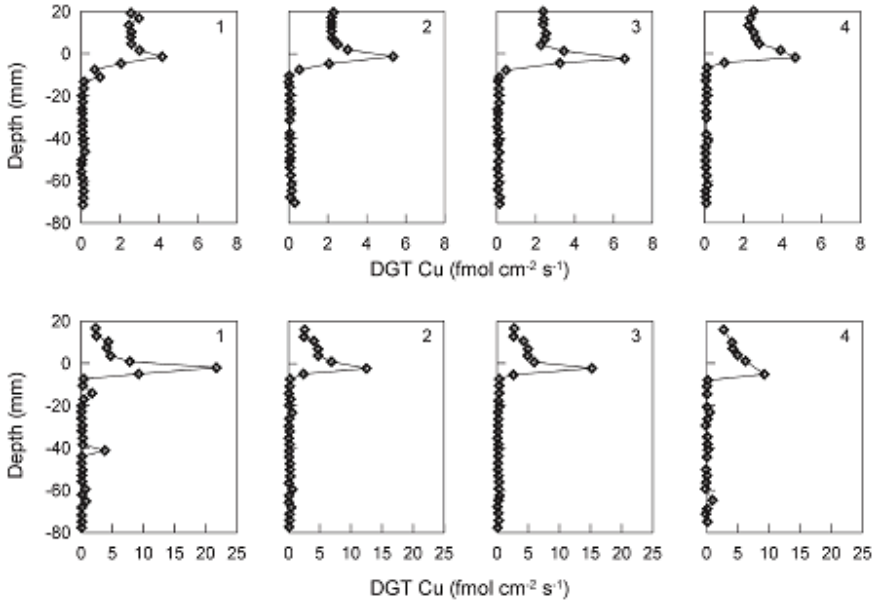

Figure 6. Vertical profiles of DGT-measured fluxes for the harbor sludge: Control (upper panel) and homogenized sediment (lower panel). Numbers 1 to 4 refer to adjacent 3 mm wide vertical columns within a single DGT probes. The location of the sediment-water interface is represented by zero. Please note the difference in scale. The results were published in Tankere-Muller et al. 2006.

Forms of Copper in the Sediment

Small blocks of undisturbed sediment were sampled in front of the DET and DGT devices at each sampling campaign. Before embedding the sediments with a methacrylate resin, the sediments were stored anoxically in formaldehyde to fix fauna and bacteria. After hardening of the resin the sediments were polished and prepared for microscopy. Semi quantitative elemental analysis was performed using an electron microscope for

elemental mapping and measurement of points. The elemental mapping showed that copper is heterogeneously distributed within the sediments. Analyzing the Cu-hotspots revealed that copper is predominantly associated with Fe-oxides and sulfides. The Fe-oxides contained traces of all contaminants and the copper concentrations ranged from 0.2 to 3% Cu (on an atomic basis). The sulfides containing Cu cover a range from a few percentage of Cu substitution in pyrite through pure chalcopyrite to almost pure Cu-sulfide. An example of sediment particles and the obtained analytical results are shown in Fig. 7.

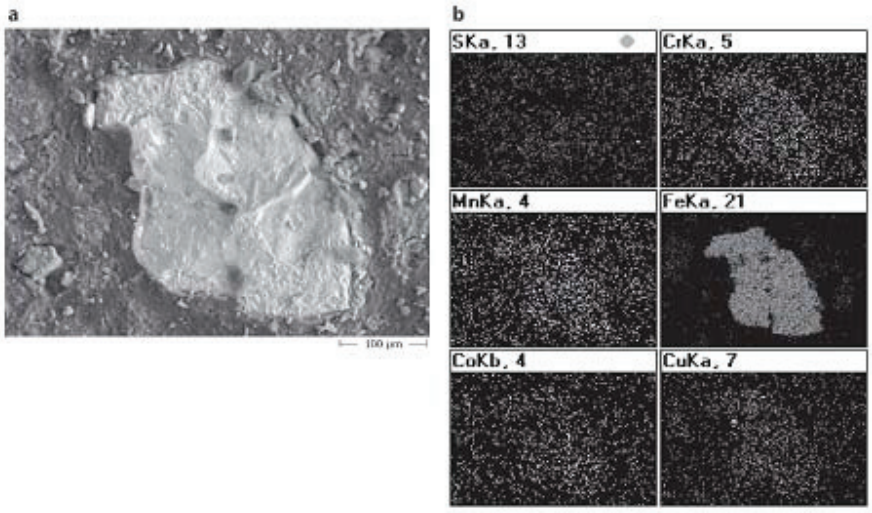

Figure 7. a Back-scattered image of Cu-containing particle in thin section of the harbor sediment. **b** Energy dispersive analysis (mapping) illustrating the distribution of selected elements in the viewed section. Operating conditions: 15 kV accelerating voltage and a total counting time of 18 min.

Discussion

Collectively these measurements show that contaminants are intensively cycled in marine sediments according to the prevailing biogeochemical conditions. After copper is introduced to the sediments (presumably as organic particles) the copper moves gradually into various inorganic forms. In the upper millimeter of the sediments, where oxic conditions prevail, the copper becomes associated with iron(III) and manganese oxides. When the oxides in the course of diagenesis are used as electron acceptors the copper is released and entrained in the sulfides. Due to bioturbation and other disturbances the sulfides are brought into the oxic sediments again where they are oxidized and a

transitory release of copper can be recorded. As metals are repeatedly cycled through these processes larger aggregates or nodules of iron and manganese oxides form in the upper sediment and sulfides in the deeper sections. With increasing time, copper is found in increasingly pure copper sulfides. This description of processes is in accordance with the findings of other workers (e.g., Parkman et al. 1999).

The high resolution measurements of the solute composition show that there are various factors that influence the small scale structure of Cu in the porewaters of sediments. There is good evidence that the productive silt sediment is laterally homogeneous, which supports the use of a vertical one dimensional model to describe the sequence of electron acceptors involved in the oxidation of org C. However, fluxes to and from the sediment can only be estimated accurately if measurements are made at mm or finer intervals because it appears that Cu is released to solution very close to the interface. The DET measurements show a sharp Cu maximum at the interface, but with DGT it is even sharper. Such an observation is consistent with rapid supply from solid phase to solution at this location. If it is sufficiently rapid to fulfill the DGT demand, while immediately above and below the site of supply the DGT demand can not be sustained, the DGT measurement will indeed have a sharper peak than the corresponding concentration profile. This highly localized remobilization at the interface would be missed by conventional measurements at typically cm resolution, which would underestimate the release flux and consequently the risk posed by the sediment.

For sandy sediments (not all results shown) the surface maximum is not so pronounced, but there is a much more heterogeneous distribution of Cu in the porewaters, both laterally and vertically. Here Cu release will depend on both diffusional fluxes at the interface and the localized chemistry in the convective pathway of the surface sediment. The analysis of the solid phase, which showed that chalcopyrite can be present in highly localized clusters, indicates that there may be some areas ($<cm^2$) of the sediment surface that have much higher Cu release rates than others. For these sediments it is inappropriate to use conventional one dimensional models of diagenesis. To develop a quantitative appreciation of the processes occurring and the resulting fluxes requires the use of a full three dimensional model of the redox reactions associated with the decomposition of organic matter. Such a model, which allows for vertical structures and localized

microniches, has recently been developed (Sochaczewski et al. in preparation). While such models can be used to simulate particular events and experimental details, their ability to predict average fluxes is limited by the intrinsic stochastic nature of the system. There can be no doubt that a full appreciation of the dynamics of metals in sediments requires measurements to be made at fine scales without lateral averaging. Quantitative interpretation of these data requires full 3 dimensional modeling of the reaction and transport dynamics of the system.

Such measurements and associated models will be able to identify cases where risks are lower than previously thought (e.g., reduced fluxes of Co and Ni), but they will also show that in some cases risks may be higher (e.g., Cu and Cd). Data sets at the required resolution are still very limited, but as more data become available in the next decade our understanding of metal dynamics in sediments is likely to increase greatly. This new found knowledge is likely to greatly benefit the risk assessment and management of contaminated sediments.

One source of the highly localized flux at the sediment-water interface is likely to be the oxidation of sulfides brought upward in the sediments due to bioturbation or other disturbance. High biological activity or other sediment disturbance is therefore likely to enhance the copper flux through the sediment-water interface, as seen in the investigated sediments.

The fluxes through the sediment-water interface as well as the concentration of copper in the porewater are only to a limited extend related to the bulk concentration of copper. This suggests that the copper compounds formed in the marine environment are rapidly turned over in the upper millimeter of the sediments. The process rate appears in fact to be high enough to ensure partial equilibrium in these sediments. Accordingly, the environmental risk is related to a combination of factors associated with sediment management (disturbance) and the size of the copper pools in the sediments.

Acknowledgments

The authors are grateful for having been invited by Ulrich Förstner and Bernhard Westrich to attend the SEDYMO symposium held in 2006 at Hamburg-Harburg University of Technology to present selected results from the TREAD study. This section

represents an overview of work which has involved financial support from various agencies particularly the EU (EVK3-CT-2002-00081), which is gratefully acknowledged.

References

BLMP (2002) Meeresumwelt 1997–1998. Bundesamt für Seeschifffahrt und Hydrographie (BSH), Hamburg und Rostock.

Burnton ED, Phillips IR, Hawker DW (2005) Geochemical partitioning of copper, lead, and zinc in benthic, estuarine sediment profiles. *J Environ Qual* 34:263–273.

Canadian Council of Ministers of the Environment (CCME) (1999) Canadian Environmental Quality Guidelines, Winnipeg.

Chapman PM (1990) The Sediment Quality Triad approach to determining pollution-induced degradation. *Sci Tot Environ* 97/98:815–825.

Chapman PM, Wang F, Janssen C, Persoone G, Allen HE (1998) Ecotoxicology of metals in aquatic sediments: Binding and release, bioavailability, risk assessment, and remediation. *Can J Fish Aquat Sci* 55:2221–2243.

Comber SDW, Gardner MJ, Boxall ABA (2002) Survey of four marine antifoulant constituents (copper, zinc, diuron and Irgarol 1051) in two UK estuaries. *J Environ Monit 4* :417–425.

Fenchel T, Glud RN (1998) Chemolithotrophic veil architectures enhance fluxes at the marine benthic interface. *Nature* 394:367–369.

Fones GR, Davison W, Grime GW (1998) Development of constrained DET for measurements of dissolved iron in surface sediments at sub-mm resolution. *Sci Tot Environ* 221:127–137.

Glud RN, Ramsing NB, Gundersen JK, Klimant I (1996) Planar optrodes, a new tool for fine scale measurements of two dimensional O2 distribution in benthic communities. *Mar Ecol Prog Ser* 140:217–26.

Lenihan HS, Peterson CH, Kim SL, Conlan KE, Fairey R, McDonald C, Grabowski JH, Oliver JS (2003) Variation in marine benthic community composition allows discrimination of multiple stressors. *Mar Ecol Prog Ser* 261:63–73.

Long ER, Field LJ, MacDonald DD (1998) Predicting toxicity in marine sediments with numerical sediment quality guidelines. *Environ Toxicol Chem* 17:714–727.

Møhlenberg F, Josefson AB, Vale C, De Deckere E (2007) Empirical relations between benthos quality and pressures in coastal waters – Identification of key indicators for WFD classification. REBECCA Deliverable 15.

Parkman RH, Charnock JM, Bryan ND, Livens FR, Vaughan DJ (1999) Reactions of copper and cadmium ions in aqueous solution with goethite, lepidocrocite, mackinawite, and pyrite. *Amer Min* 84:407–419.

Serbst JR, Burgess RM, Kuhn A, Edwards PA, Cantwell M G, Pelletier MC, Berry W J (2003) Precision of dialysis (peeper) sampling of cadmium in marine sediment interstitial water. *Arch Environ Contam Toxicol* 45:297–305.

Shuttleworth SM, Davison W, Hamilton-Taylor J (1999) Two dimensional and fine structure in the concentrations of iron and manganese in sediment pore-waters. *Envi Sci Technol* 33:4169–4175.

Sochaczewski L, Stockdale A, Zhang H, Tych W, Davison W (2007) A three dimensional model of transport and reaction dynamics in sediments: 3D-TREAD, in prep.

Tankere-Muller S, Zhang H, Davison W, Finke N, Larsen O, Stahl H, Glud RN (2007) Fine scale remobilisation of Fe, Mn, Co, Ni, Cu and Cd in contaminated marine sediment. *Mar Chem*: 192-207.

Monitoring and modelling contaminants in harbour basins: coupling hydraulic and sediment models

Conference paper (2007) “Port Development and Coastal Environment", Varna, Bulgaria.

Ole Larsen[1#] & Kyriakos Vamvakopoulos[2]

[1]DHI-NTU Water & Environment Research Centre and Education Hub, 200 Pandan Loop #08-03, Singapore

[2]Department of Biogeochemistry, Max Planck Institute for Marine Microbiology, Celsiusstrasse 1, DE-28359 Bremen, Germany

[#]Corresponding author: Ole Larsen, DHI-NTU Water & Environment Research Centre and Education Hub, 200 Pandan Loop #08-03, Singapore. T: +65 67 77 63 30, F: +65 67 77 35 37, E-mail: ola@dhi.com.sg

Abstract

In the EU Project TREAD, a huge dataset was gathered describing all major sediment processes, including rates of turn-over and fluxes of heavy metals over the sediment-water interface. The data were in the first instance used to develop a conceptual understanding of sediment processes and further to develop a 3D numerical sediment model called 3DTREAD. Several tests have been made confirming that the model is able to simulate and describe sediment processes at the scale of their occurrence. Further development allowed for simplification of the highly detailed process model into a large scale EcoLab template allowing the simulation of heavy metal species in sediments together with hydrodynamic and sediment transport models. This model is now available for the practical use in sediment management.

Introduction

Due to industrial activities and antifouling paints harbour basins are often contaminated with heavy metals. Harbour basins represent, due to the dredging activities, significant sediment traps entraining the heavy metals. Dredging and ship traffic is a major disturbance of the structure and functioning of the sediments leading to changes in the biogeochemical processes of the sediments. The dredged sediment in Europe amounts to more than 200.000.000 m³/year. Although most of the sediment is not contaminated, large amounts contain high concentrations of heavy metals. The most contaminated sediments are treated as chemical waste and the costs for disposal exceed 100 €/m³.

Predictive geochemical models, both numerical and conceptual, of elemental transformations and particularly remobilization underpin the assessment of risk posed by heavy metals in many environmental situations. The increased use of metals (e.g. copper) may critically affect the risk to intensively utilized coastal and estuarine environments. This environmental problem raises a question at a more fundamental level: what are the controls on heavy metals in marine sediments? The environmental chemistry of heavy metals has been studied during the past decades, with considerable research interest concentrated on Cd, Pb, and Cu (e.g. Serbst et al., 2003, Burnton et al., 2005, Chapman et al., 1998). For routine monitoring most sediment samples are collected directly from dredgers and analyzed as mixed bulk samples. Typically, bulk parameters like content of organic matter and total concentrations of heavy metals are measured and the results are taken as representative for a large sediment volume. However, studies (Glud et al., 1996; Shuttleworth et al., 1999, Fenchel and Glud, 1998) show that the geochemical structure of sediments is much more complicated than previously thought. Existing models are based on a 1-dimensional view of sediments with zones of microbial/chemical activity systematically layered. Biological activity is largely seen as a physical process that pertubates this state. This picture has largely developed from measurements based on horizontally slicing sediments and performing measurements on porewaters and the solid phase of the resulting volumetrically averaged sample. Measurements at one thousandth of this volumetric scale (DGT/DET/optodes/electrodes) have revealed a detailed solute structure, which suggests that sediment processes occur in microniches (Fones et al.,

1998). This new perception of sediments suggests that sediments cannot be regarded as horizontally uniform, and consequently the use of one-dimensional sediment models is called into question. Moreover, as microniches are likely to be short lived (days/weeks), the dynamic nature of the geochemical processes must be considered. At present, the transport, reactions and dynamics of copper and other heavy metals in marine sediments are known at scales much larger than the scale of the bacteria and associated microniches (1-50 μm) involved in these processes. This poses a new question: how does analytical scale affect the interpretation of sediment geochemistry in terms of processes and reactions?

In response to the lack of understanding of fundamental processes a project under the FP5 of the European Union was initiated to investigate the importance of the individual processes and their spatial distribution within sediments. In this presentation selected results from the EU project TREAD (EVK3-CT-2002-00081), will be presented. The project partners were: TU-Delft, Lancaster University, University of Copenhagen and the Max Planck Institute for Marine Microbiology in Bremen.

Methods for monitoring contaminants in harbour basins

Heavy metals are found in many forms in marine sediments. In many solids heavy metals are bound so strong that they do not readily transform into the food web. In contrast, only a small and labile part of heavy metals in sediments is able to be transformed from the sediment into the food web. Hereby, the changes in oxidation state and the complexation with various organic ligands are the prime parameters determining the ecotoxicity of the heavy metals. Hence, the ecotoxic part of the total heavy metals is the fraction moving from one solid and strongly bound state to another and is therefore measurable as the turn-over of the different pools. In marine sediments the biogeochemical processes are determined by the action of about 10^9 microorganisms per cm^3 of sediments. This very diverse community ranges from organisms (diatoms) assimilating organic matter and producing O_2 on the sediment surface to organisms (bacteria) oxidizing the organic matter with available terminal electron acceptors. Solid phases like sulfides and oxides of transition metals represent the most important sink for dissolved heavy metals in sediments.

Routinely harbour sediments are tested for their bulk concentration of heavy metals whereas measurements of the processes determining the ecotoxicity are seldomly carried out. The most important process rates to be determined are the dissolution and precipitation of heavy metals; biogechemical processes (sediment up-take of oxygen and sulphate reduction etc) and (bio)turbation. The main difficulty measuring these parameters is that the microbial community generates strong solute gradients within the sediments and the processes are only meaningful if they are described at the sub-mm scale at which the active microniches occur. Recently techniques have been developed that allow for process characterization at high temporal (seconds-hours) and high spatial resolution (20-100 μm). In table 1, a gross summary of available methods for description are delivered:

Aim of analysis	*Method*	*Reference*
Oxygen dynamics	Oxygen micro electrodes for the measurement of profiles	Revsbech, 1989
	Planar optodes for 2D imaging of oxygen at high temporal resolution	Glud RN, Ramsing NB, Gundersen JK, Klimant I (1996)
Transition element dynamics	Diffusive equilibria in thin film (DET) for measurement of solute concentration	Davison, W., Grime, G. W., Morgan, J. A. W. and Clarke K., 1991 Davison and Zhang, 1994
	Diffusive gradient thin film (DGT) for the measurement of fluxes of metals and Sulfide	Davison, W., Fones, G., Harper, M., Teasdale, P. and Zhang, H. (2000) Harper, M.P., Davison, W., Zhang, H. and Tych, W. (1998)
	Selective extractions for the different phases	Beckett PHT, 1989
	Microscopic examination of heavy metal “hot spots” in sediments	Vamvakopoulos & Larsen 2007
Sulfate dynamics	Incubation with ^{35}S labelled sulphate	Jørgensen BB (1978) Fossing H, Jørgensen BB 1989)
Bioturbation	Incubation of sediment cores with fluorescently labelled particles	

Table 1. List of selected methods for the measurement of solute and sediment dynamics that is important for the assessment of the ecotoxicity of heavy metals.

Monitoring contaminants in harbour basins

Based on the conceptual model of processes in sediments occurring at microniches, an analytical programme was launched to enable the assessment of local fluxes and concentrations in sediments at high temporal and spatial resolution. Using high resolution techniques, the fluxes of solutes (within sediments and across the sediment-water interface) in contaminated marine sediments upon disposal in the environment were investigated. Two sediments were selected: a fine-grained (silt) harbour sediment with low benthic activity and a permeable sand with high benthic activity. The harbour sediment was heavily contaminated with heavy metals while the sand from Sylt (Germany) represents pristine marine sand. The investigation included, besides a careful field site description, the sampling of several large undisturbed sediment blocks (0.18 m², 10 cm depth) that were brought to the laboratory. The sediments were installed in four mesocosms to mimic disposal of dredged material in the environment: 1) dumping at a site with high current velocities (silt was added to the sandy sediment, mimicking resuspension during a dredging event or disposal in a high-current environment – Mesocosm A), 2) dumping the sediment after reworking the sediment at a low energy environment (the silt was homogenized and slightly oxidized before settling in mesocosm D) and their respective control systems (undisturbed sand – Mesocosm B and undisturbed harbour sediments – Mesocosm C). The environmental controls of the 4 mesocosms were varied simultaneously throughout the two years the experiment lasted. Light, temperature and water flow were kept constant while, at different times, fresh supplies of benthic fauna and organic material were added and the salinity adjusted.

The vast amount of experimental data clearly demonstrated the expected high degree of horizontal and vertical heterogeneity of the sediments verifying that the process control was exerted by microniches. An example of the data is displayed in Figure 2 showing profiles of solute composition. The high resolution measurements show that the Cu concentration peaks exactly at the sediment water-interface within the 2 mm resolution of the measurement. The high concentrations at the sediment water interface suggest that there is a local source at the surface, which is probably release from the reactive organic material that is rapidly oxidized and from associated oxidants, such as manganese oxides.

Associated with the rapid remobilisation, Cu diffuses upwards and downwards from the sediment surface layer.

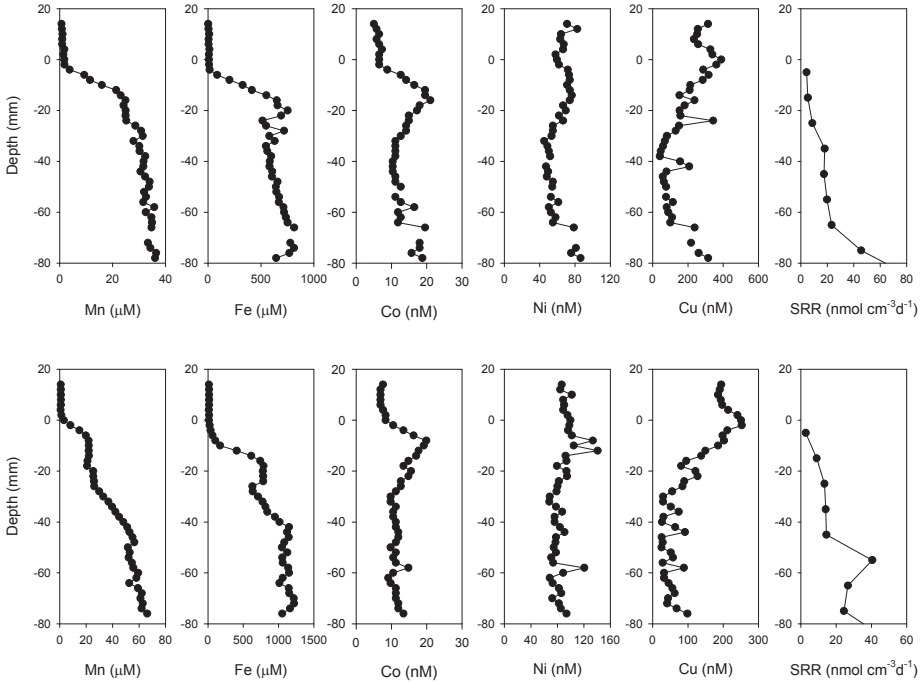

Figure 1: Concentration of metals measured with DET from the harbour sediments. The results presented in the upper panel originates were from mesocosm C (control) while the lower panel are results from the homogenized harbour sludge. SRR is the volume integrated sulphate reduction rate. The original results were published in Tankere-Muller et al., 2007 and also presented in Larsen et al., 2007).

The fluxes of Cu (and other elements) at the sediment-water interface were quantified using DGT and the sources were further characterized using microscopic techniques. The fluxes corresponding to the Cu concentration profiles displayed in Figure 1 are shown in Figure 2. In conclusion of the analytical work it can be said that all fluxes over the sediment-water interface increase dramatically as response to any change in environmental conditioning. The most dramatic effect was seen when the sediment were homogenized as result of dredging activities where the physical structure of sediments got disrupted.

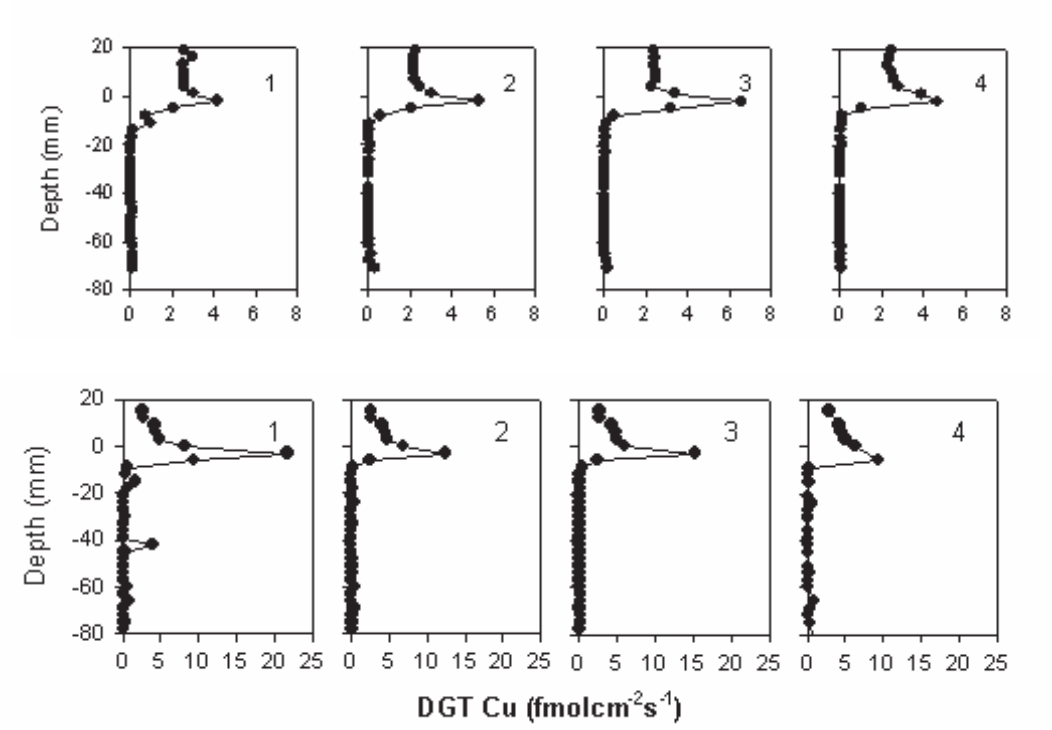

Figure 2: Vertical profiles of DGT-measured fluxes for the harbour sludge: Control (upper panel) and homogenized sediment (lower panel). Numbers 1 to 4 refer to adjacent 3 mm wide vertical columns within a single DGT probes. Please note the difference in scale. The location of the sediment-water interface is represented by zero. The results were published in Tankere-Muller et al., 2007 and also presented in Larsen et al., 2007.

Modelling biogeochemical processes in Sediments

Two major independent models have been developed during TREAD. They both incorporate a user-friendly Graphical User Interface (GUI) that provides input and output of data and specification of the problem through a series of windows. The first development was a model that describes the interaction of sediments and microniches of localized enhanced activity with the diffusive gradients in thin-films (DGT) measurement device. It is known as 2D-DIFS (two-dimensional DGT induced fluxes in sediments). The second development is a full three dimensional model of geochemical processes in sediments, incorporating the provision of microniches. It is referred to here as 3DTREAD.

3DTREAD – a model of sediment geochemistry in three dimensions

A user-friendly, object-orientated computer model that simulates biogeochemical processes in sediments in 3 dimensions has been developed. It is provisionally called 3DTREAD (three-dimensional reaction and transport dynamics). It allows for the decomposition of parcels of organic matter through linkages to the reduction of inorganic components, creating 'microniche' environments. Distributions of trace metals in solution are generated as they are released from decomposing organic material and through the reductive dissolution of iron and manganese oxides or other specified solid phases.

The 3D sediment model uses two separate modules: a 3D model solver and graphical user interface (GUI) windows. To provide a 3D sediment model solver, a 3D finite element framework is created. It deals with physical aspects (diffusion, advection) of the implementation and then results of these calculations are subject to modification by the chemical processes (oxygen reduction) described by relevant differential equations. The model is highly flexible. It is scalable according to the problem set. User-managed text files enable creation of matrices that define the 3D sediment characteristics. The solver algorithm includes three important steps: (1) initializing and assembling the model, (2) preparing necessary tools (factorizing matrices, setting time constants, introducing microniches) and (3) solving the problem and producing output text files and plots to show resulting sediment conditions. The process of solution uses a state of the art FEM library – OFELI – and some fast, scalable, highly optimized methods for introducing chemical processes in a matrix-orientated fashion. The user interface is designed to be friendly and easy to work with. Separation of the solver and GUI also gives extra functionality by providing a facility to run complicated and time-consuming series of analysis (e.g. Monte-Carlo tests of sensitivity). The initial tests of the system have shown that the time of solution is highly dependent on discretisation of the domain (the more elements, the better spatial precision) and number of time steps taken by the solver. It is only slightly influenced by the number of species and chemical processes involved in the calculations, as they are treated as fast matrix manipulations.

Using the sediment models it was possible to verify our understanding of sediment processes. A detailed description of the model and its verification can be found in Sochaczewski et al. (2007).

A fundamental problem with the process modeling is that the scale is completely different from the scale of the environmental problem in harbour basins. The modeling system MIKE from DHI provides state of the art hydraulic and sediment transport models. The models usually applied in studies of harbours for sediment management are set up in Cartesian grids or with unstructured meshes with usual element sizes of 1 to tens of meters – highly different from the 3DTREAD calculating sediment processes in 5 – 50 μm resolution. Hence, up-scaling of a factor 1000 is a necessity for a successful application in sediment management.

Modelling biogeochemical processes in Harbours, estuaries and coastal sediments: Coupling hydraulic and sediment models

A simple up-scaling of processes models of three orders of magnitude is not possible since most fluxes are determined by diffusion which is a non-linear process. Up-scaling is therefore only possible through simplification of the processes. In addition to the suite of physical models a user-friendly solver has been developed which is able to solve ordinary differential equations. This tool is called ECO Lab and is used for modeling all kinds of ecological and biogeochemical processes within the environmental systems. ECO Lab is directly coupled to the hydraulic and transport models. An ecological model with ECO Lab is completely user-defined and the user can save all defined equations and variables in a template form. The results from the TREAD activities were used to write an ECO Lab Template (free distributed) and to verify the model results.

The following compartments of heavy metals were implemented in the Heavy Metal ECO Lab template (HM):

1. The adsorption and desorption of heavy metal to solids in the water column and in the sediment;
2. The precipitation and dissolution of heavy metal species in the sediment;
3. The sedimentation and resuspension of particulate heavy metal species or heavy metal related to solids;

4. The release of heavy metal related to organic matter decomposition,
5. The diffusive transport of dissolved heavy metal at the sediment/ water interface;
6. Sediment mixing due to bio or human activity.

These pools are schematically summarized in figure 3.

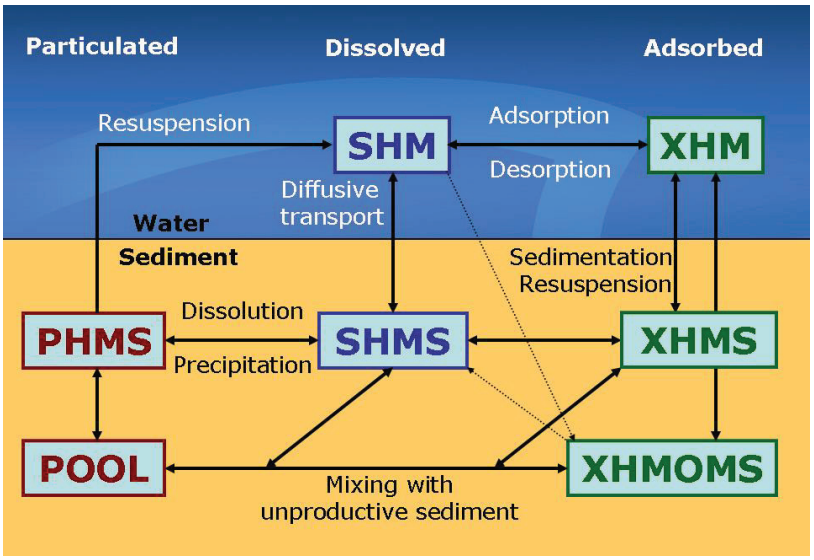

Figure 3. Schematic representation of the model processes simulating the fate of heavy metal in sediments. In this figure, SHM is dissolved Heavy metal in the water column, XHM is adsorbed heavy metal in the water column, PHMS is participated heavy metal in the sediment, SHMS is dissolved heavy metal in the sediment, XHMS is adsorbed heavy metal in the sediment related to inorganic matter, XHMOMS is adsorbed heavy metal in the sediment related to organic matter and POOL is a sink of participated heavy metal in the unproductive part of the sediment. The processes included are adsorption, desorption, sedimentation, resuspension, dissolution, precipitation, chemical alteration and mixing with unproductive sediment. The small arrows represent the organic turnover due to benthic activity.

A comprehensive description of the hundreds of processes and variables moving the heavy metals from one pool to another can be found in the Template description (Eck, 2007).

Using the developed ECO Lab template models were set-up for the mesocosms. The total concentration of heavy metals in water above the sediment is displayed for one of the examined mesocosms. An example calculated Cu concentration in the water column is displayed in Figure 4. In this particular calculation, the system shifted at t=20 and again at t=70 when the oxygen penetration depth increases due to benthic O_2 production. In

summary, the concentration levels and flux rates calculated with the ECO Lab model fits all measured values acceptable well whereby the applicability of the model was verified.

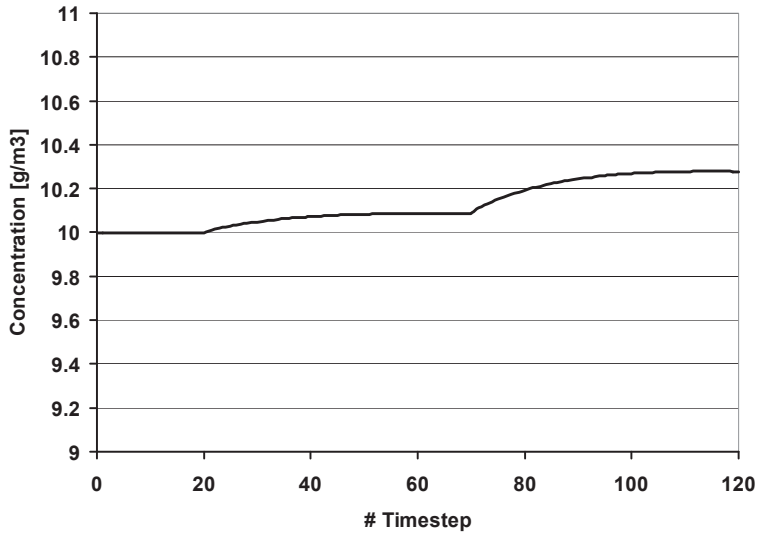

Figure 4. The Cu concentration in the water column in mesocosm experiment. At t=20, the oxygen penetration depth increases with 0.5 mm what triggers a release of heavy metals from Cu bound to the sediment particles. The amount is partially transported to the water column and partially readsorbed to inorganic matter.

References

Beckett PHT (1989) The use of extractants in studies on trace metals in soils, sewage sludges, and sludge treated soils. Advances in Soil Science 9:143-176

Burnton ED, Phillips IR and Hawker DW (2005) Geochemical partitioning of copper, lead, and zinc in benthic, estuarine sediment profiles. J Environ Qual 34: 263-273

Chapman PM, Wang F, Janssen C, Persoone G and Allen HE (1998) Ecotoxicology of metals in aquatic sediments: Binding and release, bioavailability, risk assessment, and remediation. Can. J. Fish. Aquat. Sci. 55: 2221–2243

Davison, W., Grime, G. W., Morgan, J. A. W. and Clarke K. (1991) Distribution of Dissolved Iron in Sediment Pore Waters at Submillimetre Resolution, Nature, 352, 323-325.

Davison, W and Zhang, H. (1994) In situ speciation measurements of trace components in natural waters using thin-film gels. Nature, 367, 546-548.

Davison, W., Fones, G., Harper, M., Teasdale, P. and Zhang, H. (2000). Dialysis, DET and DGT: in situ diffusional techniques for studying water, sediments and soils, in *In Situ Monitoring of Aquatic Systems – chemical analysis and speciation,* Buffle, J. and Horvai, G (Eds.), IUPAC, Wiley, Chichester, 495-569.

Eck, D. van (2007) Heavy Metals in Marine Sediment Systems. DHI Water & Environment EcoLab Template description.

Fenchel T, Glud RN. (1998). Chemolithotrophic veil architectures enhance fluxes at the marine benthic interface. Nature 394: 367-369

Fones GR, Davison W and Grime GW (1998) Development of constrained DET for measurements of dissolved iron in surface sediments at sub-mm resolution. Sci. Tot. Environ, 221: 127-137

Fossing H, Jørgensen BB (1989) Measurement of bacterial sulfate reduction in sediments: Evaluation of a single-step chromium reduction method. Biogeochemsitry 8:205-222

Glud RN, Ramsing NB, Gundersen JK, Klimant I (1996) Planar optrodes, a new tool for fine scale measurements of two dimensional O2 distribution in benthic communities. Mar. Ecol. Prog. Ser. 140:217-26

Harper, M.P., Davison, W., Zhang, H. and Tych, W. (1998) Kinetics of metal exchange between solids and solutions in sediments and soils interpreted from DGT measured fluxes. Geochimica et Cosmochimica Acta, 62, 2757-2770.

Jørgensen BB (1978) A comparison of methods for the quantification of bacterial sulfate reduction in coastal marine sediments I. Measurement with radiotracer techniques. Geomicrobiol Journal 1:11-27

Larsen O, Davison W, Vamvakopoulos K, Møhlenberg F. (2007) Transport and reactions of Contaminants in Sediments. In: Westrich and Förstner (Eds.) Sediment Dynamics and Pollutant Mobility in Rivers. Springer 2007

Revsbech, N. (1989). Diffusion characteristics of microbial communities determined by use of oxygen microsensors. J. Microbiol. Meth. 9: 111-122.

Serbst JR, Burgess RM., Kuhn A., Edwards PA, Cantwell MG, Pelletier MC., Berry WJ, (2003) Precision of dialysis (peeper) sampling of cadmium in marine sediment interstitial water. Arch. environ. contam. toxicol. 45:297-305

Sochaczewski L. Stockdale A. Davison W, Tych W and Zhang H. A 3-dimensional model of transport and reaction in sediments. In Prep.

Shuttleworth, S.M., Davison, W. and Hamilton-Taylor, J. (1999) Two dimensional and fine structure in the concentrations of iron and manganese in sediment pore-waters. Envi. Sci. Technol, 33, 4169-4175.

Tankere-Muller, S, Zhang, H, Davison, W, Finke, N, Larsen, O, Stahl, H and Glud, RN (2007) Fine scale remobilisation of Fe, Mn, Co, Ni, Cu and Cd in contaminated marine sediment. Mar. Chem., 106, 192-207.

Vamvakopoulos K & Larsen O (in prep) A biota friendly and easy to use protocol for plastifying marine sediments. Staining of microbes enclosed in the resin-matrix.

Sulfur and iron diagenesis in post-glacial limnic and brackish sediments of the Arkona Basin (Baltic Sea)

Lars Holmkvist*[a], Kyriakos Vamvakopoulos[a], Alexey Kamyshny, Jr.[a], Volker Brüchert[b], Tim Ferdelman[a] and Bo Barker Jørgensen[a,c]

[a]Biogeochemisty Group, Max-Planck Institute for Marine Microbiology, Celsiusstrasse 1, 28359 Bremen, Germany

[b]Department of Geology and Geochemistry, Stockholm University, Svante Arrhenius Väg 8c, 10691 Stockholm, Sweden

[c]Center for Geomicrobiology, Department of Biological Sciences, University of Aarhus, Ny Munkegade, Bld. 1535, 8000 Århus C, Denmark

Keywords: Baltic Sea; sulfate and iron reduction; non-steady-state diffusion; sulfide oxidation

*Corresponding author: E-mail address: lht@teknologisk.dk 22 Tel.: +45 72 70 23 95

Submitted at Geochimica et Cosmochimica Acta

Abstract

Geochemical studies of long sediment cores were carried out to investigate the geochemical alteration of sulfur and iron species across the different sedimentary units within the Arkona Basin in the southwestern Baltic Sea. This was done by combining pore water profiles with sedimentological and mineralogical analyses of the cores. The data suggest that the modern sediments of the Arkona Basin are subject to non-steady-state diffusion and diagenesis. The accumulation of sulfide in the pore water of the uppermost sediment layer and the diffusion of sulfide down into the underlying sediment lead to sulfidization and precipitation of different iron sulfide minerals. The study additionally presents a possible explanation for an unusual sulfate profile in the pore water by which high concentrations of sulfate is present within the deep limnic deposits. Our results indicate that the high sulfate concentrations are not due to oxidation of reduced sulfur species but rather due to downward diffusion of sulfate during the early Holocene history of the Baltic Sea.

Introduction

The reduction of pore water sulfate to sulfide via dissimilatory sulfate reduction is the dominant pathway of anaerobic organic carbon oxidation in ocean margin sediments (Jørgensen, 1982). Sulfate reduction often leads to a pronounced overprinting of the sediment geochemistry through sulfidization of the minerals and the organic material initially supplied to the seafloor. Studies in the Black Sea and the Baltic Sea have indicated that sulfidization is caused by sulfide formed both during mineralization of organic matter and during anaerobic oxidation of methane (Böttcher and Lepland, 2000; Neretin et al., 2004). The accumulation of sulfide in the pore water and the diffusion of sulfide down into the underlying sediment lead to the precipitation of iron sulfide minerals. The degree of sulfidization is, therefore, generally controlled by the diffusive flux of sulfide from above and the content of reactive iron in the underlying sediment layers (Neretin et al., 2004).

The distinct depth where the downward diffusing sulfide reacts with iron species in the sediment is referred to as the diagenetic front or the sulfidization front. This horizon is often recognized as a distinct black band formed as the results of an accumulation of iron monosulfides and of the magnetic mineral, greigite, Fe_3S_4. The formation of iron sulfide minerals (e.g. iron monosulfides, greigite, and pyrite) during sulfidization have been described in several earlier studies (Berner, 1970; Berner, 1984; Pyzik and Sommer, 1981). The general observation is that several complex oxidation processes of sulfur species occur along with the pyritization process. The downwards diffusing sulfide is ultimately bound by iron and partly oxidized when it reacts with iron oxides at the sulfidization front (Jørgensen et al., 2004). The products of sulfide oxidation include different sulfur intermediates such as zero-valent sulfur (e.g. S^0 and polysulfides), thiosulfate, and sulfite (Zopfi et al., 2004), all of which may undergo disproportionation to sulfide and sulfate. The different sulfur species can be oxidized all the way back to sulfate in the presence of iron and manganese oxides (Aller and Rude, 1988; Burdige and Nealson, 1986; Yao and Millero, 1996). The distribution of sulfide in marine pore waters is thus strongly controlled by the presence of reactive iron species in the sediment (Canfield, 1989b; Canfield et al., 1992). Disproportionation of intermediate oxidation

products of sulfide is also an important process in the reoxidation of sulfide to sulfate (Habicht and Canfield, 2001; Thamdrup et al., 1993; Thamdrup et al., 1994).

The Baltic Sea is the largest brackish water body on Earth and is divided into three main basins (Sohlenius et al., 1996). One of these, the Arkona Basin, is located in the southwestern part of the Baltic Sea (Fig. 1). Stratigraphic analysis of the late glacial to Holocene sediments show alternating limnic and brackish/marine deposits (Björck, 1995; Moros et al., 2002; Neumann, 1981; Neumann et al., 2005; Thiessen et al., 2006). These changes in salinity are associated with the retreat of the Fennoscandian ice sheet and the changes in water-level and connection to the ocean since the last glaciation 13 -14,000 yr BP (Andrèn et al., 2000; Björck, 1995; Moros et al., 2002). The biogeochemistry of the sediments in the Arkona Basin has consequently been subject to non-steady-state deposition and diagenesis. In particular, changing concentrations of sulfate in the sea water since the last glaciation have strongly altered the diffusion flux and depth of sulfate penetration in the sediment. Such changes have affected the rates of sulfate reduction and the degree of sulfidization within the sediment. If a particular environmental situation was maintained for a sufficient length of time, a new steady state situation became established which may be apparent from the geochemical zonation even today.

The present study aimed to understand the geochemical alteration of sulfur and iron species across the different sedimentary units within the Arkona Basin. This was done by combining pore water profiles with sedimentological and mineralogical analyses of sediment cores. The data suggest that the modern sediments of the Arkona Basin are subject to non-steady-state diffusion and diagenesis. We present a possible explanation for an unusual sulfate profile in the pore water by which high concentrations of sulfate is present within the deep limnic deposits. Our results indicate that the high sulfate concentrations are not due to oxidation of reduced sulfur species but rather due to downward diffusion of sulfate during the early Holocene history of the Baltic Sea.

Material and methods

Sampling and site description

The present study is based on two gravity cores (GC A and B) taken during a research cruise of the F/S Heincke during September 8-13, 2006, as part of the EU FP5 project

METROL. Cores were collected at Station "A6" (54° 59.24 ' N and 13° 39.86 ' E) in the Arkona Basin of the western Baltic Sea at a water depth of 45 m (Fig. 1). The position of this station is identical to that of Station 201311 described by Moros et al. (2002). A depth correction was made from the pore water concentration profiles of sulfate and sulfide in GC A and B. This correction demonstrated that 5-10 cm more surface sediment had been lost in GC A during gravity coring compared to GC B.

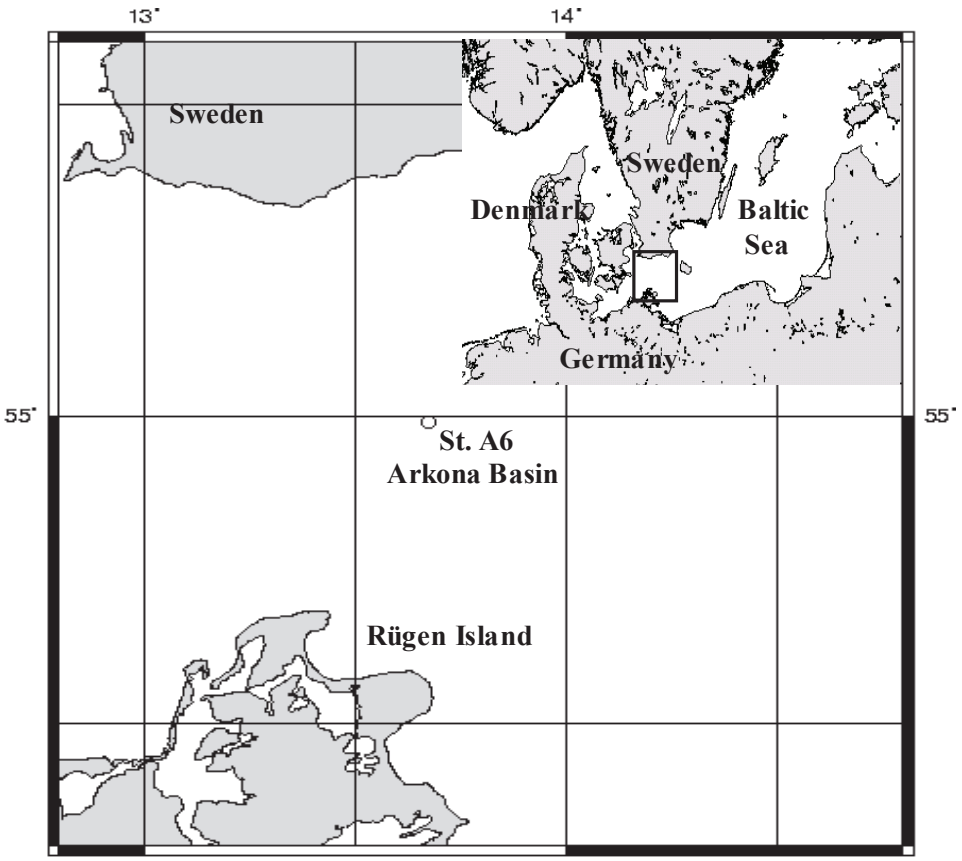

Figure. 1: Map of the study area, Arkona Basin in the Western Baltic Sea, with location of coring site "A6".

Core processing

Methane samples were taken immediately after retrieval of the first gravity core (GC A) by transferring 3 cm^3 of sediment into 20 ml serum vials with 6 ml Milli-Q water. Samples for methane were collected at 20 cm depth intervals throughout the core through small windows cut into the side of the core liner with a vibrating saw. Samples for

porosity and density were similarly taken with 10 ml cut-off syringes at the same depths as methane. Rhizone soil moisture samplers (Rhizosphere Research Products, Wageningen, The Netherlands) were used for the extraction of pore water. The rhizones consists of an inert porous polymer tube with a length of 5 cm and a pore size of 0.1 μm, through which pore fluid is extracted by vacuum created with disposable 10-ml syringes connected to the Rhizone. Pore water for sulfate and sulfide measurements in GC A was extracted from the core liner windows and fixed with 2% zinc acetate. Bottom water samples were collected from separate cores taken by a multiple corer and diluted with 2% zinc acetate for later determination of sulfate and sulfide. Gravity cores and sub-samples were stored at 4°C until processed.

Within three weeks after sampling, the GC A core was scanned for magnetic susceptibility and the GC B core was processed. Pore water was extracted from GC B with 10-cm long Rhizones by gently pushing them into predrilled holes at 5 cm depth intervals along the core. The first ~0.5 ml of extracted pore water was discarded to limit oxidation by oxygen. Pore water samples for the later determination of sulfate and sulfide were prepared by mixing ~1 ml of pore water with 250 μL 1% zinc acetate. Samples for dissolved iron were preserved by acidifying ~1 ml pore water with 100 μL 10% HCl. These samples were collected at the same depths as for sulfate and sulfide in the upper 30 cm and at every 15 cm within 30-205 cm depth. At those depths, non-acidified pore water samples were also used for analysis of polysulfide zero-valent sulfur species (ZVS). At least 5-6 ml of pore water was required from each depth in order to detect the ZVS species. The pore water for ZVS analysis was transferred into anoxic vials immediately after extraction and analyzed within a few hours to prevent oxidation by oxygen. Solid phase sub-samples were taken from the GC B at all depths where pore water was extracted. Sediment sub-samples were collected both in plastic bags and plastic tubes containing zinc acetate (20% w/v) and immediately frozen at -20°C for later analysis of iron, sulfur and carbon.

Pore water analyses

Methane in the headspace of the 20 ml serum vials was analyzed on a gas chromatograph (5890A, Hewlett Packard) equipped with a packed stainless steel Porapak-Q column (6

feet, 0.125 inch, 80/100 mesh, Aglient Technology) and a flame ionization detector. Helium was used as a carrier gas at a flow rate of 30 ml min^{-1}. Sulfate and chloride were analyzed by non-suppressed ion chromatography (100 µl injection volume, Waters, column IC-Pak^{TM}, 50 × 4.6 mm) (Ferdelman et al., 1997). The eluent was 1 mM isophthalate buffer in 10% methanol, adjusted to pH 4.5 with saturated Na borohydrate and the flow rate was 1.0 ml min^{-1}. Hydrogen sulfide (H_2S and HS^-) was determined spectrophotometrically at 670 nm (Shimadzu UV 1202) on zinc-preserved pore water and bottom water samples by the methylene blue method (Cline and Richards, 1969). Dissolved iron was measured according to Stookey (1970) with Ferrozine (1 g L^{-1} in 50 mM HEPES buffer, pH 7) spectrophotometrically at 562 nm (Shimadzu UV 1202).

The analysis of zero valent sulfur (ZVS) species included solid sulfur (S_8), colloidal sulfur (S^0), polysulfides (S_n^{2-}) and polythionates ($S_nO_6^{2-}$). The pH value of each pore water sample was measured with a pH electrode before the analysis and the value was used later for ZVS concentration calculations. A newly developed protocol for detection of ZVS species was based on four steps (Kamyshny Jr. et al., 2006): (1) The detection of inorganic polysulfides by fast single-phase derivatization with methyl trifluoromethanesulfonate (Kamyshny Jr. et al., 2006), (2) detection of the sum of colloidal S^0 and polysulfide ZVS and polythionate ZVS (n>3) with hydrogen cyanide derivatization, followed by HPLC analysis of thiocyanate by the method of Rong et al. (2005), (3) detection of the sum of polysulfide ZVS, colloidal S^0 and solid sulfur by treatment with zinc chloride followed by extraction with chloroform, and (4) the detection of polythionates (n = 4-6) by HPLC (Kamyshny et al. submitted to Limnology and Oceanography). The concentration of polysulfide ZVS was calculated as the sum of all ZVS species detected after derivatization with methyl triflate. The concentration of colloidal ZVS was calculated as the difference between results from the cyanolysis analysis and the concentration of polysulfide ZVS. Finally, the concentration of solid sulfur was calculated as the difference between the chloroform extraction analysis and results from the cyanolysis analysis.

Solid phase analyses

Whole-core magnetic susceptibility measurement was performed with a Bartington Instruments MS2 meter equipped with a MS2C sensor using a scan rate of 1 cm min^{-1}. The sediment density was determined as the wet weight per cm^{-3}. The pore water content was determined from the weight loss after drying at 60°C until constant weight. Total organic carbon (TOC) and total sulfur (TS) were determined in freeze dried sediment that was pretreated with HCl, dried again, and analyzed on a CNS analyzer (Fisons^{TM} Na 1500 elemental analyzer). AVS (acid volatile sulfide = dissolved sulfide + Fe monosulfide) and CRS (Cr-reducible S = FeS_2 + S^0) were determined using the two step acidic Cr-II method (Fossing and Jørgensen, 1989). The volatilized and trapped sulfide was determined spectrophotometrically at 670 nm (Shimadzu UV 1202) by the methylene blue method of Cline (1969). Total zero-valent sulfur (mainly S^0) was extracted from zinc acetate preserved sediment samples in 10 ml pure methanol on a rotary shaker for at least 16 h according to Zopfi et al. (2004). Total zero-valent sulfur was separated on an HPLC with a Zorbax ODS column (125 × 4 mm, 5 µm; Knauer, Germany) with methanol as the eluent (1 ml min^{-1}) and determined from the adsorption at 265 nm. Solid phase ferric iron (Fe(III)) was extracted from sub-samples of the frozen sediment in a 0.5 M HCl solution for 1 h on a rotary shaker. Fe(II) was determined in the supernatant of the HCl extracts by the Ferrozine method (Stookey, 1970). Fe(III) was calculated as the difference between the total iron (Fe(II) + Fe(III)), determined with Ferrozine + 1% (w(v) hydroxylamine hydrochloride), and the Fe(II). Total reactive iron in the sediment was extracted with dithionite-citrate-acetic acid according to Canfield (1989a) and determined with Ferrozine + 1% (w/v hydroxylamine hydrochloride). Solid manganese oxides (Mn(IV)) were measured on the supernatant of the dithionite-extracts by flame atomic absorption spectrometry (Perkin Elmer, Atomic Absorption Spectrometer 3110).

X-ray diffraction analysis (XRD) was performed on dried and homogenized sediment samples from all investigated depths in the GC B core. XRD analysis was done on a Philips X'Pert Pro multipurpose diffractometer equipped with a Cu-tube (k□ 1.541, 45 kV, 40 mA), a fixed divergence slit of ¼°, a 16 sample changer, a secondary monochromator, and a X'Celerator detector system. The sample measurement was

completed by a continuous scan from 3 – 85° 2θ, with a calculated step size of 0.016° 2θ (calculated time per step was 100 seconds). The identification of different minerals was done with the Philips software X'Pert HighScore™, which, besides the mineral identification, gives a semi-quantitative value for each identified mineral on the basis of Relative Intensity Ratio (R.I.R)-values. The R.I.R.-values were calculated as the ratio of the most intense impulse of a specific mineral to pure corundum (I/Ic) according to the "matrix-flushing method" (Chung, 1974). Finally, full quantification was done using the full-pattern quantification software QUAX (Vogt et al., 2002).

Magnetic nodules

Single magnetic nodules were collected at 68 cm sediment depth in GC B using a handheld magnet. The nodules were immediately embedded in a methacrylate resin, trimmed with a diamond band saw, and polished with an Al_2O_3 paraffin suspension. Prior to scanning electron microscopy (SEM), the surface of the polished nodules was coated with carbon to avoid charging effects. The surface morphology and texture were recorded by conventional backscattered electron and secondary electron imagery. Specific elements inside the nodules were identified using energy dispersive x-ray analysis (EDS) (Oxford INCA 300).

Sulfur and oxygen isotopes

Sulfur and oxygen isotopes in sulfate, and sulfur isotopes in sulfide and pyrite were determined on the zinc acetate preserved pore water samples and on the CRS fraction of GC B using a Thermo Delta Plus isotope ratio mass spectrometer. Pore water sulfate was precipitated as barium sulfate by the addition of 5 % barium chloride solution. The barium sulfate precipitate was collected by filtration through a 0.45 µm HA-filter and the precipitate was combusted to sulfur dioxide, catalyzed by vanadium oxide. The combustion of sulfur compounds in the precipitate for sulfide isotopes were filtered through a 45 µm HA-filter where after the filters were submerged in a 5% silver nitrate solution. The precipitate was then combusted in a mass spectrometer.

Modelling of pore water data

The modelling software, PROFILE, of Berg et al. {, 1998 #1630} was applied to the measured pore water data to calculate net rates of production or consumption of sulfate, sulfide, and dissolved iron. This one-dimensional numerical modelling program first divides the sediment into an arbitrary number of equidistant zones, each with a constant process rate, whereby an objective selection of the simplest process rate distribution that optimally reproduces the measured concentration profiles is provided. The criterion for optimal fit is to minimize the sum of squared deviations (SSE) from the data for each zone with different numbers of equally spaced zones. The model provides F tests for different fits, and suggests the minimal number of zones that provide an optimal fit. The model ensures continuity between zones and thus provides also fluxes of the solutes. The boundary conditions were:

Sulfide (H_2S+HS^-): Boundary conditions were concentration at 67.5 cm = 0.00 mM and flux at 67.5 cm = 0.00 mmol m^{-2} d^{-1}. The molecular diffusion coefficient, $D(H_2S/HS^-)$ = 11.9 10^{-6} cm^2 s^{-1} calculated from the degree of dissociation at a pH of 7.4.

Iron (Fe^{2+}): Boundary conditions were concentration at 52.5 cm = 0.00 mM and concentration at 257.5 cm = 0.346 mM. The molecular diffusion coefficient, $D(Fe^{2+})$ = 4.26 10^{-6} cm^2 s^{-1}.

Results

Four sedimentary units were identified between the surface and 3 m depth according to color and sand layers. The different sediment layers are here described as Units I to IV in accordance with the stratigraphy described from the central Baltic Sea by Böttcher and Lepland (2000) and from the southern Baltic Sea by Moros et al. (2002) (Fig. 2).

Unit IV: 0 - 45 cm depth. Holocene mud from the modern Littorina period, 0-6,500 cal yr BP. Marine/brackish olive-black mud with a strong smell of sulfide. TOC values were 3-6 wt %.

Unit III: 45 - 70 cm depth. From the Ancylus Lake, deposited ca 6,500-10,600 cal yr BP. Greyish lacustrine clay with black spots at 45 – 68 cm depth, reddish-brown clay at 68-70 cm depth, and a sand layer at 70 cm depth which probably marks the

transition from the Ancylus to the Yoldia Lake. Magnetic nodules of sub-mm to mm size were observed at the boundary between grey and reddish-brown sediment at 68 cm. TOC values were 0.6 - 2 wt %.

Unit II: 70 - 78 cm depth. The Yoldia Sea and Yoldia Lake, deposited ca 10,600-11,600 cal yr BP. Lacustrine/brackish reddish-brown clay with a thick sand layer at 78 cm which probably marks the transition from the Yoldia Lake to the Baltic Ice Lake (Billingen-2 drainage) (Moros et al., 2002). TOC values were 0.7 wt %.

Unit I: 78 - 285 cm depth. The Baltic Ice Lake, deposited >11,600 cal yr BP. Lacustrine reddish-brown clay with a sand layer at 130 cm depth which probably marks the Billingen-1 drainage (Moros et al., 2002). TOC values were >1 wt % with high values of total inorganic carbon (TIC) increasing with depth (Moros et al., 2002) (data not shown).

Geochemistry of carbon, sulfur and iron

Total organic carbon was high, 5-6% dry weight, in the most recent Holocene mud and decreased with depth to reach a constant low level of ca 0.7% from the lower part of Unit III (Fig. 2). TS was around 2% dry weight in Unit IV and decreased to <0.2% from the lower part of Unit III.

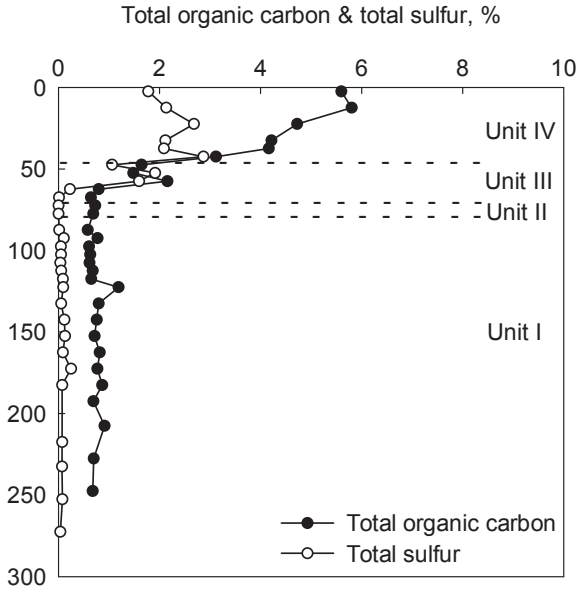

Figure 2: Total organic carbon and total sulfur (% dry weight) distributions at Station A6. The sedimentary Units I-VI are marked.

The sulfate concentration showed an unusual distribution as it decreased from 13 mM in the bottom water to a minimum of 4 mM at 22-28 cm depth below which it increased steadily to 6-7 mM at 250 cm (Fig. 3 A). The concentration of chloride dropped steeply from 318 mM in the bottom water to around 250 mM throughout the subsurface sediment (Fig. 3 A). Free sulfide was present from the sediment surface to the bottom of Unit III with maximum concentrations of 1 mM (Fig. 3 B). The concentrations of methane varied around 5 µM with no clear trend and did not exceed 10 µM at any depth (data not shown). Dissolved iron was not detected in the sulfide zone but increased from just beneath this zone at the grayish to reddish-brown sediment transition in Unit III (Fig. 3 B). Dissolved iron reached 300 - 400 µM within the non-sulfidized limnic sediment of Unit I.

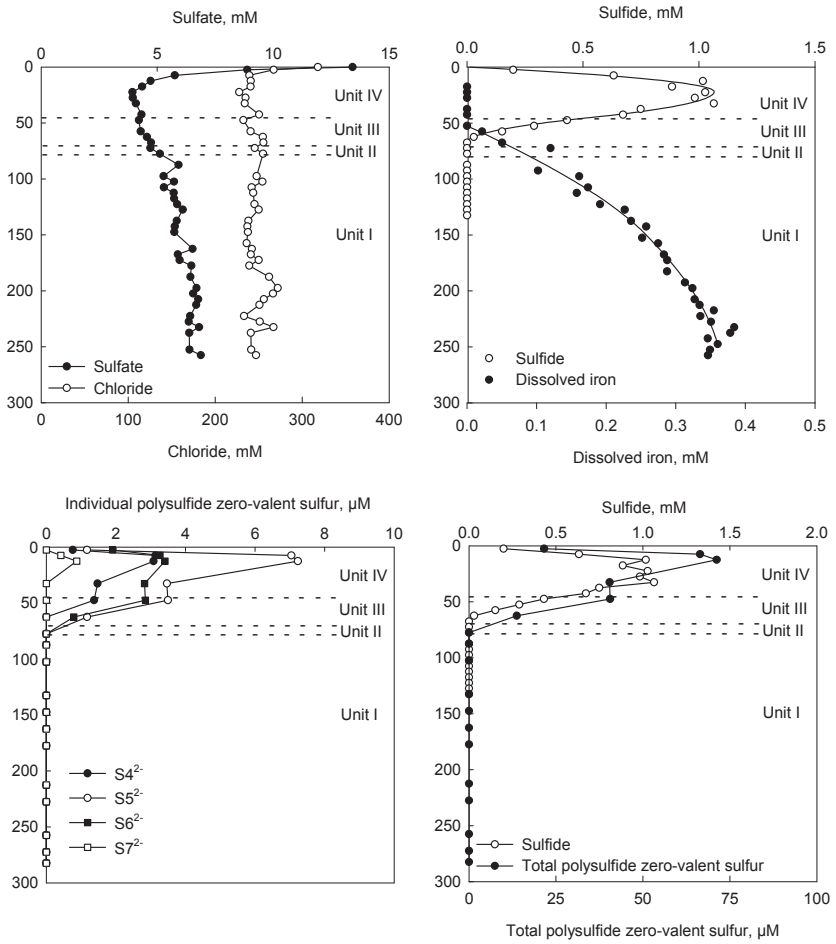

Figure 3: Pore water concentrations at Station A6 of (A) sulfate and chloride, (B) sulfide and dissolved iron as well as modeled concentrations (lines), (C) individual zero-valent sulfur species and (D) sulfide and total polysulfide zero-valent sulfur.

Estimated concentrations of sulfide and dissolved iron from PROFILE modeling followed the measured concentrations closely (Fig. 3 B), and we were able to estimate the depth integrated net production /and consumption of sulfide and dissolved iron. A net production of sulfide was found in the 0-22 and 22-45 cm depth intervals which reached 0.496 and 0.215 mmol m^{-2} d^{-1}, respectively (data not shown). Further, a net consumption of sulfide was estimated to 0.214 mmol m^{-2} d^{-1} in the 45-67 cm (data not shown). The total production of dissolved iron in the 52-250 cm depth interval was estimated to 0.0054 mmol m^{-2} d^{-1} and the total flux up to 52 cm was -0.0058 mmol m^{-2} d^{-1} (data not shown). A comparison of the flux estimates of sulfide and dissolved iron reveals that the flux of sulfide towards the sulfidization front (Unit III) is about 36 higher than the upward flux of dissolved iron.

Peak concentrations of individual polysulfide ZVS species occurred in Unit IV (Fig. 3 C). They differed according to prediction for polysulfide solutions at equilibrium with S^0 under moderately alkaline conditions, ($[S_5^{2-}]>[S_6^{2-}]>[S_4^{2-}]>[S_7^{2-}]$) (Kamyshny Jr. et al., 2004). The sum of all the polysulfide ZVS species resulted in a peak concentration of 71 µM at 12.5 cm depth (Fig. 3 D) and largely matched the depth profile of sulfide. This implies that polysulfide ZVS species were in equilibrium with sulfide in the pore water (Kamyshny Jr. et al., 2003). Dissolved manganese increased slightly with depth but remained <30 µM throughout the core, except for a stray high value at 57 cm (data not shown).

The magnetic susceptibility was low in the highly sulfidic Unit IV and increased with depth to reach a high and distinct peak of 76 SI at the transition between Unit III and II (Fig. 4 A). This peak was due to magnetic nodules which were abundant at the transition from gray to reddish-brown sediment at 68 cm depth. The magnetic susceptibility was relatively high, 25-30 SI, throughout the iron-rich, orange to brown colored limnic sediment of Unit I.

Total reactive iron was low, ca 100 µmol cm^{-3}, in the brackish sediment and increased to nearly 1000 µmol cm^{-3} in the limnic Unit I (Fig. 4 B). Total Fe(III) determined by HCl extraction was also low in Unit IV and increased down through Unit III (Fig. 4 C). A

comparison of Fig. 4 B and C shows that most iron below Unit IV was in a non-reduced state. The concentration of Mn(IV) was low throughout Units IV to II and higher in Unit I (Fig. 4 D).

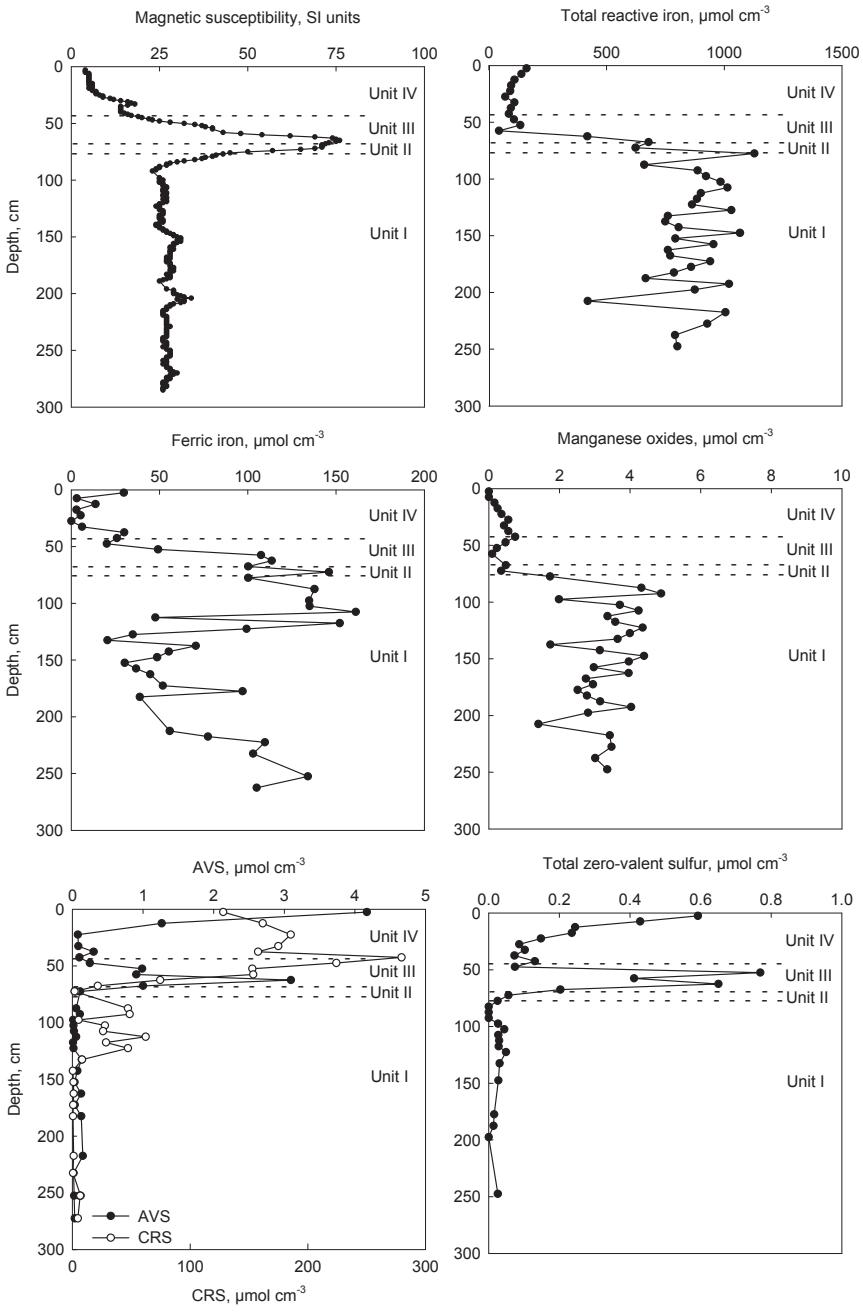

Figure 4: Depth distributions of (A) magnetic susceptibility, (B) total reactive iron, (C) ferric iron, (D) manganese oxides, (E) AVS and CRS, and (F) total zero-valent sulfur.

The AVS concentration dropped steeply with depth from 4 μmol cm^{-3} at the sediment surface to 0.1 μmol cm^{-3} at 22 cm depth. It remained low through the rest of the core with the exception of a sharp peak at the bottom of Unit III (Fig. 4 E). High concentrations of chromium reducible sulfur (CRS, mainly FeS_2) were found in Units IV and III-IV (Fig. 4 E). CRS was low through most of Units II and I with elevated values in the upper part of Unit I. The concentration of total zero-valent sulfur decreased from 0.6 to 0.1 μmol cm^{-3} between the sediment surface and 25 cm depth (Fig. 4 F). There was a second large peak in total zero-valent sulfur within the Unit III layer with a maximum concentration of 0.8 μmol cm^{-3}. In Unit I the concentration of total zero-valent sulfur did not exceed 0.05 μmol cm^{-3}.

Magnetic nodules

Magnetic nodules, extracted by a magnet, were found in the transition of gray to reddish-brown sediment (Unit III to II) where also a sharp peak of magnetic susceptibility was detected. The nodules had circular, elliptical, or irregular elongated shapes and varied in size from a few tens of μm to several mm across. Surface scans of whole, intact nodules with SEM revealed that some nodules were covered by framboidal pyrite. The EDS analyses showed that the interior of the magnetic nodules was heterogeneous and contained iron, sulfur, silicate, barium, aluminum and magnesium. Furthermore, traces of potassium, calcium, manganese and phosphorus were found. From the ratios of sulfur and iron we were able to identify iron monosulfide (FeS), greigite (Fe_3S_4) and pyrite (FeS_2) in most of the nodules. Furthermore, we were able to identify five different types of mineral associations in the magnetic nodules: (1) nodules that consisted of mostly iron and sulfur minerals such as Fe_3S_4 and FeS_2 (Fig. 5 A), (2) nodules containing iron sulfide minerals in close association with large silicate minerals (data not shown), (3) barite nodules with silicate enclosures (Fig. 5 B), (4) iron sulfide nodules composed of minor granules (Fig. 5 C-D), and (5) iron sulfide nodules that contain crystal-like structures of sulfur (Fig. 5 E-H).

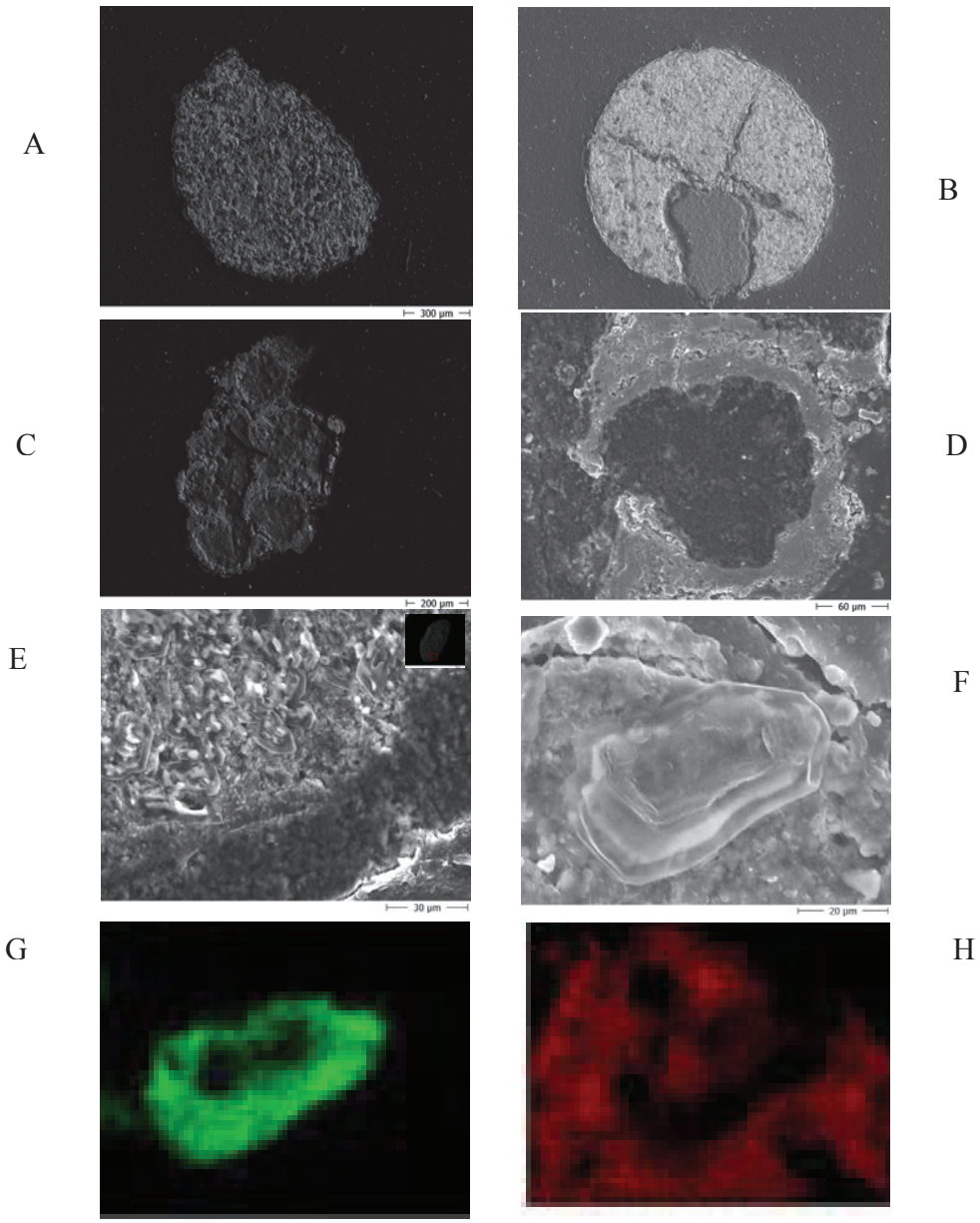

Figure. 5 Scanning electron micrographs of sliced magnetic nodules from the depth of peak magnetic susceptibility. (A) Surface scan of sliced nodule that consists mostly of iron-sulfide minerals. EDS analysis revealed the presence of Fe_3S_4 in the center and FeS_2 in the periphery of the nodule. (B) Surface scan of a sliced barite nodule. The light gray area is barite whereas the dark area consisted of silicate. (C) Surface scans of a sliced nodule with a very heterogeneous interior which probably was a conglomerate of smaller nodules. (D) Magnification of the lower region of the nodule in Fig. 5 C. EDS analysis of the dark inner area revealed FeS while the light-gray area was FeS_2. (E) Magnification of the lower region of a sliced iron-sulfide nodule (small picture in the top right corner). The gray crystal-like structures in the middle of the nodule are rich in sulfur. (F) SEM image of a large sulfur crystal. (G) The same image as in Fig. 5 G but showing sulfur in green. (H) The same image as in Fig. 5 G but showing iron in red.

X-ray diffraction

XRD analyses were done to describe the most abundant minerals, in particular those containing Fe(III). The largest heterogeneity and the highest diversity of minerals were found in Unit III. In Unit IV, on the contrary, the number of different minerals was lowest. Silicate containing minerals such as quartz (subclass tectosilicate) and albite (feldspar) were the most abundant minerals in nearly all of the investigated sediment samples. FeS_2 was detected only in Units IV and III whereas different types of Fe(III) containing silicates were found in Units I-III. For example, Fe(III)-bearing phyllosilicates such as illite, clinochlore, zinnwaldite and licate were found together with inosilicates such as magnesio-arfvedsonite, hastingsite and riebeckite in Unit III. Only the Fe(III) containing phyllosilicates, clinochlore and cronstedtiteesides, were found in Units I-II. Other interesting Fe(III)-bearing minerals, such as the hydrated phosphates, koninckite and beraunite, were observed in Units I-II.

Stable sulfur and oxygen isotopes

Fig. 6 A to D presents results from the analyses of sulfur and oxygen isotopes. The bottom water value of $\delta^{34}S_{sulfate}$ was +21‰ (Fig. 6 A), similar to the mean value of modern sea water (Böttcher et al., 2007). The pore water values of $\delta^{34}S_{sulfate}$ increased sharply just below the sediment surface where the first pore water value at 17 cm was +69 ‰ (Fig. 6 A). There was a broad maximum of $\delta^{34}S_{sulfate}$ which extended from Unit IV to I with highest values of +74 ‰. Below this peak, $\delta^{34}S_{sulfate}$ decreased gradually to ca +50‰ at the bottom of the core.

The bottom water $\delta^{18}O_{sulfate}$ was +9‰, comparable to the mean value of modern sea water (Blake et al., 2006) (Fig. 6 B). There was a steep subsurface increase in the pore water value of $\delta^{18}O_{sulfate}$ to 22 at 17 cm depth. The pore water $\delta^{18}O_{sulfate}$ remained between +22 and +24‰ throughout the rest of the core. However, a few of the data points within Unit II to III were very low, +5 to +8‰, possibly due to contamination from water bound in clay or salt minerals accompanying the $BaSO_4$ precipitate. The isotopic signature of dissolved sulfide could be measured only within Unit IV (Fig. 6 C). The $\delta^{34}S_{sulfide}$ increased steadily from -3 to +4‰ between 5 and 40 cm depth (Fig. 6 C). The $\delta^{34}S_{CRS}$

decreased from -29 to -40‰ between 2 and 42 cm depth in Unit IV and then increased from -40 to -11‰ through Unit III at 42 to 62 cm (Fig. 6 D). In Unit I the $\delta^{34}S_{CRS}$ decreased slightly to ca -20‰.

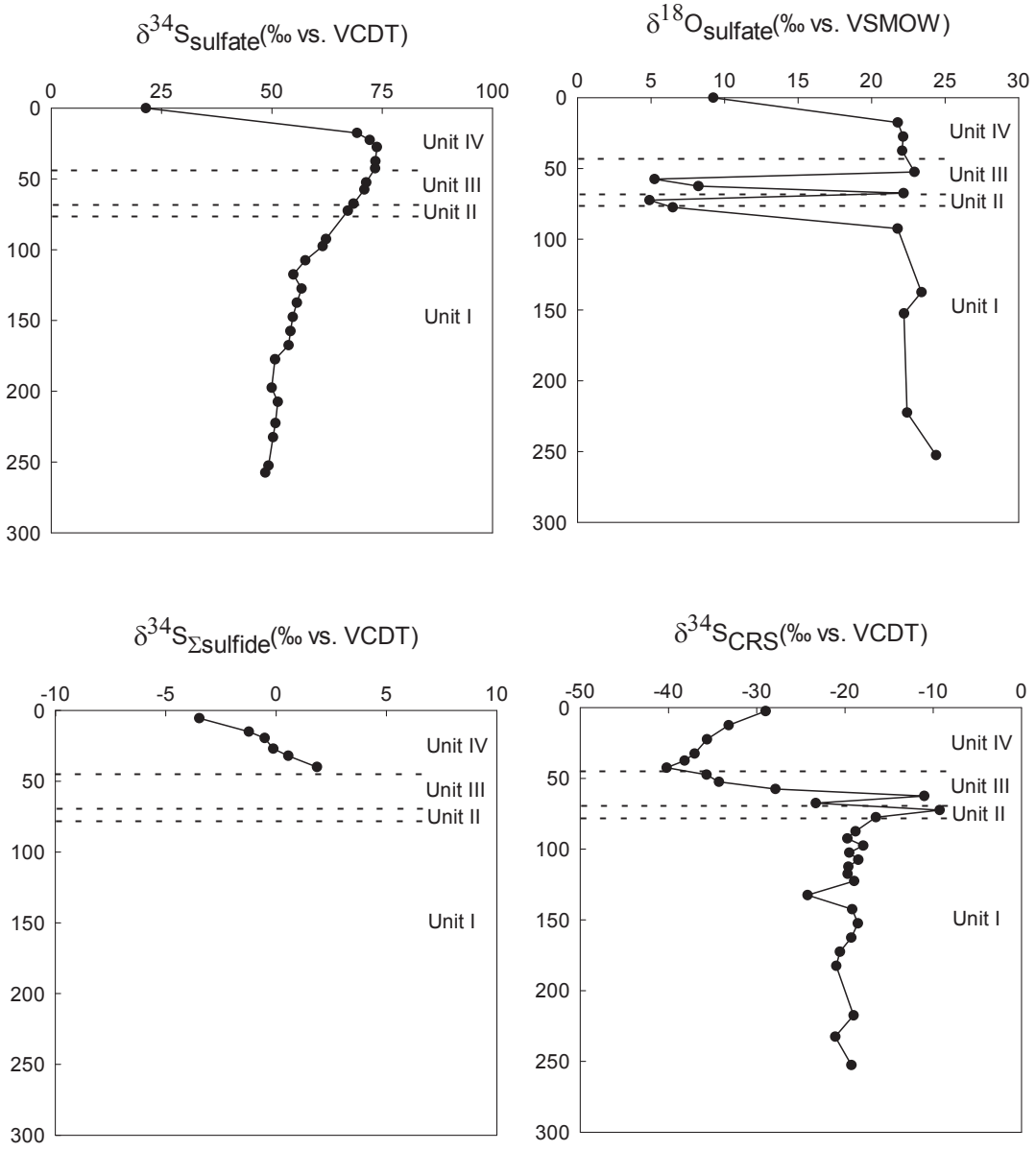

Figure 6: Figure shows results from the isotopic analysis of sulfur and oxygen isotopes of sulfate, sulfide and pyrite. (A) Isotopic composition of $\delta^{34}S_{sulfate}$ (‰ vs. VCDT) in pore water versus depth (B) Isotopic signal of $\delta^{18}O_{sulfate}$ (‰ vs. VSMOW) in pore water versus depth (C) Isotopic composition of $\delta^{34}S_{\Sigma sulfide}$ (‰ vs. VCDT) in pore water versus depth (D) Isotopic composition of $\delta^{34}S_{CRS}$ (‰ vs. VCDT) in CRS (pyrite) versus depth. The different macroscopic sedimentary units are marked as Unit I-VI.

Discussion

Sulfate reduction

Sulfate reduction took place at high rates in the Holocene mud of Unit IV as indicated by the sharp decrease in pore water sulfate just below the sediment surface and by the broad peak in free sulfide (Fig. 3 A and B). The high sulfate reduction rates implied for Unit IV are consistent with the high organic carbon concentration (Fig. 2). They are also consistent with high sulfate reduction rates measured experimentally with $^{35}SO_4^{2-}$ tracer in similar sediments from other areas of the Baltic Sea (Piker et al., 1998; Thamdrup et al., 1994).

The steep drop in the concentrations of sulfate near the sediment surface is accompanied by a drop in chloride. Yet, the sulfate/chloride ratio also showed a steep decrease, from 0.033 to 0.020 molar ratios over the top 10 cm depth interval (data not shown). This corresponds to a 40% depletion of the pore water sulfate and demonstrates that sulfate is being consumed by sulfate reduction in addition to the dilution with low-salinity pore water. Below 5 cm depth, chloride remained constant down to 250 cm depth. The sulfate concentration as well as the sulfate/chloride ratio increased again very gradually below a minimum in Unit IV. This indicates that sulfate reduction rates are low below Unit IV and that sulfate diffuses upwards from the higher concentrations in Unit I.

A previous study from the Arkona Basin showed similarly that the concentration of sulfate in the pore water increases with depth from Unit III to Unit I (Olaf, 2005). This increase was explained as the result of either, seawater contamination, sulfide oxidation during coring, sampling and storage, or in situ oxidation of downward diffusing sulfide. We have here observed a similar unusual sulfate profile after careful handling of two independent gravity cores and are confident that we can exclude the two first explanations. We propose that the sulfate profiles are correct and are due to the glacial to post-glacial history of sedimentation and sulfate reduction.

During the late-glacial melting period large amounts of organic-poor silt and clay were deposited in the Baltic Ice Lake (Unit I). The first intrusion of seawater into the Baltic occurred during the Yoldia Sea stage (10.0-9.5 kyr BP) where the salinity reached ~10‰

(Mörner, 1995; Wastegård et al., 1995). At that time, the activity of sulfate reduction within the limnic Yoldia and Baltic Ice Lake sediments was probably very low due to the low organic content and thus allowed diffusion of sulfate deep into the sediment. The barite nodules observed in our study suggest that sulfate precipitation with barium may have occurred at some time during this stage. Only after the deposition of organic-rich mud in the Littorina sediment started about 6,500 cal yr BP, sulfate reduction also gradually increased as a result of the higher sedimentation of organic detritus and the higher sulfate concentration of the water column. Sulfate may have continued to diffuse into the deep late-glacial deposits during the early Littorina stage, however, because the Holocene layer was still too thin to deplete sulfate to a minimum lower than the concentration deeper in the sediment. Only much later did the Unit IV mud grow to a thickness that reversed the sulfate gradient and led to the upwards flux of sulfate which is observed today.

Iron reduction and iron minerals

While Unit IV is dominated by sulfate reduction, the presence of active iron reduction below Unit III is indicated by the accumulation of dissolved iron (Fig. 3 B). Our data show the presence of reducible iron oxides that may be used by the iron reducing communities. Thus, the concentrations of reactive iron and Fe(III) increased strongly with depth from the bottom of Unit III and down through units II and I (Fig. 4 B–D). These iron species probably entered the Baltic Sea during the erosion of different glacial source deposits or via river inputs (Gingele and Leipe, 1997). The reddish-brown color of the sediment below 68 cm indicates the presence of hematite (Moros et al., 2002). Accordingly, the high concentration of reactive iron extracted below Unit IV (Fig. 4 B) suggests the presence of goethite and hematite. Both of these are extracted with dithionite (Canfield, 1988; Kostka and Luther, 1994), whereas easily reducible iron oxides (e.g. ferihydrite) are mainly extracted with HCl (Chou and Zhou, 1983; Kostka and Luther, 1994). The XRD analysis also revealed the presence of Fe(III)-bearing minerals within Units I-III but indicated, on the other hand, that the content of hematite is low in all sediment units (it should be taken into account that only minerals of high concentration are likely to be detected with the XRD technique).

Sulfur and oxygen isotopes

The isotopic composition of sulfate, $\delta^{34}S_{sulfate}$, was a mirror image of the sulfate concentration and supported the conclusion that the sulfate minimum in Unit IV is due to ongoing bacterial sulfate reduction (Fig. 6 A). The $\delta^{34}S_{sulfate}$ maximum of +74‰ at 25 cm depth is extremely high considering that only 40% of the sulfate was depleted due to sulfate reduction. The $\delta^{34}S_{sulfide}$ increased from -3 to +2‰ down through Unit IV (Fig. 6 B) and, thus, the isotopic difference between coexisting sulfate and sulfide reached 72‰ at the bottom of Unit IV. This strongly exceeds the isotopic fractionation observed during sulfate reduction in pure cultures and is also higher than values normally observed in marine sediments. The strong fractionation occurs here in sediment with high sulfate reduction rates and high sulfide concentration, both of which are generally associated with less sulfur fractionation. We propose that the large isotopic difference between sulfate and free sulfide may be a result of sulfide reoxidation due to reaction with the large amounts of Fe(III). When this reoxidation is coupled to disproportionation, an additional isotopic fractionation occurs (Canfield and Thamdrup, 1994).

At Station A6 the high $\delta^{34}S_{sulfate}$ values were, thus, not accompanied by a similar increase in $\delta^{34}S_{sulfide}$ and were not the result of anaerobic methane oxidation as has been observed in other sediments (Jørgensen et al., 2004). As the sulfate concentration did not drop below 40% of the relative seawater value, methane concentrations remained low, around 5 µM. In spite of the low degree of sulfate depletion, the oxygen isotope composition in sulfate indicated strong enrichment of ^{18}O in the sulfate, with $\delta^{18}O_{sulfate}$ values 13‰ more positive than those of the overlying sea water (Fig. 6 B). This indicates that the sulfate pool has undergone bacterial sulfate reduction and possibly also regeneration from sulfide oxidation, not only within the Holocene mud but also in the underlying deep limnic deposits.

The $\delta^{34}S_{CRS}$ data are difficult to interpret in terms of the modern sulfur cycle in the sediment column and are largely a result of earlier sulfur diagenesis. The $\delta^{34}S_{CRS}$ decreased down through Unit IV, from -29 to -41‰, and must have been formed from sulfide more depleted in ^{34}S than the present pore water sulfide of -3 to +2‰. The decrease in $\delta^{34}S_{CRS}$ down through Unit IV could be due to a higher degree of in situ

sulfide reoxidation and disproportionation as the early Holocene mud layer was thinner and less sulfidic. Down through Unit III, where the modern sulfidization front is located, there is apparently a transition from the marine sulfide formed under excess sulfate, and therefore highly depleted in ^{34}S, to the limnic sulfide in Unit I, formed under sulfate limitation during the late-glacial period and therefore less depleted in ^{34}S. A study by Böttcher and Lepland (2000) from the central Baltic Sea observed a similar increase in the $\delta^{34}S$ values of total sulfur (mainly pyrite) within the Unit III layer. This increase was explained from mixing of downward diffusing sulfur species with initial, syngenetic sulfur in Ancylus Lake sediments or from a reservoir effect. The high concentrations of sulfate observed in our study excludes that a reservoir effect is causing the increase in the $\delta^{34}S$ values of sulfide in the CRS fraction. Thus, our data indicate that reoxidation and/or precipitation of sulfide with reactive iron species in the Ancylus sediment (Unit III) is causing the decrease in the degree of sulfur isotope fractionation.

Sulfidization and formation of iron sulfide minerals

The color change from gray to reddish-brown within Unit III is likely the result of progressing diagenesis rather than a change in the quality of the deposited sediment (Moros et al., 2002). The color change marks the lower boundary of the downward diffusing sulfide which is produced within Unit IV and reacts with dissolved iron and iron minerals in the underlying sediment. At this sulfidization front a band of greigite nodules occurs, coinciding with a sharp peak in FeS (Fig. 4 E). It also coincides with the steepest gradient in FeS_2. Since the rate of FeS_2 accumulation is the product of its gradient and the sedimentation rate, this is also the depth where the highest rate of pyritization takes place. The Fe_3S_4 is probably an intermediate in the sequence of reactions that lead from FeS to FeS_2. Earlier studies have shown that Fe_3S_4 formation in marine sediments is favoured by a high concentration of reactive iron and low organic matter content (Kao et al., 2004). Both factors result in low sulfide concentration. At the sulfidization front these conditions of high iron and low sulfide are combined with high fluxes of both iron and sulfide. Yet, at the sulfidization front free sulfide and free iron in the pore water meet and react at very low concentration (Fig. 3 B).

The SEM and EDS analyses have helped us to identify the micro-texture and mineral types within the magnetic nodules containing Fe_3S_4. Our study therefore supports the expectancy that Fe_3S_4 rather than magnetite is the main mineral responsible for the elevated magnetic signals often observed in marine sediments (Neretin et al., 2004). The content of Fe_3S_4 in each nodule was not quantified but scans of several nodules indicated that Fe_3S_4 makes up only a minor fraction of the total amount of minerals present in each nodule. This is in accordance with Roberts and Weaver (2005), who found that Fe_3S_4 is often associated with a range of different authigenic and detrital mineral phases such as nodular and framboidal FeS_2, detrital sheet silicates, authigenic clays (smectite and illite), siderite, and gypsum. We found that Fe_3S_4 within each nodule was present mainly with iron and sulfur minerals (e.g. S^0, FeS and FeS_2). This finding also suggest that Fe_3S_4 is formed during pyrite formation in the reaction sequence from FeS to FeS_2 as proposed in several earlier studies (Berner, 1967; Berner, 1970; Berner, 1984; Sweeney and Kaplan, 1973).

The conversion of the metastable FeS fraction (the AVS fraction) into FeS_2 is still largely unresolved and has been the subject of a number of studies in which several transformation reactions are proposed. The equilibrium of polysulfides with sulfide and solid sulfur has in general been investigated intensively the past 50 years (Amend and Shock, 2001; Giggenbach, 1972; Kamyshny Jr. et al., 2004; Kamyshny Jr. et al., 2007; Maronny, 1959; Teder, 1971; Wagman et al., 1968). However, no other workers have to our knowledge previously tried to compare marine depth profiles of polysulfides with FeS_2 in the sediment. The decline in the concentration of polysulfides and the increase in FeS and FeS_2, within Unit III, suggest that FeS_2 formation occurrs with polysulfides as first proposed by Berner (1970) and Luther (1991). The calculated fluxes of sulfide and dissolved iron obtained from the PROFILE modelling showed that the downward flux of sulphide within the sulfidization front (Unit III) was much larger than the upward flux of dissolved iron. Presumably, FeS formation occurs when sulfide and dissolved iron reacts in a 1:1 stoichiometry. Interestingly, our calculated model data on sulphide and dissolved iron therefore indicate that a large excess of sulfide probably react with different solid-phase iron minerals instead of only dissolved iron.

Our data shows the existence of FeS_2 deep within the limnic sediment layers especially in the 72.5 to 142.5 cm depth interval of Unit I-II. Presumably, formation of FeS_2 within the different sediment deposits of the Arkona Basin has varied since the early history of the Baltic Sea under, because of changing biogeochemical conditions. For instance, the inwash of more saline water into the limnic sediment deposits during the Yoldia Sea stage has probably caused elevated rates of sulfate reduction and thereby a higher production FeS_2.

Oxidation of sulfur species

The present study demonstrates that much of the sulfide oxidation in this Baltic sediment takes place sub-surface, below the oxic and oxidized surface zones. A similar observation was made by Böttcher and Lepland (2000) from a study in the central Baltic Sea. Fe(III) and Mn(IV) below Unit IV most probably constitute an efficient barrier which oxidizes and binds the downward diffusing sulfide. The increasing content of reactive iron and Fe(III) within the Ancylus sediment layer (Unit III) is thus not only the result of differences in the deposition of iron minerals but may show that Fe(III) is converted into pyrite when it reacts with sulphide. The high concentrations of total zero-valent sulfur are most likely indicative of sulfide oxidation as previous studies have shown that sulfide oxidation with Fe(III) and Mn(IV) leads to the production of elemental S^0 (Burdige and Nealson, 1986; Pyzik and Sommer, 1981; Steudel, 1996; Yao and Millero, 1996). Further, the oxidation of FeS and FeS_2 with Fe(III) and/or Mn(IV) may also lead to the production of S^0 (Aller and Rude, 1988; Moses et al., 1987; Schippers and Jørgensen, 2001). The oxidation of FeS_2 involves an Fe(II)/Fe(III)-shuttle between the mineral surfaces of FeS_2 and manganese oxides (Schippers and Jørgensen, 2001). In the Arkona Basin, Fe(III) is probably the most important oxidant for sulfide since the concentration of Fe(III) is up to 30-fold larger than of Mn(IV). Yet, the high concentration of dissolved manganese in Unit III suggests that also Mn(IV) is involved in the oxidation/reduction reactions. S^0 and other intermediates of sulfide oxidation may be oxidized all the way back to sulfate through disproportionation reactions, thereby partly closing the internal sulfur cycle of the sediment.

Summary

Our data shows that the biogeochemistry of the sediments in the Arkona Basin has been subject to non-steady-state processes. In particular, changing concentrations of sulfate in the sea water since the last glaciation may have altered the diffusion flux and depth of sulfate penetration in the sediment. We present a possible explanation for an unusual sulfate profile in the pore water by which high concentrations of sulfate is present within the deep limnic deposits. Our study indicate that the high sulfate concentrations are not due to oxidation of reduced sulfur species but rather due to downward diffusion of sulfate during the early Holocene history of the Baltic Sea. Nonetheless, the increase in reactive iron and Fe(III) together with the distinct peak in total zero-valent sulfur within the Ancylus sediment layer (Unit III) suggest that reoxidation of different sulfur species (H2S, FeS and FeS2) occurs across the sediment units in the Arkona Basin.

Acknowledgements

We thank Martina Meyer, Thomas Max, Andrea Schipper, Kirsten Imhoff and Antje Vossmeyer for helpful assistance in the laboratory with mass spectrometry and geochemical analyses of sulfur speciation. We are grateful to Christoph Vogt from the Department of Crystallography at the University of Bremen (Germany) for stimulating discussions and help with the XRD analyses. We thank Benjamin Brunner at the MPI in Bremen for helpful discussions on the isotope data. Finally, we would like to thank the captain and crew of the F/S Heincke for a successful expedition. This study was financially supported by the Max Planck Society.

References

Aller R. C. and Rude P. D. (1988) Complete oxidation of solid phase sulfides by manganese and bacteria in anoxic marine sediments. *Geochimica et Cosmochimica Acta* **52**, 751-765.

Amend J. P. and Shock E. L. (2001) Energetics of overall metabolic reactions of thermophilic and hyperthermophilic Archaea and Bacteria. *FEMS Micobiology Reviews* **25**, 175-243.

Andrèn E., Andrèn T., and Sohlenius G. (2000) The Holocene history of the southwestern Baltic Sea as reflected in a sediment core from the Bornholm Basin. *Boreas* **29**, 233-250.

Berner R. A. (1967) Thermodynamic stability of sedimentary iron sulfides. *Amer. J. Sci.* **265**(AF bo), 773-785.

Berner R. A. (1970) Sedimentary pyrite formation. *Amer. J. Sci.* **268**(AF bo), 1-23.

Berner R. A. (1984) Sedimentary pyrite formation: An update. *Geochimica et Cosmochimica Acta* **48**(AF bo), 605-615.

Björck S. (1995) A review of the history of the Baltic Sea, 13.0-8.0 ka BP. *Quaternary International* **27**, 19-40.

Blake R. E., Surkov A. V., Boettcher M. E., Ferdelman T. G., and Joergensen B. B. (2006) Oxygen isotope composition of dissolved sulfate in deep-sea sediments: Eastern equatorial Pacific Ocean. In *Proceedings of the Ocean Drilling Program, Scientific Results*, Vol. 201 (ed. B. B. Joergensen, S. D´Hondt, and D. J. Miller), pp. 1-24. Online.

Böttcher M. E., Brumsack H. J., and Dürselen C. D. (2007) The isotopic composition of modern seawater sulfate: I. Coastal waters with special regard to the North Sea. *Journal of Marine Systems* **67**(1-2), 73-82.

Böttcher M. E. and Lepland A. (2000) Biogeochemistry of sulfur in a sediment core from the west-central Baltic Sea: Evidence from stable isotopes and pyrite textures. *Journal of marine Systems* **25**, 299-312.

Burdige D. J. and Nealson K. H. (1986) Chemical and microbiological studies of sulfide-mediated manganese reduction. *Geochemical J.* **4**, 361-387.

Canfield D. E. (1988) Sulfate reduction and the diagenesis of iron in anoxic marine sediments. *Ph.D. Thesis, Yale University*, 248pp.

Canfield D. E. (1989a) Reactive iron in marine sediments. *Geochimica et Cosmochimica Acta* **53**, 619-632.

Canfield D. E. (1989b) Reactive iron in marine sediments. *Geochim Cosmochim Acta* **53**, 619-632.

Canfield D. E., Raiswell R., and Bottrell S. (1992) The reactivity of sedimentary iron minerals toward sulfide. *American Journal of Science* **292**, 659-683.

Canfield D. E. and Thamdrup B. (1994) The Production of S-34-Depleted Sulfide During Bacterial Disproportionation of Elemental Sulfur. *Science* **266**(5193), 1973-1975.

Chou T. and Zhou L. (1983) Extraction techniques for selective dissolution of amorphous iron oxides from soils and sdiments. *Soil Science Society American Journal* **47**, 225-232.

Chung F. H. (1974) Quantitative interpretation of X-ray diffraction patterns, I. Matrix-flushing method of quantitative multicomponent analysis. *Journal of Applied Crystallography* **7**, 513 - 519.

Cline J. D. (1969) Spectrophotometric Determination of Hydrogen Sulfide in Natural Waters. *Limnology and Oceanography* **14**(3), 454-458.

Cline J. D. and Richards F. A. (1969) Oxygenation of hydrogen sulfide in seawater at constant salinity, temperature, and pH. *Environ.Sci.Techn.* **3**(AF bo), 838-843.

Ferdelman T. G., Lee C., Pantoja S., Harder J., Bebout B. M., and Fossing H. (1997) Sulfate reduction and methanogenesis in a Thioploca-dominated sediment off the coast of Chile. *Geochimica et Cosmochimica Acta* **61**(15), 3065-3079.

Fossing H. and Jørgensen B. B. (1989) Measurement of bacterial sulfate reduction in sediments: Evaluation of a single-step chromium reduction method. *Biogeochemistry* **8**, 205-222.

Giggenbach W. (1972) Optical spectra and equilibrium distrubution of polysulfide ions in aqueous solutions at 20°C. *Inorganic Chemistry* **11**, 1201-1207.

Gingele F. X. and Leipe T. (1997) Clay mineral assemblages in the western Baltic Sea: recent distribution and relation to sedimentary units. *Marine Geology* **140**, 97-115.

Habicht K. S. and Canfield D. E. (2001) Isotope fractionation by sulfate-reducing natural populations and the isotopic composition of sulfide in marine sediments. *Geology* **29**(6), 555-558.

Jørgensen B. B. (1982) Mineralization of organic matter in the sea bed-the role of sulfate reduction. *Nature* **296**, 643-645.

Jørgensen B. B., Boettcher M. E., Lueschen H., Neretin L. N., and Volkov I. I. (2004) Anaerobic methane oxidation and a deep H_2S sink generate isotopically heavy sulfides in Black Sea sediments. *Geochimica et Cosmochimica Acta* **68**(9), 2095-2118.

Kamyshny Jr. A., Ekeltchik I., Gun J., and Lev O. (2006) Method for the determination of inorganic polysulfide distribution in aqatic systems. *Analytical Chemistry* **78**, 2359-2400.

Kamyshny Jr. A., Goifman A., Gun J., Rizkov D., and Lev O. (2003) Kinetics of disproportionation of inorganic polysulfides in undersaturated aqueous solutions at Environmentally relevant conditions. *Aquatic Geochemistry* **9**, 291-304.

Kamyshny Jr. A., Goifman A., Gun J., Rizkov D., and Lev O. (2004) Equilibrium distribution of polysulfide ions in aqueous solutions at 25°C: a new approach for the study of polysulfides`equilibria. *Environmental Science and Technology* **38**(24), 6633-6644.

Kamyshny Jr. A., Gun J., Rizkov D., Voitsekovski T., and Lev O. (2007) Equilibrium distribution of polysulfide ions in aqueous solutions at different temperatures by rapid single phase derivazation. *Environmental Science & Technology* **41**(7), 6633-6644.

Kao S. J., Horng C. S., Roberts A. P., and Liu K. K. (2004) Carbon-sulfur-iron relationships in sedimentary rocks from southwestern Taiwan: influence of geochemical environment on greigite and pyrrhotite formation. *Chemical Geology* **203**(1-2), 153-168.

Kostka J. E. and Luther G. W. (1994) Partitioning and Speciation of Solid-Phase Iron in Salt-Marsh Sediments. *Geochimica Et Cosmochimica Acta* **58**(7), 1701-1710.

Luther III G. W. (1991) Pyrite synthesis via polysulfide compounds. *Geochimica et Cosmochimia Acta* **55**, 2839-2849.

Maronny G. (1959) Constantes de dissotiation de l`hydrogene sulfure. *Electrochimica Acta* **1**, 58-69.

Mörner N. A. (1995) The Baltic Ice Lake-Yoldia Sea transition. *Quat. Int.* **27**, 95-98.

Moros M., Lemke W., Kuijpers A., Endler R., Jensen J. B., Bennike O., and Gingele F. (2002) Regressions and transgressions of the Baltic basin reflected by a new high-resolution deglacial and postglacial lithostratigraphy for Arkona Basin sediments (western Baltic Sea). *Boreas* **31**(2), 151-162.

Moses C. O., Nordstrom D. K., Herman J. S., and Mills A. L. (1987) Aqueous pyrite oxidation by dissolved oxygen and by ferric iron. *Geochimica et Cosmochimica Acta* **51**(AF bo), 1561-1571.

Neretin L. N., Boettcher M. E., Joergensen B. B., Volkov I. I., Lueschen H., and Hilgenfeldt K. (2004) Pyritization processes and greigite formation in the advancing sulfidization front in the upper pleistocene sediments of the Black Sea. *Geochimica et Cosmochimica Acta* **68**(9), 2081-2093.

Neumann G. (1981) Lagerungsverhältnisse spät- und postglazialer Sedimente im Arkona-Becken. Ph.D. Thesis, Institut für Meereskunde, Warnemünde, Germany. *unpublished*.

Neumann T., Rausch N., Leipe T., Dellwig O., Berner Z., and Boettcher M. E. (2005) Intense pyrite formation under low-sulfate conditions in the Achterwasser lagoon, SW Baltic Sea. *Geochimica et Cosmochimica Acta* **69**(14), 3619-3630.

Olaf T. (2005) Bacterial Methane Formation and Distribution in Marine Environments: Case Studies from Arkona Basin (Western Baltic Sea) and Hotspots in the Central south Pacific. *Ph.D. Thesis, University of Christian-Albrechts Kiel*.

Piker L., Schmaljohann j., and Imhoff J. F. (1998) Dissimmilatory sulfate reduction and methane production in Gotland deep sediments (Baltic Sea) during a transition period from oxic to anoxic bottom water (1993-1996). *Aquatic Microbial Ecology* **14**, 183-193.

Pyzik A. J. and Sommer S. E. (1981) Sedimentary iron monosulfides: kinetics and mechanism of formation. *Geochimica et Cosmochimica Acta* **45**(AF bo), 687-698.

Roberts A. P. and Weaver R. (2005) Multiple mechanisms of remagnetization involving sedimentary greigite (Fe_3S_4). *Earth and Planetary Science Letters* **231**, 263-277.

Rong L., Lim L. W., and Takeuchi T. (2005) Determination of iodide and thiocyanate in seawater by liquid chromatography with poly(ethylene glycol) stationary phase. *Chromatographia* **61**, 371-374.

Schippers A. and Jørgensen B. B. (2001) Oxidation of pyrite and iron sulfide by manganese dioxide in marine sediments. *Geochimica et Cosmochimica Acta* **65**(6), 915-922.

Sohlenius G., Sternbeck J., Andren E., and Westman P. (1996) Holocene history of the Baltic Sea as recorded in a sediment core from the Gotland Deep. *Marine Geology* **134**(3-4), 183-201.

Steudel R. (1996) Mechanism for the formation of elemental sulfur from aqueous sulfide in chemical and microbiological desulfurization processes. *Industrial & Engineering Chemistry Research* **35**(4), 1417-1423.

Stookey L. L. (1970) Ferrozine - a New Spectrophotometric Reagent for Iron. *Analytical Chemistry* **42**(7), 779-&.

Sweeney R. E. and Kaplan I. R. (1973) Pyrite framboid formation: Laboratory synthesis and marine sediments. *Economic Geol.* **68**(AF bo), 618-634.

Teder A. (1971) The equilibrium between elementary sulfur and aqueous polysulfide solution. *Acta Chemica Scandinavica* **25**, 1722-1728.

Thamdrup B., Finster K., Hansen J. W., and Bak F. (1993) Bacterial disproportionation of elemental sulfur coupled to chemical reduction of iron or manganese. *Applied and Environmental Mecorbiology* **59**(1), 101-108.

Thamdrup B., Fossing H., and Joergensen B. B. (1994) Manganese, iron, and sulfur cycling in a coastal marine sediment, Aarhus Bay, Denmark. *Geochimica et Cosmochimica Acta* **58**(23), 5115-5129.

Thiessen O., Schmidt M., Theilen F., Schmitt M., and Klein G. (2006) Methane formation and distribution of acoustic turbidity in organic-rich surface sediments in the Arkona Basin, Baltic Sea. *Continental Shelf Research* **26**(19), 2469-2483.

Vogt C., Lauterjung J., and Fischer R. X. (2002) Investigation of the clay fraction (<2 μm) of the clay mineral society reference clays. *Clays and Clay Minerals* **50**(3), 388-400.

Wagman D. D., H E. W., B P. V., I H., M B. S., and H S. R. (1968) Selected values of chemical thermodynamic properties. *Natl. Bur. stand. US Goverment Office, Washington, DC., Tech. Note 270-3, 1968*.

Wastegård S., Andrèn T., Sohlenius G., and Sandgren P. (1995) Different phases of the Yoldia Sea in the north-western Baltic Proper. *Quat. Int.* **27**, 121-129.

Yao W. S. and Millero F. J. (1996) Oxidation of hydrogen sulfide by hydrous Fe(III) oxides in seawater. *Marine Chemistry* **52**, 1-16.

Zopfi J., Ferdelman T. G., and Fossing H. (2004) Distribution and fate of sulfur intermediates-sulfite, tetrathionate, thiosulfate, and elemental sulfur-in marine sediments. In *Sulfur Biogeochemistry Past and Present* (ed. J. P. Amend, K. J. Edwards, and T. W. Lyons), pp. 1-205. The Geological Society of America.

Sulfate reduction below the anaerobic oxidation of methane transition zone in Black Sea sediments

Lars Holmkvist*[a], Alexey Kamyshny, Jr.[a,b], Christoph Vogt[c], Kyriakos Vamvakopoulos[a], Timothy G. Ferdelman[a] and Bo Barker Jørgensen[a,d]

[a]Biogeochemisty Group, Max-Planck Institute for Marine Microbiology, Celsiusstrasse 1, 28359 Bremen, Germany

[b]Department of Geology and Earth System Science, Interdisciplinary Center, University of Maryland, College Park, MD 20742, USA

[c]Fachbereich Geowissenschaften, Universität Bremen, Klagenfurter Str., 28359 Bremen, Germany

[d]Center for Geomicrobiology, Department of Biological Sciences, University of Aarhus, Ny Munkegade, Bld. 1535, 8000 Århus C, Denmark

Keywords: Black Sea; sulfate reduction; potential sulfate reduction; reoxidation of sulfur species

*Corresponding author: E-mail address: lht@teknologisk.dk 22 Tel.: +45 72 70 23 95

Deep Sea Research Part I (2011), accepted

Abstract

A sudden increase in salinity about 7,000 years ago caused a shift in the deposited sediments of the Black Sea from limnic to brackish-marine. Due to the large anoxic deep water basin and the relatively high concentration of sulfate, organic matter is mineralized primarily through sulfate reduction in modern Black Sea sediments. Earlier studies have shown that sulfate-reducing bacteria are abundant within the limnic sub-surface sediment in spite of extremely low concentrations of sulfate and organic carbon. A main objective of the present study was therefore to understand the depth distribution of sulfate reduction across the different sediment units, even deep below the sulfate-methane transition. The study combined experimental measurements of sulfate reduction using 35S radiotracer with analyses of sulfur and iron geochemistry in pore water and sediment. Potential sulfate reduction rates were measured with 35S in sediment samples that were amended with sulfate and organic substrates and incubated in time-series up to 48 hours. Sulfate reduction could thereby be detected and quantified at depths where concentrations of sulfate were otherwise too low to enable calculation of the rates. The results demonstrate that sulfate-reducing bacteria are active several meters below the sulfate-methane transition in Black Sea sediments. The cryptic sulfate reduction below the sulfate-methane transition may be driven by sulfate produced from re-oxidation of sulfur compounds in pore water and sediment with oxidized iron minerals.

Introduction

The environmental conditions of the Black Sea, the largest anoxic basin on Earth, have changed strongly during the past 25,000 years. The first evidence of seawater intrusion through the Bosporus into the post-glacial lake comprising the Black Sea dates back to about 9,800 yr B.P. (Arthur and Dean, 1998, Jones and Gagnon, 1994). A permanent rise in salinity occurred only a few thousand years later, however, when seawater entered and marine conditions were established. At least three different sedimentary units have been recognized to be deposited in slope and deep-sea sediments over the past 25,000 years (Ross and Degens, 1974). Unit 1 is a carbonate-rich microlaminated sediment deposited under anoxic marine conditions within the last 3,000 years, following the invasion of planktonic coccolithophorids, Emiliania huxleyi. Unit 2 is an organic-rich microlaminated sediment deposited under anoxic marine conditions between 3,000 and 7,000 yr B.P. Unit 3 consists of alternating light and dark lutite, an organic-poor limnic sediment type of clay or silt with grain size less than 1/16 mm, deposited before 7,000 yr B.P. under oxic limnic conditions. These Pleistocene deposits of limnic origin are found throughout the modern Black Sea below a sediment depth of about one meter (Hay, et al., 1991).

Sulfate reduction within Unit I-II of the modern Black Sea plays a dominant role in the benthic mineralization of organic carbon. The process is enhanced by anoxic and sulfidic bottom water conditions while its depth in the seabed appears to be limited by downward diffusion of sulfate into the upper sediment layers. Sulfate reduction rates (SRR) peak in the sulfate-methane transition (SMT) where the activity of sulfate-reducing bacteria (SRB) is stimulated by anaerobic oxidation of methane (AOM) (Knab, et al., 2008). The high SRR within the SMT leads to an enhanced production of sulfide, which here shows peak concentration in the pore water and diffuses upwards and downwards in the sediment (Neretin, et al., 2004). The downward diffusing sulfide reacts with iron species in the sediment below and forms a distinct diagenetic sulfidization front. This front is often recognized as a black band due to a high content of iron monosulfides (FeS) and greigite (Fe_3S_4) (Berner, 1970, Berner, 1984, Neretin, et al., 2004, Pyzik and Sommer, 1981). Different oxidation processes of sulfur species takes place in the sulfidization front

that lead to an overall pyritization. The products of sulfide oxidation include different intermediates such as zero-valent sulfur (ZVS) species (i.e. elemental sulfur and polysulfides), thiosulfate, and sulfite (Zopfi, et al., 2004), all of which may undergo disproportionation to sulfide and sulfate (Thamdrup, et al., 1993, Thamdrup, et al., 1994).

Only a few studies have addressed the potential for sulfate reduction below the SMT in marine sediments. The experimental measurement of deep sulfate reduction is hindered by the low concentrations of sulfate (<50 μM) in the pore water. Thus, the activity and role of sulfate-reducing communities detected below the SMT is not known. It is possible that the SRB deep in the sediment have an important impact on the cycling of carbon, sulfur and iron. It was recently shown that sulfate-reducing communities are present several meters below the SMT in Black Sea sediments (Leloup, et al., 2007). This was demonstrated by quantitative PCR targeting their metabolic key gene, the dissimilatory (bi)sulfite reductase (dsrA). However, it is not clear how the SRB make a living below the SMT. Many sulfate-reducing prokaryotes have a versatile metabolism which apparently enables them to adapt to the extreme conditions of sub-surface sediments with low availability of electron donors and acceptors. For instance, pure culture studies of the sulfate-reducing archaea, Archaeoglobus fulgidus, show an ability to shift the metabolic pathway to different carbon sources when grown under different levels of sulfate (0.3-14 mM) (Habicht, et al., 2005). Other explanations for the presence of active sulfate reducers beneath the SMT could be the ability to ferment (Widdel and Hansen, 1992) or to reduce poorly crystalline Fe(III) oxides (Coleman, et al., 1993).

By combining activity measurements of SRR with geochemical data on sulfur and iron, we studied the activity and depth distribution of active SRB below the SMT. The results demonstrate the presence of active SRB several meters below the sulfate zone in post-glacial limnic sediments of the Black Sea. We present a possible explanation for the presence of active SRB by which sulfate is produced in the methane zone from oxidation of reduced sulfur compounds with iron minerals.

Materials and methods

Sampling and site description

The present study is based on two gravity cores (GC A and B) and a multi-corer core (MUC) taken during research cruise M75/5 of the RV METEOR in the Black Sea from May 11th to June 6th 2007. Cores were collected at Station 9 (44°39.08'N, 32°1.00'E) in the Dniepr paleodelta in the northwestern part of the Black Sea at a water depth of 1000 m. The position of this station is identical to Station "P824GC" described by Knab et al. (2008) and Station P12 described by Leloup et al. (2007). Absolute depth correction of the GC A and B cores relative to the sediment surface was not possible because sulfate was not measured in the MUC. Instead, a depth correction between the GC A and B cores was made by overlaying the two pore water concentration profiles of sulfide. This correction demonstrated that only about 5 cm more sediment had been lost from the surface during coring of GC A as compared to GC B. However, the penetration depth of sulfide was quite different between the A and B cores since the location of the black band differed (see Fig. 5 B and C).

Core processing

Immediately after retrieval of the first gravity core (GC A) methane samples were taken at 80-100 cm depth intervals through small windows cut into the side of the core liner with a vibrating saw. Sediment samples of 3 cm3 were transferred into 20 ml serum vials with 6 ml Milli-Q water, closed with a butyl rubber stopper, and crimp sealed.

The GC A and B cores as well as the MUC cores were processed in a 4°C cold room on board the METEOR within a few days after retrieval. Rhizone soil moisture samplers (Rhizosphere Research Products, Wageningen, Netherlands) were used for the extraction of pore water. The rhizones consist of an inert porous polymer tube with a length of 10 cm and a pore size of 0.1 µm, through which pore fluid is extracted by vacuum created with disposable 10 ml syringes connected to the Rhizone. Pore water for sulfate and sulfide measurements in GC A were extracted from pre-drilled holes at 10 cm depth intervals and fixed with 250 µL 2 wt. % zinc acetate. The first ~0.5 ml of extracted pore

water was discarded to limit oxidation by oxygen. Samples for dissolved iron were collected at the same depths as for sulfate and preserved by acidifying ~1 ml pore water with 100 µL 10% HCl. Pore water samples for analysis of zero-valent sulfur (ZVS) in polysulfide species were extracted in between the sulfate and sulfide pore water samples at 30-60 cm depth intervals within the upper 500 cm of the sediment and at a depth of 775 cm. At least 5-6 ml of pore water was required from each depth in order to detect the ZVS species. The pore water for ZVS analysis was transferred into anoxic vials immediately after extraction and analyzed within a few hours to prevent oxidation by oxygen.

Pore water was extracted from GC B with 10 cm long Rhizones by gently pushing them into predrilled holes at 5 cm depth intervals along the core. Pore water samples for the later determination of sulfate, sulfide and dissolved iron were prepared as with the GC A core.

Solid phase sub-samples were taken from the GC A and B cores at 10 cm and 5 cm depth intervals, respectively, in between the depths where pore water was extracted. Sediment sub-samples were collected both in plastic bags and plastic centrifuge tubes containing 10 ml of zinc acetate (20% w/v) and immediately frozen at -20°C for later analysis of iron, sulfur and carbon. Within two weeks after sampling, sediment sub-samples from the GC A core were scanned for magnetic susceptibility and all other sub-samples from both GC A and B were analyzed for carbon, sulfur and iron speciation.

Pore water analyses

Methane in the headspace of the 20 ml serum vials was analyzed on a gas chromatograph (5890A, Hewlett Packard) equipped with a packed stainless steel Porapak-Q column (6 feet, 0.125 inch, 80/100 mesh, Aglient Technology) and a flame ionization detector. Helium was used as a carrier gas at a flow rate of 30 ml min^{-1}. Sulfate was analysed by non-suppressed ion chromatography (100 µl injection volume, Waters, column IC-Pak^{TM}, 50 x 4.6 mm) (Ferdelman, et al., 1997). The eluent was 1 mM isophthalate buffer in 10% methanol, adjusted to pH 4.5 with saturated Na borohydrate and the flow rate was 1.0 ml min-1. Hydrogen sulfide (H_2S and HS^-) was determined spectrophotometrically at 670 nm (Shimadzu UV 1202) on zinc-preserved pore water and bottom water samples by the

methylene blue method (Cline, 1969). Dissolved iron was measured according to Stookey (1970) with Ferrozine (1 g L^{-1} in 50 mM HEPES buffer, pH 7) spectrophotometrically at 562 nm (Shimadzu UV 1202). Dissolved manganese in the pore water (Mn^{2+}) was determined by flame atomic absorption spectrometry (Perkin Elmer, Atomic Absorption Spectrometer 3110).

The analysis of zerovalent sulfur (ZVS) species included solid sulfur (S_8), colloidal sulfur (S_0), polysulfides (S_n^{2-}) and polythionates (SnO_6^{2-}). The pH of each pore water sample was measured with a pH electrode before the analysis and the value was used later for ZVS concentration calculations. A newly developed protocol for detection of ZVS species was based on four steps (Kamyshny, et al., 2009a): (1) The detection of inorganic polysulfides by fast single-phase derivatization with methyl trifluoromethanesulfonate (Kamyshny, et al., 2006), (2) detection of the sum of colloidal S0 and polysulfide ZVS and polythionate ZVS (n>3) with hydrogen cyanide derivatization, followed by HPLC analysis of thiocyanate (Kamyshny, 2009b, Rong, et al., 2005), (3) detection of the sum of polysulfide ZVS, colloidal S0 and solid sulfur by treatment with zinc chloride followed by extraction with chloroform, and (4) the detection of polythionates (n = 4-6) by HPLC (Kamyshny, et al., 2009b) . The concentration of polysulfide ZVS was calculated as the sum of all ZVS species detected after derivatization with methyl triflate. The concentration of colloidal ZVS was calculated as the difference between results from the cyanolysis and the concentration of polysulfide ZVS. Finally, the concentration of dispersed solid sulfur was calculated as the difference between the chloroform extraction and results from the cyanolysis.

Solid phase analyses

Sediment sub-samples were placed in a Bartington Instruments MS2 meter equipped with a MS2C sensor and scanned for magnetic susceptibility using a scan rate of 1 cm min-1. The sediment density was determined as the wet weight per cm^3. The water content in the sediment was determined from the weight loss after drying at 60°C until constant weight and sediment density as the wet weight per cm3. Total organic carbon (TOC) was determined in freeze dried sediment that was pretreated with HCl, dried again, and analyzed on a CNS analyzer (FisonsTM Na 1500 elemental analyzer). AVS (acid volatile

sulfide = dissolved sulfide + Fe monosulfide) and CRS (Cr-reducible S = pyrite + elemental sulfur) were determined using the two step acidic Cr-II method (Fossing and Jørgensen, 1989). The volatilized and trapped sulfide was determined spectrophotometrically at 670 nm (Shimadzu UV 1202) by the methylene blue method of Cline (1969). Total zero-valent sulfur (ZVS) was extracted from zinc acetate preserved sediment samples in 10 ml pure methanol on a rotary shaker for at least 16 h according to Zopfi et al. (2004). Total ZVS was separated on an HPLC with a Zorbax ODS column (125 × 4 mm, 5 µm; Knauer, Germany) with methanol as the eluent (1 ml min^{-1}) and determined from the adsorption at 265 nm.

Solid phase ferric iron (Fe(III)) was extracted from sub-samples of the frozen sediment in a 0.5 M HCl solution for 1 h on a rotary shaker. Fe(II) was determined in the supernatant of the HCl extracts by the Ferrozine method (Stookey, 1970). Fe(III) was calculated as the difference between the total iron (Fe(II) + Fe(III)), determined with Ferrozine + 1% (w(v) hydroxylamine hydrochloride), and the Fe(II). Reactive iron (towards sulfide) in the sediment was extracted with dithionite-citrate-acetic acid according to Canfield (1989) and determined with Ferrozine + 1% (w/v hydroxylamine hydrochloride). The content of total iron in the sediment was extracted from freeze dried sub-samples in a boiling HCl solution (12.5 M) for a period of 1 min according to Berner (1970) and Raiswell et al. (1988). The extracted Fe(II) from this method was determined with Ferrozine + 1% (w(v) hydroxylamine hydrochloride). Solid manganese oxides (Mn(IV)) were measured on the supernatant of the dithionite-extracts by flame atomic absorption spectrometry (Perkin Elmer, Atomic Absorption Spectrometer 3110).

Sulfate reduction

Sulfate reduction rates (SRR, Equation 1) in the MUC core were determined using the whole-core $^{35}SO_4^{2-}$ incubation method (Jørgensen, 1978). The MUC was injected with radiotracer (~300 kBq per injection) at 1 and 2 cm depth intervals and the injected core was incubated for 24 h at ca. 4?C. Sulfate reduction was terminated by sectioning the sediment cores, fixing the sections with 20 mL of 20% (w/v) zinc acetate, and freezing. A measured sulfate concentration of 16.5 mM was used for calculating the SRR in the MUC.

For the measurement of SRR in GC A, triplicate samples of 5 cm^3 were carefully collected in butyl rubber stoppered glass tubes. Sampling was done at 10 cm depth intervals, alternating with the depths of pore water extraction. The glass tubes were injected with 5 µl carrier-free $^{35}SO_4^{2-}$ tracer (~300 kb per 5 cm^3) and incubated for 24 h at ca. 4°C. The process was stopped by mixing the sample with 10 ml cold zinc acetate (20% w/v) and freezing. All samples were treated by cold chromium distillation after Kallmeyer et al. (2004) and SRR were calculated according to Jørgensen (1978):

$$SRR = [sulfate] \times (^{35}S\text{-}CRS/^{35}S\text{-}sulfate) \times 1.06/t \text{ pmol } cm^{-3} \ d^{-1} \quad \text{(Eq. 1)}$$

where [sulfate] is the sulfate concentration in pmol per cm^3 of wet sediment (1 pmol = 10-12 mol), ^{35}S-CRS is the radioactivity of total reduced sulfur at the end of incubation, ^{35}S-sulfate is the initial radioactivity of sulfate added to the experiment, 1.06 is a correction factor for the expected isotope discrimination against ^{35}S-sulfate versus the bulk ^{32}S-sulfate by the SRB, and incubation time, t, is measured in days.

In the deeper, methanogenic part of the sediment, beneath the main sulfate zone, we determined "potential sulfate reduction rates" (P-SRR) in similar 5 cm^3 samples. In this sulfate-depleted sediment below 300 cm depth, sediment samples were injected under N_2 with non-radioactive sulfate (2 mM final concentration) and organic substrates (100 µM final concentrations of propionate, acetate, lactate and formate) and then pre-incubated for 12 h. Subsequently, 10 µl carrier-free $^{35}SO_4^{2-}$ tracer (~600 kb) was injected into each sample. A five point time series experiment with incubations stopped after 0, 12, 24, 36 and 48 h was done with triplicate samples of 5 cm^3 sediment for each time point. The incubations were stopped by adding the sample into 10 ml cold zinc acetate (20% w/v) and treating as described above.

X-ray diffraction pattern analyses (XRD)

Samples for XRD analyses of mineral phases were collected from the GC A core at 30, 103, 163, 246, 316, 345 and 410 cm depths. Dried bulk samples were carefully ground to a fine powder (<20µm particle size) and prepared with a Philips back-loading system. X-ray diffractograms were measured on a Philips X'Pert Pro multipurpose diffractometer

equipped with a Cu-tube (k(alpha) 1.541, 45 kV, 40 mA), a fixed divergence slit of ¼°, a sample changer, a secondary monochromator, and a X'Celerator detector system. The measurements were done as a continuous scan from 3º to 85° 2θ, with a calculated step size of 0.016° 2θ (calculated time per step was 100 seconds). Mineral identification was done using the Philips software X'Pert HighScore™, which, besides the mineral identification, gives a semi-quantitative value for each identified mineral on the basis of Relative Intensity Ratio (RIR-values). The RIR-values are calculated as the ratio between the strongest signal from a specific mineral phase to the strongest signal from pure corundum (I/Ic), referred to as the "matrix-flushing method" after Chung (1974). In addition, mineral identification was checked with the freeware MacDiff 4.5 (Petschick et al., 1996). Full quantification was done using the full-pattern quantification software QUAX (Vogt et al., 2002).

Magnetic nodules

Sediment for the study of magnetic nodules was sampled during an earlier Black Sea cruise (METROL cruise 2004) at St. "P824GC" that was the same sample station as St. 9. Single magnetic nodules were collected from the sulfidization front at 388 cm depth using a handheld magnet. The nodules were immediately embedded in a methacrylate resin, trimmed with a diamond band saw, and polished with an Al_2O_3 paraffin suspension. Prior to scanning electron microscopy (SEM), the surface of the polished nodules was coated with carbon to avoid charging effects. The surface morphology and texture were recorded by conventional backscattered electron and secondary electron imagery. Specific elements inside the nodules were identified using energy dispersive X-ray analysis (EDS) (Oxford INCA 300).

Results

Sediment stratigraphy

Sediments from below the Black Sea chemocline consist of limnic clay, deposited before 7,500 yr BP, and overlain by microlaminated, organic-rich sapropel and modern marine coccolith ooze (Calvert and Karlin, 1991, Ross, et al., 1970). We identified four sedimentary units between the top of the GC cores and a depth of 8 m according to color,

sand layers and organic carbon content. In GC A these units were recognized as Unit I, IIa, IIb and III according to the stratigraphy defined during earlier studies (Neretin, et al., 2004) (Fig. 1). Note, however, that the description of the different depth zones of the GC cores is of uncorrected depths because absolute depth correction of the GC cores and the MUC could not be made, as described above. Based on our previous experience in the Black Sea, 10-30 cm of sediment was probably lost from the surface during GC coring.

Unit I: 0 - 30 cm depth. Laminated marine coccolith ooze deposited under anoxic conditions. Some of this upper layer was lost during GC coring. TOC values were 5-6 wt %.

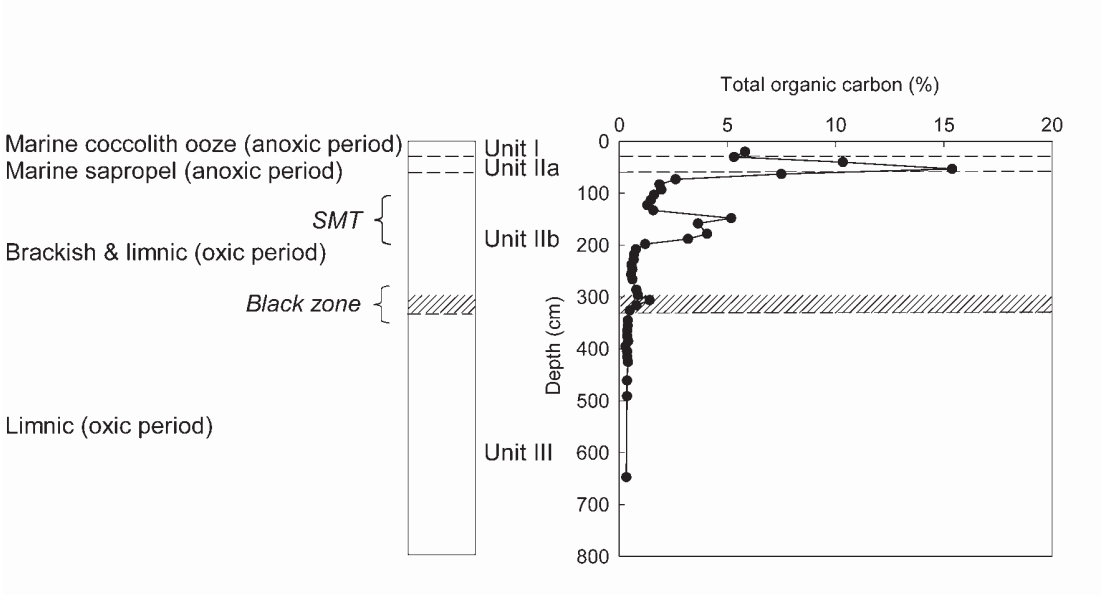

Figure 1. Total organic carbon (% dry weight) distribution at St. 9. The different sedimentary units (Units I-III) are indicated.

Unit IIa: 30-65 cm depth. Brown, marine sapropel deposited under anoxic conditions. TOC values were 7.5-15 wt %.

Unit IIb: 65- 326 cm depth. Grayish sediment of both brackish and limnic origin deposited under oxic conditions. A black band was found at 304-323 cm depth, below which a sand layer of about 3 cm thickness extended down to 326 cm. TOC values were 0.5-5 wt %.

Unit III: 326-757 cm depth. Reddish-brown limnic clay deposited under oxic conditions. The sediment was unaffected by the sulfidization process. TOC values were <1 wt %.

The TOC content was high, 5-15 % dry weight, within the recent marine coccolith ooze and sapropelic layers (Unit I and IIa). It decreased steeply with depth (<5%) in the underlying limnic Units IIb and III (Fig. 1). TOC peaked twice within Unit IIb with values reaching 5 % at 148 cm and 1.4 % at 306 cm, most probably because of differences in the deposition of organic material or perhaps due to turbidities from the upper shelf. TOC remained below 0.5% throughout Unit III in which it decreased gradually from 0.48 to 0.33 % between 325 and 650 cm depth.

The depth and thickness of the black band and of the sand layer differ slightly between the GC A and B core. In GC B, the black band was located at 359-371 cm depth. The porosity of the GC A core decreased roughly linearly with depth in the interval 15-752 cm according to the equation:

Porosity = 0.825 – 0.0005 x depth (cm) (Eq. 2)

Pore water chemistry

Pore water concentrations of sulfate, methane, sulfide and dissolved iron in core GC A are presented in Fig. 2 A-B. The sulfate concentration decreased from 12 mM at the top of the core (Unit I) to 0.1 mM at 230 cm, and further to below the detection limit of 0.01 mM at 400 cm (Fig. 2 A). From 250 cm depth, where the sulfate concentration had dropped below 50 μM, it could no longer be calibrated accurately although it still generated visible peaks on the ion chromatograms. Between 250 cm and 400 cm the low concentrations of sulfate showed a very gradual decrease with depth. Methane increased below 100 cm and reached 3.4 mM at 700 cm (Fig. 2 A). Methane had probably out-gassed below a depth of about 250 cm upon core recovery and below 400 cm the sediment was observed to crack. The sulfate-methane transition (SMT), where anaerobic oxidation of methane occurs, was situated at 100-200 cm depth.

Free sulfide was present from the top of the core and down to 321 cm depth in Unit IIb (Fig. 2 B). Sulfide showed a minor peak within the Unit I-IIa layers and a large distinct

peak within the SMT with a maximum concentration of 4 mM. Dissolved iron was not detected in the sulfide zone but increased downwards from the black band in Unit IIb (Fig. 2 B). Within the non-sulfidized limnic sediment of Unit III, the concentrations of dissolved iron were generally in the range of 2-4 mM. Dissolved manganese generally remained <10 µM throughout the core but peaked within Unit I and exhibited an increase with depth down to the upper part of Unit III (data not shown).

Peak concentrations of individual polysulfide ZVS species occurred in Unit IIb (Fig. 2 C). Our calculations revealed that individual polysulfides were not in equilibrium with elemental sulfur under moderately alkaline conditions as would have been expected according to Kamyshny Jr. et al. (2004). The sum of polysulfide ZVS species peaked at 158 cm depth with highest concentrations reaching 44 µM (Fig. 2 D). The depth of this peak largely matched the peak in sulfide, suggesting that polysulfide ZVS species were in equilibrium with sulfide in the pore water. Concentrations of ZVS species below the sulfidization front were too low to be detected.

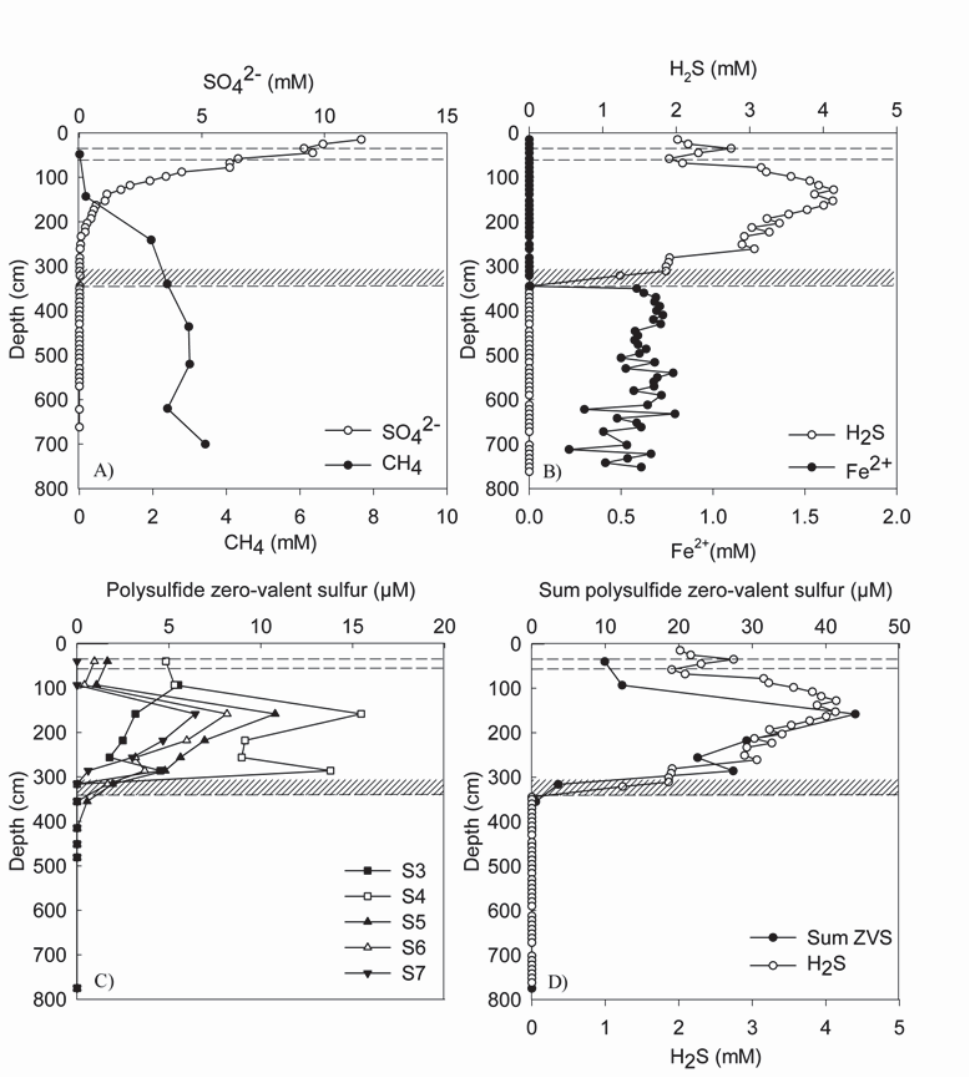

Figure 2. Pore water concentrations of (A) sulfate and methane, (B) dissolved sulfide and iron, meeting within the black band and the sand layer, (C) zero-valent sulfur present in different specific polysulfide species, (D the sum of all polysulfides compared to the free sulfide

Sediment geochemistry

Two distinct peaks in magnetic susceptibility were observed, a minor peak within the organic rich Unit IIa and a large peak within the black band of Unit IIb, with maximum values reaching 68 x 10^{-5} and 203 x 10^{-5} SI units, respectively (Fig. 3 A). The large peak in Unit IIb coincided with abundant magnetic nodules observed in the black band. Magnetic susceptibility was relatively high, 11-12 x 10^{-5} SI, throughout the iron-rich and brown colored limnic sediment of Unit III.

Total iron in Unit I-IIb peaked around 100 cm depth with highest concentration of 170 µmol cm^{-3} (Fig 3 B). Total iron increased within the limnic Unit III and reached concentrations of 400-500 µmol cm^{-3}. Reactive iron was low (<10 µmol cm^{-3}) within the sulfidic Unit I-IIb and increased sharply to about 100 µmol cm-3 in Unit III (Fig. 3 B). Fe(III) determined by HCl extraction was generally low within the upper Unit I-IIb and increased in Unit III to values reaching 7 µmol cm^{-3} at 405 cm, below which the concentration decreased again (Fig. 3 C). Sediment of Unit III was less reduced as the concentrations of reactive iron (Fig. 3 B) and Fe(III) (Fig. 3C) increased. The concentration of Mn(IV) from the dithionite extracts was low throughout the core (Fig. 3 D). Mn(IV) peaked twice in Unit IIb with maximum concentrations of 6 and 5 µmol cm-3 at 148 and 276 cm, respectively.

The concentration of total ZVS in the sediment was generally low (<5 µmol cm^{-3}) except for a sharp peak situated right within the black band with a maximum concentration of 16 µmol cm^{-3} (Fig. 3 E). There was a minor peak in AVS concentration within Unit IIa below which the concentration stayed relatively constant, <10 µmol cm^{-3}, down to the black band where there was a distinct peak with a maximum concentration of 35.5 µmol cm^{-3} at 316 cm (Fig. 3 F). Within Unit III, AVS remained low (<1 µmol cm^{-3}) throughout the rest of the core. High concentrations of chromium reducible sulfur (CRS, mainly FeS_2) were found in Units I-IIb (ca. 100-300 µmol S cm^{-3}) whereas CRS was low (<10 µmol S cm^{-3}) through the non-sulfidized Unit III (Fig. 3 F).

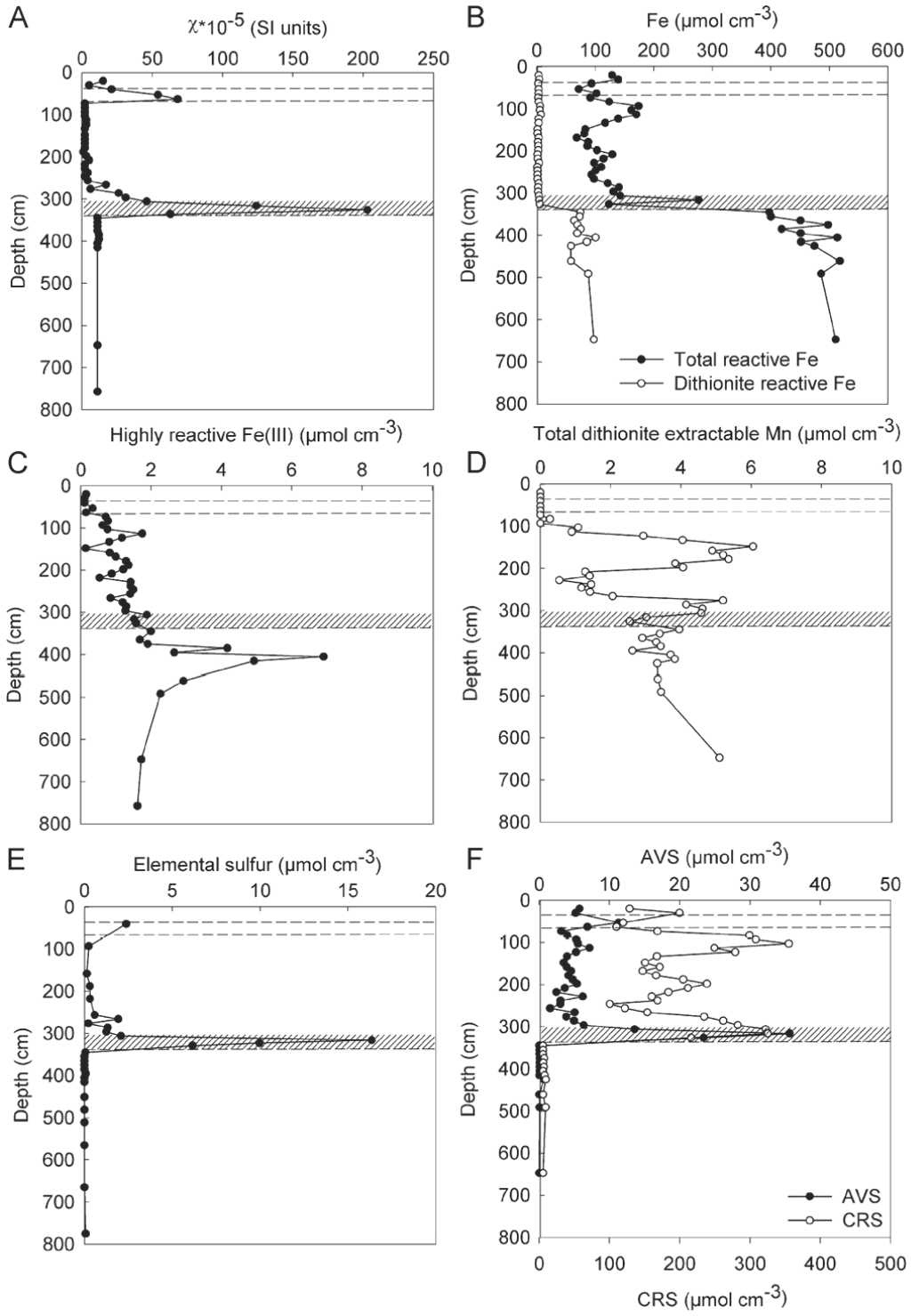

Figure 3. Depth distributions of (A) magnetic susceptibility, (B) reactive iron species, (C) highly reactive ferric iron, (D) total dithionite extractable manganese (E) elemental sulfur, and (F) acid volatile sulfide (AVS) and chromium reducible sulfur (CRS).

Magnetic nodules

Magnetic nodules collected in the black band within Unit IIb of GC A varied in size but were typically <500 µm. Surface scans of cut and polished nodules (collected in 2004) by SEM and EDS analysis showed that they had a heterogeneous interior consisting mainly of iron and sulfur. From the atomic ratios, we identified iron monosulfide (FeS), greigite (Fe_3S_4), and pyrite (FeS_2) in most of the nodules studied. As an example, the nodule presented in Fig. 4 had a core of FeS_2 surrounded by Fe_3S_4. However, a general pattern in the distribution of various iron sulphide minerals within the investigated nodules was not found.

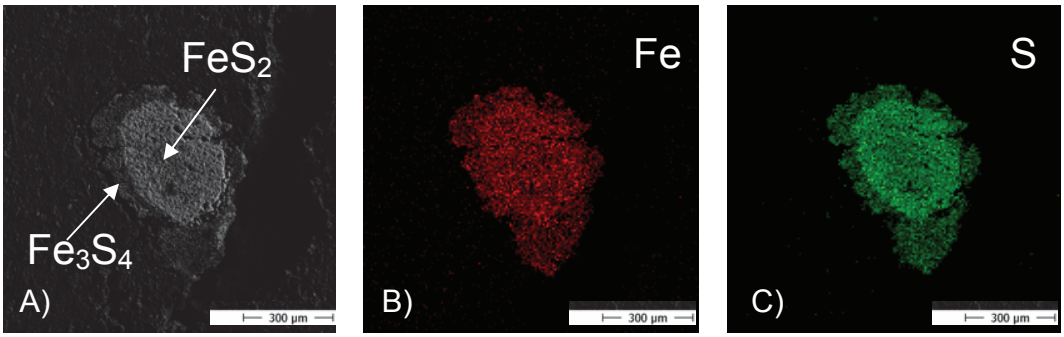

Figure 4. Scanning electron micrographs of sliced magnetic nodules from the black band with peak magnetic susceptibility at 388 cm. (A) Surface scan of sliced nodule that consists mostly of iron-sulfide minerals. EDS analysis revealed the presence of FeS_2 in the center and Fe_3S_4 in the light-gray periphery of the nodule. The same image as in Fig. 4 A is shown for only iron (B) and sulfur (C).

X-ray diffraction (XRD)

XRD analysis was performed on sediment collected from each of the different sediment units in order to identify Fe(III)-bearing minerals. It should be noted, however, that the individual minerals recognized with the XRD method show statistical distributions of minerals only. Thus, the percentage values of individual minerals identified are not an accurate measure of their quantity.

We detected iron oxides, goethite and hematite, only in the non-sulfidized limnic Unit III below a depth of 300 cm (i.e. below the sulfidization front) where they reached 1 % dry

wt. at 410 cm (data not shown). There was a great variety of silicate minerals found throughout the sediment core of which some contained Fe(III) (data not shown). These were mainly of the subclasses phyllosilicates (sheet silicates) and cyclosilicates. The largest fraction of the phyllosilicates was made up by the sum of illite and micas, ranging from 11 to 36 % dry wt, whereas other individual phyllosilicates did not exceed 6% dry wt). The different cyclosilicates did not show any particular trend with depth except that the sum of illite and micas, montmorillonites and smectites, as well as kaolinite and biotite all increased in concentration below the SMT (data not shown).

Sulfate reduction

The SRR data are separated into two graphs with different scales in order to better describe the rates within the different depth intervals of the upper 400 cm (Fig. 5 A and B). Note that the depths of the SRR for the MUC core are given relative to the sediment surface while depths for the GC A core are given relative to the core top and should therefore be shifted down, probably by 10-20 cm, to be aligned with the MUC data).

The highest SRR in the MUC reached 38,000 pmol cm-3 d-1 (or 38 nmol cm^{-3} d^{-1}; 1 pmol = 10-12 mol) at 0.5 cm (Unit I), below which depth there was a steady decrease down to 230 pmol cm^{-3} d^{-1} at 24 cm (Fig. 5 A). In GC A, SRR generally decreased with depth but peaked in the SMT with a mean rate of 410 pmol cm-3 d-1 at 123 cm (Unit IIb, Fig. 5 A). The SRR within the 200-400 cm depth interval decreased steeply and generally followed the decreasing trend of sulfate in the pore water. The SRR data below 250 cm are, however, somewhat inaccurate as the sulfate concentration approached the detection limit of our ion chromatographic technique. Below 400 cm, sulfate could not be detected and the SRR could therefore not be calculated.

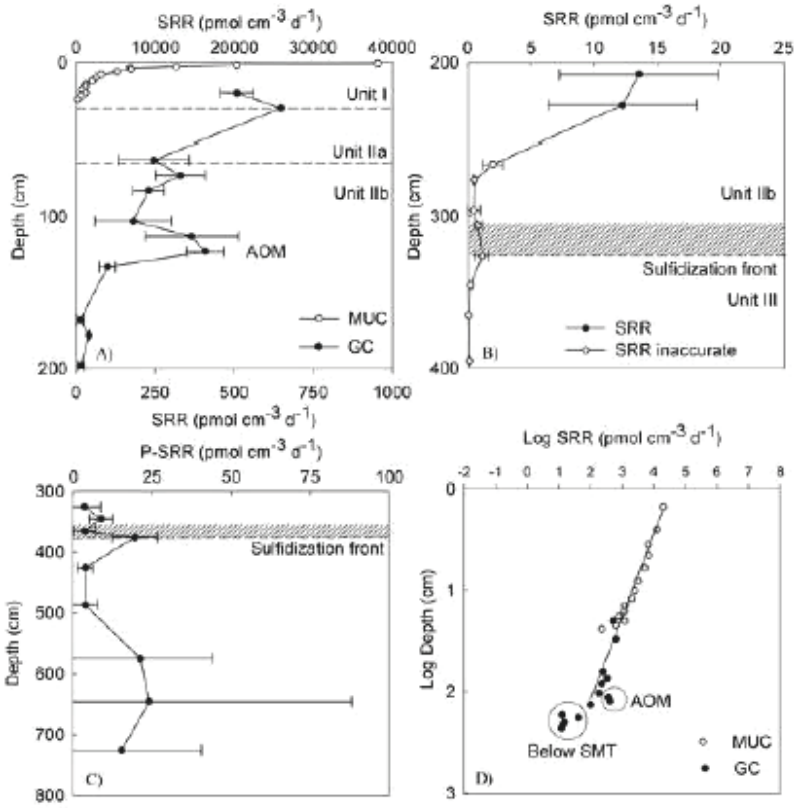

Figure 5. Sulfate reduction rates (SRR) measured experimentally using ^{35}SO42- from (A) 0-24 cm depth in the MUC (open circles, upper scale) and 0-200 cm depth in GC A (closed circles, lower scale), and (B) 200-400 cm depth in GC A. The shaded zone indicates the sulfidization front with a sand layer at the bottom. Error bars show standard deviation of triplicate measurements. (C) Potential sulfate reduction rates (P-SRR) measured experimentally using $^{35}SO_4^{2-}$ at 300-800 cm depth. (D) Log-log plot of sulfate reduction rates vs. depth in the MUC (open circles) and the GC A (closed circles). The linear regression line of the log-log transformed data above the AOM is shown. Encircled data points from within and below the AOM zone were not included in the linear regression.

We measured potential sulfate reduction rates, P-SRR, at 300-800 cm depth in GC B in the deepest part of Unit IIb and within the limnic Unit III (Fig. 5 C) in order to test whether active SRB were present also within the deeper sulfate-depleted parts of the sediment. (Note that the depth of the black band differs slightly between the GC A and B cores, as described above). The P-SRR was 4-9 pmol cm^{-3} d^{-1} in the lower part of Unit IIb with a peak of 20 pmol cm^{-3} d^{-1} at 365 cm depth in the black band (Unit IIb, Fig. 5 C). In Unit III, P-SRR increased from 4 pmol cm^{-3} d^{-1} at 400-500 cm to 15-24 pmol cm-3 d^{-1} at a depth of 600-700 cm (Fig. 5 C).

Based on these results, our study demonstrates that active SRB must be present in the limnic Unit III where the concentration of sulfate was below detection. The combined time course of P-SRR from all depths within the 325-725 cm depth interval showed that P-SRR started right away from the first incubation period and that the summed rates remained of the same magnitude (data not shown). This suggests that the size of the SRB communities did not change during the 48 h time course experiments.

The depth distribution of SRR within the sulfate zone is generally controlled by the availability of degradable organic matter which decreases over many orders of magnitude with depth and age in the sediment. In order to show this we plotted all the experimentally measured SRR (MUC and GC A data), except for the inaccurate SRR below 250 cm, as a function of depth in a double-log plot (Fig. 5 D). (Note that the depths of the SRR in the GC A core relative to the MUC are not correct since it was not possible to make an absolute depth correction). The plot shows that a linear regression analysis could be made for all the SRR data down to the SMT zone where AOM occurred. The SRR from within and below the SMT are thus not included in the linear regression since sulfate reduction in this zone is primarily AOM driven. The linear regression showed that the SRR decreased with depth in the sediment according to the following equation: Log(SRR) = -1.2544 x Log(Z) + 4.5951, where Z is depth in the sediment (cm). Below the SMT, the SRR seems to decrease even steeper than above if a linear regression had been made.

Discussion

Sulfate reduction

In a study by Jørgensen et al. (2001), modelling of SRR within the upper two meters of a Black Sea sediment resulted in average rates of around 100 pmol cm^{-3} d^{-1}. The average SRR in GC A of the upper two meters (Fig. 5A) were 260 pmol cm^{-3} d^{-1} and thus slightly above the model results. The SRR within and above the SMT (Unit I-IIb) are in general comparable to the high SRR measured experimentally with 35SO42- tracer in sediments from the same area of the Black Sea (Knab, et al., 2008). The steep decrease in sulfate and the broad peak in sulfide in Unit IIb point to a stimulated sulfate reduction due to

anaerobic oxidation of methane within the SMT (Fig. 2 A and B). This was also demonstrated by the local peak in SRR at 123 cm (Fig. 5 A) and the depletion of methane in the SMT (100-200 cm depth interval) (Fig. 2 A). The minor peak in sulfide in Unit I (Fig. 2 B) and the high SRR in this zone (Fig. 5 A) are on the other hand consistent with the high content of organic carbon near the sediment surface (Fig. 1). It is not clear whether the near-surface H_2S peak is a transient phenomenon or an artifact. If not, then the H_2S minimum at the Unit IIa/IIb transition at 65 cm depth should indicate a strong H_2S sink right at that depth which is not consistent with, for example, the depth distribution of reactive iron.

The P-SRR experiments were used to detect bacteria with the ability to reduce sulfate in the deep methanogenic sediment of limnic origin, where the concentration of sulfate was too low to calculate in situ SRR directly from radiotracer experiments. Since the SRR and P-SRR estimates were obtained under different experimental conditions, these rates are not directly comparable. In the P-SRR experiments, the SRB were stimulated by the addition of sulfate and organic substrates in order to analyze the metabolic capacity of the existing SRB community. Given the rather short incubation times and the constant level of SRR over time, it is unlikely that the SRB community grew during the P-SRR experiments. There was reduction of sulfate at relatively high rates during the first half hour immediately after the injection of $^{35}SO_4^{2-}$, which indicates that the community already possessed the physiological capacity for dissimilatory sulfate reduction. We found that the mean P-SRR from the GC B core at 0.5, 1, 1.5 and 2 days after injection of 35S tracer was 610, 390, 360, and 155 pmol cm-3 d-1, respectively (data not shown).

In contrast to P-SRR measurements, SRR are determined under in situ conditions where the availability of substrates was limiting. The P-SRR below 300 cm depth was accordingly much higher than the SRR (Fig. 5 B and C). The data show that SRB were not limited to the upper sediment layers, which are rich in sulfate, but that they also maintained the capacity for sulfate reduction deep beneath the SMT and even beneath the sulfidization front. These data support the observations by Leloup et al. (2007), who quantified the SRB communities in deep sediment cores from the same site by Q-PCR targeting their metabolic key gene, dissimilatory (bi)sulfite reductase (dsrA). The authors showed that SRB occurred throughout the methane zone at 200-500 cm depth in numbers

of 0.8-1.5 x 106 cells g-1. The proportion of SRB relative to the total microbial cell number was even as high in the methane zone as in the sulfate zone, namely 5-10%. Our study now shows that SRB in the methane zone are capable of performing sulfate reduction when provided with appropriate substrates.

When SRR were calculated using the measured concentrations of sulfate in the pore water, the rates reached zero below 400 cm. However, we now speculate that the SRR do not quite decrease to zero but that the sulfate concentration in the pore water below 400 cm was simply too low to enable proper calculations of the SRR. It therefore seems likely that sulfate reduction occurs also in the methane zone within the limnic Pleistocene sediment (Unit III). For future studies of sulfate reduction within sub-surface sediments it is thus crucial that analytical methods are used which can accurately detect sulfate also below 50 μM.

Geochemistry of sulfur and iron

As a result of high SRR, reduced sulfur species (i.e. sulfide, polysulfides, elemental sulfur, AVS and CRS) were present at high concentrations within the upper marine Units I-IIb. In contrast, concentrations of reduced sulfur species were low in the limnic Unit III (Fig. 2 B, Fig. 3 E and F), where a steep gradient of dissolved iron demonstrates active iron reduction (Fig. 2 B). The distribution of reducible iron oxides (Fig. 3 B, C and D) showed that these were abundantly available for iron reducing microorganisms from the top of Unit III and down. XRD analyses below the sulfidization front also confirmed the presence of iron oxides as well as Fe(III)-bearing clay minerals in this sediment unit (data not shown).

The black band in Unit IIb marked the lower boundary of downward diffusing sulfide produced within the SMT. At the transition to Unit III or just within this unit the downward diffusing sulfide reacted with iron minerals and with dissolved iron diffusing upwards from the deeper sediment. It is not clear why the sulfidization front occurred exactly at the 3-5 cm thick sand layer marking the transition between Unit III and IIb. There might be a lateral pore fluid transport associated with this permeable horizon which locks the sulfide-iron interface at this position. The coincidence may also be due to a shift

in geochemistry, e.g. to a step-up in total iron with a high capacity to react with sulfide (Fig. 3 B).

A sharp peak in magnetic susceptibility occurred within the black band and coincided with peaks in AVS and CRS (Fig. 3A and F). Although the black color of sediments may not be a simple indicator of AVS (Rickard and Morse, 2005), it seems reasonable to assume that, in this Black Sea sediment, the black color of the sulfidization front was due to AVS (Fig. 3F). We found numerous greigite nodules within the black band and the presence of this paramagnetic iron-sulfur mineral explained the magnetic susceptibility data (Fig.3 A). SEM and EDS analyses of nodules collected with a magnet demonstrated that these contained both greigite (Fe_3S_4) and pyrite (FeS_2) (Fig. 4). The content of Fe_3S_4 in each nodule was not quantified, but scans of several nodules indicated that Fe_3S_4 makes up only a fraction of the total amount of minerals present in each nodule. This is in accordance with a study from the Baltic Sea where similar magnetic nodules were collected at the transition of two sedimentary units (Holmkvist et al., 2009, in prep).

The Fe_3S_4 may be an intermediate in the sequence of reactions leading from FeS to FeS_2. However, the formation of FeS_2 from the metastable FeS fraction (the AVS fraction) has not been completely resolved. Our study shows that sulfur intermediates were abundant within Unit IIb where the formation of FeS2 could occur via either polysulfides (Berner, 1970, Luther, 1991), elemental sulfur (Berner, 1970), or sulfide in the pore water (Rickard and Luther III, 1997).

The finding of a deep sulfidization front where sulfide produced within the SMT is trapped at depth has been observed also in other continental shelf sediments such as the Angola Basin (Pruysers, 1998), the Baltic Sea (Boesen and Postma, 1988), and the Bay of Aarhus (Denmark) (Holmkvist et al., 2009, in prep). Below the sulfidization front iron sulfides (FeS and FeS_2, Fig. 3 F) occurred at low concentration, which indicates that sulfide production had occurred. This is consistent with the finding of active sulfate reducers in the limnic sediment layers, but it may also be the result of iron sulfide formation during the earlier history of the Black Sea, at the time when the limnic deposit was formed.

Deep production of sulfate and active SRB below the SMT

One of the aims of the present study was to demonstrate whether SRB below the SMT do indeed reduce sulfate and to explain their presence within sub-surface sediments in terms of the availability of electron donors- and acceptors. The SRR measurements showed that SRB, which are present several meters below the SMT (Leloup, et al., 2007), are indeed actively reducing sulfate. The P-SRR data showed that their capacity for sulfate reduction in the 326-395 cm depth interval is 3-140-fold higher than the in situ rates and probably relatively even higher deeper in the limnic Unit III (Fig. 5 C). The in situ activity is thus highly constrained by the low concentration and reactivity of TOC and possibly also by the low sulfate concentration.

Sulfate dropped steeply with depth from 12 mM at the GC core top to about 0.01 mM at 400 cm, below which sulfate could no longer be detected. We suggest that the measured low concentrations of sulfate below the SMT were not just "background" concentrations although the concentrations below 250 were inaccurate. As discussed in a comparable study from Aarhus Bay (Holmkvist et al. 2009, in prep), at least three possible explanations may be proposed for the low background concentrations of sulfate in the methane zone:

a) The background could be a handling artifact due to chemical or biological oxidation of free sulfide during the time between coring and sulfate measurement. However, the storage, sampling and analysis of the cores were done very carefully in order to minimize sample oxidation and exclude such possible artifacts. For example, gravity cores were sectioned and kept upright in the core liners on the ship and during transport to avoid air contact at the outside of the sediment core. The sampling of pore water using rhizons inserted into the middle of the core took place on the day of coring which should not have allowed sufficient time for diffusion of oxygen and sulfate from the core periphery to the centre. The first extracted pore water was always discarded as it had been in contact with air and pore water was immediately fixed with zinc acetate to prevent sulfide oxidation. It is therefore most probable that there was no significant oxidation of sulfide during the pore water extraction, which could have affected the extracted sulfate data. This was also demonstrated in the study from Aarhus Bay, where pore water was extracted under strict anoxic conditions inside an anaerobic glove box in order to test whether auto-oxidation of sulfide occurred during the extraction in open air. This experiment showed that there was

no significant difference between the low concentrations of sulfate extracted in open air with those extracted under controlled anoxic conditions.

b) The sulfate could be a biologically unavailable background or even be passively diffusing down into the methane zone, because it was not being consumed by sulfate-reducing microorganisms. The sulfate background could be biologically unavailable because the concentration was below a physiological threshold for uptake and respiration. However, the fact that the sulfate concentration did drop to undetectable concentration beneath 400 cm speaks against the hypothesis of an untouchable threshold concentration. Besides, it also seems unlikely that the background sulfate was fed continuously by diffusion from above since there was a concentration drop beneath the SMT at 200-300 cm depth (Fig. 5B).

c) The sulfate could be generated in situ down in the methane zone by reaction between free sulfide or iron sulfide minerals with oxidized iron buried with the sediment. We propose that this is indeed the main explanation for the measured low sulfate concentrations, as discussed in further detail by Holmkvist et al. (in prep).

The iron oxides within the non-sulfidized Unit III (Fig. 3 B, C and D) constitute an efficient barrier which oxidizes and traps the downward diffusing sulfide at the sulfidization front as described above. The parallel decrease in sulfide and sulfate above the sulfidization front suggests a close association between the formation of sulfate and in situ re-oxidation of sulfide. From the XRD analyses we found that hematite and goethite were present below the sulfidization front. This was consistent with an increase in reactive iron below the sulfidization front (Fig. 3 B) since the dithionite method extracts hematite and goethite (Kostka and Luther, 1994).

The cryptic formation of sulfate within the methane zone is, however, not simple to explain based on reactions between free sulfide and solid-phase Fe(III). Based on earlier considerations on pyrite formation from sulfide and Fe(III) reactions (Berner, 1967, Berner, 1970, Drobner, et al., 1990, Rickard, 1997), disproportionation of intermediate sulfur species to sulfide and sulfate (Canfield and Thamdrup, 1996), and a removal of excess reducing power in the form of H2 by methanogenic archaea, the study from Aarhus Bay proposed a revised redox balance of the reactions between sulfide and

oxidized iron we propose the following net equation (Eq. 3) (Holmkvist et al. 2009, in prep):

$$16\ H_2S + 8\ FeOOH \rightarrow 8\ FeS_2 + 4\ H_2 + 16\ H_2O \qquad \text{(Eq. 3)}$$

In the set of reactions behind this net equation, a transient formation of sulfate (but no overall net production of sulfate) could occur by the partial oxidation of sulfide with iron oxides and subsequent disproportionation of the intermediate sulfur species to sulfate. The iron oxy-hydroxide chosen as an example for the proposed reaction (Equation 5) is goethite (FeOOH). However, other less reactive Fe(III)-containing minerals such as sheet silicates detected with XRD are more likely to be responsible.

The transient production of sulfate could stimulate and maintain active SRB within the methane zone. In the Black Sea sediments, elemental sulfur (a fraction of the total sum of ZVS in Fig. 3 E) may form when sulfide is oxidized chemically by metals according to well known oxidation reactions described by Burdige and Nealson (1986) and Pyzik and Sommer (1981). Oxidation of sulfide (or other sulfur intermediates) seems to be particularly intensive at the sulfidization front as indicated by the large peak in total ZVS (Fig. 3 E). This finding is in agreement with the increasing content of easily reducible iron oxides down through the sulfidization front (reactive iron in Fig. 3 B). Further, the presence of ZVS species, ranging from 0.2-2 μmol cm^{-3}, in sediment extending from the SMT and down to the sulfidization front (Fig. 4 E) supports our expectancy of Fe(III) driven sulfide oxidation.

It is an interesting observation that active SRB were found also within the limnic sediment of Unit III (Fig. 5 C), although sulfate and sulfide were not detected in the pore water. We suspect that the SRB present in Unit III reduce sulfate also in situ since the radioactive 35^S counts in the TRIS fraction from the SRR samples were significantly above the blank values (data not shown). It therefore seems likely that sulfate was present below the sulfidization front, but concentrations were too low to be detected (<50μM), and that the sulfide produced from sulfate reduction was removed immediately from the pore water due to reaction with Fe(III).

ZVS species could not be detected below a depth of 345 cm. This indicates that only a very limited re-oxidation of free sulfide occurs in Unit III and that rapid removal of ZVS

via disproportionation prevented accumulation. Re-oxidation of free sulfide according to equation 5 may not be the only explanation for the production of sulfate below the sulfidization front, however. Re-oxidation of iron sulfide minerals, such as FeS or FeS_2 (the AVS and CRS fraction, respectively, Fig. 3 F) to elemental sulfur and subsequent disproportionation, might also lead to a sub-surface production of sulfate in Unit III. The re-oxidation of iron sulfide minerals with iron oxide minerals has been proposed from several previous studies (Burdige and Nealson, 1986, Pyzik and Sommer, 1981, Steudel, 1996, Yao and Millero, 1996).

The oxidation of FeS_2 could also be due to deeply buried Mn(IV). This reaction between two solid mineral phases has been suggested to involve an Fe(II)/Fe(III)-shuttle between the mineral surfaces of FeS_2 and manganese oxides (Aller and Rude, 1988, Moses, et al., 1987, Schippers and Jørgensen, 2001). In Black Sea sediments, Fe(III) and MnO_2 were extracted from the sediment below the SMT in equal quantities (Fig. 3 C and D). However, the fraction of poorly-reactive iron oxides and/or iron silicates, defined as the difference between the content of total iron and reactive iron fraction (Fig. 4 B), made up by far the largest fraction of iron oxides which potentially could re-oxidize sulfur compounds in the sediment. The predominant role of iron was also indicated by the high amount clay minerals by which some may contain Fe(III) detected in Unit III by XRD (data not shown).

The P-SRR in Unit III increased with depth (Fig. 5 C) and showed a high potential for sulfate reduction of the microbial community. The SRB living down in the methane zone are apparently adapted to low concentrations of sulfate and must have high affinity to sulfate at low concentrations. Ingvorsen and Jørgensen (1984) found that fresh-water strains of SRB grown in batch culture were able to sustain growth at sulfate concentrations down to 5 µM. Perhaps the SRB within Unit III originate from fresh-water strains from the time when the Black Sea was still a lake. Alternatively, it may well be that marine sulfate-reducing bacteria develop high sulfate affinity when growing under limiting sulfate concentrations.

Conclusions

The potential sulfate reduction data from the present study show for the first time that SRB present several meters below the SMT in Black Sea sediment are apparently active sulfate reducers. We propose that there is an ongoing cryptic sulfur cycle in the deep methane-rich sediment by which Fe(III) and Mn(IV) minerals oxidize sulfide or other reduced sulfur species in pore water and sediment. The immediate oxidation products are sulfur species of intermediate oxidation steps, such as elemental sulfur. Through disproportionation reactions these may be partly oxidized to sulfate, which serves as electron acceptor for the sulfate-reducing bacteria.

Acknowledgement

We thank Martina Meyer, Thomas Max, Andrea Schipper and Kirsten Imhoff at the Max Planck Institute for Marine Microbiology for assistance in the laboratory with analyses of sulfur speciation. We thank Nina Knab (University of Southern California, USA) for sampling the sediment used to study the magnetic nodules and Vera Lukies from the Center for Marine Environmental Sciences (MARUM in Bremen, Germany) for assistance with magnetic susceptibility measurements. XRD analyses were performed by the research group Crystallography, Dept. of Geosciences, University of Bremen. We are grateful to Christian Borowski from the MPI for planning and leading the M75/5 METEOR cruise. Finally, we thank the captain and crew of the RV METEOR for a successful expedition. This study was financially supported by the Max Planck Society.

References

Aller, R.C. and Rude, P.D., 1988. Complete oxidation of solid phase sulfides by manganese and bacteria in anoxic marine sediments. Geochimica et Cosmochimica Acta. 52, 751-765.

Arthur, M.A. and Dean, W.E., 1998. Organic-matter production and preservation and evolution of anoxia in the Holocene Black Sea. Paleoceanography. 13, 395-411.

Berner, R.A., 1967. Diagenesis of iron sulfide in recent marine sediments. Estuaries. 268-272.

Berner, R.A., 1970. Sedimentary pyrite formation. Amer. J. Sci. 268, 1-23.

Berner, R.A., 1984. Sedimentary pyrite formation: An update. Geochimica et Cosmochimica Acta. 48, 605-615.

Boesen, C. and Postma, D., 1988. Pyrite formation in anoxic environments of the Baltic. American Journal of Science. 288, 575-603.

Burdige, D.J. and Nealson, K.H., 1986. Chemical and microbiological studies of sulfide-mediated manganese reduction. Geochemical J. 4, 361-387.

Calvert, S.E. and Karlin, R.E., 1991. Relationships between sulphur, organic carbon, and iron in the modern sediments of the Black Sea. Geochimica et Cosmochimica Acta. 55, 2483-2490.

Canfield, D.E., 1989. Reactive iron in marine sediments. Geochim Cosmochim Acta. 53, 619-632.

Canfield, D.E. and Thamdrup, B., 1996. Fate of elemental sulfur in an intertidal sediment. FEMS Microbiology Ecology. 19, 95-103.

Chung, F.H., 1974. Quantitative interpretation of X-ray diffraction patterns, I. Matrix-flushing method of quantitative multicomponent analysis. Journal of Applied Crystallography. 7, 513 - 519.

Cline, J.D., 1969. Spectrophotometric determination of hydrogen sulfide in natural waters. Limnology and Oceanography. 14, 454-458.

Coleman, M.L., Hedrick, D.B., Lovley, D.R., White, D.C. and Pye, K., 1993. Reduction of Fe(III) in sediments by sulphate-reducing bacteria. Nature. 361, 436-438.

Drobner, E., Huber, H., Waechtershaeuser, G., Rose, D. and Stetter, K.O., 1990. Pyrite formation linked with hydrogen evolution under anaerobic conditions. Nature. 346, 742-744.

Ferdelman, T.G., Lee, C., Pantoja, S., Harder, J., Bebout, B.M. and Fossing, H., 1997. Sulfate reduction and methanogenesis in a Thioploca-dominated sediment off the coast of Chile. Geochimica et Cosmochimica Acta. 61, 3065-3079.

Fossing, H. and Jørgensen, B.B., 1989. Measurement of bacterial sulfate reduction in sediments: Evaluation of a single-step chromium reduction method. Biogeochemistry. 8, 205-222.

Habicht, K.S., Salling, L., Thamdrup, B. and Canfield, D.E., 2005. Effect of low sulfate concentrations on lactate oxidation and isotope fractionation during sulfate reduction by Archaeoglobus fulgidus strain Z. Appl Environ Microbiol. 71, 3770-3777.

Hay, B.J., Arthur, M.A., Dean, W.E., Neff, E.D. and Honjo, S., 1991. Sediment Deposition in the Late Holocene Abyssal Black-Sea with Climatic and Chronological Implications. Deep-Sea Research Part a-Oceanographic Research Papers. 38, S1211-S1235.

Ingvorsen, K. and Jørgensen, B.B., 1984. Kinetics of sulfate uptake by freshwater and marine species of Desulfovibrio. Arch. Microbiol. 139, 61-66.

Jones, G. and Gagnon, A., 1994. Radiocarbon chronology of Black Sea sediments. Deep - Sea Research I. 41, 531-557.

Jørgensen, B.B., 1978. A comparison of methods for the quantification of bacterial sulfate reduction in coastal marine sediments. III. Estimation from chemical and bacteriological field data. Geomicrobiology Journal. 1, 49-64.

Jørgensen, B.B., Weber, A. and Zopfi, J., 2001. Sulfate reduction and anaerobic methane oxidation in Black Sea sediments. Deep-Sea Research I. 48, 2097-2120.

Kallmeyer, J., Ferdelman, T.G., Weber, A., Fossing, H. and Jørgensen, B.B., 2004. A cold chromium distillation procedure for radiolabeled sulfide applied to sulfate reduction measurements. Limnology and Oceanography: Methods. 2, 171-180.

Kamyshny, A., Borkenstein, C.G. and Ferdelman, T.G., 2009a. Protocol for Quantitative Detection of Elemental Sulfur and Polysulfide Zero-Valency Sulfur Distribution in Natural Aquatic Samples. Geostandards and Geoanalytical Research. 33, 415-435.

Kamyshny, J.A., 2009b. Improved Cyanolysis Protocol for Detection of Zero-valent Sulfur in Natural Aquatic Systems. Limnology and Oceanograph: Methods. 7, 442-448.

Kamyshny, A., Ekeltchik, I., Gun, J. and Lev, O., 2006. Method for the determination of inorganic polysulfide distribution in aqatic systems. Analytical Chemistry. 78, 2359-2400.

Kamyshny, A., Goifman, A., Gun, J., Rizkov, D. and Lev, O., 2004. Equilibrium distribution of polysulfide ions in aqueous solutions at 25°C: a new approach for the study of polysulfides equilibria. Environmental Science and Technology. 38, 6633-6644.

Knab, N.J., Cragg, B.A., Hornibrook, E.R.C., Holmkvist, L., Borowski, C., Parkes, R.J. and Jørgensen, B.B., 2008. Regulation of anaerobic methane oxidation in sediments of the Black Sea. Biogeosciences Discussions. 5, 2305–2341.

Kostka, J.E. and Luther, G.W., 1994. Partitioning and speciation of solid-phase iron in salt-marsh sediments. Geochimica Et Cosmochimica Acta. 58, 1701-1710.

Leloup, J., Loy, A., Knab, N.J., Borowski, C., Wagner, M. and Jørgensen, B.B., 2007. Diversity and abundance of sulfate-reducing microorganisms in the sulfate and methane zones of a marine sediment, Black Sea. Environmental Microbiology. 9, 131-142.

Luther, G.W., 1991. Pyrite synthesis via polysulfide compounds. Geochimica et Cosmochimia Acta. 55, 2839-2849.

Moses, C.O., Nordstrom, D.K., Herman, J.S. and Mills, A.L., 1987. Aqueous pyrite oxidation by dissolved oxygen and by ferric iron. Geochimica et Cosmochimica Acta. 51, 1561-1571.

Neretin, L.N., Böttcher, M.E., Jørgensen, B.B., Volkov, I.I., Lueschen, H. and Hilgenfeldt, K., 2004. Pyritization processes and greigite formation in the advancing sulfidization front in the upper pleistocene sediments of the Black Sea. Geochimica et Cosmochimica Acta. 68, 2081-2093.

Petschick, R., Kuhn, G. and Gingele, F., 1996. Clay mineral distribution in surface sediments of the South Atlantic: sources, transport, and relation to oceanography. Marine Geology. 130, 203-229.

Pyzik, A.J. and Sommer, S.E., 1981. Sedimentary iron monosulfides: kinetics and mechanism of formation. Geochimica et Cosmochimica Acta. 45, 687-698.

Raiswell, R., Buckley, F., Berner, R.A. and Anderson, T.F., 1988. Degree of pyritization of iron as a paleoenvironmental indicator of botom water oxygenation. Journal of Sedimentary Petrology. 58, 812-819.

Rickard, D., 1997. Kinetics of pyrite formation by the H2S oxidation of iron (II) monosulfide in aqueous solutions between 25 and 125 degrees Celsius: The rate equation. Geochimica et Cosmochimica Acta. 61, 115-134.

Rickard, D. and Morse, J.W., 2005. Acid volatile sulfide (AVS). Marine Chemistry. 97, 141-197.

Rickard, D.T. and Luther III, G.W., 1997. Kinetics of pyrite formation by the H2S oxidation of iron (II) monosulfide in aqueous solutions between 25 and 125 degrees Celsius: The mechanism. Geochemica et Cosmochimica Acta. 61, 135-147.

Rong, L., Lim, L.W. and Takeuchi, T., 2005. Determination of iodide and thiocyanate in seawater by liquid chromatography with poly(ethylene glycol) stationary phase. Chromatographia. 61, 371-374.

Ross, D.A. and Degens, E.T., 1974. Recent sediments of Black Sea. Amer. Assoc. Petrol. Geol. 20, 183-199.

Ross, D.A., Degens, E.T. and Macllvaine, J., 1970. Black Sea: recent sedimentary history. Science. 170, 163-165.

Schippers, A. and Jørgensen, B.B., 2001. Oxidation of pyrite and iron sulfide by manganese dioxide in marine sediments. Geochimica et Cosmochimica Acta. 65, 915-922.

Steudel, R., 1996. Mechanism for the formation of elemental sulfur from aqueous sulfide in chemical and microbiological desulfurization processes. Industrial & Engineering Chemistry Research. 35, 1417-1423.

Stookey, L.L., 1970. Ferrozine - a new spectrophotometric reagent for iron. Analytical Chemistry. 42, 779-781.

Thamdrup, B., Finster, K., Hansen, J.W. and Bak, F., 1993. Bacterial disproportionation of elemental sulfur coupled to chemical reduction of iron or manganese. Applied and Environmental Mecorbiology. 59, 101-108.

Thamdrup, B., Fossing, H. and Jørgensen, B.B., 1994. Manganese, iron, and sulfur cycling in a coastal marine sediment, Aarhus Bay, Denmark. Geochimica et Cosmochimica Acta. 58, 5115-5129.

Vogt, C., Lauterjung, J. and Fischer, R.X., 2002. Investigation of the clay fraction (<2 μm) of the clay mineral society reference clays. Clays and Clay Minerals. 50, 388-400.

Yao, W.S. and Millero, F.J., 1996. Oxidation of hydrogen sulfide by hydrous Fe(III) oxides in seawater. Marine Chemistry. 52, 1-16.

Two-dimensional mapping of photopigments distribution and activity of *Chloroflexus*-like bacteria in a hypersaline microbial mat

Ami Bachar[1], Lubos Polerecky[1], Jan P. Fischer[1], Kyriakos Vamvakopoulos[1], Dirk de Beer[1], Henk M. Jonkers[1,2,#]

[1]Max-Planck-Institute for Marine Microbiology, Celsiusstrasse 1, D-28359 Bremen, Germany

[2]Delft University of Technology, Postbox 5048, NL-2600 GA Delft, The Netherlands

Key words: Chloroflexaceae, photopigments, hyperspectral imaging, microbial mat

[#]Corresponding author: Henk M. Jonkers, Henk M. Jonkers, Delft University of Technology, PO Box 5048, 2600 GA Delft, The Netherlands. Tel.:131 0 15 278 2313; fax: 131 0 15 278 6383; e-mail: h.m.jonkers@tudelft.nl

FEMS Microbiol Ecol 65 (2008) 434–448

Abstract

Pigment analysis in an intact hypersaline microbial mat by hyperspectral imaging revealed very patchy and spatially uncorrelated distributions of photopigments Chl a and BChl a/c, which are characteristic photopigments for oxygenic (diatoms and cyanobacteria) and anoxygenic phototrophs (Chloroflexaceae). This finding is in contrast to the expectation that these biomarker pigments should be spatially correlated, as oxygenic phototrophs are thought to supply the Chloroflexaceae members with organic substrates for growth. We suggest that the heterogeneous occurrence is possibly due to sulfide, whose production by sulfate-reducing bacteria may be spatially heterogeneous in the partially oxic photic zone of the mat. We furthermore mapped the near-infra-red-light controlled respiration of Chloroflexaceae under light and dark conditions and found that Chloroflexaceae are responsible for a major part of oxygen consumption at the lower part of the oxic zone in the mat. The presence of Chloroflexaceae was further confirmed by FISH probe and 16S rRNA gene clone library analysis. We assume that species related to the genera Oscillochloris and 'Candidatus Chlorothrix', in contrast to those related to Chloroflexus and Roseiflexus, depend less on excreted photosynthates but more on the presence of free sulfide, which may explain their presence in deeper parts of the mat.

Introduction

Filamentous anoxygenic phototrophic bacteria related to the family Chloroflexaceae are conspicuous bacteria that have been found to be quantitatively important community members in both hot spring and hypersaline microbial mats (Castenholz, 1988; Pierson et al., 1994; N¨ ubel et al., 2001, 2002; van der Meer et al., 2003, 2005). The family accommodates so far six scientifically described genera, of which the species of two genera (Heliothrix and Roseiflexus) only produce bacteriochlorophyll a (BChl a), while species of the other four genera (Chloroflexus, Chloronema, Oscillochloris and 'Candidatus Chlorothrix') produce BChl c and other possible bacteriochlorophylls in addition to BChl a (Klappenbach & Pierson, 2004). All the Chloroflexaceae members characterized so far are generally described as anoxygenic phototrophs. Enzymatic studies have shown that Chloroflexus aurantiacus apparently uses the 3-hydroxypropionate pathway for inorganic carbon fixation during autotrophic growth (Strauss & Fuchs, 1993). The finding that homologous genes encoding for different steps in that pathway also occur in Roseiflexus-like organisms suggests that representatives of this genus might also be capable of autotrophic bicarbonate fixation (Klatt et al., 2007). In addition to phototrophy, at least some of the cultured and physiologically characterized species of the Chloroflexaceae family appear to be able to additionally perform aerobic respiration (Pierson & Castenholz, 1974). In two recently published studies, it was shown by near-infra-red (NIR) light manipulations that BChl c-containing Chloroflexaceae were likely responsible for a significant part (up to 100% in certain cases) of the microbial mat's community aerobic respiration (Bachar et al., 2007; Polerecky et al., 2007). These and other reported studies on the in situ physiology of Chloroflexaceae members (Bateson & Ward, 1988; van der Meer et al., 2003, 2005) contributed to the notion that these organisms may play an important role in carbon and sulfur cycling in at least some microbial mats.

Although the metabolic switch from anoxygenic photosynthesis under NIR light illumination to aerobic respiration under NIR light-deprived conditions for C. aurantiacus was proved in pure culture (Bachar et al., 2007), the direct link between the presence of an organism and a certain physiological property in intact natural systems is often obscured by the presence of other community members. Moreover, the spatial

heterogeneity both in the vertical and in the horizontal direction of such ecosystems often hampers our ability to establish a firm relationship between the presence of specific community members (community structure) and their function.

Currently, a practical difficulty in establishing the two-dimensional (2-D, i.e., both horizontal and vertical) distribution of different Chloroflexaceae species in microbial mats is that specific fluorescent gene probes for FISH studies are available only for two (Chloroflexus and Roseiflexus)of the six known Chloroflexaceae genera (N¨ ubel et al., 2002). However, bacteriochlorophyll c (BChl c), which is produced presumably by oxygen-respiringmembers of Chloroflexaceae (Bachar et al., 2007; Polerecky et al., 2007), could be used as another possible, although less specific, biomarker. Bacteriochlorophylls and other photopigments are routinely quantified by HPLC. However, this method requires extraction of pigments from mat sections, which limits the vertical spatial resolution to 0.25–0.5mm, and smears possible horizontal patchiness.

In this work, we applied hyperspectral imaging to visualize the 2-D distribution of BChl a and c and other photopigments in the mat. This was done to test the working hypothesis that Chloroflexaceae members are spatially correlated with oxygenic phototrophs (e.g. Cyanobacteria), which are thought to supply the former with organic substrates for growth (D'Amelio et al., 1987; Bateson & Ward, 1988; Castenholz, 1988; Hanada & Pierson, 2006; Nübel et al., 2002). Furthermore, we exploited the observation that NIR light can inhibit Chloroflexaceae respiration and adopted the recently developed NIR light manipulation method (Polerecky et al., 2007) to map Chloroflexaceae respiration activity in 2-D, with the aim to compare it with the distribution of the photosynthetic activity and to establish a link with the 2-D BChl c distribution in the mat. Additionally, we used HPLC to provide supplementary data on vertical pigment distribution, and applied available FISH probes and additional 16S rRNA gene techniques to investigate the presence, distribution and diversity of Chloroflexaceae members in the investigated mat. Several characterized species of the Chloroflexaceae family are known to be able to use sulfide as source of electrons for energy generation in the process of cyclic electron transport as well as for CO_2 fixation. Therefore, we measured sulfide concentration profiles and sulfate reduction rates in distinct depth zones to additionally establish the potential availability of sulfide as an electron donor for anoxygenic photosynthetic

activity. Finally, we used microsensors to measure light and oxygen penetration in undisturbed mat samples to estimate their availability for photosynthesis and aerobic respiration, respectively.

Materials and Methods

Microbial mats

A microbial mat was maintained in a continuous flow-through mesocosm consisting of an open plastic basin (1.2m x 1.2m x 0.5m) with a continuous in- and outflow of hypersaline water. The mesocosm system was inoculated withmat samples taken fromthe hypersaline Lake Chiprana, Spain ((41°14'20''N, 0°10'54''W), and grown over 3 years in water with a salt composition similar to the natural lake water (seawater plus 80 g/l $MgSO_4.7H_2O$). The mats were illuminated with a light intensity of 500 µmol photons m^{-2} s^{-1} and a light regime of 16 h light and 8 h dark.

Microsensor measurements

A microbial mat piece was taken from the mesocosm system and incubated in the laboratory in a continuous flow-through chamber at room temperature. After c. 5 h of mat stabilization, high spatial resolution depth profiles of oxygen (O_2), sulfide (H_2S), pH and light were measured continuously after light conditions were changed (switch from light,

500 µmol photons m^{-2} s^{-1}, to dark and vice versa) until a steady state was reached. O_2 was measured using a Clark- type oxygen microsensor with a guard cathode (Revsbech, 1989), which had a tip diameter < 10 µm and a response time < 1s. H_2S and pH were measured with microsensors made and calibrated as described by Kühl et al. (1998). Light spectra inside themat in the region from 400 to 900 nm were measured in 500-µm intervals using a fiber-optic scalar irradiance microprobe (Kühl & Jørgensen, 1992, 1994) connected to a spectrometer (USB2000, Ocean Optics). The recorded light intensity at each wavelength was normalized to the intensity measured at the mat surface.

Oxygen imaging and rate calculation

O2-sensitive planar optodes were used to map the distributions of oxygen concentration, net oxygenic photosynthesis and NIR light-dependent respiration in intact microbial mat

samples. A piece of the mat was taken from the mesocosm system, vertically cut and placed in an aquarium against a glass wall equipped with a planar oxygen optode. The optode was constructed by depositing a thin (c.20 μm) layer of an oxygen-sensitive cocktail (see Precht et al., 2004, for cocktail composition) onto a fused fiber-optic bundle element (Fiber Optic Faceplate, 50 × 50 × 10 mm; SCHOTT North America Inc.), which was subsequently glued into an opening in the aquarium's side wall. The mat was illuminated from above by two warm-white high-power light-emitting diodes (LEDs; LXHL-MWGC Lumileds) emitting in the visible region (VIS, 400–700 nm; intensity 200 mmol photons m^{-2} s^{-1}). The saturating NIR light (NIR, 715–745 nm, lmax = 740 nm; intensity c.60 mmol photons m^{-2} s^{-1}) was generated by an array of NIR LEDs (ELD-740-524, Roithner Lasertechnik) equipped with a band-pass filter (730AF30, Omega Optical). The wavelength region was selected so as to match specifically the in vivo absorption maximum of BChl c. The mat was illuminated from the side through the optode window to ensure maximal exposure of the BChl c-containing organisms to NIR light. The VIS and NIR LEDs could be switched on and off independently of each other. Each of the four possible illumination combinations (VIS1NIR, VIS-only, NIR-only and dark) lasted for 3 h, during which oxygen images were recorded at 5-min intervals using an oxygen imaging system (see Holst & Grunwald, 2001 for details). Temperature was maintained constant at 20 °C and the overlying water was aerated during the measurement.

NIR light-dependent respiration of BChl c-containing bacteria was calculated from the steady state oxygen images by expanding the 1-D method described by Polerecky et al. (2007) to 2-D. Specifically, O_2 images measured at the end of the VIS1NIR and VIS-only periods were subtracted from each other to obtain the differential oxygen image during VIS illumination, denoted as δO2(+VIS). The same was done for the images measured at the end of the NIR-only and dark periods to obtain differential oxygen image in the absence of VIS illumination, denoted as ΔO2(-VIS). Subsequently, 2-D maps of the respiration activity of the BChl c-containing bacteria (supposedly Chloroflexaceae) in the VIS light [RC(+VIS)] and in the dark [RC(-VIS)] were calculated from the second derivative of the respective differential oxygen images and oxygen diffusion coefficient D, as suggested by Polerecky et al. (2007). For simplicity, the second derivatives were calculated only in the vertical (z) direction, i.e., $R_C(\pm\text{VIS}) \approx -D\ \partial^2\Delta O_2(\pm\text{VIS})/\partial^2 z$. This

was done numerically by applying the Savitzky–Golay filter on the vertical profiles extracted from each differential oxygen image. 2-D maps of net photosynthesis in the VIS light and dark were calculated similarly but using the respective oxygen images, i.e. $NP(\pm VIS) \approx -D\, \partial^2 O_2(\pm VIS, -NIR)/\partial^2 z$.

Photopigment analysis by HPLC and hyperspectral imaging

For HPLC pigment analysis, frozen microbial mat cores (0.9 cm diameter) were horizontally sliced in 250- μm thick sections using a rotary HM 505E cryomicrotome (Micron) from the surface down to 10mm depth. Pigments were extracted in 5-mL 100% acetone for 24 h at -35 °C in the dark. Extracts were subsequently centrifuged for 10min at 16 000 g and supernatant aliquots were analyzed by HPLC as described before (Jonkers et al., 2003). Standards for chlorophyll a (Chl a) and Zeaxanthin were obtained from DHI Water and Environment, Denmark. Cultures of *Thiocapsa roseopersicina* (BChl a), C. *aurantiacus* (BChl c) and *Chlorobium tepidum* (BChl c) were used as a source for the respective bacteriochlorophyll standards. Because no quantitative bacteriochlorophyll standards were available, these pigments were quantified only in arbitrary units (A.U.).

2-D mapping of photopigment distribution in the mat was carried out using a newly developed hyperspectral imaging system (L. Polerecky et al., unpublished data). Briefly, the system comprises a laboratory hyperspectral camera (Resonon Inc., Bozeman) attached to a motorized stage (VT-80, Micos), which is mounted onto a heavy stand. The hyperspectral camera allowed simultaneous acquisition of light spectra from a line of 480 pixels in the wavelength region 460–913 nm (resolution c. 2 nm). A 1-mm thick vertical mat section was placed between two microscope slides and kept moist with hypersaline water. The slides were gently pressed to achieve maximal optical contact with the mat, and to ensure that the imaged face of the mat was flat. The sample was then placed c. 5 cm in front of the objective lens and illuminated from above. The hyperspectral images were acquired by moving the camera (at 80 $\mu m s^{-1}$) over the sample while recording the spectral information from the line of pixels at 3.75 fps. The resulting hyperspectral images had a spatial resolution of c.30 μm x 30 μm.

Both the absorption and the autofluorescence properties of the pigments in the mat were used for hyperspectral pigment imaging. For the absorption measurements, the sample was placed on a white standard substrate (Spectra-lon), which allowed simultaneous acquisition of the reference and reflected spectra in one scan, and illuminated by either a combination of warm-white and NIR LEDs or a halogen lamp emitting in the VIS+IR region (Table 1). Spectral reflectance R(λ) in each pixel of the mat was obtained by dividing the spectrum of the light reflected from the sample with that reflected from the white standard. The emission spectra were measured under illumination by a narrow band LED equipped with a 51 collimating optics (LXHL-NX05-5; Lumileds) and a short-pass optical filter, and the emitted autofluorescence was imaged through a complementary long-pass optical filter (see Table 1 for the light source+filter combinations used). During these measurements, the sample was placed on a black substrate to minimize reflections of the excitation light.

HS imaging mode:	Light source:	Excitation / Emission filter:	Target group:
Absorption	LXHL-MWGC[1] (450–720 nm)	-	Diatoms
	+ ELD-740-524[2] (710–770 nm)	-	Cyanobacteria
	or halogen lamp (450–900 nm)	-	BChl *a* and *c*- producing bacteria
Emission	LXHL-LR5C[1]	455DF70/510ALP[3]	Diatoms
	(λ_{max} = 455 nm, blue)	(λ_c = 510 nm)	BChl *a* and *c*- producing bacteria
Emission	LXHL-LL3C[1]	DC-Red/R-61[4]	Cyanobacteria
	(λ_{max} = 590 nm, amber)	(λ_c = 610 nm)	

[1]Lumileds; [2]Roithner Lasertechnik; [3]Omega Optical; [4]Linos Photonics

Table 1. Combinations of light sources together with excitation and emission filters used for hyperspectral imaging of pigments in the mat

The hyperspectral images obtained were analyzed using the available in vivo absorption and fluorescence characteristics of the targeted pigments (Table 2). Specifically, the fourth derivative of the reflectance in the wave length corresponding to the absorption maximum (λmax; Table 2) of a given pigment was taken as a relative measure of the local pigment concentration, i.e. [pigment] ≈ $d^4R(\lambda_{max})/d\lambda^4$ (Butler & Hopkins, 1970; Fleissner et al., 1996). The emission spectra were fitted by a linear combination of Lorenzian and/or Gaussian peak functions centered at specific wavelengths corresponding to *in vivo* emission maxima of the targeted pigments (Table 2), similar to that performed

by Combe et al. (2005) and Barille et al. (2007) for reflectivity spectra. The magnitude of the peaks was then taken as a relative measure for the local concentration of the corresponding pigment. In both absorption and emission measurement modes, the calculated concentrations of the targeted pigment were color-coded and displayed as R, G and B channels in composite RGB images. To allow quantitative comparison with the 1-D HPLC-determined pigment distributions, the 2-D maps were also horizontally averaged over 0.5-mm intervals and plotted as vertical profiles.

Pigment:	Absorption maximum (λ_{max}):	Excitation/Emission maximum (λ_{max}):	Target group:
Chl a	673 nm	455 / 677 nm	Diatom*s*
Chl a	673 nm	-	*Cyanobacteria*
Phycocyanin[1]	622 nm	590 / 652 nm	*Cyanobacteria*
BChl *a*[2]	807 + 845 nm	455 / 867 nm	Chloroflexaceae / Purple sulfur bacteria
BChl *c*[3]	733 nm	455 / 756 nm	Green sulfur bacteria / some *Chloroflexaceae*

[1]Hofstraat *et al.*, (1994); [2]Kühl & Fenchel (2000); [3]Saga & Tamiaki (2004)

Table 2. Absorption and emission characteristics of pigments found in the studied mat; only spectral features associated with target microorganisms of this study are listed.

Distribution of Chloroflexaceae in intact mat samples by FISH analysis

The spatial distribution of two specific groups within the *Chloroflexaceae* family was studied by FISH using previously developed specific probes (Nübel et al., 2002). The FISH probing was limited to members phylogenetically related to two genera, *Chloroflexus* and *Roseiflexus*, as specific probes for the other four genera within the *Chloroflexaceae* family (*Chloronema, Heliothrix, Oscillochloris* and '*Candidatus Chlorothrix'*) were not available at the time of this study. As the members of the genera Chloroflexus and Roseiflexus characterized so far produce BChl a+c, and BChl a but not BChl c, respectively, we assumed in this study that the applied FISH probes targeted corresponding pigment-producing phylotypes of these two genera. For the FISH procedure, mat pieces were firstly fixed in filter-sterilized 4.5% formaldehyde in seawater

for 12 h at room temperature. Subsequently, formaldehyde was rinsed out twice with a saline phosphate buffer ((1.37 M NaCl, 85 mM $Na_2HPO_4.2\ H_2O$, 27 mM KCl, 15 mM KH_2PO_4). In order to maintain the spatial organization, the mat was then embedded in a methacrylate resin, which enabled precise vertical sectioning of thin samples (30 μm) using a rotary HM 505E cryomicrotome (Microm). These sections were hybridized with probes CFX1238 (CGCATTGTCGTGGC CATT) attached to fluorophore Alexa 647 and RFX1238 (CGCATTGTCGGCGCCATT) attached to fluorophore Alexa 488, targeting Chloroflexus- and Roseiflexus-related phylotypes, respectively (Nübel et al., 2002). Sections of thus plasticized mat samples were mixed with a 5-μL probe and 45-μL hybridization buffer (40% formamide) in a 125- μL reaction vial, incubated for 6 h at 45 1C and washed in prewarmed washing buffer for 10min at 47 °C. Hybridized mat sections were subsequently covered with antifading immersion oil (Citifluor Ltd, UK) and evaluated using a fluorescence microscope (Axio Imager M1, Zeiss, equipped with Plan Apochromat objectives).

Chloroflexaceae diversity in the ma*t*

As the FISH probe analysis carried out in this study targeted phylotypes of only two out of six known *Chloroflexaceae* genera, a 16S rRNA gene clone library was additionally constructed in order to obtain an estimate of the diversity of *Chloroflexaceae* genera present in the mat. Specific PCR primers (CCR-344-F and CCR-1338-R) developed by Nübel et al. (2001), targeting the 16S rRNA gene of all presently known *Chloroflexaceae* members, were applied. Genomic DNA was extracted from a 1-cm thick intact mat sample by phenol–chloroform extraction and purified with the Wizard® DNA clean-up system (Promega, Madison, WI). Approximately 1000-bp fragments of the present 16S rRNA genes were amplified from genomic DNA using the specific primers. PCR conditions were applied as described in Nübel et al. (2001). The PCR product was subsequently visualized on an agarose gel, and the 16S rRNA gene band was excised. The excised PCR product was then purified using the QIAquick Gel Extraction Kit (Qiagen, Hilden, Germany). Two microliters of purified product was ligated into the pGEM T-Easy vector (Promega) and transformed into Escherichia coli TOP10 cells (Invitrogen, Carlsbad, CA) according to the manufacturer's recommendations. Over night

cultures were prepared from positive transformants in a 2-mL 96-well culturing plate. Plasmid DNA was extracted and purified using the Montage Plasmid Miniprep 96 kit (Millipore, Billerica). Purified plasmids were sequenced in one direction with the M13F primer using the BigDye Terminator v3.0 Cycle Sequencing kit (Applied Biosystems, Foster City, CA). Samples were run on an Applied Biosystems 3100 Genetic Analyzer. Sequences of > 800 bp were matched with the nucleotide–nucleotide BLAST (BLASTN) tool (www.ncbi.nlm.nih.gov/blast/Blast.cgi) and closest matches with sequences fromboth environmental clones and isolated bacteria present in the database were determined.

Sulfate reduction rates

For the determination of sulfate reduction rates in distinct deep layers of the mat, 1.5-cm diameter microbial mat cores overlain with 2mL water were injected each with 3MBq 35 $^{35}SO_4^2$ divided over five injections of 5 μL each to ensure an equal distribution of tracer. Triplicate cores were incubated for 5 h either under light (500 mmol photons m^{-2} s^{-1})or dark conditions at room temperature. Cores were fixed in liquid nitrogen after incubation. Duplicate control cores were fixed in liquid nitrogen immediately after tracer injection. Cores were then horizontally cut into 4-mm thick slices to a depth of 24mm and fixed in 20% zinc acetate solution. Reduced-labeled sulfate was extracted following the single-step chromium reduction method according to the procedure described in Kallmeyer et al. (2004) and quantified with a liquid scintillation counter (2500 TR, Packard) using Lumasafe Plus (Lumac BV, Holland) scintillation cocktail. Microbial mat pore water sulfate was quantified by ion chromatography to enable calculation of specific sulfate reduction rates (Kallmeyer et al., 2004).

Results

General description of the microbial mat

The mesocosm-incubated microbial mat investigated consisted of distinctly colored layers (Figs 1, 6a and 7a). Microscopic analysis revealed that the top c. 2-mm thick yellow–brown layer was mainly composed of various morphotypes of diatoms and thin filamentous bacteria. Below this layer, a 3–4-mm-thick green layer was dominated by filamentous cyanobacteria. Underneath this layer was a 2–3-mm-thick purple layer

dominated by filamentous bacteria and purple sulfur-like bacteria (1–5-mm diameter spherical bacteria with apparent sulfur inclusions).

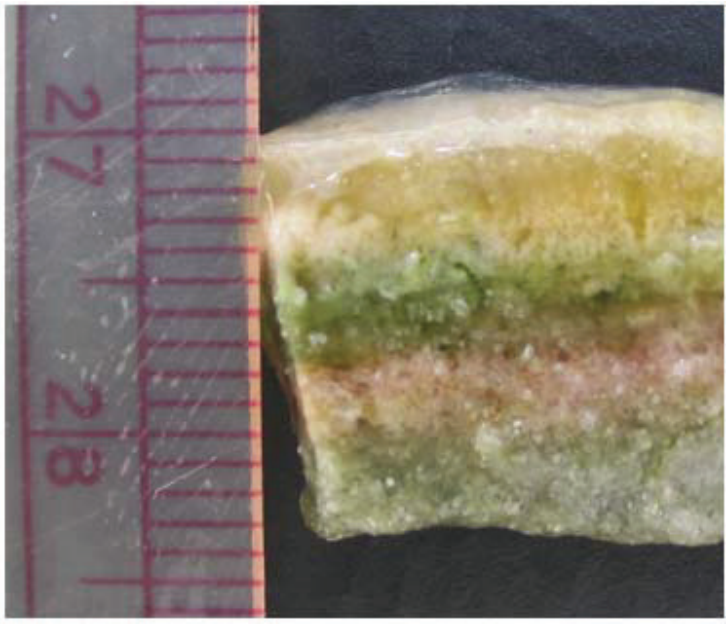

Figure 1: Photograph of a vertically cut subsample of a mesocosm incubated microbial mat used in this study for oxygen, sulfide and light microsensor measurements, HPLC photopigment determination, *Chloroflexus* and *Roseiflexus* FISH analysis and sulfate reduction measurements. For oxygen and hyperspectral imaging, other subsamples of the same mat were used (see Figs 3, 4, 6 and 7). Scale with 0.5-cm intervals is depicted on the paper beside the mat.

Vertical profiles of oxygen, light intensity, sulfide and sulfate reduction rates

Oxygen, measured both with microsensors and planar optodes, penetrated down to c. 2 and 6–9mm in the dark and light incubated mats, respectively (Figs 2a and 3). Light microsensor measurements (Fig. 2b) revealed that NIR light, which can be used by the BChl α- and c-producing bacteria, penetrated in significant amounts to depths 47mm. On the other hand, the intensity of the VIS light at 673 nm, which corresponds to the *in vivo* absorption maximum of Chl α, decreased below 1% of the surface value already at depths of 4–4.5mm. Free sulfide was detected only in deeper parts of the mat, both under dark (>7mm) and under light (>8mm) conditions (Fig. 2a). ^{35}Sulfate-radiotracer measurements revealed that in dark incubated mats, sulfate reduction occurred throughout the entire mat (thickness, c. 2 cm), reaching a maximum at depths 8–12mm. In illuminated mats, significant rates of sulfate reduction were detectable in deeper anoxic parts

(>12mm) of the mat, although low rates were also observed in the 4–8mm zone (Fig. 2c). It thus appears that in this mat sulfate reduction was not restricted to anoxic zones only but also occurred in the oxic zone of the mat (Fig. 2c).

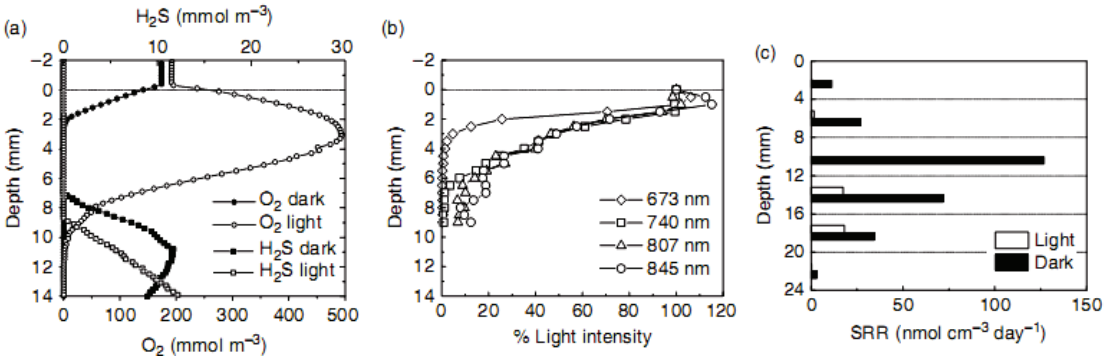

Figure 2. **(a)** Oxygen and total free sulfide (H_2S+HS^-+$S2^-$) concentration profiles in the mat measured in the dark and under visible illumination (500 µmol photons $m^{-2}s^{-1}$.**(b)** Vertical profiles of scalar irradiance in the mat at selected wavelengths corresponding to absorption maxima of targeted pigments (see Table 2). Values are expressed as percentage of the irradiance at the mat surface. **(c)** Vertical profiles of sulfate reduction rates in dark and light (500 µmol photons $m^{-2}s^{-1}$) incubated mat samples.

Spatial distribution of photopigments

As for this study, the hyperspectral imaging technique was optimized for the detection of BChl α and c in addition to other major photosynthetic pigments (Chl α and phycobilins); the results of this technique (Figs 6 and 7) are compared with those obtained with traditional HPLC photopigment detection (Fig. 5). The presence of Chl α (produced by algae and cyanobacteria), BChl α (produced by purple and green sulfur bacteria and *Chloroflexaceae*) and BChl c (produced by some green sulfur bacteria and some *Chloroflexaceae*) in the mat was detected by both HPLC and hyperspectral methods. The typical cyanobacterial pigments phycocyanin (a phycobilin) and zeaxanthin (a carotenoid) detected by hyperspectral imaging and HPLC analysis, respectively, were used as specific proxies for the distribution of cyanobacteria.

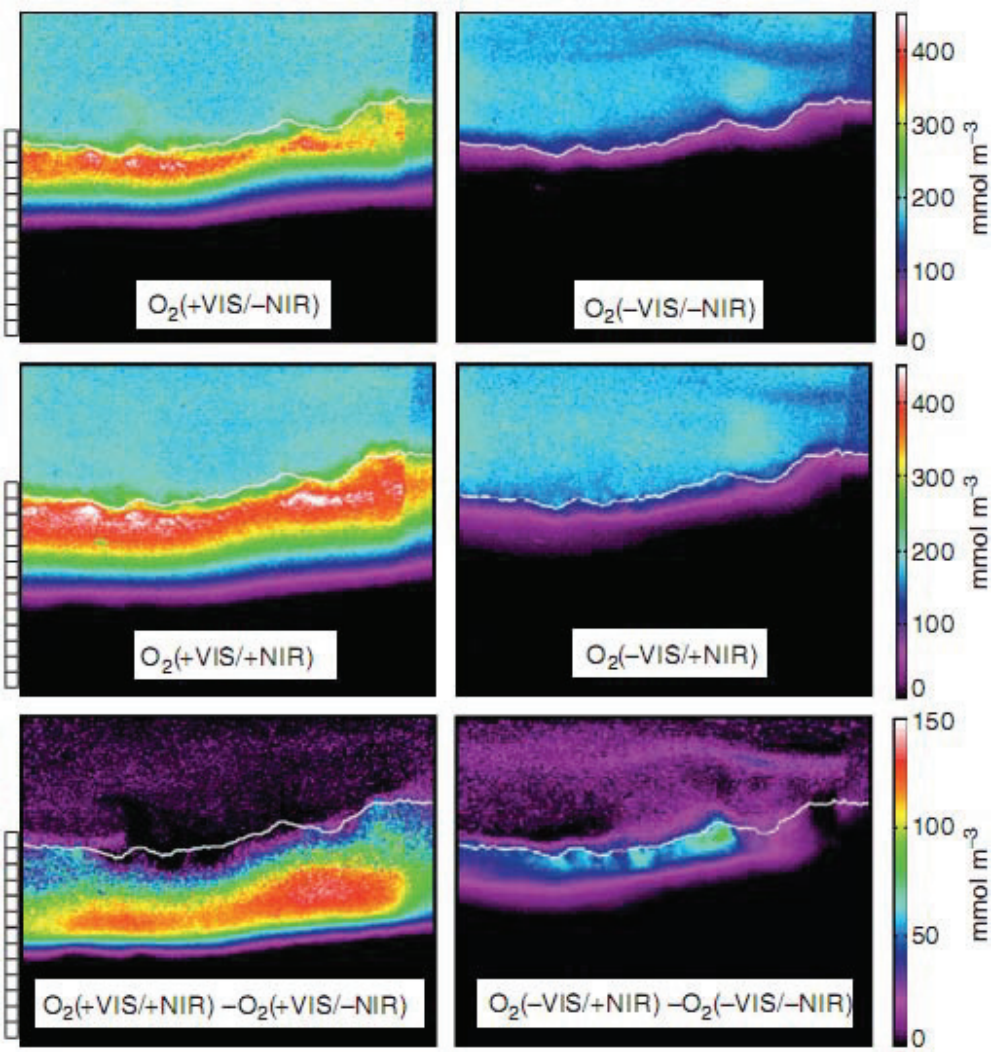

Figure 3. Oxygen imaging across a vertical section of the microbial mat (shown in Fig. 7a) using planar optodes. Top and middle panels show steady-state oxygen distributions at four combinations of illumination by visible (VIS) and saturated NIR lights, respectively. + and - indicate the presence and absence of the light, respectively. Differential oxygen images, calculated as the difference between the oxygen distributions obtained with (middle panel) and without (top panel) NIR illumination, are shown in the bottom panel. Approximate mat surface is depicted by a white horizontal line; scale bar in mm is shown on the left, and color scaling on the right.

HPLC analysis revealed abundant Chl α content in the top 8mm of the mat, reaching local maxima at depth zones of 2–3 and 6–7mm (Fig. 5). These maxima coincided well with the bands in which zeaxanthin was observed. BChl α was almost not detected by HPLC in the top 5.5mm of the mat (with the exception of depth c. 3.5mm), but was found only at depths of 5.5–7mm. In contrast, BChl c was detected only in a narrow zone at depths

of 3–4mm, coinciding with low amounts of BChl α, the local minimum of zeaxanthin and depreciated Chl α concentrations.

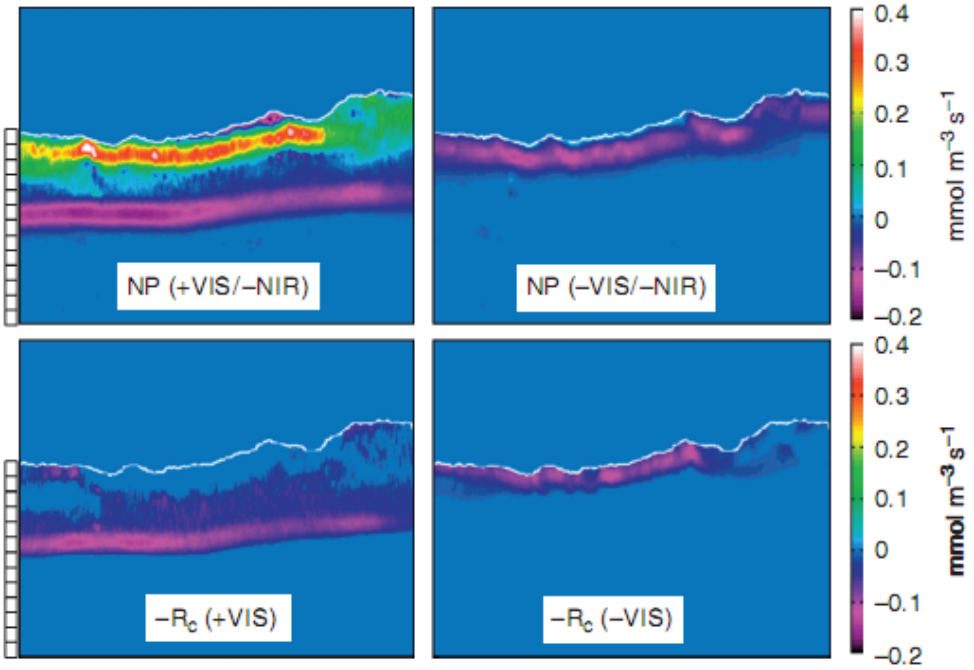

Figure 4. Distributions of rates of net photosynthesis (NP; top) and respiration by BChl c-producing Chloroflexaceae (RC; bottom) in the presence (left) and absence (right) of illumination by visible light (NIR illumination was absent in both cases). NP and RC images were calculated from the oxygen images in the top row and from the differential oxygen images in the bottom row of Fig. 3, respectively. Positive and negative NP values represent net production and consumption, respectively. Note that RC is displayed as a negative value to enable direct visual comparison with the NP rates. Approximate mat surface is depicted by the white horizontal line; scale bar in mm is shown on the left and color scaling on the right.

Hyperspectral imaging was sensitive to detect target photopigments in both absorption and emission modes. In the absorption mode, the presence of a pigment was detected as a pronounced valley in the reflectance spectrum centered at a specific wavelength λ_{max} corresponding to the pigment's in vivo absorption maximum (Fig. 6e, Table 2). In the emission mode, pigment was detected by its strong autofluorescence. Detection of Chl α (in algae and cyanobacteria) and BChls α and c was possible using blue excitation (λ_{max} = 455 nm) and emission at 677, 867 and 756 nm, respectively, while phycocyanin (in cyanobacteria) could be detected using amber excitation (λ_{max} = 590 nm) and emission at 652 nm (Fig. 6f, Table 2). Although more emission peaks were observed using these two

excitation wavelengths, only those mentioned above were analyzed in more detail to remain focused on the targeted groups of microorganisms.

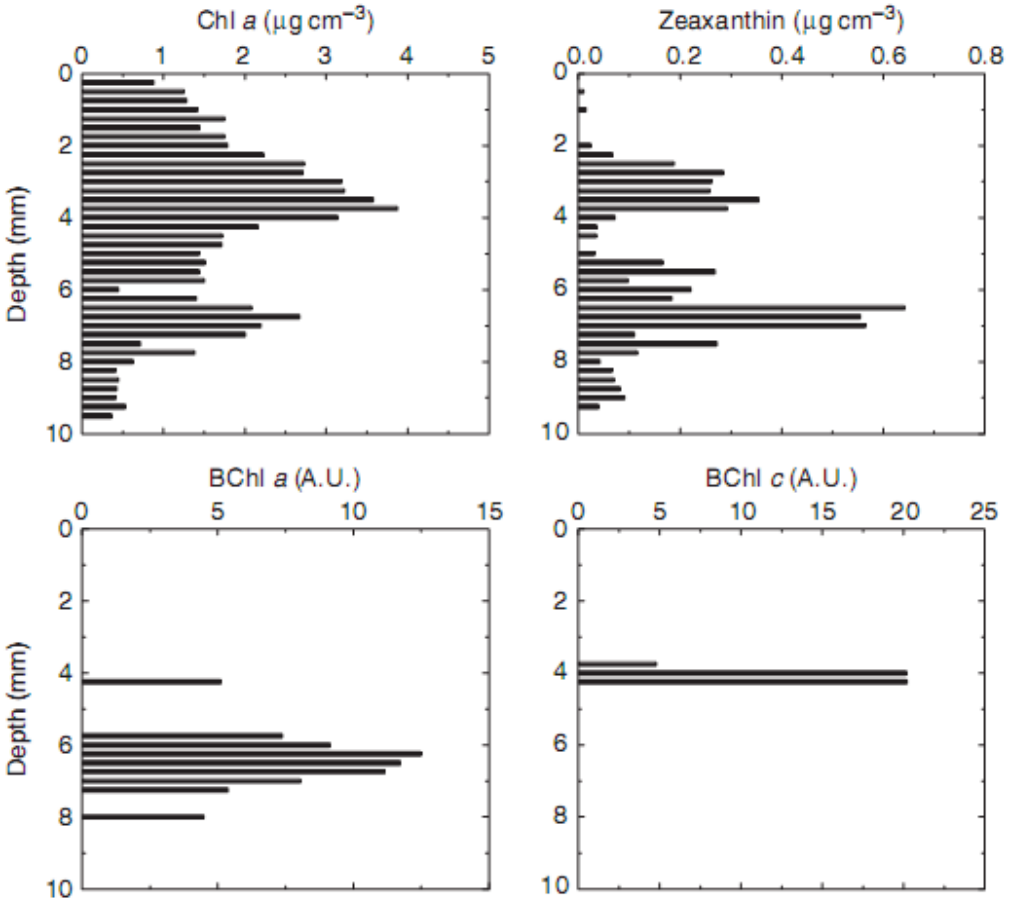

Figure 5. Vertical profiles of photopigments in the mat, as determined by HPLC analysis of 0.25-mm thin mat sections. Chl α and zeaxanthin are presented in µgcm^{-3} of the mat, while the other pigments are in A.U. due to lack of calibration standards.

Pigment distributions in the studied mat derived from hyperspectral imaging exhibited a very patchy character, with pronounced vertical and horizontal heterogeneities (Fig. 6b–d). When horizontally averaged, the vertical pigment distributions matched mostly well with those determined by HPLC (compare Figs 5 and 6g–i). Namely, local Chl α maxima due to the presence of algae (diatoms) were observed in the top c. 1mm of the mat, while wide but pronounced peaks of Chl α and phycocyanin corresponding to dense cyanobacterial populations were observed at depths of c. 3 and 4–5mm.

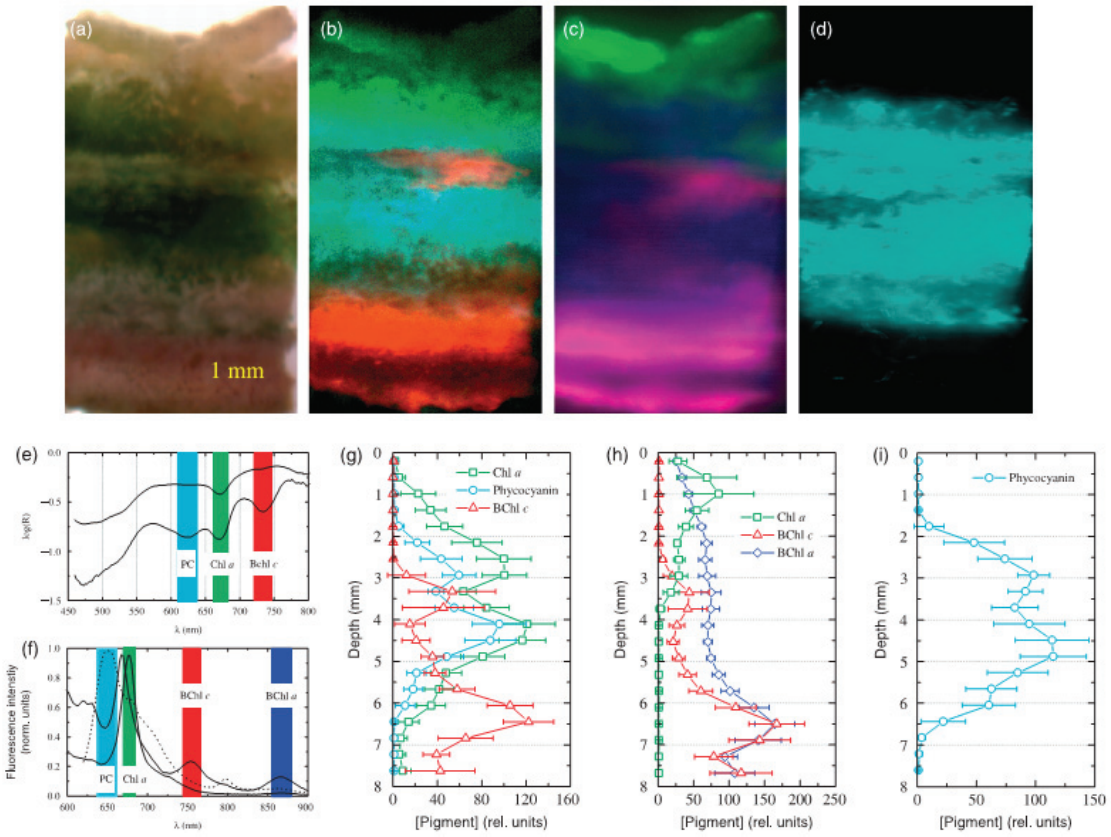

Figure 6. Hyperspectral imaging of pigments in the microbial mat. (a) True-color image of the mat, as seen by a naked eye under white illumination. (b) Relative concentrations of photopigments Chl α (green), phycocyanin (PC, blue) and BChl c (red) across a vertical section of the mat, as calculated from the second derivative of the reflectance spectra at specific wavelengths. Examples of the reflectance spectra, together with the spectral features corresponding to the target pigments, are shown in (e). (c–d) Relative concentrations of photopigments across the mat calculated from the magnitudes of the auto-fluorescence peaks emitted when excited by blue (c) and amber (d) lights (Tables 1 and 2). Examples of normalized emission spectra obtained using blue and amber excitation are shown in (f) by solid and dotted lines, respectively. Associations between the emission peaks and the target pigments are also shown. Red, green and blue colors in (c) correspond to photopigments BChl c,Chl α and BChl α, respectively, while cyan color in (d) corresponds to phycocyanin. Note that mix-colored regions represent areas where more than one pigment are concurrently detected (e.g. in B, cyan = blue+green indicates concurrent presence of Chl α and phycocyanin; in C, magenta = blue+red indicates the concurrent presence of BChl α and c). (g), (h) and (i) show the vertical profiles of relative pigment concentrations obtained by horizontal averaging of the corresponding channels in images (b), (c) and (d), respectively.

Local maximum of BChl c was detected as a pronounced patch at a depth of 3–4mm, i.e., in the zone where Chl α and phycocyanin exhibited local minimum. Similar complementarities were seen in the HPLC data. However, unlike HPLC analysis, hyperspectral imaging revealed evidence of absorption at 733 nm as well as emission at 756 nm in deeper parts of the mat (>4mm, peaking at c. 6.5mm), suggesting abundant

presence of BChl c also at these zones of the mat. Furthermore, in contrast to the HPLC analysis, which detected BChl α only below c. 5.5mm, hyperspectral imaging suggests detectable amounts of BChl a throughout the entire mat (0–8mm), reaching a maximum at depth c. 6.5mm (Fig. 6h).

Hyperspectral analysis of another subsample of the same mat, which was also used for O_2 imaging, revealed a similar degree of patchiness in the pigment distribution, as demonstrated by large variability of colors in the composite RGB image in Fig. 7c–d. Chl α was abundant throughout the mat, reaching a wide maximum at c. 3mm depth, while phycocyanin became abundant only at depths below 2mm. Evidence for the presence of BChl c (i.e. pronounced absorption at 733 nm) was found throughout the mat, starting at lower concentrations also at the mat surface and reaching a wide maximum at 3–7mm (Fig. 7f).

As diatoms (and other algae) produce only Chl α, while cyanobacteria produce Chl α, in addition to zeaxanthin and phycocyanin, it can be concluded from these profiles that diatoms and other algae are responsible for the upper Chl α maximum (0–1.5mm depth; Chl α but insignificant zeaxanthin or phycocyanin present), while at least two apparently different populations of cyanobacteria occur in deeper parts of the mat. BChl α and c-producing bacteria (purple and green sulfur bacteria and *Chloroflexaceae*; see Discussion) exhibited profound maxima at 6–7 and 3–4+6–7mm depths, respectively.

Hyperspectral imaging revealed a high degree of horizontal heterogeneity, in addition to vertical stratification, in the distribution of major phototrophic groups of microorganisms in the mat. Particularly striking is the patchy distribution pattern of BChl c, depicted by the red channel (i.e. as red, magenta or orange) in the composite images in Figs 6b–c and 7d. It appears that BChl c-producing *Chloroflexaceae* are spatially not closely associated with the oxygenic phototrophs (diatoms and/or cyanobacteria) present in the mat, as was hypothesized in this study, but are rather ‘sandwiched’ in their own specific locations, possibly determined by factors other than excretion of organics by oxygenic phototrophs.

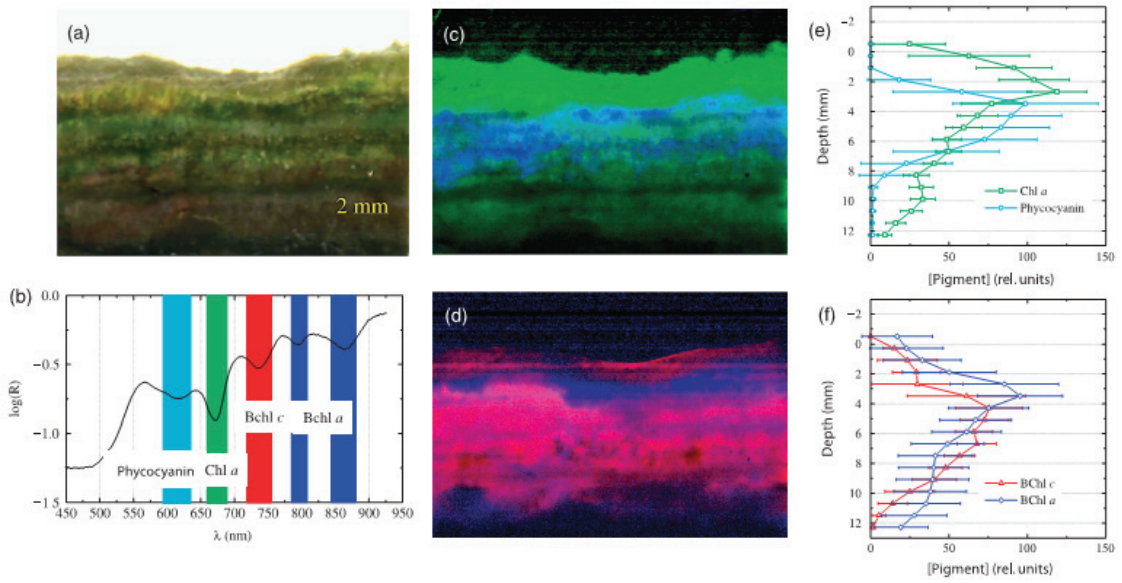

Figure 7. (a), (b), (c+d) and (e1f) correspond to the same quantities as those displayed in Fig. 6a, b, e and g, respectively, except for the fact that the measurements were conducted on the same mat subsample for which O_2 imaging was carried out (see Figs 3 and 4). Note again mixed colors in (c) and (d): cyan = blue+green, i.e. concurrent occurrence of phycocyanin and Chl α, magenta = blue1red, i.e. concurrent occurrence of BChl a and BChl c..

Number of clones (<97% similarity)	Closest isolate / % similarity	Closest clone sequence / % similarity
20	'Candidatus Chlorothrix halophila' / 90-97% (AY395567)	Uncultured CLB / 92-99% (DQ103661)
2	'Candidatus Chlorothrix halophila' / 93% (AY395567)	Halotolerant bact P4-I-O / 93% (AJ308497)
2	*Oscillochloris* sp. / 89-90% (AF146832)	Uncultured CLB / 92-95% (AJ309642)
2	*Chloroflexus* sp. / 89% (AJ308498)	Uncultured CLB / 98-99% (DQ329967)
3	*Roseiflexus castenholzii* / 58-76% (AB041226)	Uncultured CLB / 97-98% (DQ329903)

Table 3. BLAST analysis of 16S rRNA gene sequences obtained from a clone library prepared with *Chloroflexaceae*-specific PCR primers.

Chloroflexaceae-related phylotype diversity and depth distribution of selected species

Analysis of the 16S rRNA gene clone library carried out with specific primers revealed the presence of sequences related (58–97%) to characterized members of four of the six known genera of the Chloroflexaceae Family (Table 3). Members of three of these genera

are known to produce BChl c (*Chloroflexus* sp., *Oscillochloris* sp. and '*Candidatus Chlorothrix halophila*'), while members of the fourth genus are known to produce BChl α only (Roseiflexus castenholzii). By far most of the analyzed unique sequences (22 out of 29, i.e. 76%) appeared to be related to '*Candidatus Chlorothrix halophila*'.

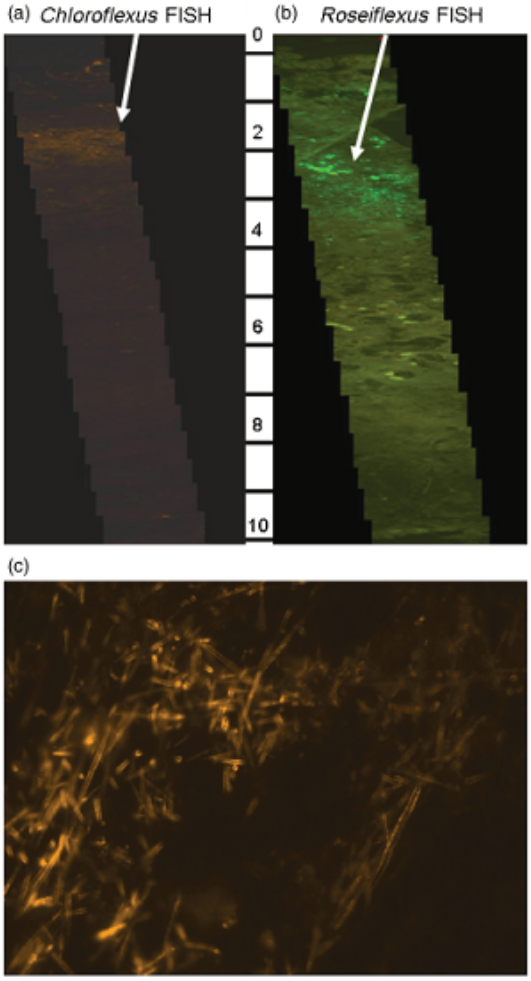

Figure 8: Images of the microbial mat hybridized with (a) Chloroflexusand (b) Roseiflexus specific FISH probes. Scale bars indicate depth in millimeters from the mat surface. (c) Close-up of (a) showing positive hybridization of probe CFX1238 with filamentous bacteria.

FISH analysis with probes designed to specifically target representatives of the genera *Chloroflexus* and *Roseiflexus* indicated that related phylotypes of both groups were indeed present in the mat. Their distribution, as estimated from the brightness of the FISH probe signal (Fig. 8), appeared to be mainly concentrated in the 2–4mm depth zone. *Chloroflexus* relatives appeared to be concentrated at a somewhat shallower depth than

the Roseiflexus relatives. However, the fluorescent signal of both FISH probes was also visible in other mat zones (e.g. at depth c. 6mm). This suggests that although the species related to these two genera were concentrated in a specific zone, they were present throughout the entire mat, which is a result similar to that revealed by hyperspectral imaging.

Imaging of oxygen and oxygen production/consumption rates in the mat

2-D oxygen distributions in the mat showed pronounced horizontal heterogeneity in the upper 2–4mm of the mat (Fig. 3, top row). Under VIS illumination (light intensity of c. 200 μmol photons m^{-2} s^{-1}), peak oxygen concentrations varied between 320 and 420 μM. The top 3–4mm of the mat were photosynthetically net producing (maximum NP rates ranging between 0.15 and 0.4 mmol m^{-3} s^{-1}), while respiration exceeded photosynthesis at depths below 4–5mm, reaching maxima of 0.1–0.18 mmol m^{-3} s^{-1}at the oxic/ anoxic interface (Fig. 4, top-left). In the dark, the oxic zone was only 2–3mm thick and the respiration rates in this zone were similar (0.1–0.15 mmol m^{-3} s^{-1}; Fig. 4, top-right).

To estimate the contribution of BChl c-producing *Chloroflexaceae* to this respiration, the mat was additionally illuminated by saturating NIR illumination (λ_{max} = 740 nm, corresponding to the specific in vivo absorbance of BChl c), which was shown to inhibit respiration by *Chloroflexaceae* species (Polerecky et al., 2007). Upon this additional NIR illumination, oxygen penetration depth in the mat significantly increased by 1–2mm (Fig. 3, middle row). This was accompanied by a dramatic increase in oxygen concentrations in the top mat layers (by 60–140 mM in the VIS light and by 40–60 mM in the dark), most pronounced at depths of 4–6mm in the VIS light and immediately below the mat surface in the dark (Fig. 3, bottom row). When this change in oxygen concentrations was converted into the respiration rates of BChl c-producing *Chloroflexaceae* using the method proposed earlier (Polerecky et al., 2007), it was found that, in the zones where NP was negative, the rates were comparable in magnitude and spatially correlated with the (negative) rates of net photosynthesis in the dark- or VIS-light-only illuminated mat (compare the dark-blue-to-magenta patches in the top and bottom rows in Fig. 4). This means that the respiration of BChl c-producing Chloroflexaceae constituted a significant part of total respiration in the mat's oxic zone.

Discussion

Comparison between HPLC and direct hyperspectral pigment imaging techniques

The most important advantage of the hyperspectral imaging of photopigments (either by detecting their absorption or auto-fluorescence) over the traditional HPLC detection technique is that the structural composition of the sample and thus the spatial organization of the pigmented community members can remain undisturbed. This is because direct imaging does not require pigment extraction before the analysis (Wiggli et al., 1999). The detection limit of the hyperspectral technique appeared to be low (high sensitivity), because pigment concentrations were not diluted as was done in extracts obtained for HPLC analysis in this study, although this could be improved by concentrating the pigment extracts before analysis. Imaging of auto-fluorescence also largely cuts back on the need for pigment separation before analysis, as the combination of specific excitation wavelengths with sophisticated spectral analysis allows detection of individual pigments in a complex mixture (Wiggli et al., 1999).

Although hyperspectral imaging of reflectance spectra combined with the fourth derivative approach for the identification of pigments did provide a valuable insight into the distribution of pigments targeted by this study, hyperspectral imaging in the emission mode appeared to be superior. This was mainly due to a higher degree of specificity, offered by the higher degree of choice of the excitation wavelengths, as well as due to a more direct relationship between the observed fluorescence peak magnitude and the local pigment concentration, which is not to such a large degree as the spectral reflectance measurement affected by the scattering properties of the sample. Another reason for the preferential choice of auto-fluorescence imaging is the fact that the number of identifiable and spectrally separable fluorescence peaks is generally considerably larger than that of specific absorption features.

Important disadvantages of the HPLC analysis are that not all pigments can be readily extracted from the cells, that pigments may be altered during the pigment extraction procedure and that pigments may not be well separated from each other as well as from other interfering compounds present in the mat, which hampers correct identification.

One of these factors may have been the reason why the deeper BChl c maximum (at 6–7mm depth) and/or the rather abundant presence of BChl α throughout the mat observed by hyperspectral imaging was not detected, or at least not correctly identified, by HPLC. Another possibility could be due to the presence of sulfide in the mat, as this strongly reducing agent may have altered the structure of BChl α/c during the extraction procedure. Particularly for these reasons we are confident that a further improvement of hyperspectral imaging, for example, by calibrating the method using pigment standards and pure cultures of characterized phototrophic algae and bacteria, may yield a valuable method for pigment analysis in undisturbed complex microbial communities.

Spatial distribution of Chloroflexaceae and NIR light-dependent respiratory activity
Previous studies reported that characterized Chloroflexaceae species apparently preferentially use organic photosynthates, excreted particularly by cyanobacteria, for photo-heterotrophic growth (Bateson & Ward, 1988; Castenholz, 1988; Hanada & Pierson, 2006; Hanada et al., 2002; van der Meer et al., 2003; Berg et al., 2005). Based on these findings, we hypothesized that the spatial distribution of Chloroflexaceae members in the microbial mat would be closely associated with the distribution of oxygenic phototrophs. However, as determined by HPLC and hyperspectral imaging in this study, distributions of the photopigments BChl c, which is produced by members of four of the six known Chloroflexaceae genera, and Chl α and/or phycocyanin, produced by oxygenic phototrophs, were more complementary than similar. Whereas distinct Chl α maxima were located in mat zones at depths around 1, 2–3 and 4–5mm, most of the BChl c was found at depths of 3–4mm and below 5–6mm. All the pigments investigated exhibited not only pronounced vertical stratification, but were to a large extent, especially BChl c and a, heterogeneous also in the horizontal direction. Although one part of the BChl c-producing population (at 3–4mm depth) did occur in the oxygen-saturated photic zone of the mat, its patchy rather than a more stratum-like horizontal distribution indicated that the availability of excreted photosynthates was likely not the prime factor determining their spatial distribution.

From studies in which Chloroflexaceae members were physiologically characterized, it is known that in addition to photosynthates, most isolates and enrichments can use sulfide as a growth substrate, i.e. as an electron donor for photoautotrophic CO_2 fixation (Pierson

& Castenholz, 1974; Klappenbach & Pierson, 2004; van der Meer et al., 2005). This raises a question of whether the availability of sulfide or another potential electron donor for autotrophic growth would influence the occurrence and spatial distribution of BChl c-producing Chloroflexaceae. Measured sulfide concentration profiles showed that free sulfide occurred at depths Z7mm, which is too deep for the population present in the 3–4mm zone, but not for the deeper positioned (6–7mm) BChl c-containing population, which showed a somewhat more homogenous horizontal distribution according to the 2-D hyperspectral pigment analysis. The sulfate reduction rate measurements, however, revealed that this process did occur in all mat zones, including the 0–4mm zone, although primarily under dark and anoxic conditions. As we determined sulfate reduction rates only in layers that were relatively thick (4mm), we can only speculate about the 2-D distribution of this process. However, it is plausible that the occurrence of sulfate reduction and its rate may have a patchy distribution, particularly in the upper photic zone of the mat where the oxygen concentration strongly fluctuates during a 24 h light/dark cycle, and thus influence the distribution of the Chloroflexaceae members. In several previous studies, sulfate reduction was found to occur in the upper and even fully oxygenated photic zone of mats (Canfield & Desmarais, 1991; Frund & Cohen, 1992; Jørgensen, 1994; Ludwig et al., 2005). Rates in distinct depth zones, however, were found to be highly variable (Ludwig et al., 2005), which may indicate that the process, particularly in the upper, mostly oxygenated, photic zone is highly horizontally heterogeneous. Using a silver foil technique for 2-D mapping of sulfate reduction in lithified modern stromatolites, which can be considered as structural homologues of microbial mats, Visscher found a horizontally heterogeneous sulfate reduction activity (Visscher et al., 2000). The reason why sulfate reduction in oxygenated mat zones may show a heterogeneous rather than a homogenous distribution in the horizontal direction is likely because the process is influenced by a combination of several factors such as differences in the oxygen tolerance of different species of sulfate-reducing bacteria (Cypionka, 2000), availability of suitable organic substrates and success in the competition for those substrates against other microbial community members (Jonkers et al., 2005). Although we did not find significant sulfate-reducing activity in the upper photic zone under light and oxygenated conditions, small pockets may have occurred.

Moreover, as significant sulfate reduction in this zone did occur under dark and anoxic conditions, pockets of sulfide, or only partly oxidized sulfur compounds, may have continued to exist in the upper photic zone at least during the initial part of the next light period.

Taking the above-listed considerations into account, i.e. that BChl c-containing characterized Chloroflexaceae members can use photosynthates excreted by oxygenic phototrophs for (photo)heterotrophic growth as well as sulfide or partly oxidized sulfur compounds for photoautotrophic growth, we hypothesize that their occurrence in the oxygenated upper zone of the mat is maximal in those locations where both photosynthate excretion and sulfate reduction occur during a light/dark cycle. If sulfate reduction had a heterogeneous distribution, which would probably be due to differences in oxygen tolerance of different species, it would primarily influence the horizontal spatial distribution of BChl c-containing Chloroflexaceae in the upper, often oxygenated photic zone of the mat. The metabolic flexibility of Chloroflexaceae would give them, in those locations, a competitive advantage over community members with a more restricted physiology (e.g. either photosynthate or sulfide utilization).

Although in addition to certain *Chloroflexaceae* members some green sulfur bacteria are also known to produce BChl c, we assume that species of the former group are responsible for its occurrence in the oxygenated photic zone (at 3–4mm depth) of the mat, as all characterized species of the green sulfur bacteria are strict anaerobes (Pfennig & Tr¨ uper, 1992). The second and larger BChl c maximum found by the hyperspectral analysis in the lower (6–7mm) part of the photic zone was also likely of Chloroflexaceae origin, as oxygen was found to penetrate to a depth of 8mm in illuminated mats.

BChl α maxima were observed by both HPLC and hyperspectral imaging in deeper zones of the mat (Z6mm), although some BChl α was also detected by the spectral imaging technique in other mat zones (0–6mm). Although this pigment is produced by *Chloroflexaceae* members, most of the BChl α in the deeper layer may have originated from oxygen-tolerant purple sulfur bacteria (de Wit & van Gemerden, 1990), as is indicated by the intense purple coloration of this mat zone. The microsensor light measurements showed that NIR light at wavelengths 8071845 and 740 nm, corresponding

to the in vivo absorbance maxima of BChl α and c, respectively, was still available in sufficient amounts below 6mm, which indicates that purple sulfur bacteria and Chloroflexaceae could potentially perform anoxygenic photosynthesis, as free sulfide was also detected in this zone.

One of the two FISH probes that were applied in this study targeted Roseiflexus-related species. Characterized species of this genus produce BChl α but not BChl c and were found to be able to grow photoheterotrophically under anaerobic conditions (Hanada et al., 2002). However, as oxygen does not affect bacteriochlorophyll synthesis in Roseiflexus (Hanada et al., 2002), it is not surprising that theirmaximal occurrence in this study was found in the fully oxic upper photic zone. In previous studies, these filamentous bacteria were found to be spatially tightly associated with cyanobacteria, and were in fact found to occur within polysaccharide sheaths of cyanobacterial filament bundles (D'Amelio et al., 1987; Ley et al., 2006). Such a spatial and structural association with filamentous cyanobacteria, which probably supply Roseiflexus relatives with organic growth substrates, may in fact have determined the rather shallow depth distribution of these preferentially photoheterotrophic (D'Amelio et al., 1987; Pierson et al., 1994) organisms.

The other FISH probe that was applied in this study targeted *Chloroflexus*-related species, i.e., only one of the four known BChl c-producing *Chloroflexaceae* genera. Significant probe signal was observed only in the upper part of themat at depths 2–4mm, i.e. in the zone where clear BChl c maxima were observed by HPLC and hyperspectral analyses. This result indicates that Chloroflexus-related species were responsible for at least a part of the observed upper, but likely not for the deeper BChl c maximum. Clone library data revealed that in addition to *Chloroflexus*, *Oscillochloris* and '*Candidatus Chlorothrix*'-related sequences also occurred in the mat. As characterized members of the latter two genera are also known to produce BChl c, and particularly sequences related to the latter genus dominated the clone library (76%), species related to these genera were most likely responsible for the lower, and possibly for a part of the upper BChl c maximum. In line with our hypothesis stated above, we suggest that *Chloroflexus*-related members found (by FISH analysis) in the upper part of the photic zone depend for growth both on the presence of excreted photosynthates and reduced sulfur compounds, while

Chloroflexaceae members responsible for the lower BChl c maximum (*Oscillochloris*- and/or '*Candidatus Chlorothrix'*- related species) depend for growth less on excreted photosynthates but more on the presence of free sulfide. If the proportion of sequences in the clone library truly reflected the relative abundance of species, the conclusion would be that '*Candidatus Chlorothrix*'-related species were the dominant *Chloroflexaceae* in this mat. '*Candidatus Chlorothrix halophila*' is a recently characterized mesophilic and halophilic filamentous anoxygenic phototrophic bacterium that was obtained from a hypersaline microbial mat from Guerrero Negro, Mexico, and cultured in the laboratory in a highly enriched state (Klappenbach & Pierson, 2004). Although sulfide-dependent phototrophic CO_2-fixation was observed in culture (Klappenbach & Pierson, 2004), (photo)heterotrophic growth on organic photosynthates was not determined in that study. In contrast, characterized Oscillochloris representatives were shown to use organic compounds as additional carbon sources to CO_2 (Berg et al., 2005). As specific FISH probes for 'Candidatus Chlorothrix'- and Oscillochloris-related species are not yet available, their spatial distribution and contribution to BChl c maxima as observed in the hypersaline mat of this study remains to be quantified.

The second aim of this study was to establish a direct relationship between the presence of BChl c and NIR light-dependent respiration occurring in the microbial mat. The NIR light spectrum (715–745 nm, λ_{max} = 740 nm) applied in this study was selected to specifically target BChl c and to some extent BChl d- and e-producing species, as other types of bacteriochlorophyll show maximum in vivo absorbance at different wavelengths (BChl α: 805+830–890 nm; BChl b: 835–850+1020–1040 nm; BChl g: 670+788 nm; whereas BChl c: 740–755 nm; BChl d: 705–740 nm; BChl e: 719–726 nm) (Kühl & Fenchel, 2000; Madigan et al., 2000). Comparing Figs 4 (bottom) and 7d, which were measured on the same subsample of the mat, it can be seen that pronounced NIR light-dependent respiration activity of *Chloroflexaceae* determined by planar oxygen optodes is found in locations where abundant concentrations of BChl c are found with hyperspectral imaging, and both of these distributions have a very patchy character. Although the quality of the oxygen data and the noncalibrated character of the hyperspectral data did not allow a more accurate correlation analysis, at least a qualitative match of these two datasets demonstrates that BChl c-producing *Chloroflexaceae* are indeed responsible for

the respiration in the mat that can be decreased or even completely inhibited by adding specific NIR illumination. Numerical analysis of our oxygen data further suggested that this group is responsible for a major part of respiration in the oxygenated zone in the mat, which is a conclusion similar to that reached in our previous study conducted in a different mat with the same origin (Polerecky et al., 2007).

Acknowledgements

A.B. was supported by a grant (DFG JO-412) from the German Research Foundation. The development of the hyperspectral imaging technique was supported by European Commission (project ECODIS, project number 518043). We are grateful to Harald Osmers, Paul Faerber, Alfred Kutsche and Georg Herz for their technical wizardry offered during the development of the spectral imaging system.

References

Bachar A, Omoregie E, de Wit R & Jonkers HM (2007) Diversity and function of Chloroflexus-like bacteria in a hypersaline microbial mat: phylogenetic characterization and impact on aerobic respiration. Appl Environ Microbiol 73: 3975–3983.

Barille L, Meleder V, Combe JP, Launeau P, Rince Y, Carrere V & Morancais M (2007) Comparative analysis of field and laboratory spectral reflectances of benthic diatoms with a modified Gaussian model approach. J Exp Mar Biol Ecol 343: 197–209.

Bateson MM & Ward DM (1988) Photoexcretion and fate of glycolate in a hot spring cyanobacterial mat. Appl Environ Microbiol 54: 1738–1743.

Berg IA, Keppen OI, Krasil'nikova EN, Ugol'kova NV & Ivanovsky RN (2005) Carbon metabolism of filamentous anoxygenic phototrophic bacteria of the family Oscillochloridaceae. Microbiology 74: 258–264.

Butler WL & Hopkins DW (1970) Analysis of fourth derivative spectra. Photochem Photobiol 12: 451. Canfield DE & Desmarais DJ (1991) Aerobic sulfate reduction in microbial mats. Science 251: 1471–1473.

Castenholz RW(1988) The green sulfur and nonsulfur bacteria of hot springs. Green Photosynthetic Bacteria (Olson JM, ed), pp. 243–255. Plenum Press, New York.

Combe JP, Launeau P, Carrere V, Despan D,Meleder V, Barille L & Sotin C (2005) Mapping microphytobenthos biomass by non-linear inversion of visible-infrared hyperspectral images. Remote Sensing Environ 98: 371–387.

Cypionka H (2000) Oxygen respiration by Desulfovibrio species. Annu Rev Microbiol 54: 827–848.

D'Amelio ED, Cohen Y & DesMarais DJ (1987) Association of a new type of gliding, filamentous, purple phototrophic bacterium inside bundles of Microcoleus chthonoplastes in hypersaline cyanobacterial mats. Arch Microbiol 147: 213–220.

de Wit R & van Gemerden H (1990) Growth and metabolism of the purple sulfur bacterium Thiocapsa roseopersicina under combined light dark and oxic anoxic regimens. Arch Microbiol 154: 459–464.

Fleissner G, Hage W, Hallbrucker A & Mayer E (1996) Improved curve resolution of highly overlapping bands by comparison of fourth-derivative curves. Appl Spectr 50: 1235–1245.

Frund C & Cohen Y (1992) Diurnal cycles of sulfate reduction under oxic conditions in cyanobacterial mats. Appl Environ Microbiol 58: 70–77.

Hanada S & Pierson BK (2006) The family Chloroflexaceae. The Prokaryotes: An Evolving Electronic Resource for the Microbiological Community, release 3.11 (Dworkin M, ed), pp. 1–41. Springer, Heidelberg, Germany.

Hanada S, Takaichi S, Matsuura K & Nakamura K (2002) Roseiflexus castenholzii gen. nov., sp. nov., a thermophilic, filamentous, photosynthetic bacterium that lacks chlorosomes. Int J Syst Evol Microbiol 52: 187–193.

Hofstraat JW, van Zeijl WJM, de Vreeze MEJ, Peeters JCH, Peperzak L, Colijn F & Rademaker TWM (1994) Phytoplankton monitoring by flow-cytometry. J Plankton Res 16: 1197–1224.

Holst G & Grunwald B (2001) Luminenscence lifetime imaging with transparent oxygen optodes. Sensors and Actuators B-Chemical 74: 78–90.

Jonkers HM, Ludwig R, de Wit R, Pringault O, Muyzer G, Niemann H, Finke N & de Beer D (2003) Structural and functional analysis of a microbial mat ecosystem from a unique permanent hypersaline inland lake: 'La Salada de Chiprana' (NE Spain). FEMS Microbiol Ecol 44: 175–189.

Jonkers HM, Koh IO, Behrend P, Muyzer G & de Beer D (2005) Aerobic organic carbon mineralization by sulfate-reducing bacteria in the oxygen-saturated photic zone of a hypersaline microbial mat. Microb Ecol 49: 291–300.

Jørgensen BB (1994) Sulfate reduction and thiosulfate transformations in a cyanobacterial mat during a diel oxygen cycle. FEMS Microbiol Ecol 13: 303–312.

Kallmeyer J, Ferdelman TG, Weber A, Fossing H & Jørgensen BB (2004) A cold chromium distillation procedure for radiolabeled sulfide applied to sulfate reduction measurements. Limnol Oceanogr Meth 2: 171–180.

Klappenbach JA & Pierson BK (2004) Phylogenetic and physiological characterization of a filamentous anoxygenic photoautotrophic bacterium 'Candidatus Chlorothrix halophila' gen. nov., sp. nov. recovered from hypersaline microbial mats. Arch Microbiol 181: 17–25.

Klatt CG, Bryant DA &Ward DM (2007) Comparative genomics provides evidence for the 3-hydroxypropionate autotrophic pathway in filamentous anoxygenic phototrophic bacteria and in hot spring microbial mats. Environ Microbiol 9: 2067–2078.

Kühl M & Fenchel T (2000) Bio-optical characteristics and the vertical distribution of photosynthetic pigments and photosynthesis in an artificial cyanobacterial mat. Microb Ecol 40: 94–103.

Kühl M & Jørgensen BB (1992) Spectral light measurements in microbenthic phototrophic communities with a fiberoptic microprobe coupled to a sensitive diode-array detector. Limnol Oceanogr 37: 1813–1823.

Kühl M & Jørgensen BB (1994) The light-field of microbenthic communities - radiance distribution and microscale optics of sandy coastal sediments. Limnol Oceanogr 39: 1368–1398.

Kühl M, Steuckart C, Eickert G & Jeroschewski P (1998) AH2S microsensor for profiling biofilms and sediments: application in an acidic lake sediment. Aquat Microb Ecol 15: 201–220.

Ley RE, Harris JK, Wilcox J, Spear JR, Miller SR, Bebout BM, Maresca JA, Bryant DA, Sogin ML & Pace NR (2006) Unexpected diversity and complexity of the Guerrero Negro hypersaline microbial mat. Appl Environ Microbiol 72: 3685–3695.

Ludwig R, Al-Horani FA, de Beer D & Jonkers HM (2005) Photosynthesis-controlled calcification in a hypersaline microbial mat. Limnol Oceanogr 50: 1836–1843.

Madigan MT, Martinko JM & Parker J (2000) Brock – Biology of Microorganisms, 9th edn. Prentice-Hall Inc., Upper Saddle River, NJ.

N¨ubel U, BatesonMM,MadiganMT, K¨ uhlM&Ward DM(2001) Diversity and distribution in hypersaline microbial mats of bacteria related to Chloroflexus spp. Appl Environ Microbiol 67: 4365–4371.

Nübel U, Bateson MM, van Dieken V, Wieland A, K¨ uhl M & Ward DM (2002) Microscopic examination of distribution and phenotypic properties of phylogenetically diverse Chloroflexaceae-related bacteria in hot spring microbial mats. Appl Environ Microbiol 68: 4593–4603.

Pfennig N & Trüper HG (1992) The family Chromatiaceae. The Prokaryotes, 2nd edn (Balows A, Tr¨ uper HG, Dworkin M, Harder W & Schleifer KH, eds), pp. 3200–3221. Springer-Verlag, Berlin.

Pierson BK & Castenholz RW (1974) Studies of pigments and growth in Chloroflexus aurantiacus, a phototrophic filamentous bacterium. Arch Microbiol 100: 283–305.

Pierson BK, Valdez D, Larsen M, Morgan E & Mack EE (1994) Chloroflexus-like organisms from marine and hypersaline environments – distribution and diversity. Photosynth Res 41: 35–52.

Polerecky L, Bachar A, Schoon R, Grinstein M, Jørgensen BB, de Beer D & Jonkers HM (2007) Contribution of Chloroflexus respiration to oxygen cycling in a hypersalinemicrobial mat from Lake Chiprana, Spain. Environ Microbiol 9: 2007–2024.

Precht E, Franke U, Polerecky L & Huettel M (2004) Oxygen dynamics in permeable sediments with wave-driven pore water exchange. Limnol Oceanogr 49: 693–705.

Revsbech NP (1989) An oxygen microsensor with a guard cathode. Limnol Oceanogr 34: 474–478.

Saga Y & Tamiaki H (2004) Fluorescence spectroscopy of single photosynthetic light-harvesting supramolecular systems. Cell Biochem Biophys 40: 149–165.

Strauss G & Fuchs G (1993) Enzymes of a novel autotrophic CO_2 fixation pathway in the phototrophic bacterium Chloroflexus aurantiacus, the 3-hydroxypropionate cycle. Eur J Biochem 215: 633–643.

Van der Meer MTJ, Schouten S, Damste JSS, de Leeuw JW&Ward DM (2003) Compound-specific isotopic fractionation patterns suggest different carbon metabolisms among Chloroflexus-like bacteria in hot-spring microbial mats. Appl Environ Microbiol 69: 6000–6006.

Van der Meer MTJ, Schouten S, Bateson MM, N¨ ubel U, Wieland A, K¨ uhl M, de Leeuw JW, Damste JSS &Ward DM (2005) Diel variations in carbon metabolism by green nonsulfur-like bacteria in alkaline siliceous hot spring microbial mats from Yellowstone National Park. Appl Environ Microbiol 71: 3978–3986.

Visscher PT, Reid RP & Bebout BM (2000) Microscale observations of sulfate reduction: correlation of microbial activity with lithified micritic laminae in modern marine stromatolites. Geology 28: 919–922.

Wiggli M, Smallcombe A & Bachofen R (1999) Reflectance spectroscopy and laser confocal microscopy as tools in an ecophysiological study of microbial mats in an alpine bog pond. J Microbiol Methods 34: 173–182.

Conclusions & perspectives

During this stimulating period of method development, verification and application we were able to reach our primary aim namely to cast with a water-permeable resin highly hydrated marine habitats (sediments and microbial mats) in a biota-friendly manner minimizing chemical and physical stress. As salinity is unimportant during plastification we conclude that the method should also be applicable without any modifications to freshwater environments. Questions as how to sample, how to impregnate and how to prepare the sections are now hopefully answered. Inevitably, also, it was impossible to reach agreement on all points and approaches and some compromises were made (e.g. use of ethanol).

This thesis is intended to serve as a working manual and a guide. Above all, it is intended to lead to a more easy approach to the possibilities using the plastification method. Considering the diverse and heterogeneous natural systems it will be very difficult to uniform the results. However, it is hoped that the examples described in the previous pages will stimulate further development and applications in many areas. Thus, we expect that this work will be a welcomed and appreciated contribution by more and more scientists in an increasing number of disciplines when consolidation of hydrated materials is necessary.

Microscopic images taken directly from polished faces of polished sections have being analysed. Leaving and non-leaving information could be in situ revealed. Microorganisms within the resin matrix were successfully stained and identified. Lack of a motorised microscope stage in our lab hindered the synthesis of composite images from contiguous fields of view e.g. generating large-scale images of bacterial cell distributions. It would definitely be interesting to discover if there are any quantitative discrepancies counting bacteria on filters and in plastified sections. Problems with out-of-focus fluorescence especially in cell aggregates and high non-specific background autofluorescence could be perhaps circumvented by using laser scanning microscopy. Laser scanning microscopy could also be used to produce optical sections of a sample enabling 3D-rendering.

Fluorescent labelling of prokaryotic communities in undisturbed hypersaline mats gave us the possibility to investigate their spatial organization and their aggregation. FISHing bacteria with a specific metabolic capability in plastified sections could be further used as a proxy indicative of a particular process in a spatial context. Certain progress with dyes which do not easily bleach, which bind very specific, which are electrically neutral to avoid binding on cationic or anionic sites would facilitate future research.

Submicroscopic investigations using the scanning electron microscope and energy dispersive X-ray analysis have been successfully applied on plastified sediment sections. Mineral features such as abundance, size, shape and composition that form part of a field description could be observed in several levels of detail from different marine ecosystems. Coarse, sand and fine mud samples from the North, the Black, and the Baltic Sea were embedded and analyzed in the context of greigite, pyrite, and chalcopyrite formation. Within the frames of the EU project TREAD in a mesocosm experiment the 2D spatial distribution of oxides and sulphides in marine fine sediments could be precisely determined. Post-embedding mineral analysis of sediment attached on an oxygen optode foil revealed details of metal-bearing mineral phases and oxygen distribution in 2D. Thus, important aspects of dominant processes in sediments like pyritization and bioturbation could be revealed.

Combination of bacteria visualization techniques and substrate elemental analysis have shown in two cases the spatial relationship among iron minerals and microbes, presenting, for the very first time, details from an undisturbed microbes-substrate relationship. This demonstrates the great potential of optical / electron microscopy and x-ray analysis to complement each other in a micrometer scale following the plastification procedure. We therefore strongly recommend the application and combination of optical microscopy with electron microscopy and energy dispersive X-ray analysis. To our knowledge, at present, there are not available any electron microscopes equipped with an epifluorescence microscope. This could be in particular helpful when both tools are required. Researchers seeking for microbial inhabited minerals following out protocol are advised to start with substrate analysis and a detailed micromorphological description as a precursor to the selection of samples for detailed examination with staining and optical microscopy techniques.

Data on microbes and minerals in resin sections were incorporated in a number of studies complementing methods like the digital gradient technique, microsensor measurements, hyperspectral imaging, pigment analysis, 16S rRNA gene clone library analysis, sulphate reduction, isotopic measurements and other. Combined mineral, chemical and biological descriptions are thus advisable.

Embedding and subsequent direct visualization of the textural interplay between organic matter, microbes, and minerals may also be valuable in experiment and model design helping to identify mechanisms of interaction between the biologic, organic and mineral constituents in natural sediments. The development and application of models of ecosystems require reliable quantitative estimates of biotic and abiotic parameters. Based on the overriding principle that our samples have not been disturbed either during sampling or subsequently make us believe that our protocol could be applied in reliable quantification procedures related to species composition and abundance with respect to sediment depth and different physicochemical regimes in modelling studies.

Further, improved methods for sampling deep sea sediments, marine aggregates, and other detritus that preserve the material in the undisturbed state might be areas of possible extension of the embedding technique. Technical advances in sophisticated instrumentation (ion microscope, electron probe microanalyser) and in current laboratory techniques e.g. ion milling as an alternative to thin sectioning, or two-photon laser scanning fluorescence microscopy, could open new pathways in exploring bacteria spatial distribution in natural samples and associated consequences.

Manuscripts contributions

A biota friendly and easy to use protocol for plastifying marine sediments. Staining of microbes enclosed in the resin-matrix

Kyriakos Vamvakopoulos & Ole Larsen

Kyriakos Vamvakopoulos wrote the paper and is the corresponding author of the paper. He performed all the experimental work. He prepared all the figures.

Transition metal oxides and sulfides in marine sediments and their associated heavy metals

Kyriakos Vamvakopoulos, Niko Finke & Ole Larsen

Kyriakos Vamvakopoulos wrote most of the paper and is the corresponding author of the paper. He performed almost all the experimental work. He prepared all figures.

Transport and reactions of contaminants in sediments

Ole Larsen, Bill Davison, Kyriakos Vamvakopoulos, Flemming Møhlenberg

Kyriakos Vamvakopoulos performed sampling and analysis of copper minerals. He wrote part of the paper, prepared figures and commented.

Monitoring and modelling contaminants in harbour basins: coupling hydraulic and sediment models

Ole Larsen & Kyriakos Vamvakopoulos

Kyriakos Vamvakopoulos contributed to the experimental design, data acquisition, commented and discussed outcomes.

Sulfur and iron diagenesis in post-glacial limnic and brackish sediments of the Arkona Basin (Baltic Sea)

Lars Holmkvist, Kyriakos Vamvakopoulos, Alexey Kamyshny, Jr., Volker Brüchert, Tim Ferdelman and Bo Barker Jørgensen

Kyriakos Vamvakopoulos was responsible for experiments on solid phase analysis. Assisted on sampling strategy and performed all work for EDS-SEM analysis. He also contributed to the method, results, discussion part and commented the paper.

Sulfate reduction below the anaerobic oxidation of methane transition zone in Black Sea sediments

Lars Holmkvist, Alexey Kamyshny, Jr., Christoph Vogt, Kyriakos Vamvakopoulos, Tim Ferdelman and Bo Barker Jørgensen

Kyriakos Vamvakopoulos was responsible for experiments on solid phase analysis. Assisted on sampling strategy and performed all work for EDS-SEM analysis. He also contributed to the method, results, discussion part and commented the paper.

Two-dimensional mapping of photopigments distribution and activity of Chloroflexus-like bacteria in a hypersaline microbial mat

Ami Bachar, Lubos Polerecky, Jan Fisher, Kyriakos Vamvakopoulos, Dirk de Beer, Henk M. Jonkers

Kyriakos Vamvakopoulos performed literature research and was responsible for sampling, fixation, plastification, probes ordering and testing, hybridization and digital image acquisition. He interpreted the results, wrote parts of the paper and prepared the respective figures.

Note: The plastification procedure was additionally applied at: Cook P & Røy H (2006) Advective relief of CO_2 limitation in microphytobenthos in highly productive sandy sediments. *Limnol. Oceanogr.*: 51(4), 1594–1601.